

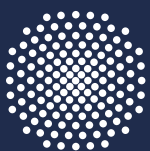
BEITRÄGE ZUR UMFORMTECHNIK



Herausgeber: Prof. Dr.-Ing. Dr. h.c. Mathias Liewald MBA
Institut für Umformtechnik, Universität Stuttgart

Fei Han

92 A new criterion to determine wrinkling
in deep drawing and stretch forming
processes



Universität Stuttgart

A new criterion to determine wrinkling in deep drawing and stretch forming processes

Von der Fakultät Konstruktions-, Produktions- und Fahrzeugtechnik
der Universität Stuttgart
zur Erlangung der Würde eines Doktor-Ingenieurs (Dr.-Ing.)
genehmigte Abhandlung

Vorgelegt von
Fei Han MSc
aus Nanjing, Jiangsu / P.R. China

Hauptberichter: Prof. Dr.-Ing. Dr. h.c. Mathias Liewald MBA

Mitberichter: Prof. Dr.-Ing. Wolfram Volk, Technische Universität München

Tag der mündlichen Prüfung: 15.07.2021

Institut für Umformtechnik der Universität Stuttgart

2021

Fei Han, M. Sc.
Institute for Metal Forming Technology
University of Stuttgart

Univ.-Prof. Dr.-Ing. Dr. h.c. Mathias Liewald MBA
Institute for Metal Forming Technology
University of Stuttgart

D93

ISBN 978-3-946818-17-5

Institute for Metal Forming Technology

Universität Stuttgart
Holzgartenstraße 17
70174 Stuttgart
www.ifu.uni-stuttgart.de

Printed in Germany

Geleitwort des Herausgebers

Die langjährige Buchreihe „Beiträge zur Umformtechnik“ enthält Forschungsberichte und abgeschlossene Dissertationen, die am Institut für Umformtechnik (IFU) der Universität Stuttgart aus einer mehrjährigen wissenschaftlichen Arbeit zu einem Forschungsthema aus der Umformtechnik entstanden sind. Auch sind in dieser Buchreihe Abschlussberichte von Forschungsarbeiten zu aktuellen Fragestellungen der Umformtechnik enthalten.

Umformen ist die gezielte Änderung der Form, der Oberfläche und der Eigenschaften eines metallischen Körpers unter Beibehaltung von Masse und Stoffzusammenhalt.

Diese Definition für das Umformen von metallischen Körpern in Anlehnung an DIN 8580 beschreibt nicht nur die gezielte Änderung der Form, sondern auch die der Oberfläche und der Eigenschaften des Produktes durch den Umformvorgang. Die Technik des Umformens befasst sich daher nicht nur mit Arbeiten zur Erlangung eines vertieften Prozessverständnisses und der Auslegung von Betriebsmitteln, sondern auch mit Methoden für eine zuverlässige Vorausbestimmbarkeit der finalen Produkteigenschaften. Dabei kommt der mathematischen Beschreibung des Umformvorganges und der Modellierung grundlegender physikalischer Phänomene wie z.B. der verfahrensspezifischen Tribologie und dem Werkstoffverhalten eine besondere Bedeutung bzgl. der Güte von numerischen Simulationsrechnungen mit der Methode der Finiten Elemente (FEM) zu.

Oftmals geht dabei die intuitive, auf aktuellen Grundlagenerkenntnissen basierende Forschung in der Umformtechnik mit einer experimentellen bzw. empirisch basierten Herangehensweise an neue Fragestellungen einher. Die dabei erzielten Forschungsergebnisse dienen dem allgemeinen Wissenserwerb und dem Grundlagenverständnis von werkstofflichen und verfahrensspezifischen Phänomenen und Zusammenhängen. Solche Arbeiten sind somit nicht nur für Wissenschaftler, sondern auch für die in der Praxis stehenden Ingenieure von grundsätzlicher Bedeutung.

Kurze Entwicklungszeiten für neue Produkte der Umformtechnik einerseits und veränderte Wertschöpfungsketten, die Dynamik von Märkten, neue Technologien sowie veränderte Randbedingungen andererseits erfordern in den Unternehmen heute eine Intensivierung von spezifischer Forschung. Auch gewinnt das schnelle Lernen im Umfeld von Produktionstechnologien in den sich volatil verändernden, oftmals globalen Wertschöpfungsketten immer mehr an Bedeutung. Moderne Forschungsstellen stehen daher im engen Dialog mit solchen Unternehmen und sind in beide Prozesse eingebunden: zum einen in die Grundlagenforschung mit Blick auf Werkstoffe, Verfahren und Maschinen der Umformtechnik und zum anderen in vorwettbewerbliche bzw. anwendungsorientierte integrierte Lösungen über neue Prozessketten hinweg.

Motivation für die Herausgabe dieser Berichte ist die Publikation solcher grundlagenorientierten und auch praxisorientierten Forschungs- und Entwicklungsarbeiten, die an meinem Institut entstehen. Ein weiteres Ziel der Buchreihe ist das Bereitstellen eines aktuellen Wissens- und Kenntnisstandes für weiterführende wissenschaftliche Arbeiten auf internationalem Niveau.

Acknowledgement

The present work was carried out during my work as a research assistant at the Institute of Metal Forming at the University of Stuttgart.

First of all, I would like to express my deepest appreciation to my supervisor, Mr. Univ.-Prof. Dr.-Ing. Dr. h.c. Mathias Liewald MBA, who is director of Institute for Metal Forming Technology. Thank you for your guidance and discussion on my projects and academics during my time at the institute. It was these four years in the institute that made me grow rapidly in the field of sheet metal forming technology. It was also these four years that allowed me to make great progress in my work style and ability to solve problems independently.

I would also like to extend my deepest gratitude to Mr. Prof. Dr.-Ing. Stefan Wagner, who is my direct leader in Materials Department at the institute until the end of 2015. Thank you for your long-term trust and encouragement, thank you for your support and help in my daily work at the institute. It was due to your continuous encouragement that made it possible for me to improve myself continuously, and I will not be afraid in the face of difficulties.

I would also like to extend my gratitude to Mr. Dr.-Ing. Klaus Drotleff, who was my direct leader in Materials Department at the institute and Dr.-Ing. Kartik Jamadar, who was the project leader from Volkswagen (VW). Thank you for your inspiration and suggestions when I was at a loss. Without your help, the project would have only stayed on the original plan and there wouldn't have been any breakthrough. Special thanks to Dr.-Ing. Kartik Jamadar for the continuous support of the project, opinions towards my personal future development, and long-term concern.

Furthermore, I also had great pleasure of working with Dr.-Ing. Siu Ping Afonichev (Li), Dr.-Ing. Markus Singer, Dr.-Ing. Ranko Radonjic, Dr.-Ing. Dennis Hofmann, Dipl.-Ing. Matthias Schneider und Dr.-Ing. Martin Barthau. Without your support and help in my daily work and life, I couldn't have successfully completed this project. I would also like to thank the employees of the companies DynaMore GmbH (Stuttgart office), AutoForm Engineering Deutschland GmbH (Esslingen and Dortmund office), and CADFEM GmbH for the expert support in using the FEM programs. I would like to acknowledge the help of Mrs. B.Sc. Chen Meng and Mr. Ralf Schmidt, thank you for the valuable support and constructive discussions about the FEM software AutoForm. I would like to acknowledge the help that I received from Dipl.-Ing. Ekaitz Moral Trebolazabala, thank you for your help by trying out the parts used in this thesis in GESTAMP.

Finally, I would like to thank my wife, Dr.rer.nat Tingting Yu, and my parents for the support, understanding, and inexhaustible patience in carrying out this work.

Stuttgart, Dezember 2020

Table of Contents

Geleitwort des Herausgebers	<i>i</i>
Acknowledgement	<i>ii</i>
Table of Contents.....	<i>iii</i>
Abbreviations	<i>vi</i>
Formula symbols	<i>vii</i>
Abstract.....	<i>xi</i>
Deutsche Kurzfassung.....	<i>xiii</i>
1 Introduction.....	<i>1</i>
2 State of the art.....	<i>5</i>
2.1 Sheet metal material properties and material testing.....	<i>5</i>
2.1.1 Yield locus modelling.....	<i>5</i>
2.1.2 Flow rules, flow curve, effective strain and stress	<i>8</i>
2.1.3 Hardening curve – experimental procedure and its characterisation	<i>10</i>
2.1.4 Elastic and plastic deformation stage defined in uniaxial tensile test.....	<i>12</i>
2.1.5 Types of failure in the deep drawing process	<i>18</i>
2.2 Standard tests in the laboratory to investigate wrinkling formation.....	<i>24</i>
2.2.1 Buckling bending test	<i>24</i>
2.2.2 Buckling test performed with original and modified Yoshida specimen.....	<i>25</i>
2.2.3 Wrinkling test by using special designed specimen	<i>27</i>
2.2.4 Conical cup test.....	<i>28</i>
2.2.5 Car-fender based geometry produced with segment-elastic blankholder	<i>30</i>
2.3 Conventional wrinkling criteria applied in FEA	<i>35</i>
2.3.1 Wrinkling criteria based on the forming-limit diagram	<i>35</i>
2.3.2 Wrinkling criteria based on critical stress level	<i>39</i>
3 Objective of this Thesis.....	<i>47</i>
4 Development of a simplified model for predicting wrinkles of second order .	<i>51</i>
4.1 Motivation.....	<i>51</i>
4.1.1 Limitation of the criteria based on the force–displacement curve.....	<i>52</i>
4.1.2 Limitation of the strain-distribution-based wrinkling criterion	<i>56</i>
4.2 Description of wrinkle formation using a simplified, stress based model	<i>63</i>
4.2.1 Analysis of maximum compressive stress emerging at wrinkling initiation.....	<i>64</i>

4.2.2	Analysis of the change in stress state after wrinkling initiation	67
4.2.3	Using development of surface compressive stress to establish a simplified model	72
4.3	Conclusion on the simplified model for predicting wrinkles of second order....	74
5	Criterion considering tool contact - Concept of newly developed approach .	77
5.1	Basic concept of the developed approach	78
5.1.1	Definition of wrinkling using two boundary conditions.....	78
5.1.2	Detecting bifurcation by analysing the stress state.....	80
5.1.3	Identification of both wrinkling initiation and developed wrinkling.....	82
5.1.4	Characterising the degree of wrinkling by evaluating the development of stress	85
5.2	Application of the newly developed concept in post processing FEA code.....	87
5.3	Conclusion.....	90
6	Regression models considering factors affecting wrinkling process	92
6.1	Essential factors affecting the wrinkling process	92
6.2	Influence of material on the difference in surface stress.....	93
6.2.1	Influence of sheet thickness on the difference in surface stress	93
6.2.2	Conclusion on the influence of sheet metal materials on wrinkling behaviour.....	94
6.3	Influence of sheet thickness on the difference in surface stress	95
6.3.1	Wrinkling initiation when materials have different thicknesses	95
6.3.2	Conclusion on the influence of sheet thickness.....	96
6.4	Influence of local curvature on the critical stress level	97
6.4.1	Determination of principal local curvature in experiments	97
6.4.2	FEA results gained from the conical-cup test	99
6.4.3	Conclusion on the influence of local curvature on wrinkling behaviour	101
6.5	Linear-regression models for predicting the critical value of surface stress ...	102
6.5.1	Linear-regression models for sheet metal material HC420LA.....	103
6.5.2	Linear-regression models for material HC340LA and DX54D	105
7	Examining the simulation accuracy and reference simulations	106
7.1	Case study 1 – Buckling test with modified Yoshida specimen.....	106
7.1.1	Experiment details – Buckling test with modified Yoshida specimen	107
7.1.2	Simulation details – Buckling test with modified Yoshida specimen.....	107
7.1.3	Examining of surface stress development on outer and inner side of specimen.....	109
7.1.4	Results and conclusion – Buckling test with modified Yoshida specimen	110
7.2	Case study 2 – Mini conical cup test.....	111
7.2.1	Experiment and simulation details – Mini conical cup test.....	111
7.2.2	Examining of surface stress development on outer and inner side of wrinkling area	113

7.2.3	Evaluating surface quality by applying Eisele's approach	116
7.2.4	Surface defect – wrinkling height and surface deviation	119
7.2.5	Conclusion on the mini conical-cup test	120
7.3	Case study 3 – car-fender-based geometry	123
7.3.1	FE model for rigid blank holder.....	123
7.3.2	FE model for the elastic blank holder	124
7.3.3	Results – experiments conducted with car-fender-based geometry.....	126
7.3.4	Conclusion on experiments performed with car-fender-based geometry	128
8	Validation of developed approach by applying in industrial part analysis.....	129
8.1	User-defined-variable files in AutoForm software	129
8.2	Validation study 1 – exterior lower-side part	131
8.3	Validation study 2 – Part C-Pillar-Reinforcement.....	137
8.4	Validation study 3 – Part Door-Frame-Adapter.....	140
9	Conclusion and Outlook.....	143
9.1	Conclusion of this work.....	143
9.2	Outlook and future works	146
10	Appendix.....	148
10.1	Applied sheet metal materials	148
10.2	Results regarding regression models using Minitab 17	149
11	Bibliography	150
	Curriculum Vitae	158

Abbreviations

Abbreviation	Description
AHSS	Advanced high strength steel
BBC_2005	Banabic 2005 Yiled criterion
BBT	Buckling Bending Test
BCC	Body-Centered Cubic
BLC	Bending limit curve
CCT	Conical Cup Test
DoE	Design of Experiment
DSCS-approach	Double Surface Compressive Stress Approach
DW	Developed Wrinkle
DMV	Donell-Mushtari-Vlashitari theory
FCC	Face-Centered Cubic
FWA	Flange Wrinkle Amplitude
FEA	Finite Element Analysis
FFL	Fracture Forming Limit
FLC	Forming Limit Curve
FLD	Forming Limit Diagram
GFLC	Generalised Forming Limit Concept
GISSMO	Failure criterion, GISSMO model
HSS	High strength steel
IFU	Institut für Umformtechnik
ISO	International Organisation for Standardisation
KVG	Car Fender Shaped Geometry
LYS	Lower yield strength point
M-CCT	Mini conical cup test
M-YBT	Buckling Test with Modified Yoshida Specimen
M-YBT-K	Buckling Test with Modified Yoshida Specimen (small shoulder radius)
M- YBT-G	Buckling Test with Modified Yoshida Specimen (large shoulder radius)
OEM	Original Equipment Manufacturer
OYS-approach	Offset yield strength approach
SWA	Sidewall Wrinkle Amplitude
SE	Simultaneous Engineering
SEB	Segment-Elastic Blankholder
SEM	Scanning electron microscopy
SFFL	Shear Fracture Forming limit
UDV	User Defined Variables

UHSS	Ultra high strength steel
UTS	Ultimate tensile stress
UYS	Upper yield strength point
WI	Wrinkling Initiation
WLC	Wrinkling Limit Curve
YBT	Yoshida Buckling Test
YPE	Yield point elongation
YID_2000	Barlat 2000 Yield criterion

Formula symbols

Symbol	Unit	Description
A	[mm ²]	Reduced current cross-sectional area of tensile specimen
A_0	[mm ²]	Initial cross-sectional area of tensile specimen
A_1	[mm ²]	Wrinkling area of modified Yoshida specimens
A_2	[mm ²]	Area of specimen wings of Yoshida specimens
a	[-]	Anisotropic material constants in Barlat yield criterion
a_c	[mm]	Effective length of assumed wrinkling area
a_f	[mm]	Crack length of assumed “internal flaw” and “surface flaw”
b_c	[mm]	Effective width of assumed wrinkling area
c	[-]	Anisotropic material constants in Barlat yield criterion
d_c	[mm]	Die cavity in bulge test
h	[-]	Anisotropic material constants in Barlat yield criterion
h_d	[mm]	Dome height of the formed part in bulge test
l_0	[mm]	Initial length of tensile specimen
l_1	[mm]	Effective length of original Yoshida specimen
l_2	[mm]	Effective width of original Yoshida specimen
Δl	[mm]	Increased length of the tensile specimen during the test
n	[-]	Strain hardening exponent
n_H	[-]	Work hardening exponent of Hollomon’s power law
n_L	[-]	Work hardening exponent of Ludwig’s power law
n_S	[-]	Work hardening exponent of Swift’s law
p	[-]	Anisotropic material constants in Barlat yield criterion
t	[mm]	Sheet metal thickness
t_0	[mm]	Initial thickness (cross-sectional area) of tensile specimen
t_d	[mm]	Dome apex thickness of the formed part in bulge test
t_i	[mm]	Initial thickness of the specimen in bulge test
$w = f(x, y)$	[-]	Surface failure model

w_0	[mm]	Initial width (cross-sectional area) of tensile specimen
D^E, D^P	[GPa*mm ³]	Elastic and plastic bending rigidity
E	[GPa]	Elastic modulus
$E_{pri.}$	[GPa]	Primary path deformation energy in Kim' s model
$E_{sec.}$	[GPa]	Secondary path deformation energy in Kim' s model
E_s	[GPa]	Secant Modulus
E_t	[GPa]	Tangential modulus
F	[N]	Force without considering principal direction
F_1, F_2	[N]	Force in first principal and second principal direction
F_{MD}	[N]	The vertical force acted on piezo load cell
F_Z	[N]	Tensile force existing in the side wall
G^Y	[-]	Constants specific of the anisotropy state
H^Y	[-]	Constants specific of the anisotropy state
H^W	[mm]	Wrinkling height
H^B	[mm]	Buckling height
V^P	[mm]	Position deviation
ΔL	[mm]	Increased length of the wrinkling area
$L_{\alpha\beta k\gamma}$	[-]	Instantaneous moduli
$\bar{L}_{\alpha\beta k\gamma}$	[-]	Instantaneous moduli for plane stress condition
K	[MPa]	Material strength coefficient
K_H	[MPa]	Material strength coefficient of Hollomon' power law
K_L	[MPa]	Material strength coefficient of Ludwig' s power law
K_S	[MPa]	Material strength coefficient of Swift' s law
$K_{\alpha\beta}$	[-]	Bending strains components
N^Y	[-]	Constants specific of the anisotropy state
$N_{\alpha\beta}$	[-]	Membrane stress resultants
M	[-]	Constants specific of the anisotropy state
$M(x)$	[N]	Bending moment
$M_{\alpha\beta}$	[-]	Bending moments components
$ MP_i $	[mm]	Vector length used in Eisele' s approach
Q^Y	[-]	Constants specific of the anisotropy state
$1/R_1$	[1/mm]	Local curvature in first principal direction
$1/R_2$	[1/mm]	Local curvature in second principal direction
O_O	[-]	Investigated point O on the outer side to calculated critical stress
O_I	[-]	Investigated point O on the inner side to calculated critical stress
R_{00}	[-]	Lankford anisotropy value in rolling direction 0°

R_{45}	[-]	Lankford anisotropy value in rolling direction 45°
R_{90}	[-]	Lankford anisotropy value in rolling direction 90°
$R_{an.}$	[-]	Lankford anisotropy value without considering rolling direction
R_p	[mm]	Punch radius defined in conical cup test
R_d	[mm]	Radius of the die entry
R_z	[mm]	Length at one-third of drawing depth defined in conical cup test
R_m	[MPa]	Tensile strength
$R_{P0.2}$	[MPa]	Yield strength
S_{ij}	[-]	Stress deviator, $i, j = 1, 2$
T	[s]	Time
W_f	[-]	Wrinkling factor in Kim's model
W_{tm}	[mm]	Effective width of gripper in original Yoshida specimen
$Z_{eff.}$	[mm]	Effective measured depth in conical cup test
Z_d	[mm]	Drawing depth in conical cup test
Z^*	[mm]	Position one-third of drawing depth in side wall of a conical cup
ΔT^C	[W]	Work performed by membrane forces in Cao's model
ΔU^C	[W]	The internal energy of buckled plate in Cao's model
α	[-]	Stress state according to Levy-mises flow rule
α^S	[-]	Angle between the punch and sidewall
β_0	[-]	Bifurcation factor
β_1	[-]	Bifurcation factor
β_2	[-]	Bifurcation factor
k_1	[-]	Specimens "1" based on M-YBT-K specimen
k_2	[-]	Specimens "2" based on M-YBT-K specimen
γ_1	[-]	Invariant of the stress tensor
γ_2	[-]	Invariant of the stress tensor
σ_{11}	[MPa]	First principal stress, = σ_1
σ_{22}	[MPa]	Second principal stress, = σ_2
σ_{33}	[MPa]	Third principal stress, = σ_3
$\sigma_{\alpha\beta}$	[-]	Stress components, $\alpha, \beta = 1, 2$
$\bar{\sigma}$	[MPa]	Effective stress
$\bar{\sigma}_b$	[MPa]	Equi-biaxial effective stress in bulge test
σ_c	[MPa]	Critical stress by testing specimens with assumed "flaws"
σ_Y	[MPa]	Yield stress
σ_{WI}	[MPa]	Critical stress level at "wrinkling initiation"
σ_{DW}	[MPa]	Critical stress level at "developed wrinkle"
$\sigma_{eng.}$	[MPa]	Engineering stress

$\sigma_{resultant}^{O_o}$	[MPa]	Resultant stress at point O_o on the outer side
$\sigma_{resultant}^{O_I}$	[MPa]	Resultant stress at point O_I on the inner side
ε_1	[-]	First principal strain
ε_2	[-]	Second principal strain
ε_3	[-]	Third principal strain
$\varepsilon_{\alpha\beta}$	[-]	Strain components, $\alpha, \beta = 1, 2$
$\varepsilon_{eng.}$	[-]	Engineering strain
ε_t	[-]	Thickness strain in bulge test
$\bar{\varepsilon}$	[-]	Effective strain
$\bar{\varepsilon}_b$	[MPa]	Equi-biaxial effective strain in bulge test
δ_{ij}	[-]	Kronecker delta
ϑ	[-]	Poisson's ratio
ρ	[-]	Radius of local curvature
ρ_f	1/[mm]	Local curvature of assumed "internal flaw" and "surface flaw"

Abstract

At present, in order to improve the global warming effect and the deterioration of the environment, series of solutions have been proposed for the automotive industry that uses fossil fuels as the driving energy source. The lightweight of cars is one of the most important solutions. The light weight of a car implies that the car's body weight should be reduced as much as possible while ensuring the strength and safety performance of the car, thereby improving the power of the car, reducing fuel consumption, and reducing exhaust pollution. However, thinner and lighter sheet formed parts, although successfully reducing the weight of the body, they have presented unprecedented challenges and requirements for the metal forming technology. The major problems faced by the forming technology applied in automotive industry are, for example, how to use lightweight materials to maintain the structural properties, or to get even better properties than traditional formed parts, and how to avoid and reduce the defects often appearing in forming processes.

For this reason, the accuracy of finite element analysis (FEA) in metal forming technology is more important than ever, since the used new lightweight materials and the thin sheet materials usually have reduced bending resistance which can easily lead to surface defects like wrinkles during manufacturing process like deep drawing and stretch forming. If such surface defects can be predicted in production design stage and SE-stage (Simultaneous Engineering), the manufacture period and cost of a new car model will be reduced by changing the part and structure design in advance.

This work focuses on the wrinkling criteria used in FEA to predict surface defects in forming process. For that reason, two kinds of conventional wrinkling criteria were first reviewed in Chapter 4. The first conventional wrinkling criteria mentioned in this work was based on force-displacement curve determined from experiments, for example “turning point” approach and “gradient of wrinkling height development” approach was reviewed in Chapter 4.1. However, these approaches cannot be used in FEA to predict surface defects caused by wrinkling. Furthermore, the second conventional wrinkling criteria discussed in this work was based on the wrinkling limit curve (WLD) in forming limit diagram (FLD). The feasibility of this kind of strain-based wrinkling criterion is also discussed in Chapter 4.1. Experiments at the Institute for Metal Forming Technology (IFU) have shown that this strain-based wrinkling criterion does not accurately reflect the wrinkles in the complex deep drawing situations. Only simple geometry like conical-cup test (CCT) and car-fender-based geometry (KVG) can be validated with strain-based wrinkling criterion under limited conditions.

As shown in this work, firstly, conventional wrinkling criteria do not accurately predict wrinkles during the forming process. Secondly, traditional wrinkling criteria cannot predict changes in surface quality during the forming process. Therefore, a new criterion that can predict wrinkles and changes in surface quality during manufacturing process was developed in this work. For that reason, this new

criterion aims to establish a new approach for predicting the surface quality of sheet metal parts, taking into consideration tool contact. This newly developed criterion is called “Double-Surface Compressive-Stress-Approach” (DSCS-approach). By using this approach, not only wrinkles, but also wrinkling initiation and slight surface defects, like surface lows and buckling effects, can be predicted using FEA.

Two essential time points, namely “wrinkling initiation” (WI) and “developed wrinkle” (DW), can be defined using DSCS-approach by evaluating the surface stress difference between outer side and inner side of component in FEA. By using these two time points, the development of surface defects caused by wrinkling phenomenon can be observed according to reference experiments at IFU. The introduced and performed reference experiments are, buckling tests with modified Yoshida specimens and mini-conical-cup tests.

In the time point “wrinkling initiation”, the investigated part region, which reveals wrinkling tendency, shows the maximum buckling height and tends to change surface defect type from “buckling” to “wrinkling”. When the local bending resistance is high, the surface profile remains in a buckling state. The phenomenon was observed during buckling tests with G-Series modified Yoshida specimen (M-YBT-G, “G” means specimen with large shoulder radius) and by performing mini conical cup tests with thick materials. On the other hand, when the local bending resistance is low, a typical wrinkled surface profile occurs. This phenomenon was observed during buckling tests with K-Series modified Yoshida specimen (M-YBT-K, “K” indicates specimens with small shoulder radius), and by performing mini conical cup tests with thin sheet metal materials.

The concept of DSCS-approach was continuously developed as regression model considering the effecting parameters “sheet metal thickness” and “local curvature” in this work. Finally, regression model was prepared as User-Defined-Variable-Files (UDV-Files) which can be implemented in FEM software like AutoForm R6 and R7. The DSCS-approach was validated. The validation results show that the DSCS-approach can accurately predict the location of surface defects. In addition, by using the DSCS-approach, the first wrinkles can be predicted at the correct drawing depth. In addition, by setting the critical strain value in the UDV-file, it is possible to detect the wrinkles in the elastic deformation stage (small effective strain value). Since the DSCS-approach is a stress-based criterion, there is no need to consider the effects of non-linear strain paths in UDV-files.

In future, if enough sheet metal materials are validated, an individual model should be developed to calculate the critical value of stress between outer side and inner side at defined “wrinkling initiation” and “developed wrinkles”. By using this stress-based wrinkling criterion, the wrinkling position actually cannot be stored in AutoForm software. In this work, the wrinkling positions were manually marked at corresponding drawing depth.

Deutsche Kurzfassung

Heutzutage sind die Forderungen nach Leichtbauweisen in der Rohkarosserie insbesondere für batteriebetriebene Fahrzeuge größer als je zuvor. Somit ist die Verwendung von neuen Materialien und dünnen Stahl/Aluminium-Blechwerkstoffen immer häufiger anzutreffen. Neue Materialien und dünne Blechwerkstoffe weisen beide das gleiche Merkmal auf, und zwar eine geringere Biegesteifigkeit. Daher ist es heute wichtiger denn je, über genaue Finite-Elemente-Analysen in der Blechumformung zu verfügen. Insbesondere treten bei Tiefziehprozessen Faltenbildungen häufiger auf, wenn neuere Materialien und dünne Blechwerkstoffe eingesetzt werden.

Zunächst werden konventionelle Faltenbildungskriterien behandelt. In Kapitel 4.1 werden Faltenbildungskriterien basierend auf Kraft-Weg-Kurven wie zum Beispiel die “Wendepunkt“-Methode oder die “Gradient der Faltenbildung” -Methode vorgestellt. Jedoch können diese Ansätze in der Finiten-Elemente-Analyse zur Vorhersage von Faltenbildung nicht eingesetzt werden. Darüber hinaus wird das klassische Faltenbildungskriterium, bei dem eine Faltenbildungskurve aus dem Grenzformänderungsdiagramm hervorgeht, in Kapitel 4.1 behandelt. Experimentelle Arbeiten am IFU haben gezeigt, dass mit solch einem dehnungsbasierten Faltenkriterium eine genaue Faltdetektion in komplexen tiefgezogenen Bauteilen nicht möglich ist. Mit dem dehnungsbasierten Faltenkriterium können lediglich einfache Geometrien, wie es beim konischen Napf und dem Kotflügel der Fall ist, validiert werden. Mit dem konventionellen Faltenkriterium ist die Möglichkeit einer Vorhersage sowohl der Faltenbildung als auch der Änderung in der Oberflächenqualität nicht gegeben.

Die vorliegende Arbeit zielt darauf ab, ein neues Kriterium zur Vorhersage der Oberflächenqualität von durch Blechumformung hergestellten Teilen unter Berücksichtigung der Werkzeugkontakte zu entwickeln. Das neue Kriterium wird als DSCS-Ansatz bezeichnet. Durch die Verwendung des neuen Ansatzes können nicht nur Falten, sondern auch Falteninitiierung und leichte Oberflächendefekte wie Einfallstellen und Beulen detektiert werden. Mit dem DSCS-Ansatz können zwei wesentliche Zeitpunkte, nämlich der Zeitpunkt der Falteninitiierung und der voll ausgebildeten Falte, durch Bewertung der Oberflächenspannungsdifferenzen zwischen der äußeren und der inneren Seite der untersuchten Elemente in der FEA definiert werden. Mithilfe der beiden Referenzexperimente (Beulversuche mit modifizierten Yoshida-Proben (M-YBT) und Mini konischer Napf-Versuche (M-CCT)) kann bestätigt werden, dass Oberflächendefekte vor der „Falteninitiierung“ als Beulen behandelt werden. Zwischen den Zuständen “Falteninitiierung” und “voll ausgebildete Falte” können leichte Falten oder Beulen beobachtet werden.

Im Falteninitiierungszustand weist die untersuchte Oberfläche, welche die Tendenz zur Faltenbildung besitzt, die maximale Beulhöhe auf, der Typ des Oberflächendefekts neigt vom Beulen zur Faltenbildung. Ist der Biege­widerstand groß genug, verbleibt die Oberfläche in einem Beulzustand. Dieses Phänomen wurde anhand von Beulversuchen mit modifizierten Yoshida-Proben der G-Serie (M-YBT-G, "G" bezeichnet Proben mit großem Schulterradius) und Mini-konische Napfversuche mit großer Materialdicke ermittelt. Ist der lokale Biege­widerstand hingegen klein, so tritt die typische Faltenbildung der Oberfläche auf. Dieses Phänomen wurde anhand von Beulversuchen mit modifizierten Yoshida-Proben der K-Serie (M-YBT-K, "K" bezeichnet Proben mit kleinem Schulterradius) und Mini-konische Napfversuche mit geringer Materialdicke ermittelt.

Es können 3 Stufen der Oberflächenqualität durch Anwendung der beiden zuvor erwähnten Zeitpunkte "Falteninitiierung" und "Voll ausgebildete Falten" definiert werden. Der Oberflächenfehler mit der Bezeichnung "surface low" kann als der Faltenbildungsprozess bis zum Erreichen der maximalen Beulhöhe bzw. der Falteninitiierung angesehen werden. Die Ergebnisse der experimentellen Untersuchungen von M-YBT mit verschiedenen Materialien zeigen, dass die Faltenhöhe im Zustand der Falteninitiierung etwa 0,04 mm beträgt (Probendicke 1,0 mm). Der Bezeichnung "Falten" wird für den Zustand eingeführt, in dem die Falten sich bereits voll ausgebildet haben. Die Ergebnisse der experimentellen Untersuchungen von M-YBT mit verschiedenen Materialien zeigen, dass die Faltenhöhe der voll ausgebildeten Falten etwa 1,2 mm beträgt (Probendicke 1,0 mm). Zwischen den definierten Zuständen "Falteninitiierung" und "voll ausgebildete Falten" liegen zeitgleich die Oberflächenfehler Beulen und Faltenbildung vor. Dieser Zustand wird hier als kleine "dimension wrinkles" bezeichnet. Die DSCS-Methode wurde kontinuierlich anhand eines Regressionsmodells unter Berücksichtigung der Einflussparameter entwickelt. Letztendlich wurde das Regressionsmodell als benutzerdefinierte Variablen-Datei aufbereitet, die im FEM-Programm AutoForm implementiert werden kann.

Die DSCS-Methode wurde anhand von Außen- und Innenblechen von Karosserieteilen validiert. Die Ergebnisse der Validierung zeigten, dass der Ort des Oberflächenfehlers mittels der DSCS-Methode genau vorhergesagt werden kann. Auch kann mit der DSCS-Methode die erste Faltenbildung der jeweiligen Ziehtiefe vorhergesagt werden. Weiterhin kann durch Eingabe der kritischen Dehnwerte in die UDV-Datei die Faltenbildung in der elastischen Deformationsphase (mit kleinen effektiven Formänderungen) detektiert werden. Aufgrund der Tatsache, dass die DSCS-Methode ein spannungsbasiertes Kriterium darstellt, ist es in dieser Arbeit nicht nötig, den Einfluss von nichtlinearen Dehnpfaden zu berücksichtigen. Im weiteren Verlauf sollte, nachdem eine Validierung von ausreichend Blechwerkstoffen durchgeführt wurde, ein individuelles Modell zur Berechnung der kritischen Spannungswerte zwischen der äußeren und der inneren Seite, an definierten Stellen der Falteninitiierung und der voll ausgebildeten Falten, entwickelt werden.

1 Introduction

To reduce the time and costs for research and development, for years car body development performed by OEMs or suppliers is supported by SE (Simultaneous Engineering). Supported by simultaneous engineering method, the feasibility of all sheet metal parts of car body can be evaluated using FEM software, like AutoForm, LS-Dyna or Pam-Stamp. One of the most important duties of stamping SE-Engineering for sheet metal parts is to predict best achievable quality of the produced parts made of sheet metal or composite materials. Therefore, nowadays the criteria proposed for split detection, wrinkling formation and springback prediction play a more and more important role. Since risk of potential splits, undesired wrinkles and accurate amount of springback can be predicted in the part design phase, time and costs will be saved later in the manufacturing phase. The layout of forming stages of stamping process and part design of car body depends mainly on the precision of FEA analysis (results) in the field of sheet metal forming.

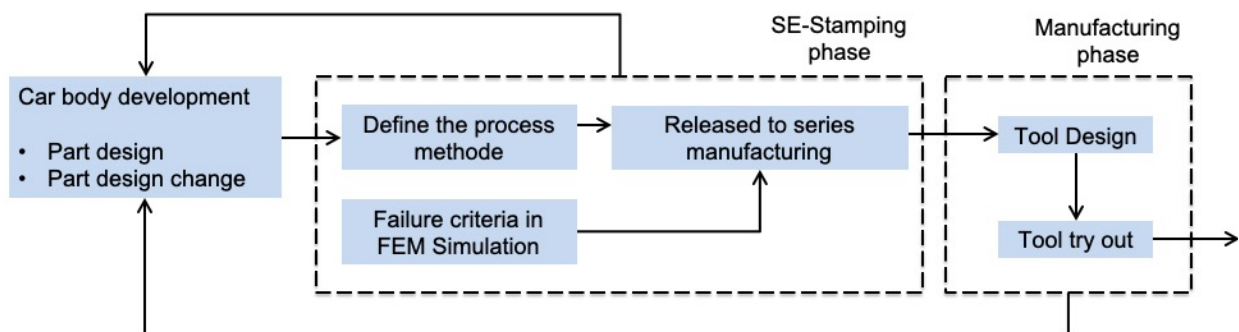


Figure 1-1: Working content of the SE-Stamping phase between car body design and tool manufacturing phase in automobile industry

Unlike splits and springback [Ran20], surface defects or distortion like wrinkles and slight waviness of exterior parts directly effect the product appearance [Pap16]. Usually, consumers have requirements for the apprerance (misspelled) of a product, and this kind of demand exits (misspelled) not only in the automotive industry, but also in appliance and consumer electronis (misspelled) industry, and so on. According to a marketing research [Mid20], in Aisa (misspelled), especially in the countrys (misspelled) like China, Korea and Japan, at the small price level the product appearance plays a more important role than product performance in whether consumers want to buy a product. Besides, consumers are more inclined to buy products manufactured with metallic parts. Thus, a robust criterion to predict surface qulity (misspelled) during the forming process of a designed exterior sheet metal part, especially desined (misspelled) with thin thikniss (misspelled) (less than 0.6 mm) is disiered (misspelled) in products and parts design phase.

In some situations, it is not enough to only predict at which drawing depth severe wrinkles will occur [Bla12], because slight surface defects may take place prior to appearance of severe wrinkles. Also, buckling phenomenon sometimes occurs at a very small strain level leading to

unacceptable surface quality. Consequently, it is important to predict the development of the surface quality of the exterior parts made from sheet metal during deep drawing process.

Unfortunately, due to lack of robust scientific tools it is difficult to predict occurring slight surface defects and surface distortions during forming operation. Most scientific works in the last 20 years have focused only on the onset of wrinkling or buckling. Less attention has been paid to the change of surface quality during the deep drawing process.

Furthermore, in the case of wrinkles, only the types of the first and second order have been intensively studied in practical applications [Bla12]. The wrinkles of the first order refer to the occurrence of wrinkles between the blank holder and die. Thus, no matter for industrial application or forming process research, usually more less attention was paid to the wrinkles of first order than the second orders, because the wrinkles of first order, which located in the deep drawing part flange, are less relevant to the surface quality of a part. This fact also indirectly explains why the wrinkles of second order are widely concerned in the field of applied research area [Bla12].

Research works for predicting second order wrinkles by using stress-based approach started from 1958. At that time, R. Hill presented a general analytical study of plastic wrinkling based on the bifurcation theory [Hil58]. Later, J.W. Hutchinson derived a bifurcation function from Hill's theory. Later the Donell-Mushtari-Vlasov (DMV) theory of plates and shells was developed, which enables the study of wrinkling effects in the plastic stage [Hut85]. Another analytical approach based on "Cao's energy method", presented by J. Cao, was used to study wrinkling behaviour in buckling tests using Yoshida Specimens and wrinkling phenomena in square cup forming [Wan00] [Yos81]. The previous studies from J.W. Hutchinson and J. Cao indicated that compressive stress values beyond a critical value could induce wrinkles of second order in the free forming region of a formed part. However, in deep drawing processes with complex geometries, it is difficult to identify the dimension of potential wrinkling areas. Based on this fact, if the deep drawn components are shaped complex, the critical value of compressive stress which be able to lead to wrinkles of second order cannot be accurately determined. Therefore, this critical value should be calculated in advance based on useful models or valid wrinkling criteria, respectively [Cao97].

Another conventional way to predict second order wrinkles is to use the strain-based approach in the forming limit diagram (FLD). In the last twenty years, many studies have been conducted to determine a strain distribution-based criterion based on the FLD [Doe98] [Li12]. However, according to experimental results, Li [Li00] indicates that no wrinkling limit curve (WLC) based on FLD can be estimated because the critical strain value for detecting "wrinkling initiation" is not a material property. Wrinkling phenomenon in sheet metal forming is complex. It is affected

by many factors such as part geometry, sheet thickness, mechanical properties of used sheet metal material, strain path and forming history, boundary conditions, etc.

Despite this, many studies still have been performed to establish strain-based approaches to predict wrinkles during and after forming process; for example, wrinkling limit curves in the FLD which is similar to the forming limit curve (FLC). Experimental works based on modified Yoshida specimens have shown that the specimen geometry affects the location of determined wrinkling limit curve in FLD. As a result, it is difficult to generate a relationship between the location of wrinkling limit curve and specimen geometries. Also, it is difficult to determine the effective dimensions of the compressive region in sheet metal specimen objectively.

In this work, the wrinkling behaviour during deep drawing and stretch forming processes was investigated. Based on this investigation, the new time-dependent, stress-based criterion “Double-Surface-Compressive-Stress-Approach” (DSCS-approach) was introduced and validated with forming parts. First of all, the DSCS-approach was tested by using mini conical cup test. Furthermore, this new approach was prepared as UDV files that can be implemented in FEM Software to predict the onset of wrinkles of exterior and interior parts regarding industrial application.

In Chapter 2, basic concepts on characterisation and test methods of sheet metal materials were firstly reviewed. Then the basic concepts on deep drawing process and test procedures for gaining the FLC for sheet metal materials were also introduced. Finally, conventional wrinkling criteria used in industry were discussed. In conclusion, an effective approach to predict slight surface defects or wrinkles for the usage regarding real exterior parts should be investigated, because the nowadays applied criteria regarding prediction of surface quality are not effective.

In Chapter 3, the main objective and five tasks of this work were introduced to realise the application of DSCS-approach in practical applications.

In Chapter 4, the motivation to develop a new wrinkling criterion was first reviewed. In the second part of Chapter 4, a simplified model was proposed based on the development of compressive stress on the outer side of sheet metal component for predicting wrinkles of the second order.

In Chapter 5, the simplified model proposed in Chapter 4 was continued to develop further to a “specific concept” in order to predict surface defects and wrinkles considering the tool contact of instantaneous workpiece shape. Here the concept of DSCS-approach was firstly introduced. According to the results in Chapters 4 and 5, the entire wrinkling process can be sub-divided into three different time stages during formation of wrinkles to evaluate the change in surface quality of investigated drawn part.

In Chapter 6, regression models which will be used in FEA were established by using concept of DSCS-approach. The regression models introduced in Chapter 6 were determined by considering essential factors like sheet thickness and local curvature of wrinkling area. In Chapter 7, corresponding simulative investigations were carried out and the results of buckling test performed with modified Yoshida specimen and mini-conical-cup test are presented as reference simulations. The FEA results showed that tendency of the development of both outer and inner surface stress value emerge in good agreement compared to results of the analysis in Chapters 4 and 5.

Finally, in Chapter 8, the proposed DSCS-approach was validated additionally by analyzing further deep drawing processes of three real car body parts: a Door-Frame-Adapter, a C-Pillar-Reinforcement and a Side-Low-Outer. The results showed that the AutoForm used in strain-based wrinkling criterion – “potential wrinkles”, are not sensitive to slight wrinkles when evaluating complex deep drawing components. The wrinkles and surface defects can be predicted and detected more accurately by using DSCS-approach than by using strain-based “potential wrinkles” approach.

In conclusion, the developed DSCS-approach aims to enhance the accuracy of used the FEA for industrial application. First of all, by using the DSCS-approach the location of the surface defects which take place during the forming process on a sheet metal part was able to be predicted better than conventional wrinkling criteria. Furthermore, by using DSCS-approach a pre-defined critical wrinkling height can be used as criterion to predict surface quality of a formed sheet metal part. Thus, with the help of the new developed approach the surface quality of a designed part can be predicted more accurately in the product design stage.

However, the plastic and elastic wrinkles can not be freely defined by using DSCS-approach. To distinguish plastic and elastic wrinkles, a critical strain level should be pre-defined in DSCS-approach. This kind of critical strain level can only be determined by performing M-YBT tests.

In the future, the DSCS-approach should be tested and validated by using more different commercial softwares. Until now, this new approach was validated by using AutoForm software. In order to adapt to more software codes, the logic of the developed DSCS-approach will become more complete and the applicability will become broader.

2 State of the art

As discussed before, the importance of FEA in metal forming technology of automobile industry has been continuously increasing. Also, it is well known that the accuracy of FEA mainly depends on the numerical simulation of the metal forming process and the modelling of the material behavior of the used sheet metal material [Bru14]. Therefore, information and basic concepts about material behavior, standard material test procedures were firstly reviewed in Chapter 2. Chapter 2.1 starts with a discussion of available contributions in the yield locus. The concept of flow rules, effective strain/stress and hardening behavior is also introduced in Chapter 2.1. In the last part of Chapter 2.1, the standard material test procedures and common failure types are discussed. In Chapter 2.2, standard tests in the laboratory to investigate wrinkling formation, such as buckling tests, conical cup test and tests with car-fender shaped geometry, are reviewed additionally. Finally, in Chapter 2.3, relevant acknowledgements and information related to conventional wrinkling criteria, namely strain-based and stress-based wrinkling criteria, were presented.

2.1 Sheet metal material properties and material testing

The numerical simulation of a sheet metal forming process requires the implementation of material models to characterise the flow behaviour of the sheet material. An accurate description of a sheet metal material requires the following three pieces of information [Bru14], yield criterion (see Chapter 2.1.1), flow rule (see Chapter 2.1.2), and hardening rule (see Chapter 2.1.3). Together with anisotropy values, the sheet metal material failure, which are usually presented as forming limit curve (FLC) and fracture forming limit curve (FFLC), see Chapter 2.1.4, can be defined.

2.1.1 Yield locus modelling

The yield locus models do define the condition for the elastic/plastic behavior limit under multi-axial states of stress. After reaching the yield locus, the material continues to be deformed plastically until it fails. In case of plastic deformation, the formed material shows the hardening behavior. Starting with the pioneering contributions of von Mises (1928) and R. Hill (1948), many anisotropic yield criteria have been introduced. Especially in the past 20 years, with the extension of the application of FEA in sheet metal forming industry, the trend of proposing advanced yield functions has been greatly increased. In addition to the Hill yield criteria, there is a model of isotropic formulation based on Hershey. Hosford “rediscovered” Hershey’s model in 1972 and used it for the development of an anisotropic yield criterion. Barlat et al. and Banabic et al. [Ban10], as well as some other researchers, proposed further extensions of the model. The most commonly used yield locus models in industrial application are based solely on uniaxial or equibiaxial tests, namely BBC 2005, Barlat-2000-2d and Barlat-1989 yield criterion.

Tresca and von Mises Yield Criterion

The first yield criterion was proposed by Tresca in 1864 based on the fact that plastic strain appears by crystallographic gliding undergoing shear stresses. According to this observation from Tresca, it can be assumed that metal materials can change the forming state from elastic to plastic state when the maximum shear stress τ_{max} reaches a critical level. The general Tresca yield criterion can be formed in Equation 2.1, where σ_{11} , σ_{22} and σ_{33} are principal stresses:

$$\max\{|\sigma_{11} - \sigma_{22}|, |\sigma_{22} - \sigma_{33}|, |\sigma_{33} - \sigma_{11}|\} = \sigma_Y \quad (2.1)$$

Later Huber and von Mises developed a yield criterion based on the observation that a hydrostatic pressure does not influence the yielding of a metal material. As a result of that, Huber and von Mises proposed that only the elastic energy distortion do influences the transition from an elastic state to plastic state. The yield criterion now refers to the von Mises criterion, which can be written in the following Equation 2.2 by considering results gained by uniaxial tensile test. For plane stress state, Equation 2.2 represents an ellipse in the coordinate plane of the principal stress, which is circumscribed to the Tresca criterion (polygon standard).

$$(\sigma_{11} - \sigma_{22})^2 + (\sigma_{22} - \sigma_{33})^2 + (\sigma_{33} - \sigma_{11})^2 = 2\sigma_Y^2 \quad (2.2)$$

Hill developed a quadratic yield criterion for anisotropic materials in 1948 [Hil48]. The material should have the anisotropy of three orthogonal symmetric planes. The yield criterion is represented by a quadratic function of the following types in Equation 2.3:

$$2f(\sigma_{ij}) = Q^Y(\sigma_{22} - \sigma_{33})^2 + G^Y(\sigma_{33} - \sigma_{11})^2 + H^Y(\sigma_{11} - \sigma_{22})^2 + 2L^Y\sigma_{23}^2 + 2M^Y\sigma_{31}^2 + 2N^Y\sigma_{12}^2 = 1 \quad (2.3)$$

Here $f(\sigma_{ij})$ is the yield function. Q^Y , G^Y , H^Y , L^Y , M^Y , and N^Y are constants specific to the anisotropy state of the material. The numbers “1”, “2” and “3” indicate the principal anisotropic direction. In the case of sheet metal materials, “direction 1” usually stands for the rolling direction, “direction 2” is parallel to the transverse direction, and the “direction 3” is defined as the normal direction of the sheet thickness.

Through the modelling of anisotropic materials, the Hill 1948 yield criterion reveals the advantages of easy to understand equations from 2.4 to 2.5. The parameters being included in the yield function do have a direct physical meaning. This leads to the wide application of Hill 1948 yield function in industrial practice. The material parameters of Hill 1948 are determined only using anisotropy values ($R_{an.}$) along 0° (R_{00}), 45° (R_{45}) and 90° (R_{90}) to the rolling direction [San13]. The desired $R_{an.}$ Values and yield stress values can be obtained by performing standard tensile tests using specimens in different rolling directions.

$$G^Y = \frac{1}{1 + R_{00}} \quad (2.4-a)$$

$$H^Y = \frac{R_{00}}{1 + R_{00}} \quad (2.4-b)$$

$$Q^Y = \frac{R_{00}}{R_{90}(1 + R_{00})} \quad (2.4-c)$$

$$N^Y = (R_{45} + 0.5) \left(\frac{1}{R_{00}} + \frac{1}{R_{90}} \right) H^Y \quad (2.4-d)$$

Under plane stress conditions ($\sigma_{33} = \sigma_{23} = \sigma_{13} = 0$), according to Equations 2.3 and 2.4, the Hill 1948 yield criterion can be expressed as:

$$\sigma_{11}^2 - \frac{2R_{00}}{1 + R_{00}} \sigma_{11}\sigma_{22} + \frac{R_{00}(1 + R_{90})}{R_{90}(1 + R_{00})} \sigma_{22}^2 + \frac{R_{00} + R_{90}}{R_{90}(1 + R_{00})} (2R_{45} + 1) \sigma_{12}^2 = \sigma_Y^2 \quad (2.5)$$

Barlat 1989 Yield Criterion

By generalising the Hosford isotropic criterion (see Equation 2.6), F. Barlat introduced a new criterion, described in Equation 2.7, together with Richmond [Bar87].

$$Q^Y |\sigma_{22} - \sigma_{33}|^a + G^Y |\sigma_{33} - \sigma_{11}|^a + H^Y |\sigma_{11} - \sigma_{22}|^a = 2\sigma_Y^a \quad (2.6)$$

$$f = |\gamma_1 + \gamma_2|^M + |\gamma_1 - \gamma_2|^M + |2\gamma_2|^M = 2\sigma_Y^M \quad (2.7)$$

Here γ_1 and γ_2 are invariants of the stress tensor while M indicates an integer exponent, which has the same significance as the “exponent a ” used by Hosford in Equation 2.6. Parameters γ_1 and γ_2 can be obtained from Equation 2.8:

$$\gamma_1 = \frac{\sigma_{11} + \sigma_{22}}{2} \quad (2.8)$$

$$\gamma_2 = \sqrt{\left(\frac{\sigma_{11} - \sigma_{22}}{2}\right)^2 + \sigma_{12}^2}$$

In 1989, Barlat and Lian published the general equations regarding metallic materials with planar anisotropic behavior by introducing the following yield functions. For face-centered cubic (FCC) materials, M = 8 is recommended and for body-centered cubic (BCC) materials, M can usually be defined as 6 [Lsd12].

$$f = a|\gamma_1 + \gamma_2|^M + a|\gamma_1 - \gamma_2|^M + c|2\gamma_2|^M = 2\sigma_Y^M \quad (2.9)$$

The coefficients k_1 and k_2 can be obtained by:

$$k_1 = \frac{\sigma_{11} + h\sigma_{22}}{2} \quad (2.10)$$

$$k_2 = \sqrt{\left(\frac{\sigma_{11} - h\sigma_{22}}{2}\right)^2 + p^2\sigma_{12}^2}$$

Considering this, there are two ways to calculate anisotropic material constants “ a ”, “ c ”, “ h ” and “ p ”. Firstly, material constants “ a ”, “ c ”, “ h ” and “ p ” values can be identified by the following equation published by D. Banabic [Ban10]:

$$a = 2 - c = \frac{2 \left(\frac{\sigma_Y}{\sigma_{22}} \right)^M - 2 \left(1 + \frac{\sigma_Y}{\sigma_{90}} \right)^M}{1 + \left(\frac{\sigma_Y}{\sigma_{90}} \right)^M - \left(1 + \frac{\sigma_Y}{\sigma_{90}} \right)^M} \quad (2.11)$$

$$h = \frac{\sigma_Y}{\sigma_{90}}$$

$$p = \frac{\sigma_Y}{\sigma_{12}} \left(\frac{2}{2a + 2^M c} \right)^{\frac{1}{M}}$$

In the second way, these four constants can be calculated by Equation 2.11 directly through anisotropy values R_{00} , R_{45} and R_{90} by considering $c = 2 - a$. The p -value can be calculated using the form in Equation 2.10.

$$a = 2 - c = 2 - 2 \sqrt{\frac{R_{00}}{1 + R_{00}} \frac{1 + R_{90}}{R_{90}}} \quad (2.12)$$

$$h = \sqrt{\frac{R_{00}}{1 + R_{00}} \frac{1 + R_{90}}{R_{90}}}$$

2.1.2 Flow rules, flow curve, effective strain and stress

Conventional flow rules in the plastic stage

In elastic deformation, the relevant strain value can be determined by Hooke's law. However, in the plastic phase, the so-called "flow rule" is used to determine the strain in the following form:

$$d\varepsilon_{ij} = d\lambda \left(\frac{\partial f}{\partial \sigma_{ij}} \right) \quad (2.13)$$

Where f is the function of σ_{ij} that describes yielding criterion. Usually, f can be defined by the name "plastic potential". For example, strain values in third direction can be determined by using von Mises criterion reviewed in Chapter 2.1.1:

$$\begin{aligned} d\varepsilon_1 &= d\lambda \left[\sigma_1 - \left(\frac{1}{2} \right) (\sigma_2 + \sigma_3) \right] \\ d\varepsilon_2 &= d\lambda \left[\sigma_2 - \left(\frac{1}{2} \right) (\sigma_3 + \sigma_1) \right] \\ d\varepsilon_3 &= d\lambda \left[\sigma_3 - \left(\frac{1}{2} \right) (\sigma_1 + \sigma_2) \right] \end{aligned} \quad \text{with } d\lambda = d\bar{\varepsilon}/\bar{\sigma} \quad (2.14)$$

The expression of $d\lambda$ is shown in the Equation 2.14. It becomes obviously, that $d\lambda$ is a material behavior that is dependent on the $\bar{\sigma} - \bar{\varepsilon}$ curve. Usually, the $\bar{\sigma} - \bar{\varepsilon}$ curve will be determined by experiments and is defined as "hardening curve" which was widely used in FEA to calculate the amount of effective strain when applying effective stress. The von Mises effective strain and stress can be simply expressed when considering $\sigma_1 > \sigma_2 > \sigma_3$:

$$d\bar{\varepsilon} = \sqrt{\left(\frac{2}{3} \right) (d\varepsilon_1^2 + d\varepsilon_2^2 + d\varepsilon_3^2)} \quad (2.15)$$

Assuming that straining is proportional to a constant ratio of $d\varepsilon_1 : d\varepsilon_2 : d\varepsilon_3$, the total effective strain can be written as:

$$\bar{\varepsilon} = \sqrt{\left(\frac{2}{3}\right) (\varepsilon_1^2 + \varepsilon_2^2 + \varepsilon_3^2)} \tag{2.16}$$

Taking into account the von Mises yield criterion, the critical value of the effective stress can be expressed as:

$$\bar{\sigma} = (\sqrt{1 - \alpha + \alpha^2})\sigma_1 \quad (\text{with } \alpha = \frac{\sigma_2}{\sigma_1}, \sigma_3 = 0) \tag{2.17-a}$$

$$\frac{d\varepsilon_1}{2 - \alpha} = \frac{d\varepsilon_2}{2\alpha - 1} = \frac{d\varepsilon_3}{-(\alpha + 1)} \tag{2.17-b}$$

$$\alpha = \frac{2\beta + 1}{2 + \beta} \quad \beta = \frac{2\alpha - 1}{2 - \alpha} \tag{2.17-c}$$

In the principal stress space, it can be understood as an ellipse graphics presented in Figure 1-1. Flow rule means that which strains will be associated with the stress state when the element deforms. According to Levy-mises flow rule, deviatoric stresses will be important when a yield locus develops with shape change. Furthermore, the ratio of the strain increments will be the same as the ratio of the deviatoric stresses. This relationship is expressed in Equation 2-17-b. The relationship between stress and strain can be understood as formular. If an element deforms under a given stress state (α), and the ratio of the strain can be calculated according to Equation 2-17-c

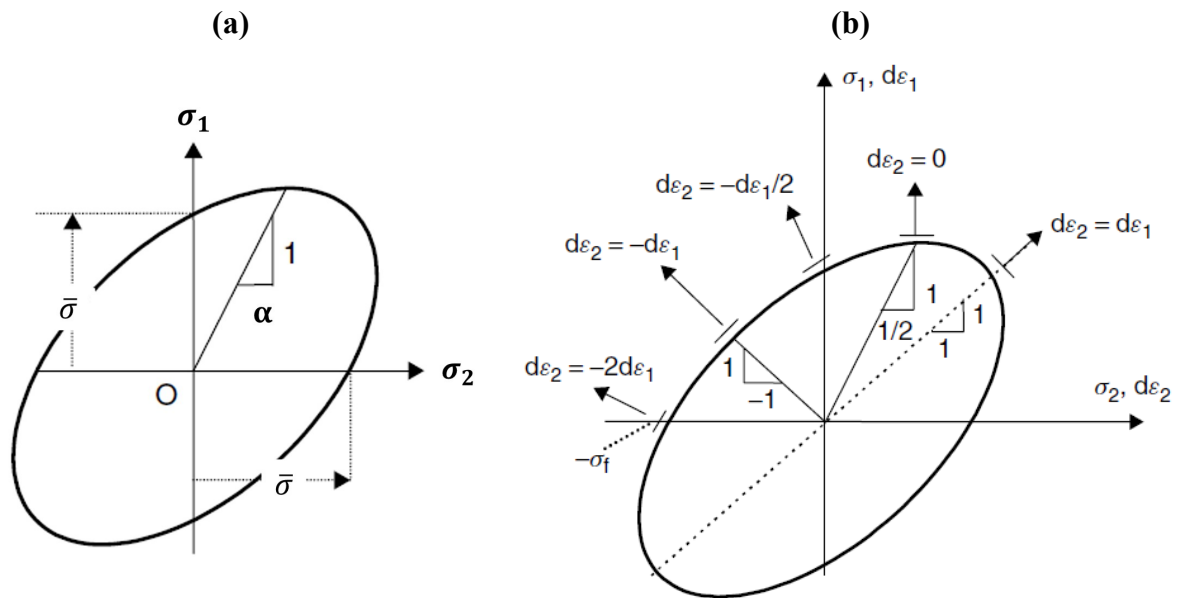


Figure 2-1: (a) Yield locus for plane stress refer to von Mises yield condition; (b) Diagram presenting the strain increment components regarding different stress states, around von Mises yield Locus

2.1.3 Hardening curve – experimental procedure and its characterisation

In the first part of Chapter 2.1.3, determination of hardening curve ($\bar{\sigma} - \bar{\epsilon}$ curve) based on standardised uniaxial tensile test was presented. In the second part of this chapter, the method to determine hardening curve ($\bar{\sigma} - \bar{\epsilon}$ curve) by using bulge test under biaxial stress state is also introduced. Finally, hardening models and methods to fit hardening curve ($\bar{\sigma} - \bar{\epsilon}$ curve) are explained. Furthermore, details regarding determination of “hardening coefficient” n by using tensile test were reviewed.

Approaches to determine true stress – true strain curves based on uniaxial tensile test results

The uniaxial tensile test is a standardized, widely used approach to determine material properties. Not only metal materials, but also plastic and composite materials can be tested by using tensile test according to ISO 527-1 [ISO12]. In this work, testing approaches applied regarding sheet metal materials are based on ISO-16808 [ISO14]. By using uniaxial tensile test, the following essential mechanical properties of tested materials can be directly determined, like yield strength $R_{p0.2}$ and tensile strength R_m , uniform and total elongation, as well as Lankford’s anisotropy coefficients R_{an} . Required hardening curve ($\bar{\sigma} - \bar{\epsilon}$ curve) only can be determined by using uniaxial tensile test, when the following three steps described in Table 2-1 will be performed. Moreover, strain hardening index “ n ” can also be calculated directly from the determined hardening curve ($\bar{\sigma} - \bar{\epsilon}$ curve).

Table 2-1: Three steps to determine true stress – true strain curve based on uniaxial tensile test

Step 1: The Force-extension diagram	Obtained directly from the tensile test
Step 2: The engineering stress-strain curve	Based on initial cross-sectional area of specimen
Step 3: The true stress-strain curve	Based on actual cross-sectional area of specimen

First of all, through the tensile test, a load – extension curve can be directly obtained from the test results. By defining an initial cross-sectional area, $A_0 = w_0 * t_0$, the engineering stress-strain curve can be obtained by Equation 2.18, where w_0 is the initial width and t_0 is the initial thickness of the cross-section area of specimen.

$$\sigma_{eng.} = \frac{F}{A_0} \quad (2.18-a)$$

$$\epsilon_{eng.} = \frac{\Delta l}{l_0} \times 100\% \quad (2.18-b)$$

However, the engineering stress-strain curve is rarely used for the analysis of sheet metal forming processes, as the curve is based only on the initial cross section of the studied tensile specimen, rather than on the reduced current area (A) during the test. The hardening curve ($\bar{\sigma} - \bar{\epsilon}$ curve) based on the instantaneous value of the cross-sectional area was calculated in Equations 2.19-a/b:

$$\bar{\varepsilon} = \int d\varepsilon = \int_{l_0}^l \frac{dl}{l} = \ln \frac{l}{l_0} \quad (2.19-a)$$

$$\bar{\sigma} = \frac{F}{A} = \frac{F}{A_0} \frac{A_0}{A} = \sigma_{eng.} \frac{l}{l_0} = \sigma_{eng.} \left(1 + \frac{\varepsilon_{eng.}}{100}\right) \quad (2.19-b)$$

Approaches to determining hardening curve based on bulge test

The standard approach to calculate the $\bar{\sigma} - \bar{\varepsilon}$ curve based on a bulge test is defined by ISO 16808 [Iso14]. In this ISO-standard test, a circular sheet specimen is clamped along its circumference and deformed in a dome shape by hydraulic pressure. The set-up of bulge test is shown in Fig. 2-2. The diameter of the die cavity (d_c) and the die radius (R_c) refer to the constant parameters, whereas the dome height (h_d), the pressure (p), the dome apex thickness (t_d) and the curvature radius R_d measured during the experiments belong to the instantaneous variables.

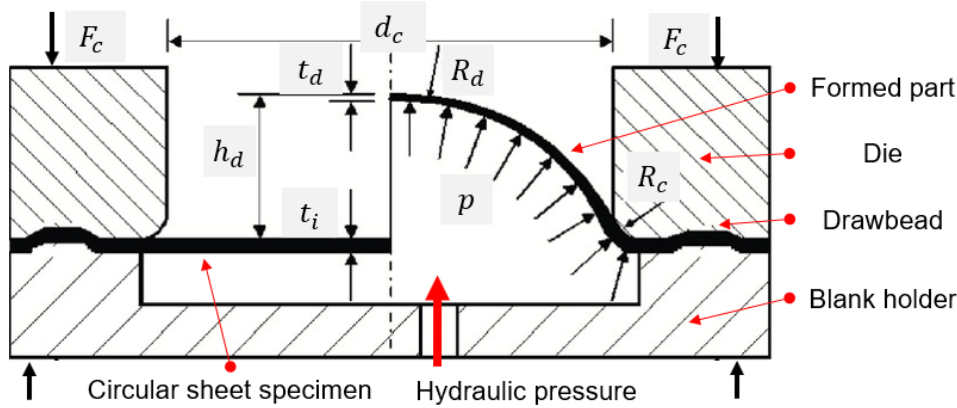


Figure 2-2: Schematic diagram regarding bulge test

The magnitude of effective strain and effective stress can be calculated concerning the geometry changes of specimen measured in the experiments by using ARAMIS measuring system. Assuming an isotropic material behavior during the hydraulic bulge process, the equi-biaxial flow stress ($\bar{\sigma}_b$) at the dome apex of the formed specimen can be obtained from the following Equation 2.20-a. Regarding constant volume theory, the effective strain ($\bar{\varepsilon}_b$) at the dome apex of the formed specimen is derived as in Equation 2.20-b.

$$\bar{\sigma}_b = \frac{p}{2} \left(\frac{R_d}{t_d} + 1 \right) \quad (2.20-a)$$

$$\bar{\varepsilon}_b = -\varepsilon_t \ln \left(\frac{t_0}{t_d} \right) \quad (2.20-b)$$

Approaches to characterise hardening curve ($\bar{\sigma} - \bar{\varepsilon}$ curve) based on phenomenological models

In order to apply hardening curve to predict plastic behaviour of metallic materials in FEA, the determined hardening curve should be firstly characterised using phenomenological models. Hollomon's power law, Ludwig's power law and Swift's power law are the most used phenomenological models in FEA in the industry.

Hollomon's power law is presented in Equation. 2.21-a, where $\bar{\sigma}$ and $\bar{\varepsilon}$ indicate the true stress and true strain, respectively. K_H and n_H indicate material strength coefficient and work hardening exponent of Hollomon's power law. K_H and n_H can be determined from the slope and interception of an $\ln \bar{\sigma} - \ln \bar{\varepsilon}$ plot (see Equation. 2.21-b).

$$\bar{\sigma} = K_H \bar{\varepsilon}^{n_H} \quad (2.21-a)$$

$$\ln \bar{\sigma} = \ln(K_H) + n_H \ln(\bar{\varepsilon}) \rightarrow n_H = \frac{\ln \bar{\sigma}}{\ln \bar{\varepsilon}} \quad (2.21-b)$$

Ludwig's power law is presented in Equation 2.22-a, where $\bar{\sigma}$ and $\bar{\varepsilon}$ indicate the true stress and true strain, respectively. K_L and n_L indicate material strength coefficient and work hardening exponent of Ludwig's power law. Compared to Hollomon's power law, the work hardening exponent of Ludwig's law is mainly analysed using "differential Crussard-Jaoul (C-J) method" [Bol14]. The logarithmic form of Ludwig law's power after differentiation with respect to effective strain $\bar{\varepsilon}$ is shown in Equation 2.22-b. In a $\ln \left(\frac{d\bar{\sigma}}{d\bar{\varepsilon}} \right) - \ln \bar{\varepsilon}$ plot, the slope can be calculated by using the value $(n_L^{C-J} - 1)$, while the intersection of slope can be calculated by using the value $\ln(K_L^{C-J} n_L^{C-J})$. In this way, the parameters n_L , K_L and σ_Y can be determined.

$$\bar{\sigma} = \sigma_Y + K_L \bar{\varepsilon}^{n_L} \quad (2.22-a)$$

$$\ln \left(\frac{d\bar{\sigma}}{d\bar{\varepsilon}} \right) = \ln(K_L^{C-J} n_L^{C-J}) + (n_L^{C-J} - 1) \ln \bar{\varepsilon} \rightarrow n_L = n_L^{C-J} - 1 \quad (2.22-b)$$

Swift's power law is presented in Equation. 2.23, which is especially suitable for predicting effective stress-strain relationship at large deformations. Scientific works figured out that the results from Swift's power law are really close to reality. The determination of work hardening exponent regarding Swift's power law is not shown here.

$$\bar{\sigma} = K_S (\varepsilon_0 + \bar{\varepsilon})^{n_S} \quad (2.23)$$

2.1.4 Elastic and plastic deformation stage defined in uniaxial tensile test

To better understand the meaning of elastic and plastic deformation regarding metal forming process, the determined force-displacement curve and the calculated true stress – true strain curve based on material HC340LA with thickness 1.0 mm are shown as example in Fig. 2-3-a and Fig. 3-2-c, respectively. According to the force-displacement curve characterised by software and control of tensile test machine, the entire forming process can be normally divided into three stages: "elastic stage", "uniform plastic stage" and "non-uniform plastic stage", see Fig. 2-3-a.

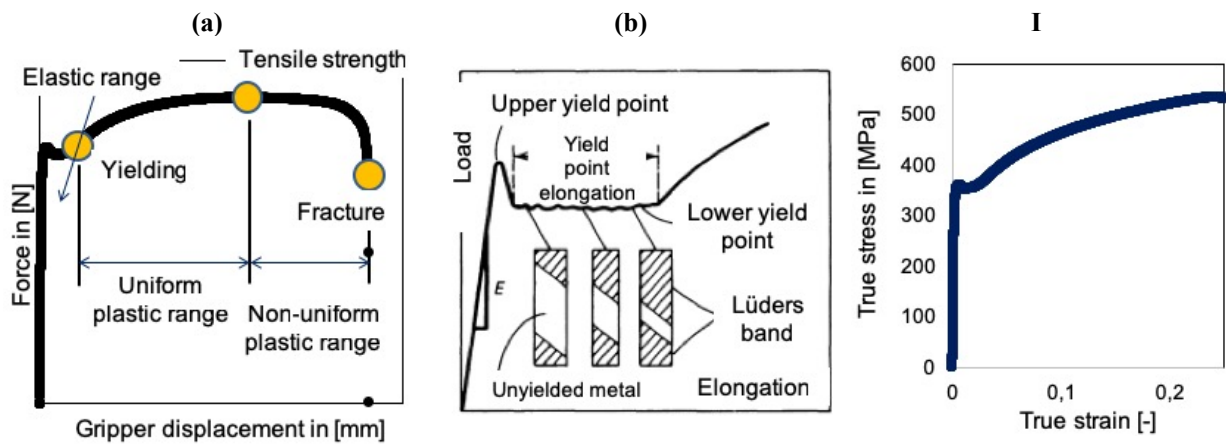


Figure 2-3: (a) Force-displacement curve based on tested material HC340LA (thickness 1.0 mm) with definition of “yielding”, “tensile strength” and “fracture”, (b) illustrated “Yield point elongation“ with definition of upper/lower yield points of typical low-carbon steel [Dav04], (c) true stress – true strain curve based on tested material HC340LA with thickness of 1.0 mm calculated from force displacement curve presented in Fig. 2-3-a

Elastic deformation stage (from beginning of the test until “yielding point”)

First, in the elastic deformation stage, the tensile force is proportional to the elongation. Elastic deformation is recovered when the applied tensile force is removed at this stage. At higher force, it can be observed that plastic deformation occurs when the applied force is higher than the “yielding point” defined in Figure 2-3-a. Compared to elastic deformation, it can be observed that plastic deformation is not recoverable.

Uniform plastic deformation stage (from “yielding point” to “instability” under uniaxial tension stress state)

(a) *Definition of “yielding” based on curve with phenomenon “yield point elongation”*

The typical “yield point elongation” (YPE) phenomenon is depicted in Fig. 2-3-b. It can be observed that, the determined force increases steadily with strain in elastic stage. And then the force drops suddenly after arriving at a critical value which is defined as “upper yield strength point” (UYS). The determined force fluctuates until to the “lower yield strength point” (LYS). After “LYS”, the force rises again as the strain increases.

Typically, the elongation that occurs under “constant force” is called “yield point elongation” as illustrated in Fig. 2-3-b [Dav04]. The deformation that occurs during the elongation of the entire yield point is uneven. However, in DIN EN 10002-1:2001, four types of “force development between UYS and LYS” have been classified. The type depicted in Figures 2-3-a and 2-3-c belongs to the “type C” [DIN01].

At UYS points, discrete deformed metals that are usually easy to see come out of the present stress concentration, this phenomenon is called “Lüders Band”. In line with the formation of the “Lüders

Band”, force falls to LYS. It is then transmitted along the length of the specimen, resulting in the elongation of the yield point. After the phenomenon of “Lüders band”, the force increases itself with strain, which can be described by the “strain hardening phase”. This phenomenon is described in the next section.

(b) Definition of “yielding” based on curve without phenomenon “yield point elongation”

According to J.R. Davis, the critical value of stress measured at “yielding point” depends on the sensitivity of measurement device in tensile machine. Furthermore, ductile metal materials show mainly a “gradual transition”, which is defined as the area between the presented black line and black dotted line in Fig. 2-4-a, from elastic to plastic deformation stage. Thus, “yielding point” is more difficult to be defined with precision in this case.

Normally, three approaches have been explained to define “yielding point” in tensile test, namely, “elastic limit” approach, “proportional limit” approach (see Fig. 2-4-a) [Roy01] and “offset yield strength” (OYS) approach. Nowadays, “offset yield strength” approach is widely used in practice, since by using this robust approach, the disadvantages of “elastic limit” approach and “proportional limit” approach can be overcome [Dav04]. The principle of “offset yield strength” approach is illustrated in Fig. 2-4-a by constructing a dotted straight line which is parallel to the “initial linear portion” in elastic stage with offset by true strain value $\bar{\epsilon}$ equal to 0.002 (or 0.2%) (see OYS line), an “intersection point” can be determined between OYS line and $\bar{\sigma} - \bar{\epsilon}$ curve. The yield strength ($R_{p0.2}$) is defined as the stress value measured at this determined “intersection point”.

(c) Definition of “tensile strength” and “tensile instability”

The tensile strength is the maximum stress that a material can withstand. The value of tensile strength can be directly determined by analysing hardening curve ($\bar{\sigma} - \bar{\epsilon}$ curve). During “the uniform plastic deformation stage”, the specimen tested with tensile machine remains evenly deformed until the maximum critical stress is reached, that is, the tensile strength of R_m . However, after the maximum critical stress is reached, the plastic deformation will localise and a undesired phenomenon of “necking” occurs. “Necking” is defined as “tensile instability” or “plastic instability” by Hosford in [Hos07]. In summary, this tensile strength R_m is also named “ultimate tensile stress” (UTS). “Onset of necking” indicates the “occurring of instability” (or defined as “onset of localised deformation”) of a tensile specimen under uniaxial tensile stress. The beginning of the necking can be found by analysing “true stress – true strain curve ($\bar{\sigma} - \bar{\epsilon}$ curve)” based on Considère criterion [Hos07]. Therefore, the beginning of tensile instability can be calculated according to Equation 2.21.

$$\frac{d\bar{\sigma}}{d\bar{\epsilon}} = \bar{\sigma} \quad (2.21)$$

Therefore, the “onset of necking” which is defined with the maximum measuring force based on the force-displacement curve, can be determined through the $\bar{\sigma} - \bar{\epsilon}$ curve by finding that the strain hardening rate equals the stress, see Fig. 2-4-b.

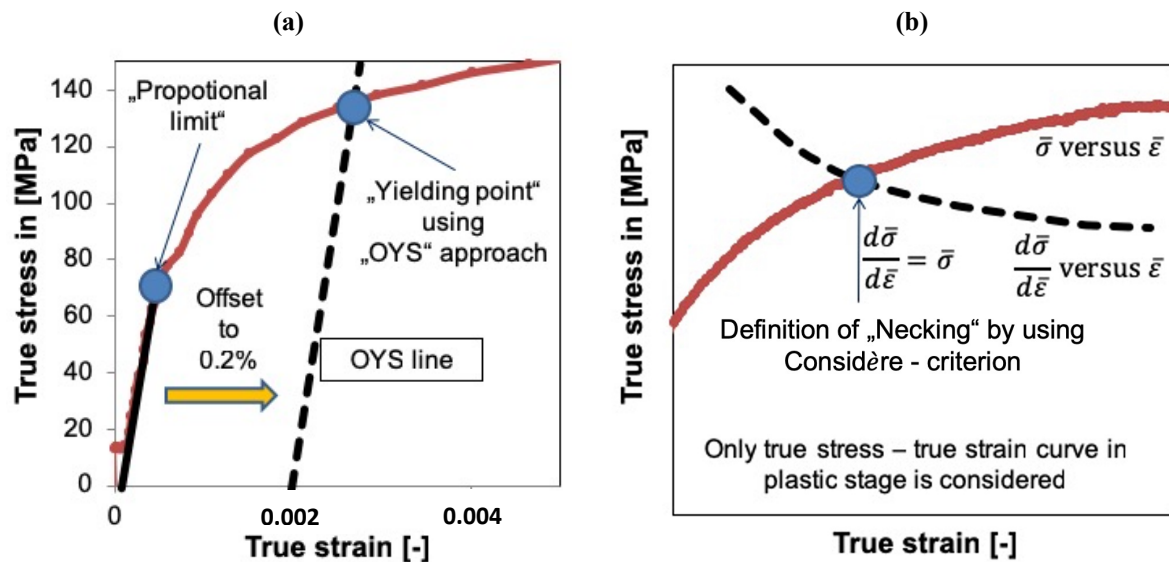


Figure 2-4: Definition of “yielding” and “necking” based on tensile test, the used true stress – true strain curve determined from material DX54D with thickness of 1.0 mm, (a) Definition of “yielding point” according to the “offset yield strength” approach, (b) Definition of “necking” according to “Considère criterion” [Hos07]

Non-uniform plastic deformation (after “necking” until to the fracture of the specimen)

During the non-uniform plastic stage, the true stress $\bar{\sigma}$ must be calculated from the measured force and current real cross-section area (A) located in the necking region. When the necking takes place, because of the material instability, the width of the middle part of the test sample begins to decrease. With continuous extension, almost all deformation is concentrated only in the necking region, and the stress state in the necking area cannot remain uniaxial plane stress anymore [Kop99].

(a) Ductile fracture observed in tensile test

The development of ductile fracture from “necking” is illustrated in Fig. 2-5 from Fig. 2-5-a to Fig. 2-5-d [Pin16]. In the case of ductile material, the “initiation of voids” is assumed to be induced by “particle-matrix decohesion” phenomenon. This phenomenon is discussed in [Ach13]. Fig. 2-5-g shows the “particle-matrix decohesion” phenomenon explained by using “inclusion particle of Al_2O_3 ” and “ferrite matrix” in [Ach13]. The existence of “inclusion particles” was also observed by Colangelo and Heiser in [Col87], see Fig. 2-5-f. They pointed out that those kinds of “inclusion particles” cannot be avoided in metallurgical process.

The phenomena of voids growth and deformation are caused by the change of stress state from two-biaxial stress state to triaxial stress state [Kop99]. The triaxial stress state in the necking region

introduces a large amount of plastic deformation, which is beneficial to the continuous growth and deformation of the cavity. There are some models to explain the “voids coalescence”, like “internal necking”, “internal shearing”, and “necklace formation”, but the real physical meaning of “void coalescence” is not clear according to [Pin16]. At last a crack is formed after the occurrence of void coalescence. A typical ductile fracture surface is shown in Fig. 2-5-h.

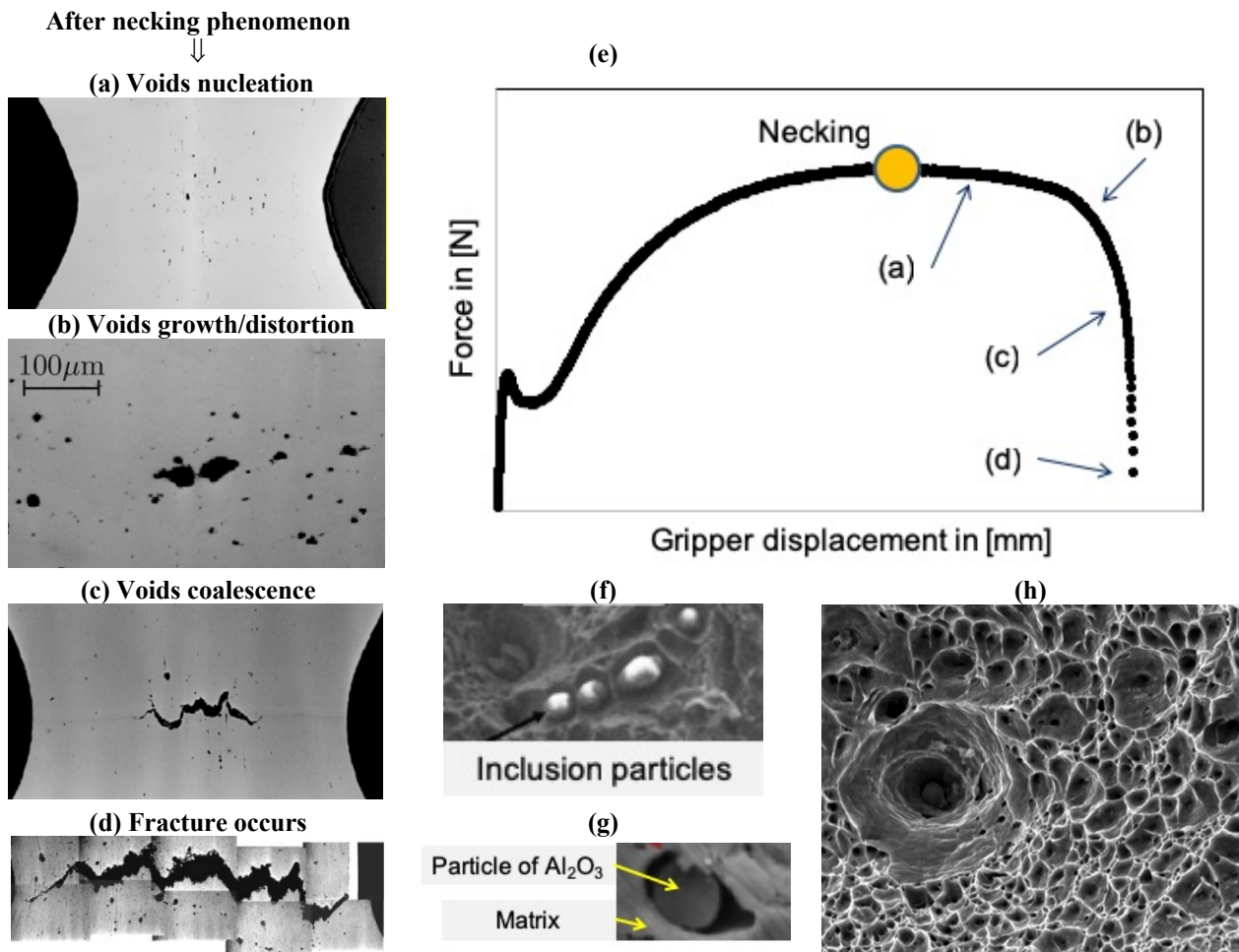


Figure 2-5: From voids nucleation to ductile fracture, (a) Photo of “voids nucleation” in [Ben04]; (b) Photo of “voids growth and voids distortion” in [Ben04]; (c) Photo of “voids coalescence” in [Ben04]; (d) Photo of “fracture of the specimen” in [Pin16]; I Schematic diagram of the force-displacement curve which corresponds to the observed phenomena from Fig. 2-5-a to 2-5-d; (f) Observed “inclusion particles” in [Col87]; (g) The “particle-matrix decohesion” phenomenon explained by using Al_2O_3 particle and ferrite matrix in [Ach13]. (h) Typical damaged ductile surface in [Pin16].

(b) Brittle fracture observed in tensile test

W.T. Becker reported a relationship between specimen having geometry with “notch tip radius” and yield strength [Bec02]. The experiments performed by Becker (named with “surface cracks”) are comparable with Griffith crack model (named with “internal cracks”) [And95].

In the situation of “surface cracks”, the “beginning of fracture” performed using tensile test, marked with yellow circles in Fig.2-6-a, depends on the “section thickness”, “crack length” and

“notch tip radius”. All these three factors were concluded by Becker as “constraint”. When the “section thickness” and “crack length” increases, the determined yield strength, marked with blue circles in Fig. 2-6-a, is increased. Meanwhile, the total tensile elongation at fracture is reduced. When a specimen having small enough notch tip radius was tested, the fracture occurs before reaching yield strength. To explain brittle fracture at both situations, surface flaw (see Fig. 2-6-b), internal flaw and also the principle of “flaws induced stress concentration” (see Fig. 2-6-c) are introduced. “Flaw” is defined here as micro cracks. When propagation of cracks is along the grain boundaries, type “intergranular brittle fracture” takes place, see Fig. 2-6-e. Besides, in the type “transgranular brittle fracture”, the cracks transcend from one grain to another grain.

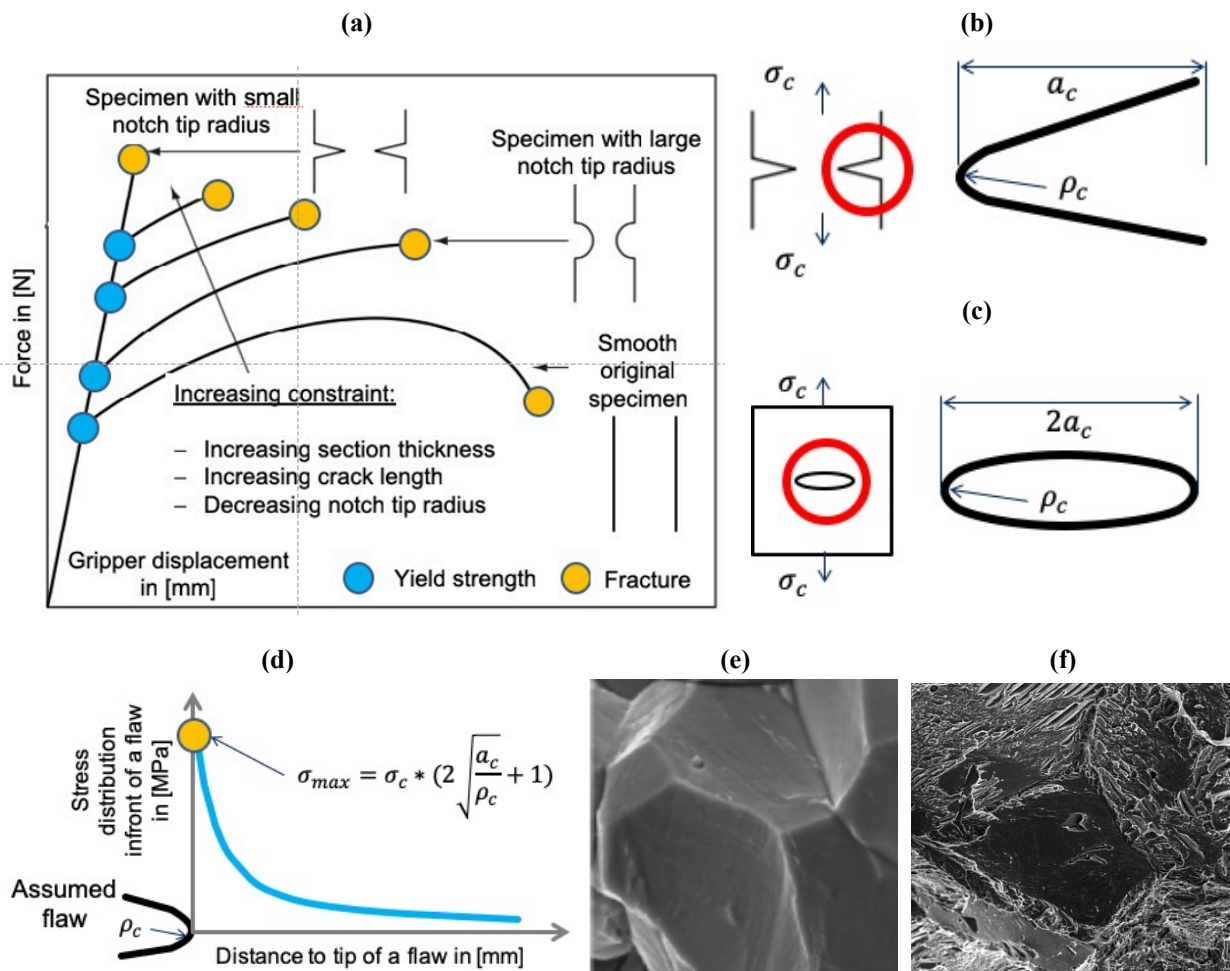


Figure 2-6: Schematic regarding brittle fracture, (a) Influence of the notch tip radius on fracture and yield strength determined from tensile test in [Bec02], (b) “surface flaw” introduced by Becker with definition of crack length and local curvature of assumed flaw; (c) “internal flaw” supposed by Griffith with definition of crack length and local curvature of assumed flaw; (d) Schematic of stress distribution in front of a flaw corresponding to distance to the tip of a flaw; I SEM micrograph regarding intergranular damaged brittle surface in [Hoj17]; (f) SEM micrograph regarding mixed trans- and intergranular damaged brittle surface in [Pok10]

2.1.5 Types of failure in the deep drawing process

Type of failure 1: Necking and fractures

Cracks and splits are the most important type of failure regarding the formed parts. If those failures are detected after manufacturing, the formed parts (no matter the structure parts or outer skin parts) cannot be used any more. Due to this reason, the necking and fracture phenomena were intensively investigated in the last 20 years to prevent or predict failures based on FEA. According to results, three kinds of fracture curves can be defined (under different loading conditions) and depicted in Fig. 2-7 [Isi14]. The conventional FLC curve represents the limit of necking from the biaxial strain state ($\varepsilon_1/\varepsilon_2 = 1$) to the uniaxial strain state ($\varepsilon_1/\varepsilon_2 = -2$). The transition from the FLC curve to the crack curve (Case 2, FFL) indicates the transition from necking to fracture. SFFL (Fracture line Case 3) is determined by planar-shear test, and the planar shear test can predict the fracture regarding strain path from $\varepsilon_1/\varepsilon_2 = -2$ to $\varepsilon_1/\varepsilon_2 = -1/2$. Furthermore, in order to investigate forming limit under different forming conditions, Marciniak, Duncan and Hu proposed a concept of “forming window for plane stress” considering necking, fracture and wrinkling in 2002 [Mar02]. Since FLC curve can be conveniently determined and implemented in commercial FEM-software to predict failures of formed parts, until today, the forming limit curve (FLC) in FLD can still be seen as the most popular criterion to predict forming failure in the industry [Vol11]. Nowadays, this approach is standardised by ISO 12004 which recognises the localised necking (under different loading conditions) as forming limit [Iso08]. However, some of the drawbacks regarding FLC curve limits its application for predicting failures in the deep-drawn parts suffered from complex loading conditions. The most well-known disadvantage refers to the influence of “non-linear strain path”, which is caused by forming history, on the location of FLC curve in FLD. In short, the location of FLC curve, which is defined as a strain-based criterion used in FLD, can be affected by forming history.

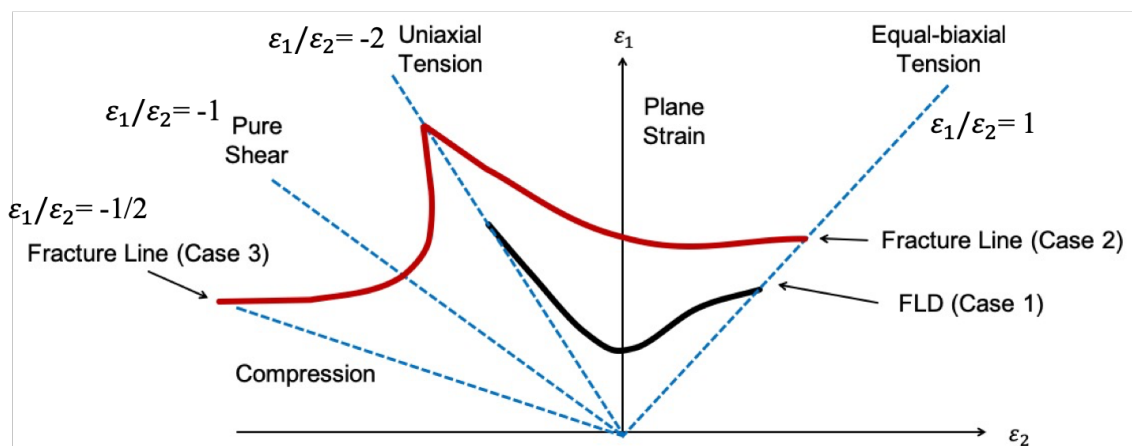


Figure 2-7: Forming limit curves (Case 1), fracture line (Case 2) and fracture line (Case 3) in FLD [Isi14]

To overcome this problem, the approach by using FLC curve to predict failures must be continuously developed. The IFU-FLC-criterion was one of the solutions to overcome the drawbacks of criterion based on FLC. This new criterion was firstly proposed by Drotleff and can predict failure by considering the change of the strain path in case of a complex drawn part [Wer13]. In order to create a nonlinear strain path (forming history regarding different loading conditions), the material is pre-stretched by using Marciniak test. Then, a secondary Nakajima sample was made from the stretched formed parts. Furthermore, in order to save time in determining the new failure IFU-FLC-criterion, an enhanced method of IFU-FLC-criterion was proposed in 2015 by Drotleff as well. This new approach can significantly reduce the experimental effort and material costs to determine the new failure curve [Dro15]. Besides, to solve the problem of effects of nonlinear strain path, W. Volk et al. proposed a generalised forming limit concept (GFLC) in 2013 [Vol13]. This approach uses the strain ratio as a measure to identify the loading type at a given material point. Later F. Andrade presented an incremental model based on GFLC model [And15]. However, F. Andrade mentioned in his work that damage-based models (GISSMO model, [Neu09]) are more general and useful than FLC-based criterion.

The fracture curves introduced in Figure 2-7 describe only the cracks caused by mechanism “membrane instability”. When considering the entire forming process, it can be observed that the bending or hemming process also causes cracks and failures [Kau13]. However, the crack mechanism of bending or hemming does not belong to the mechanism “membrane instability” [Den11]. Thus, the evaluation of bending results regarding damage and failure is still an important topic in labs and series production. To address these problems, the bending limit curve (BLC), which locates over the FFL curve in FLD, was developed. By using the concept of bending limit curve (BLC), the influence of hydrogen embrittlement on forming ability of AHSS DP1180 was determined [Gao16a][Gao16b].

Type of failure 2: Wrinkles of first and second order, surface defect

Apart from necking and cracks, wrinkling and surface defects also represent an important kind of failure in drawn parts. Surface defects affect the surface quality of outer panels significantly. However, slight surface defects in structural parts can be accepted, if surface defects or wrinkles are not located in the functional area (mating surface and welding surface) of a formed part. To better understand wrinkling phenomenon, E. Doege proposed the concept that refers to two types of wrinkling phenomena in 1995 [Doe95]. The first type involves wrinkles in the flange area which are called “wrinkles of the first order” (see Fig. 2-8-a). The other type “wrinkles of the second order” (see Fig. 2-8-b) is defined as wrinkles in the free forming zone especially between the punch radius and die radius.

The experimental procedure for predicting the formation wrinkles of first order can be summed up in two categories. Firstly, by using analytical models, the critical stress levels can be determined to predict the onset of wrinkles. Secondly, the wrinkles of first order formation can be detected by determining the critical binder pressure.

First of all, the usage of “critical stress levels” to predict wrinkle formation is a widely accepted approach in the industrial application, because a critical value of stress can be conveniently applied in the post-processing of conventional FEM software, like LS-DYNA and AutoForm. Based on this, great deal of works has been done using analytical models to predict first order wrinkles. For example, X. Wang uses an analytical model to predict flange wrinkling [Wan00a] by combining the use of energy conservation and plastic bending theory. The analysed model is based on the wrinkle criterion proposed by J. Cao and M.C. Boyce in 1997 [Cao 97]. The material parameters K , strain hardening index n and pressure P were found to have a significant effect on the calculated critical stress at onset of wrinkling.

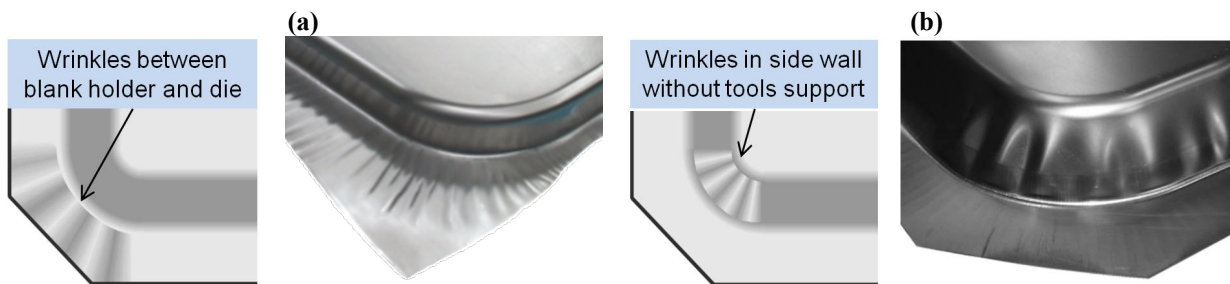


Figure 2-8: Surface failure of wrinkles according to the car-fender-based geometry (KVG geometry) tests in [Bla12], (a) Wrinkles of first order occur between blank holder and die in [Lie08]; (b) Wrinkles of second order take place in the free forming region in [Lie08]

Since the wrinkles of first order in deep drawing process can be controlled by verifying the binder force, the industry pays more attention to the phenomenon of wrinkles of second order. According to the theory from W.F. Hosford, if too much material is allowed to be drawn into the die, compressive hoop stress may be generated in unsupported wall areas (eg. Free forming area in drawing test, see Fig. 2-8-b). This compressive stress can cause wrinkles of second order. The approach for predicting the formation of wrinkles of second order can be summed up in three categories. Firstly, the onset wrinkles of second order can be defined by using the critical stress levels calculated by using analytical models. Secondly, the wrinkles of second order can be detected by using geometrical method during the forming process. At last, by using the theory of “bifurcation” the onset of wrinkles of second order can be detected by analysing the surface stability in FEA.

First of all, the usage of “critical stress levels” to predict second-order wrinkles is also a widely used approach in the industrial application. To calculate the desired critical stress levels, special

designed specimens, like Yoshida buckling test and conical cup test, have been investigated using analytical models. Due to simple geometrical shapes and experimental devices, both of these approaches are chosen as reference for FEA investigation and experiments. In addition, in order to validate developed wrinkle criteria, these two experiments are mainly selected as standard procedure both in scientific works (described in Chapter 2.3) and in the industry.

The geometrical method is mainly used to predict wrinkle formation in laboratory. To evaluate the side wall surface quality of a conical cup [She04], Z.Q. Sheng et al. defined two indexes, namely “flange wrinkle amplitude (FMA)” and “sidewall wrinkle amplitude (SAM)”. Although wrinkling initiation can be defined as a critical buckling height or wrinkle height, it is difficult to directly determine surface deviation. In addition, a robust method should be developed to study the development of surface deviation in the deep drawing process. Only in this way, the difference between buckling initiation and wrinkling initiation can be judged, and the surface quality of the side wall can be evaluated. Eisele reports a method for predicting the beginning of side wall wrinkles, which applies not only to simple symmetrical parts such as conical cups, but also to asymmetric parts such as car-fender-based geometry, which is usually named with KVG geometry. The advantage of this approach is obvious. By using Eisele’s approach, the surface contour of the side wall can be characterised at any drawing depth. In this way, the critical wrinkling height can be exactly determined at defined wrinkling initiation.

R. Narayanasamy and C. Loganathan studied wrinkling behavior by using conical and tractrix dies [Nar08]. They also proposed a strain-based WLC in FLD and pointed out that high value of normal anisotropy postponed the wrinkle formation.

Furthermore, “bifurcation” theory can be used in analysing “wrinkling initiation”, since the wrinkling phenomenon can be seen as a kind of “instability” regarding investigated wrinkling area. When the studied region (drawn part) loses its structural stability, wrinkling initiation occurs. Numerical procedures to predict wrinkle formation of the second order can be generalised into two categories:

- Linear bifurcation analysis of a perfect structure (eigenvalue buckling analysis) [Hut74]
- Non-linear bifurcation analysis employing initial imperfections [Kim00a].

Linear buckling analysis is a widely used method to analyse simple structure geometry in practice, since the used time in FEA for linear bifurcation analysis are much more shorter than for a non-linear bifurcation analysis. In general, when the stiffness matrix $[K_T^{Lin}]$ for linear analysis is equal to zero, instability takes place.

Furthermore, the $[K_T^{Lin}]$ can be expressed by using $[K_m + \lambda K_g]$. Here $[K_m]$ indicates the material contribution matrix and $[K_g]$ represents geometric stiffness matrix. Thus the condition $[K_T^{Lin}] = 0$ can be seen as an eigenvalue problem, see equation 2.26.

$$[K_T^{Lin}]\{u\} = \{0\} \quad \rightarrow \quad [K_m + \lambda K_g]\{u\} = \{0\} \quad (2.26-a)$$

In general, by using linear buckling analysis, critical load is usually overestimated (see Fig. 2-9-a). The bifurcation point indicates the point when the structure starts to lose its stability even though it has been bended or deformed for a certain time, while the limit load is the load with which the structure starts to bend or deform and thus loses its functionality. The classic linear buckling analysis considers only elastic material behaviour. Also the effects of imperfections, which influence the FEA results significantly [Lia11], are not taken into account. The load-extension curve determined by using non-linear buckling method is illustrated in Fig. 2-9-b. The non-stable stage in the case of non-linear buckling occurs when the value of the load begins to decrease. The phenomenon of the “non-stable” stage is called “collapse” in [Dia10].

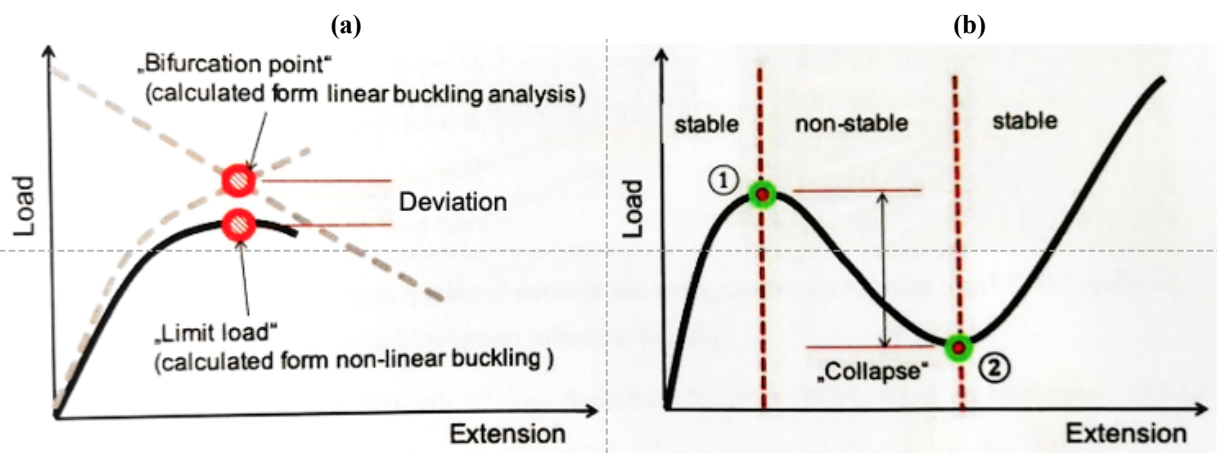


Figure 2-9: (a) Comparison between “bifurcation point” calculated from “linear buckling” method and “limit load” determined from “non-buckling” method; (b) Determined load-extension curve using “non-buckling” method with the definition of stable and non-stable stage

The bifurcation theory was adopted by J.B. Kim et al. [Kim00b] to study the wrinkling initiation and its growth using Yoshida buckling specimen. In his work, the wrinkle initiation can be found by examining the determination of the stiffness matrix at each iteration, and the finite element is based on the incremental deformation theory and the elastoplastic model. Compared with experimental results, it can be concluded that the proposed modified Yoshida specimen can be used in the verification of the finite element code for wrinkling analysis.

J. Cao and M.C. Boyce proposed a non-bifurcation procedure to predict wrinkles by implementing imperfection [Cao97]. This program is robust after introducing imperfection, which appears in the form of a randomly distributed thinning part with an intermediate surface offset. In this way, buckling wavelengths and buckling stresses can be expressed as functions of adhesive pressure.

Compared with conical cup and square cup test, the correct wrinkling initiation behaviour can be obtained.

While typical wrinkles of first/second order can be detected using FEA in the part development stage [Klo10], the surface defects like surface low, small dimension wrinkles and surface distortion remain difficult to be predicted by FEA [Hor12]. Sometimes surface defect can be observed even if forming process is followed after deep drawing [Por08]. However, in this work, only the surface defect in deep drawing process will be handled and discussed.

In practice, surface defect “surface low” can be measured by the depth of the low and the area of the low. The measurement results indicated that when a surface defect “surface low” is deeper than 0.002 mm, the die need to be re-worked. Hu et al. reported a “stoning algorithm” in post-processing of Dynaform V5.5 to evaluate and predict surface defect like type “surface low” at Chrysler LLC [Hu08].

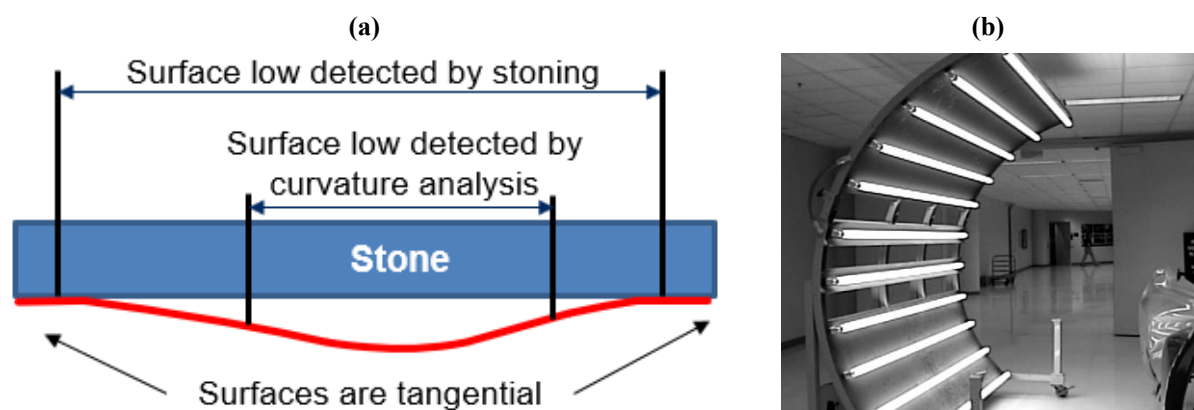


Figure 2-9: (a) Evaluating the surface quality of surface low using treatment stoning [Aut19]; (b) Surface low measurement using blue/green reflection [Hu08]

Surface defect – type “surface distortion” was described by H.P. Wang et al. as undesired subtle waves and irregularities in formed parts [Wan08]. Wang reported that even the depression or waves only between 0.002 to 0.05 mm that deviated from the reference surface can be noticed in a panel without optical measurement devices. In the year 2008, some of surface distortion problems cannot be detected due to the limited understanding of the surface distortion and lack of robust tools to predict surface defects [Wan08].

2.2 Standard tests in the laboratory to investigate wrinkling formation

In chapter 2.2, standard tests to investigate wrinkling formation will be reviewed. Buckling bending test (BBT) is firstly introduced in Chapter 2.2.1. Buckling test performed with original Yoshida specimen and modified Yoshida specimen will be presented in Chapter 2.2.2. Later in Chapter 2.2.3, tests with special designed specimens are shown. In order to determine the wrinkling behavior in the real deep drawing process, the conical cup test (CCT) is explained in Chapter 2.2.4. Finally, in Chapter 2.2.5, the car fender shaped geometry (KVG) with the help of segment-elastic blankholder (SEB) is introduced which was used to establish the real drawing conditions in laboratory. In Chapter 2.2.5, the method of controlling material flow using a closed-loop control system will also be described.

2.2.1 Buckling bending test

Buckling test is a commonly used approach to test structure or specimen instability under in-plane compression or shear load [Ble52] [Nas71]. The buckling bending test (BBT test) introduced in Fig. 2-11 is a kind of buckling test and is used mainly for investigating stability and buckling behavior of a flat specimen under uniaxial compressive stress.

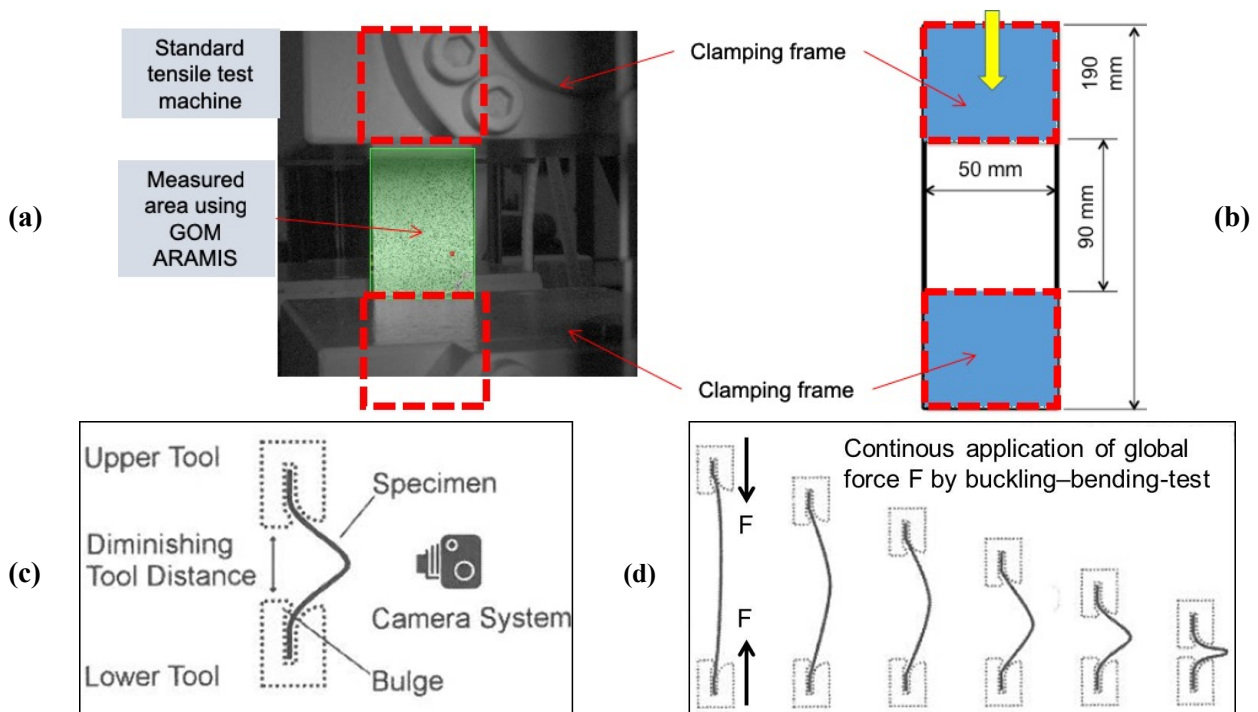


Figure 2-10: Buckling bending test performed at IFU, (a) Buckling bending specimen clamped in tensile test machine; (b) Sketch of buckling bending specimen, clamping area and measurement area; (c) Position of the tensile test machine and ARAMIS optical measurement system in experiment [Hoe13]; (d) Development of surface contour during the BBT test [Hoe13].

The usage of BBT tests to investigate buckling behaviour regarding sheet metals was concentrated mainly in FEA. Li reported an approach to study the plastic instability of sandwich sheet made

from the construction of metal-plastic-metal based on the BBT specimen by using LS-DYNA [Li12]. In this way, the “limit load” determined from load-extension curve can be observed. Furthermore, to enhance the accuracy of calculated bending strain by using FEA, Hönle investigated the influence of combination regarding hardening models and yield locus models on the bending strain [Hoe16]. Since the details of the BBT specimen used by Li and Hönle were not shown, the BBT specimens were tested and optimised in the year 2015 at IFU. Besides, BBT test is not a standard test, the BBT specimen used in this work was only optimised according to the real condition of clamping area regarding applied tensile test machine, and the measuring real condition by using GOM ARAMIS in experiments (see Fig. 2-11c). In this way, the buckling process was able to be observed by optical measuring equipment, and the onset of buckling can be defined in laboratory.

The in this work adopted BBT specimen geometry is shown in Fig. 2-11-b. The total length of the specimens is 190 mm while the effective buckling area for measuring with GOM ARAMIS is 50 mm * 90 mm (see Fig. 2-11-b). First of all, the red dotted line marked areas were clamped in a conventional tensile machine (see Fig. 2-11-a and Fig. 2-11-b). Then the upper clamping frame moved downward with a speed of 20 mm/min (yellow arrow illustrates the direction in Fig. 2-11-b). When the “effective area” loses its structure stability under compressive stress, the initial buckling occurs. The changes in the profile of the specimen during the test are illustrated in Figure 2-11-d. The wrinkle height can be measured by using GOM ARAMIS. The details of experimental results, like structure stability and instability, are shown in Chapter 4.2.1.

2.2.2 Buckling test performed with original and modified Yoshida specimen

Compared to BBT test, buckling test with Yoshida specimens is used mainly for investigating stability and buckling behavior under tensile-compressive stress state (as shown in Fig. 2-12-a). By modifying the original Yoshida specimen, the buckling behavior under pure-shear stress (as shown in Fig. 2-12-c) can be observed and investigated.

Buckling test to be performed with Yoshida specimen is mainly called “Yoshida Buckling Test” (abbreviated as YBT test) which is named after an experimental approach performed by K. Yoshida [Yos81]. The principle of YBT test is, when the compressive stress generated by specimen center exceeds the specific critical compressive stress level, the “buckling initiation” of the specimen occurs. Due to the rhomboid geometry of the YBT specimen, in the center of the specimen, the compression zone is generated vertically in the tensile direction while the load increases. Besides, the elastic buckling behavior based on the YBT test can be explained by the theory of Timoshenko [Tim85]. According to this theory, the tensile and compression

superposition regarding the middle area of specimen leads to the shear stress. When the shear stress exceeds the specific stability limit, the onset of buckling takes place.

To enhance the accuracy of the predictability of Yoshida buckling tests, two kinds of new modified Yoshida sample (K-series and G-series specimens) were modified using FEA in 2014 [Han14]. By considering the energy theory of J.W. Hutchinson in the forming process, the different buckling behaviours based on K- and G-series specimens are explained.

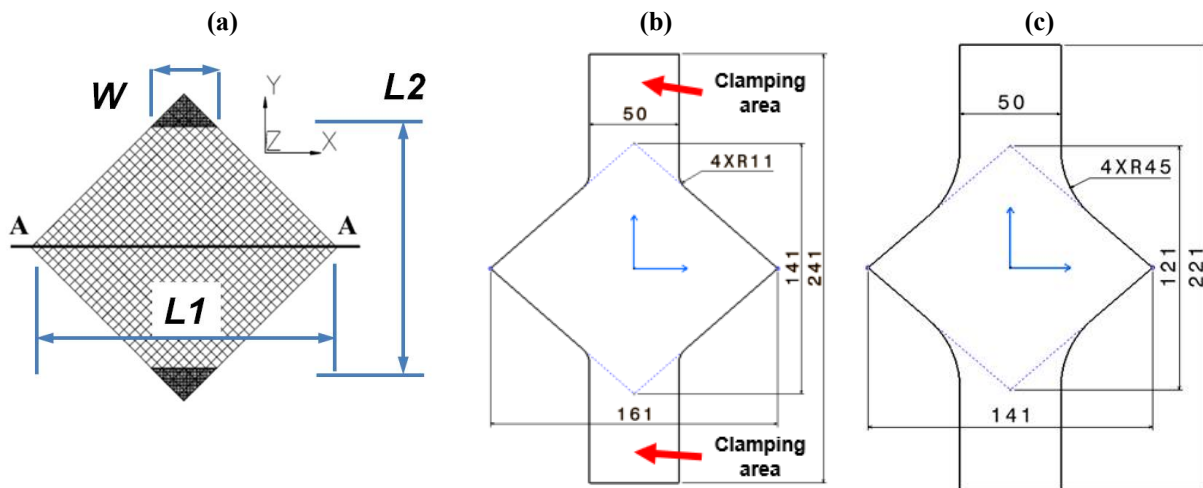


Figure 2-11: (a) Schematic illustration of the original Yoshida buckling specimen; (b) Schematic of the modified Yoshida buckling specimen with a small radius (K-Series) (c) Schematic of the modified Yoshida buckling specimen with a large radius (G-Series)

According to the actual situation, buckling tests based on six modified Yoshida specimens (3 different shoulder radius and 3 specimen width) were carried out on tensile testing machine and simulated in LS-DYNA. Two holders were added to the original rhomboid Yoshida specimen to better accommodate the tensile test machine. Additionally, each specimen is divided into two variations – K series and G series with small and large curved radius (see Fig. 2-12-b/c). According to the research results published by Schleich by using specially modified buckling specimens [Sch09], buckling test with M-YBT specimens was able to be summarized as following:

- 1) Advantage of Yoshida buckling test: Yoshida test is an effective and simple method to study the wrinkling/buckling behavior). And the experimental results can be directly compared with FEA results. Thus, the accuracy of FEA can be ensured.
- 2) Disadvantage of Yoshida buckling test: Yoshida buckling test is not a standard test to evaluate the wrinkling tendency of sheet metal materials. Thus, Yoshida specimen should have to be modified according to experimental equipments and sheet material.

In conclusion, Yoshida buckling test und Buckling bending test are the suitable method to study the wrinkling behavior in laboratory. These two experiments need only conventional tensile test machine. Unlike the following introduced specimens and experimental methods, special test machine is required to evaluate wrinkling behavior.

2.2.3 Wrinkling test by using special designed specimen

To predict wrinkling initiation in sheet metal specimen by using strain-based approach, like wrinkling limit curve (WLC) based on FLD, more specimen shape variants should be developed to induce wrinkling formation under different load conditions. Thus, some kinds of special designed specimens were developed in the last 20 years to determine the wrinkling limit curve.

In 1989, A. Simon et al. attempted to determine a wrinkling limit curve by using a “wedge specimen” illustrated in Fig. 2-13-a. This especially designed specimen aimed to determine a WLC regarding initiation of the wrinkles of second order. This specimen reveals a total length of 260 mm. The width at A-side and B-side are different and the specific values, like angle α^s , can be freely defined according to actual experimental needs. The basic idea of this experiment is to apply a tensile force at the clamped A-side along the direction of blue arrow, while the B-side was clamped. Since the width at A- and B-side is different, compressive stress was induced vertically in the tensile direction during the elongation process.

Experimental results indicated that determined wrinkling limit curve (red line in Fig. 2-13-a) had a shifted origin (reason: stress state and strain path before onset of wrinkling) by using this wedge specimen. When the wrinkles reached a defined wrinkling height, the measured ε_1 and ε_2 was recorded. After testing enough amount of specimens, a red line can be fitted based on FLD, see Fig. 2-13-a/b. This red line is the wrinkling limit curve defined by Simon in 1989. The wrinkling limit curve determined by using Simon’s specimen can be seen as the function $\varepsilon_1 = k \cdot \varepsilon_2 + b$.

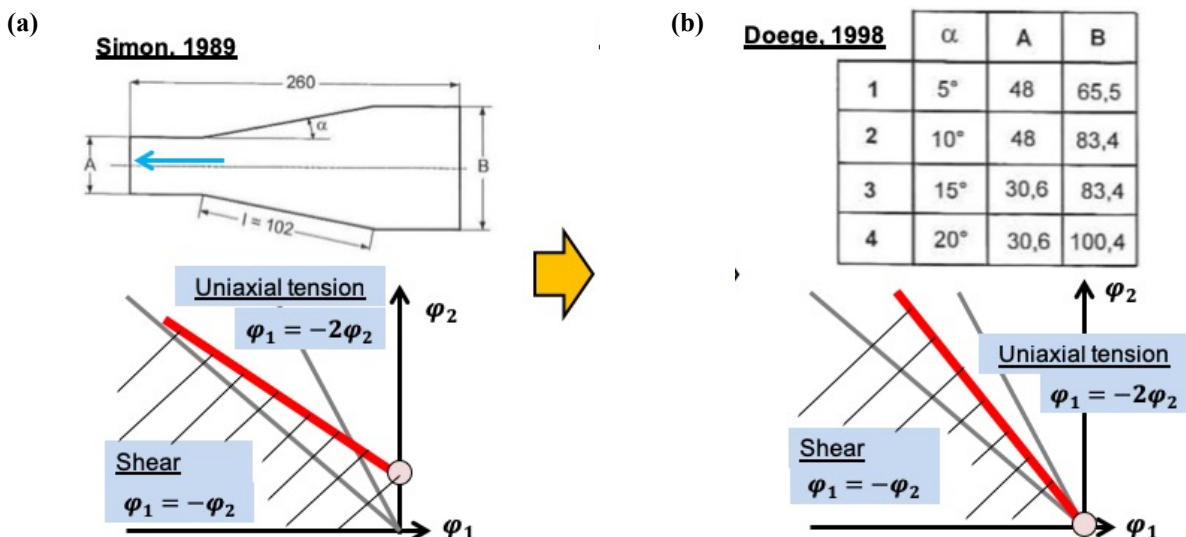


Figure 2-13: Experimental results, (a) Determination of a wrinkling limit curve using special designed wedge specimen by Simon in 1989 [Sim89]; (b) by determination of a wrinkling limit curve using modified Simon’s specimen [Doe98]

Doege et al. modified this wedge specimen by verifying the following three parameters to enhance the accuracy of the location referred to as wrinkling limit curve in FLD [Doe98]. The details about

the “width of the A-side” (30.6 mm, 48 mm), “width of the B-side” (65.5 mm, 83.4 mm and 100.4 mm), and “wedge angle α ” (5° , 10° , 15° and 20°) are listed in Fig. 2-13-b. By fitting the experimental results, the wrinkling limit curve can be defined as the function $\varepsilon_1 = k \cdot \varepsilon_2$.

The wrinkling limit curve determined by [Doe98] was based on four different modified shapes of specimens. The result was comparable with the wrinkling limit curve determined by using conical cup test [Bla08]. In the following section, details regarding conical cup test will be introduced.

2.2.4 Conical cup test

The conical cup test is mainly used to study the wrinkling behavior of sheet metal materials regarding symmetrical and simple deep drawing part. W.F. Hosford pointed out that by introducing enough tensile stress can prevent the wrinkling formation [Hor07]. Usually, the needed tensile stress can be increased by applying higher blank holder force and using draw beads. Therefore, the wrinkles of first order that occur between the blank holder and the die can be prevented by directly raising the blank holder force. However, wrinkles of second order cannot be eliminated by only adjusting the blank holder force, since the failure (cracks and splits) takes place, when not enough sheet metal materials flow in the die. Until now, how to prevent and predict wrinkles of second order for real drawn parts in product design phase is still a challenging topic. The conical cup test can be seen as a standard test to study the formation of wrinkles in the free forming area during deep or stretch drawing.

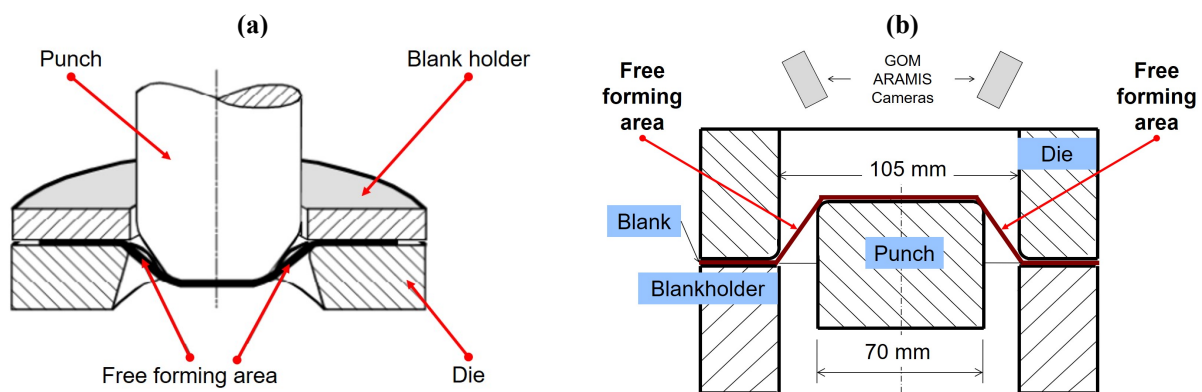


Figure 2-14: (a) Schematic regarding tools of conical cup test according to [Lan90] and [Doe10]; (b) new set up with GOM ARAMIS optical measurement system to capture the change of side wall contour during deep drawing process [Hor15]

A scheme of tools regarding conventional conical cup is shown in Fig. 2-14-a [Lan90] and [Doe10]. The disadvantage of this kind of set up is that, the change of the surface contour in free forming region, see Fig. 2-14-a, during deep drawing process cannot be captured by optical measurement system, for example by using optical measurement GOM ARAMIS. To solve this problem, the experimental set up performed with conical cup test was improved in the work of Horwath. The new set up equipped with GOM ARAMIS is depicted in Fig. 2-13-b. In this way,

the captured surface contours of free forming areas in the side wall can be recorded during the forming process.

The reasons for the initiation of wrinkles of second order in free forming area were explained deeply by Schmidt in [Sch53]. He explained the reason based on conical cup test by showing distribution of stresses in the part wall during deep drawing in Fig 2-14.

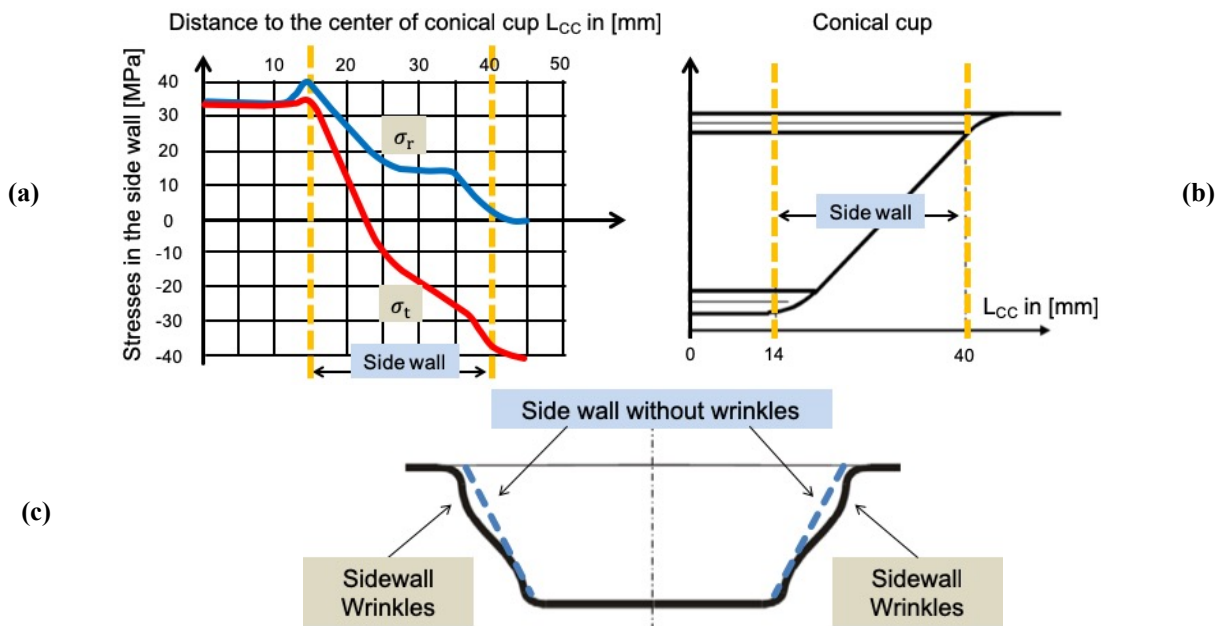


Figure 2-15: Stress distribution in side wall and emergence of wrinkles in conical cup test, (a) Distribution of tangential stress σ_t and radial stress σ_r as function of L_{CC} in [Sch53]; (b) Schematic diagram of side wall area in conical cup [Sch53]; (c) Schematic diagram of tangential stress σ_t and radial stress σ_r in side wall area; (d) Ideal side wall contour and side wall wrinkles

Fig. 2-15-a depicts the relationship between the “distribution of stresses in radial and tangential direction” in side wall and “ L_{CC} ” which is defined as “distance to center of the investigated conical cup” in Fig. 2-15-b. Clearance between die and punch disclose the value of 25 mm which is illustrated in Fig-2-15-a (between the L_{CC} distance 15 mm and 40 mm). The red curve in Fig. 2-15-a indicates the distribution of “tangential stress” σ_t in the side wall. The blue curve shows the distribution of “radial stress” σ_r in the side wall. Since a plane stress state was assumed by Schmidt in his work, the stress in the thickness direction σ_n was assumed as zero.

Obviously, according to results from [Sch53], the stress σ_r in the free forming region is tensile stress, see L_{CC} distance from 14 mm to 40 mm in Fig. 2-15-a. In contrast, the tangential stress σ_t from L_{CC} distance 14 mm to approximately 22 mm is tensile stress. From L_{CC} distance 22 mm to 40 mm, the tangential stress is compressive stress. Thus, from L_{CC} distance 14 mm to approximately 22 mm, the side wall of the investigated conical cup suffers biaxial tensile stress, meanwhile rest part of side wall remains in the tensile-compressive stress state which indicates “wrinkling tendency”. When the value of σ_t reaches a critical value of a given sheet metal material,

wrinkles in the side wall take place. The conventional approaches to determine those critical values will be introduced in Chapter 2.3. As shown in Fig. 2-15-c, to better understand the wrinkles of second order, the formed wrinkles are depicted as an example as a black curve. The dotted blue line in Fig. 2-15-c indicates the assumed straight side wall without wrinkles.

2.2.5 Car-fender based geometry produced with segment-elastic blankholder

The approaches to investigate wrinkles formation during deep drawing were introduced in Chapter 2.2.1 to 2.2.4. However, only simple specimens are used which cannot reflect the complex situations prevailing in deep drawing of real components designed for car body application. To investigate wrinkling behavior under the conditions which more similar to reality of this work, experiments with car fender-based (KVG) geometry are introduced in Section 2.2.5. In Fig. 2-16, the technology iteration relationship from the usage of segment-elastic blankholder (SEB) to the application of closed-loop-controlled SEB was shown. This technology iteration aims to research wrinkling behavior based on the car-fender-based geometry (KVG geometry)

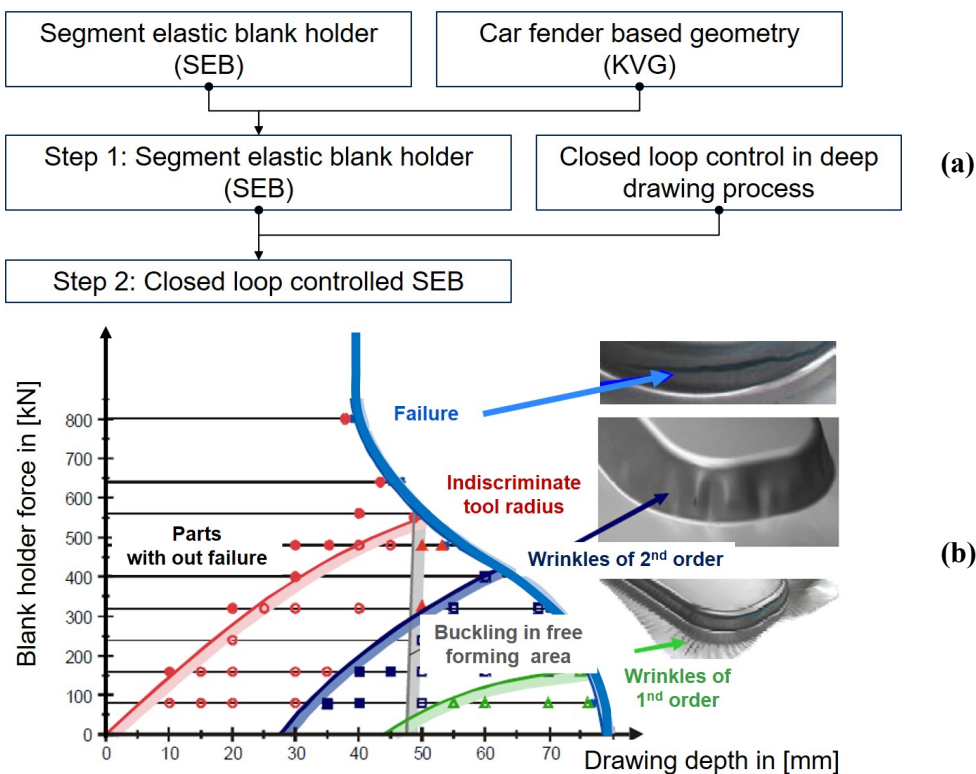


Figure 2-16: Two steps to investigate the influence of SEB and closed loop controlled SEB on local quality of drawn parts produced with a car fender-based geometry; (b) Concept of process window from Blaich [Bla12]

By using SEB and closed-loop-controlled SEB, the process window of the deep drawing process based on KVG geometry is able to be expanded, and the robustness of the drawing process can be improved. “Process window” is usually applied for predicting failures (cracks and splits) and wrinkles of first- and second-order during the deep drawing process using the relationship between blank holder force and drawing depth [Bla12]. Within the “safe” process window, the drawn parts

reveal no failures or wrinkles. Outside of the “safe” process window, the failures and wrinkles appear. The details referring to SEB and closed-loop-controlled SEB will be discussed in the following sections.

The name of car-fender-based geometry – “KVG” comes from the German expression (Kotflügelähnliche Versuchsgeometrie). The KVG geometry was designed and used mainly for investigating wrinkling behavior under unsymmetrical and complex deep drawing part. The originating idea of KVG geometry came from the works of Hishida in the year 1993 [His93a], [His93b]. Afterwards, this geometry was intensively investigated based on use of SEB and closed-loop-controlled SEB at IFU. Fig. 2-17-a shows the car fender part by a dotted red closed curve based on a real car. Simplified car fender based part geometry for lab work is presented in Fig. 2-17-b. Since the drawing process by using KVG geometry simulates the first deep drawing process of a real car fender, this special design is intended to investigate formation of wrinkles of second order in the corner regions.



Figure 2-17: (a) formed part (outer panel) – Car fender; (b) the formed part with KVG [Bla12], [Hae02]

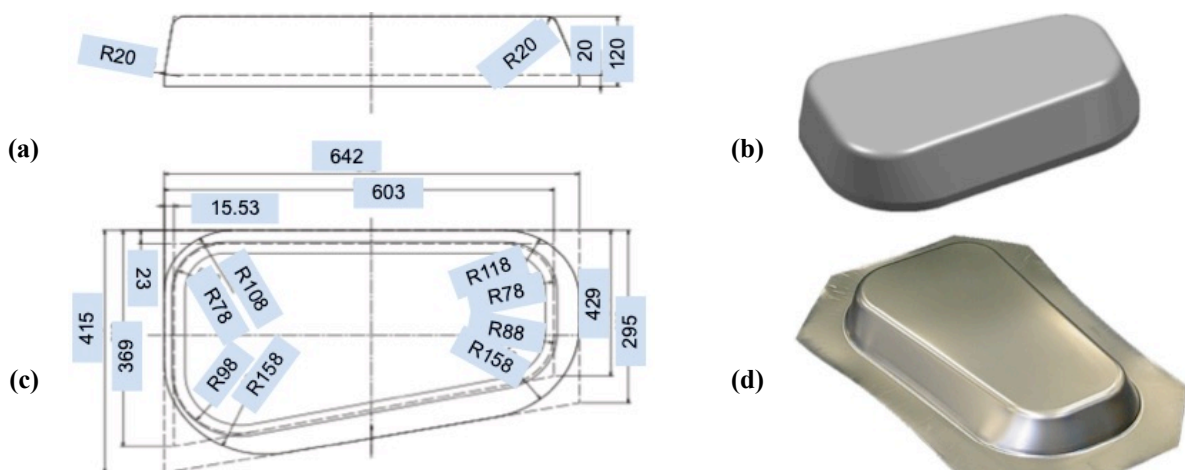


Figure 2-18: (a) Dimension of the KVG geometry (side view) in [Hae02]; (b) Punch of KVG geometry; (c) Dimension of the KVG geometry (top view) in [Hae02]; (d) A drawn part showing KVG geometry

Furthermore, to investigate wrinkles formation and its development during the forming process, the four side walls of KVG geometry is intentionally designed with different side angles to produce different gaps between blank holder and die (see Fig. 2-18-a). In this way, the wrinkles of second order in the free forming area under varied gaps can be generated.

Segment-elastic blank holder (SEB)

As the drawing depth increases, the side with small gaps between punch and die is easily prone to produce failure (cracks). For normal blank holder, it is difficult to produce a drawn part without wrinkles and failures (cracks). Therefore, Häussermann used the concept SEB proposed by [Sie98] to study the feasibility of KVG geometry. The SEB consists of a blank holder plate, cylindrical segments and an adaptor plate, as shown in Figure 2-18-a. The details of the applied cylindrical segment are shown in Figure 2-18-b. The main advantage of the SEB concept is that the local pressure on the blank holder plate can be controlled by adjusting the drawing pin force F_{ch} , which enables the blank draw-in in the tools during the forming process to be controlled. This principle is shown in Figure 2-18-c. If the drawing pin force F_{ch} increases (see increased F_{ch} in Figure 2-18-c), the local surface pressure acting on the sheet metal is enlarged. By employing this method, the value of the local pressure on the blank holder plate can therefore be controlled, which also enables the blank draw-in in the die to be controlled. If the produced part exhibits (local) wrinkling, the blank draw-in can be reduced through increased drawing pin force F_{ch} . Furthermore, when the local pressure is faced with failure (cracks), more material can be intentionally controlled to flow in the die by reducing the drawing pin force F_{ch} .

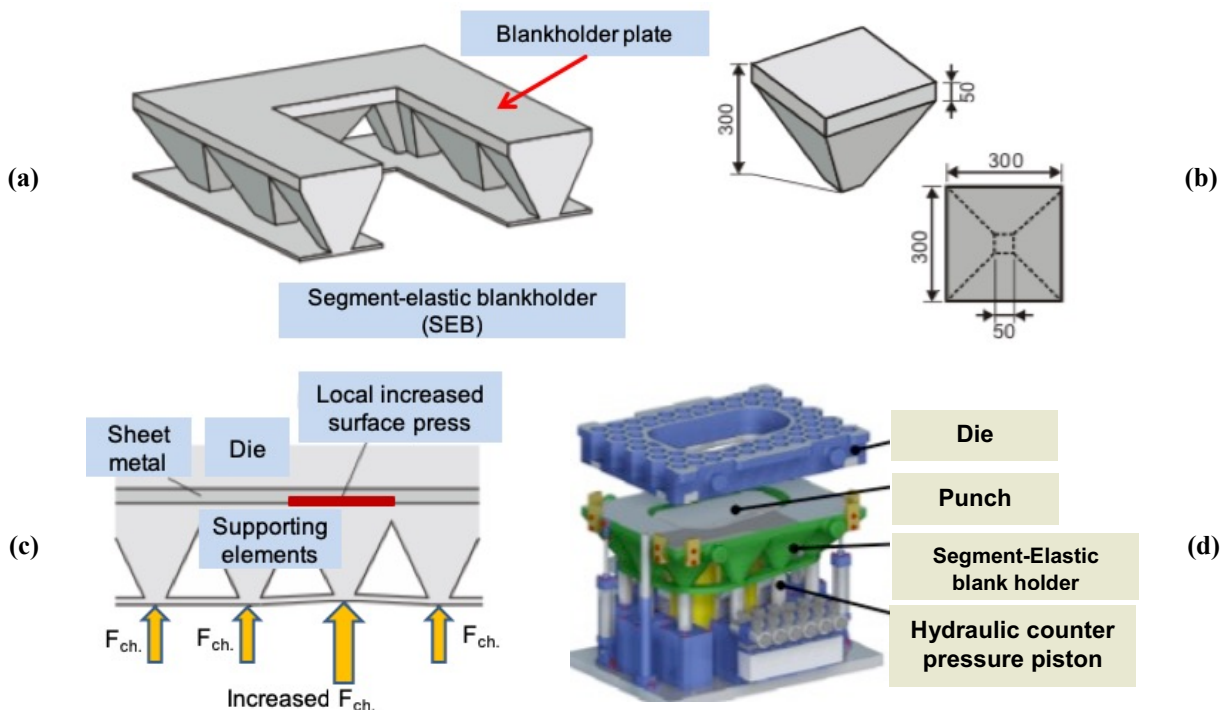


Figure 2-19: (a) Concept of supporting system, consists of Blankholder plate, segment-elastic blankholder and adaptor plate; (b) Details of individual segment-elastic blankholder; (c) Principle of supporting system; (d) Developed tools for forming with supporting system [Hae02]

The piston transfers the local pressure to the segment elastic blank holder, which is connected to the cover plate (blank holder plate) as illustrated in Figure 2-18-b. This design therefore also avoids

marks on the deep drawn component resulting from the separating line between the individual blank holder segments. The complete die set depicted in Figure 2-18-d was developed by Haeussermann. Each segment integrated into the SEB has a separate, hydraulically driven piston.

Segment elastic blank holder (SEB) with closed-loop control system and sensor

The conventional SEB was further developed by C. Blaich and M. Barthau to feature a closed-loop control system for controlling the flow of sheet metal material to avoid local failures (cracks) and second order wrinkles. The principle of the closed-loop system is explained in [Bar17a] and [Bar17b]. However, in this section, only the sensors used to obtain input signals for closed-loop control systems will be introduced since the closed-loop control system applied to the KVG with an SEB will not work without robust and accurate input signals.

A “command variable” defined in [Bla08] and [Wur11] or “state variable” defined in [Bar17a] and [Bar17b] should be measured in a robust manner and as thoroughly as possible, and can describe the behaviour of the closed-loop control system used in their work. The “command variable” and “state variable” in this case have the same function. In this thesis, for the sake of convenience, these two parameters will be referred to as the “input variable”.

S. Beck et al. developed a measuring concept with a “part wall stress sensor” for measuring the mechanical load of the die/punch radius during the deep drawing process. This “part wall stress sensor” is shown in Figure 2-19-a, and the concept of this stress sensor is depicted in Figure 2-19-b. According to the results of Beck and Blaich [Lie18], the “side wall stress” is chosen as the input variable used in the closed-loop control system employed in this work.

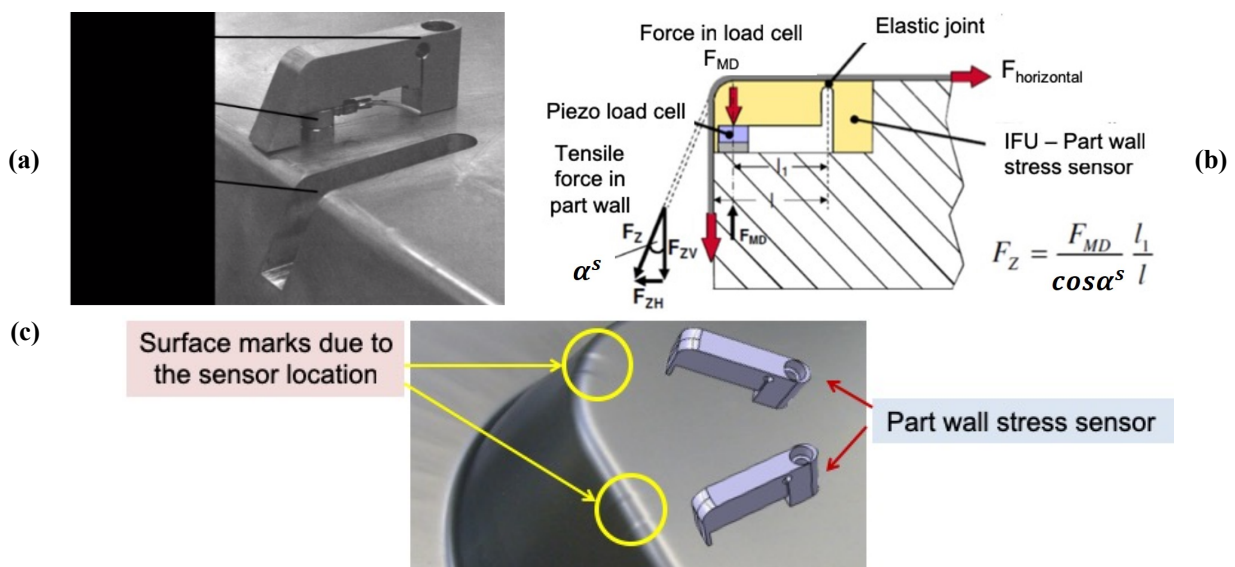


Figure 2-12: Part wall stress sensor used at IFU: (a) photo of part wall stress sensor inserted in punch; (b) schematic principle for calculating tensile force F_z acting in the sidewall zone of the part; (c) surface marks induced by part wall stress sensor, designed as an insert in the punch surface [Lie18]

As shown in Figure 2-19-b, the “part wall stress sensor” in the very first stage of development mainly consists of a piezoelectric load sensor and an elastic joint. In this case the sensor acts to produce measures which are more or less proportional to acting forces onto the punch corner. To calculate a synonym “load” of desired side wall stress, the side wall tensile force F_Z should first be determined. The method used to determine this force F_Z is described in Figure 2-19-b. The tensile force F_Z acting onto the punch corner radius induced by the sidewall of component under tension can be calculated by considering “ratios of l_1/l ”, the vertical force acting on piezo load cell “ F_{MD} ”, and the “ α^s angle” between the punch and sidewall. The method for calculating the “side wall stress” induced by the tensile force F_Z was introduced in the dissertation of S. Beck [Bec04]. The advantage of the “part wall stress sensor” is, firstly, to facilitate its capability by providing tensile stress conditions specific to the drawing outline. Secondly, this sensor can provide stable “input variables” during the drawing process because the tensile stress can be measured very effectively in the first stretch-forming stage and the deep drawing phase alike. This stable signal source provides assurance to the closed-loop control system.

However, using the “part wall stress sensor” significantly affects the surface quality of the drawn part. First of all, unacceptable surface marks can be observed on the formed parts, as shown in Figure 2-19-c, which depicts forming parts with high surface quality requirements, such as the outer panel components of a passenger car. In addition, the use of this sensor can cause surface marks when sensors are located on the punch surface not being properly assembled.

To overcome this problem, a new measuring concept was developed in 2006 by Hengelhaupt and Vulcan [Hen06]. This new sensor employed for measuring sidewall stress is a “piezoelectric measuring sensor” and is illustrated in Figure 2-20-a. To avoid surface marks (as shown in Figure 2-19-c), piezoelectric measuring sensors are inserted directly into the drawing die, die bodies, or cams, as shown in Figure 2-20. In this way, there is no contact between the sensor and the drawn parts. The surface quality of the drawn parts produced can thus be guaranteed.

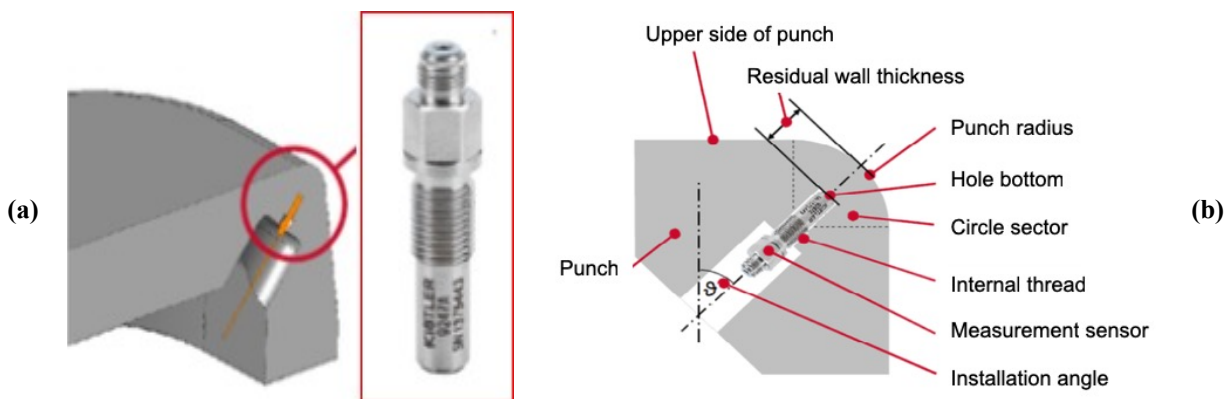


Figure 2-13: Applied piezo-electric measuring sensor, (a) Modified punch and installation position of a piezo-electric measuring sensor; (b) Details of punch and sensor

2.3 Conventional wrinkling criteria applied in FEA

This chapter introduces the traditional approaches for predicting the initiation of wrinkling, namely strain- and stress-based approaches. Firstly, in section 2.3.1, the strain based wrinkling criteria based on FLD [Doe98] are introduced. Subsequently, section 2.3.2 outlines the criteria, for which the most important task is determining the critical compressive stress level leading to wrinkles or at least waviness in the part wall. When the observed compressive stress reaches such a critical level, wrinkling initiation is detected as “occurring”. Usually, there are two approaches for determining the critical compressive stress level, namely by using the “energy method” or “bifurcation method” discussed in section 2.3.2 [Cao97][Kim03]. Compared with traditional approaches, a very promising method of predicting buckling initiation based on the new analysis model will be reviewed in section 2.3.3.

2.3.1 Wrinkling criteria based on the forming-limit diagram

In the first part of section 2.3.1, the conventional strain based wrinkling criterion and its usage in FEA are introduced. The wrinkling limit curve (WLC) is usually used for the strain based wrinkling criterion in FEA. The functionality of the WLC, its origin and its position in FLD are explained here. In the second part of this section, the application of WLC in FEA is introduced with consideration of the non-linear effects in conventional FEA software.

Conventional wrinkling limit curve in FLD and its application in FEA

The FLD used in industrial sheet metal processing is dependent on the major strain ε_1 and minor strain ε_2 . The conventional WLC based on FLD can thus be described in accordance with the following equation considering the major strain ε_1 and minor strain ε_2 : [Doe98]

$$\varepsilon_1 = k\varepsilon_2 \quad (2.27)$$

Figure 2-21-a visualises the WLC, which is illustrated as a dotted line passing through the origin of diagram. The value k indicates the slope of the WLC in FLD. According to the theoretical analysis and practical tests, the k value located between the ratio $\varepsilon_1/\varepsilon_2$ is equal to -2 (uniaxial tensile state) and -1/2 (uniaxial compressive state) [Nar08].

The ratio of “ $\varepsilon_1/\varepsilon_2$ ” is calculated at every drawing depth of component within investigated elements. If ratio $\varepsilon_1/\varepsilon_2$ meets or is located below the determined WLC in FLD (see Figure 2-21-a), the wrinkling initiation is defined as “occurring”. The blue arrows in Figure 2-21-a indicate the strain path (forming history) before a defined wrinkling initiation. According to F. Han [Han13], the wrinkling tendency increases if WLC rotates to the uniaxial stress state. Conversely, if the investigated WLC rotates to a deep drawing strain state, the wrinkling tendency decreases. This

conclusion was proved by testing different materials in accordance with [Doe98], as shown in Figure 2-21-b.

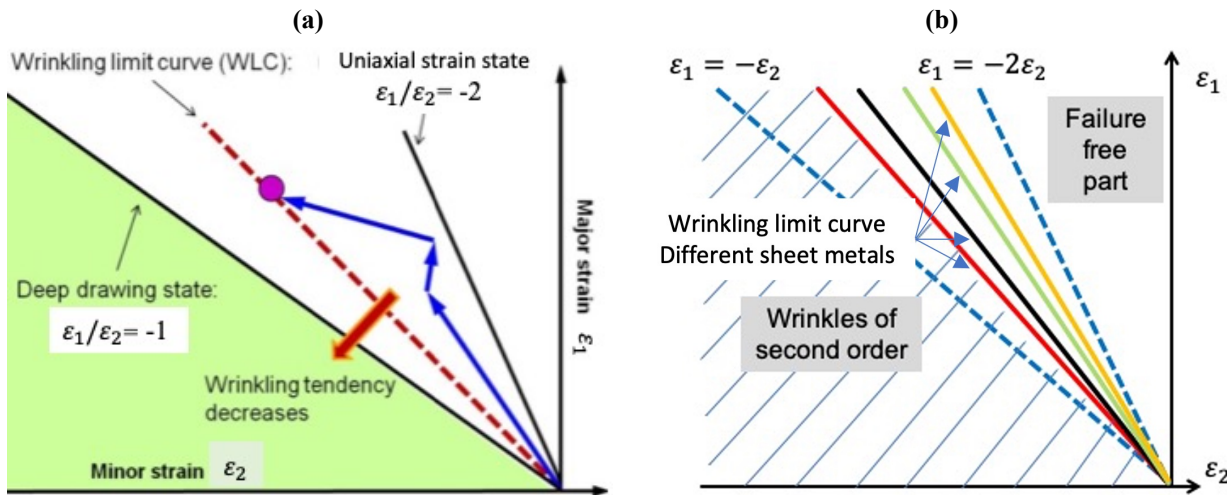


Figure 2-14: (a) Wrinkling limit curve (WLC) in FLD and defined wrinkling initiation (purple circle); (b) various wrinkling limit curves determined using the specimen depicted in Figure 2-11-b [Doe98]

(a) Detection of wrinkles considering the influence of the non-linear strain path in FLD

In 2014 and 2016, respectively, S. Dambach and D. Y. Chen proved using experiment results that forming history does indeed affect the location of the WLC in FLD. The influence of the forming history on the WLC must therefore be taken into account when the strain based wrinkling criteria are used to predict wrinkle formation in FEA. In this section, the strain based wrinkling criterion “potential wrinkling” applied in the software code AutoForm will be introduced considering the influence of the forming history. “Potential wrinkling” is a standardized, strain based wrinkling criterion used in AutoForm that aims to analyse the wrinkling tendency during stretch and deep drawing processes.

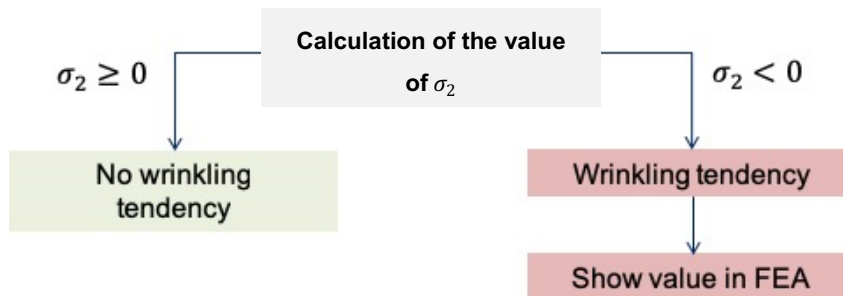


Figure 2-15: Logic of calculating “potential wrinkling” in AutoForm to identify the “wrinkling tendency” areas

The logic and functionality of the approach called “potential wrinkling” implemented in AutoForm code is shown in Figure 2-23. To save calculation time in FEA, only the finite elements which have the wrinkling tendency will be considered. If the amount of the minor stress σ_2 of a finite element is smaller than zero, this element can be considered as have “wrinkling tendency”. Only in this case is the determined compressive stress compared with the defined, critical compressive stress

level in post-process. If the value of the calculated minor stress σ_2 is higher than the value 0, no wrinkling tendency is considered in AutoForm. The value of the minor stress σ_2 in AutoForm can be calculated according to Equation 2.27 assuming the finite element of a shell. The value of minor stress depends on the factor λ , anisotropy value R , and the major and minor strain in FLD.

$$\sigma_2 = \lambda \left(\varepsilon_2 + \frac{R}{1+R} \varepsilon_1 \right) \quad (2.27)$$

$$\varepsilon_{WC}^{lin} = \max \left[- \left(\varepsilon_2 + \frac{R}{1+R} \varepsilon_1 \right), 0 \right] \quad (2.28)$$

(b) Value “ ε_{WC}^{lin} ” and linear strain path in FLD

As mentioned, if the calculated minor stress of the investigated element is less than zero, a “wrinkling tendency” is determined. This assumption is similar to the idea proposed by W. F. Hosford [Hos07] stating that wrinkling during deep drawing may occur when the minor stress is compressive/negative. Figure 2-24-a and Figure 2-24-b illustrate this idea from both AutoForm and W. F. Hosford.

Both the idea from AutoForm and from W. F. Hosford can be explained using the relationship between the “uniaxial-tension line” and “actual strain path” calculated in post-processing (in FEA). As shown in Figure 2-24-a, the red arrow indicates the actual strain path in FEA. If the actual strain path is located to the right of the “uniaxial-tension line”, this situation can be interpreted as “no wrinkling tendency”. However, if the strain path is located to the left of the “uniaxial-tension line”, a wrinkling tendency is determined. Since the “degree of wrinkling” (slight or severe wrinkles) cannot be defined by a wrinkling height in the AutoForm FEA software, a special value “ ε_{WC}^{lin} ”, as defined in Equation 2.28, is introduced to determine the “degree of wrinkling” in post-processing.

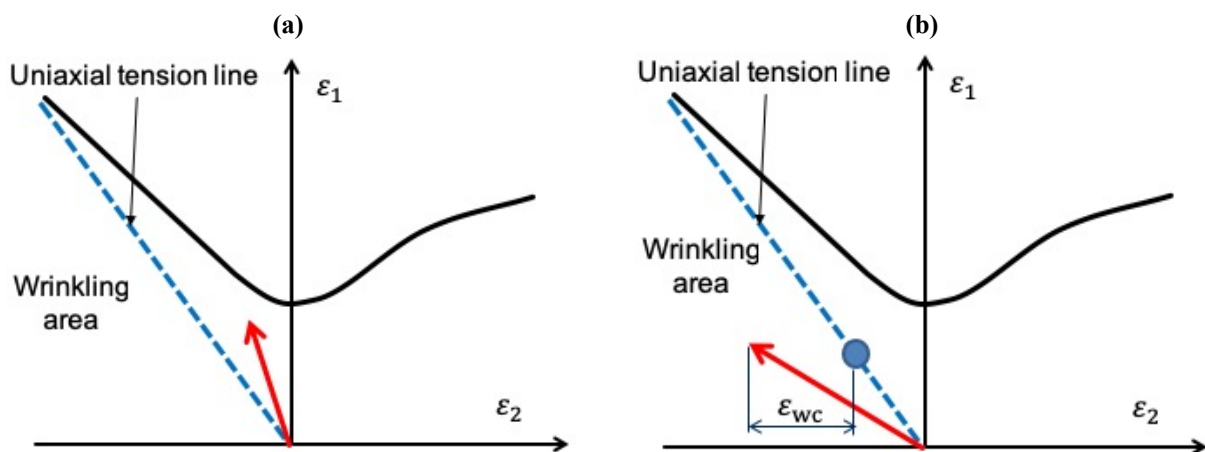


Figure 2-16: Definition of the “potential wrinkling area” based on FLD in [Hos07] and [Aut19]: (a) observed strain path without wrinkling tendency; (b) observed strain path is recognised located in the wrinkling area indicated by the defined value of “potential wrinkling” ε_{WC}^{lin}

The special value “ ε_{WC}^{lin} ” more or less has a geometric meaning of “distance from the uniaxial-tension line” in the inverse direction along the minor strain axis, which is illustrated in Figure 2-24-b. As shown in Equation 2.28, if the minor stress σ_2 is equal to 0, the “distance from the uniaxial-tension line” ε_{WC}^{lin} is equal to 0. If the minor stress σ_2 is smaller than 0, this indicates that compressive stress is existing. The value of ε_{WC}^{lin} in this case is adopted as $-\left(\varepsilon_2 + \frac{R}{1+R}\varepsilon_1\right)$.

(c) Value “ ε_{WC}^{Non} ” considering non-linear strain path in FLD

To enhance the accuracy of the “potential wrinkling” analysis, the forming history should be considered during the FEA, therefore the expression of the value “ ε_{WC}^{Non} ” for predicting the degree of wrinkling is modified in Equation 2.29 as follows:

$$\varepsilon_{WC}^{Non} = \varepsilon_{WC}^{lin} - \min\left[\left(\varepsilon_2 + \frac{R}{1+R}\varepsilon_1\right)\right] = \varepsilon_{WC}^{lin} + \varepsilon_{between} + \varepsilon_{history} \quad (2.29)$$

The geometric interpretation of the modified model is explained in Figure 2-24-a and Figure 2-24-b. Supposing the first strain path is only to the right of the uniaxial-tension line (see Figure 2-24-a), the following strain path then passes through the uniaxial-tension line and at its end it is located to the left of this line. In this situation, the value “ ε_{WC}^{Non} ” consists of ε_{WC}^{lin} , $\varepsilon_{between}$, and $\varepsilon_{history}$. The geometric meanings of these three terms are explained in Figure 2-25-b.

In summary, whenever the strain path angles further to the left and the slope becomes less than the uniaxial-tension line, values start to occur for potential wrinkling. Furthermore, the value of ε_{WC} and ε_{WC}^{Non} cannot provide the actual wrinkling height, rather only wrinkling factors.

$$\varepsilon_{WC}^{Non} = \varepsilon_{WC}^{lin} - \min\left[\left(\varepsilon_2 + \frac{R}{1+R}\varepsilon_1\right)\right] = \varepsilon_{WC}^{lin} + \varepsilon_{between} + \varepsilon_{history} \quad (2.29)$$

The geometric interpretation of the modified model is explained in Figure 2-24-a and Figure 2-24-b. Supposing the first strain path is only to the right of the uniaxial-tension line (see Figure 2-24-a), the following strain path then passes through the uniaxial-tension line and at its end it is located to the left of this line. In this situation, the value “ ε_{WC}^{Non} ” consists of ε_{WC}^{lin} , $\varepsilon_{between}$, and $\varepsilon_{history}$. The geometric meanings of these three terms are explained in Figure 2-25-b.

In summary, whenever the strain path angles further to the left and the slope becomes less than the uniaxial-tension line, values start to occur for potential wrinkling. Furthermore, the value of ε_{WC}^{lin} and ε_{WC}^{Non} cannot provide the actual wrinkling height, rather only wrinkling factors.

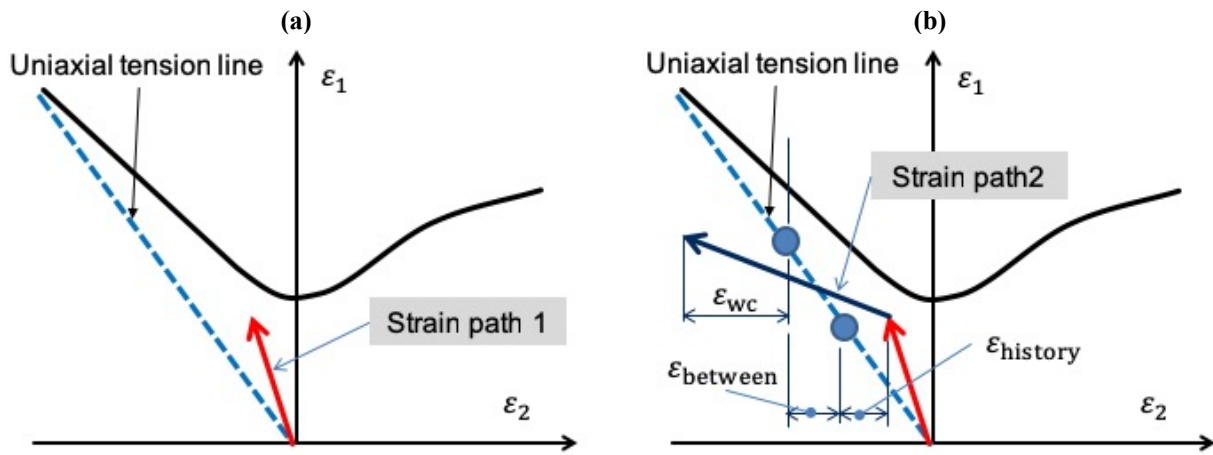


Figure 2-17: Definition of the value of “ ε_{WC}^{Non} ” based on the non-linear strain path in FLD [Aut19]: (a) the first strain path in FLD; (b) the second strain path and definition of the three terms “ ε_{WC}^{lin} ”, “ $\varepsilon_{between}$ ”, and “ $\varepsilon_{history}$ ”

2.3.2 Wrinkling criteria based on critical stress level

Over the past 20 years, the main stress based approaches employed to analyse wrinkling/buckling phenomena are the “bifurcation method” and the “energy method” [Kim03]. By employing the “bifurcation method” and the “energy method”, the desired critical, compressive stress applied in FEA as a criterion for judging whether initiation has occurred can be determined. In the following sections, Hutchinson’s bifurcation method is reviewed first. The “energy model” as defined by Cao and Kim will subsequently be explained.

2.3.2.1 Bifurcation method for determining the critical stress level

By exploiting the fact that the short wavelength modes are shallow and can be analysed using “shallow-shell theory” and “DMV theory”, Hutchinson and Neale [Hut85] presented the approach of plastic-buckling analysis for studying a local wrinkling area, which is assumed by J. W. Hutchinson to be a doubly curved wrinkling region, see Figure 2-26.

A comprehensive discussion about buckling theory and the relations for the DMV “shallow-shell theory” using “J2 flow theory” is reviewed by Hutchinson. By applying this theory to the wrinkling analysis, a “general constitutive law” for studying plastic wrinkling is given, as shown in Equation 2.30. Moreover, with the “J2 flow theory”, the incremental plane-stress moduli $\bar{L}^{\alpha\beta\kappa\gamma}$ can be calculated with Equation 2.31.

The letter “S” in Equation 2.36-a represents the wrinkling region with a thickness t where the wrinkling phenomena occur. Equation 2.36-a is determined by Equations 2.30 to 2.35. “ $\dot{K}_{\alpha\beta}$ ” (Equation 2.33) and “ $\dot{E}_{\alpha\beta}$ ” (Equation 2.32) denote the “bending strain” and “stretching strain”, respectively. In Equations 2.32 and 2.33, $\dot{U}_{\alpha \text{ and } \beta}$ ($\alpha = 1, \beta = 2$) represents the incremental displacements in the defined surface coordinate directions x_1 and x_2 , which are illustrated in Figure 2-26. Additionally, w is the incremental buckling displacement in direction x_3 (normal to

the centre of the investigated wrinkling region). Furthermore, $b_{\alpha\beta}$ is the curvature tensor of the wrinkling area before buckling initiation (pre-buckling state). The ‘‘comma’’ denotes covariant differentiation regarding in-plane surface coordinates (see Figure 2-26). Incremental stress results $\dot{N}_{\alpha\beta}$ and bending moments $\dot{M}_{\alpha\beta}$ are given in Equations 2.34 and 2.35.

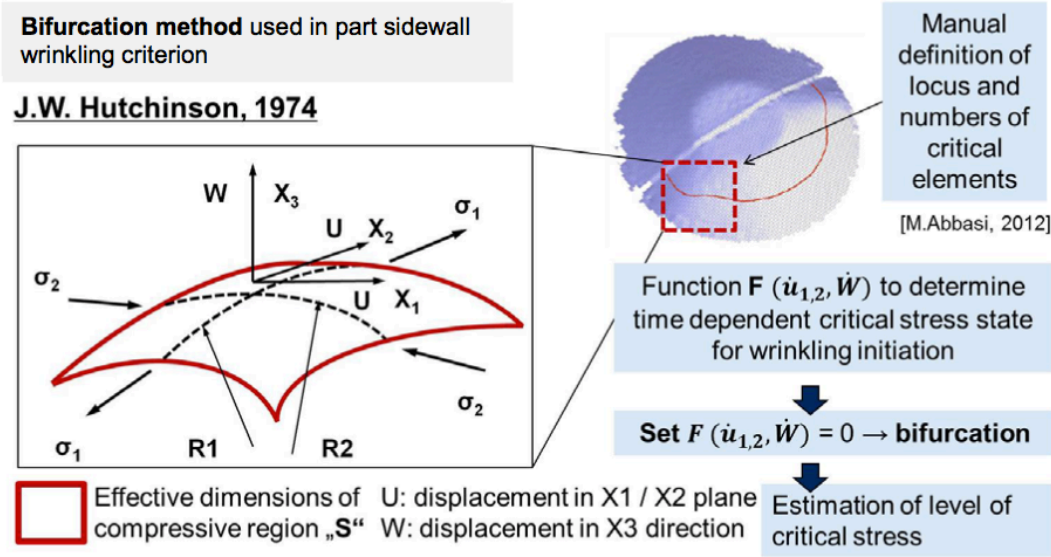


Figure 2-18: Application of bifurcation method to predict wrinkling initiation when using the conical-cup test [Lie16]

$$\dot{\sigma}^{\alpha\beta} = \bar{L}^{\alpha\beta k\gamma} \dot{\epsilon}_{k\gamma} \quad (2.30)$$

$$\bar{L}^{\alpha\beta k\gamma} = L^{\alpha\beta k\gamma} - \frac{L^{\alpha\beta 33} L^{33 k\gamma}}{L^{3333}} \quad (2.31)$$

$$\dot{E}_{\alpha\beta} = \frac{1}{2} (\dot{U}_{\alpha,\beta} + \dot{U}_{\beta,\alpha}) + b_{\alpha\beta} \dot{W} \quad (2.32)$$

$$\dot{K}_{\alpha\beta} = -\dot{w}_{,\alpha\beta} \quad (2.33)$$

$$\dot{N}_{\alpha\beta} = t \bar{L}_{\alpha\beta k\gamma} \dot{K}_{k\gamma} \quad (2.34)$$

$$\dot{M}_{\alpha\beta} = \frac{t^3}{12} \bar{L}_{\alpha\beta k\gamma} \dot{K}_{k\gamma} \quad (2.35)$$

$$F(\dot{u}_{\alpha\beta}, \dot{w}) = \int_s \left\{ \frac{t^3}{12} \bar{L}_{\alpha\beta k\gamma} \dot{K}_{\alpha\beta} \dot{K}_{k\gamma} + t \bar{L}_{\alpha\beta k\gamma} \dot{E}_{\alpha\beta} \dot{E}_{k\gamma} + N_{\alpha\beta} \dot{u}_{3,\alpha} \dot{u}_{3,\beta} \right\} dS \quad (2.36-a)$$

$$F(\dot{u}_{\alpha\beta}, \dot{W}) = \frac{1}{2} St \left(\frac{t}{L} \right)^2 \{u\}^T [M] \{u\} \quad (2.36-b)$$

$$[M] = \begin{pmatrix} M_{11} & M_{12} & M_{13} \\ M_{21} & M_{22} & M_{23} \\ M_{31} & M_{32} & M_{33} \end{pmatrix} \Rightarrow \det[M] = 0 \quad (2.37)$$

According to Hutchinson et al., the onset of buckling occurs when the ‘‘bifurcation function’’ $F(\dot{u}_{\alpha\beta}, \dot{W})$ described in Equation 2.36-b becomes zero. By considering ‘‘failure models’’ (assumed sine-wave-shaped wrinkles described by the ‘‘short-wavelength shallow’’ model) in three major principal directions (namely x_1 , x_2 , and x_3), the ‘‘buckling function’’ $F(\dot{u}_{\alpha\beta}, \dot{W})$ can be determined. Details of the failure models can be found in [Nea90]. Here, $\{u\}$ indicates a

“displacement amplitudes” vector that contains the relative displacement amplitude in three directions (x_1 , x_2 , and x_3). In this way, the plastic buckling can be analysed using linear-buckling methods, it means that, when the value of $\det[M]$ equals zero, wrinkling begins to occur.

Furthermore, based on the assumption that wrinkles are aligned with one of the principal curvatures, the critical value of the compressive stress (both in the first and second principal directions) can be simplified and calculated with Equation 2.38 [Hut74]. Here, E_s denotes the secant modulus, and E_t is the tangential modulus.

$$\begin{aligned}\sigma_1^{cr.} &= \frac{1+r}{\sqrt{3(1+2r)}} \frac{t}{R_2} \sqrt{E_s E_t} \\ \sigma_2^{cr.} &= \frac{1+r}{\sqrt{3(1+2r)}} \frac{t}{R_1} \sqrt{E_s E_t}\end{aligned}\quad (2.38)$$

In addition, the critical strains at the onset of wrinkling can also be determined by using Equation 2.39. Firstly, the loading ratio ρ (also called “strain path”; defined as $\varepsilon_1/\varepsilon_2$) during the pre-wrinkling stage remains proportional, which can be proved through experiments. Furthermore, assuming that the flow curve of a sheet metal material obeys Hollomon’s power law, the critical strain can be expressed using Equation 2.39. Here, the critical strain is only shown in the first principal direction.

Equations 2.38 and 2.39 show that the onset of buckling depends not only on the material properties (namely “strain-hardening coefficient” and “mean vertical anisotropy”), but also on the geometry of the wrinkling area (e.g. the local curvature of component and sheet thickness).

$$\varepsilon_1^{cr.} = \frac{1}{\sqrt{3}} \frac{\sqrt{(1+2r)}}{1+r+\rho r} \sqrt{n} \frac{t}{R_1}\quad (2.39)$$

Table 2-2 summarises the influencing factors of the wrinkling/buckling analysis. According to the analysis models of J.W. Hutchison and A. Selman [Sel99], five factors in total do reveal a significant effect on the wrinkling/buckling process, namely “strain path” (during the pre-wrinkling process), “sheet thickness”, “local curvature”, “strain-hardening coefficient”, and “mean vertical anisotropy”.

Table 2-2: Factors that affect the effective stress and strain value at the onset of wrinkling

Strain path in the pre-wrinkling process:	ρ
Sheet thickness:	t
Local curvature:	$\frac{1}{R_1}, \frac{1}{R_2}$
Strain-hardening coefficient:	n
Mean vertical anisotropy:	$R_{ave.}$

2.3.2.2 Cao's energy method for determining the critical stress level

Cao's energy method is a widely used approach for determining the critical compressive stress at the onset of wrinkling. Usually, Cao's model is applied to calculated critical compressive stress based on Yoshida specimen. Then the determined critical value will be used in the FEA to predict wrinkling initiation [Cao97]. However, before introducing Cao's energy method, S. P. Timoshenko's energy method introduced in 1936 should be mentioned. By employing Timoshenko's energy method, the elastic buckling of thin plates and shells has been intensively studied with boundary conditions [Tim85].

With this energy method, the critical buckling condition can be assessed by balancing the "internal energy of the buckled plate" ΔU^C with "the work performed by the in-plane membrane forces" ΔT^C . This means that the investigated plates or shells remains in a stable equilibrium if the "internal energy" for every possible assumed deflection is larger than "the work produced by membrane forces". Therefore, the stability state for the topic of elastic buckling can be expressed in Equation 2.35 as follows:

$$\Delta T^C \leq \Delta U^C \quad (2.35)$$

Energy method used in the sidewall wrinkling criterion

J. Cao, 2000

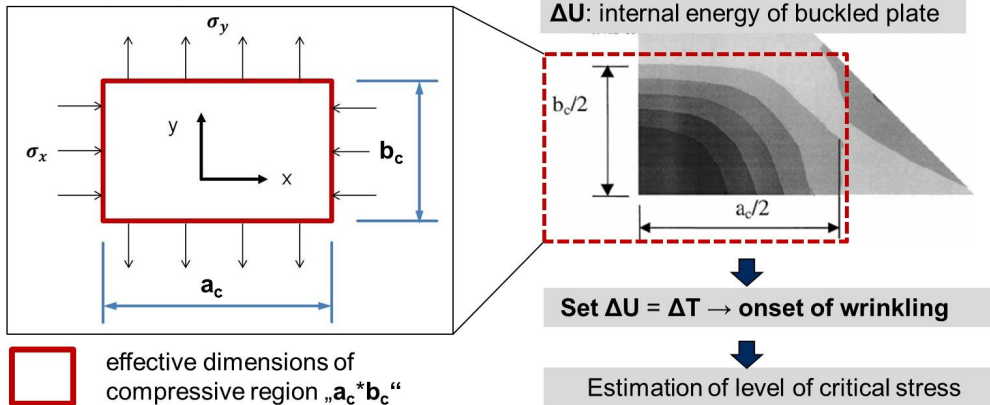


Figure 2-19: Application of bifurcation method to predict the onset of wrinkling using Yoshida's specimen [Lie16]

Cao's study aims to investigate the onset of wrinkling based on Timoshenko's energy method while taking possible boundary conditions (for example, the "effective dimensions of the compressive region" in Figure 2-26) into account. However, Cao's energy model can only predict wrinkles of second order without considering the local curvature of a wrinkling area. In other words, the specimens validated with Cao's energy model (e.g. the Yoshida buckling test, see Figure 2-27, and square-cup test) all have the flat geometry of the wrinkling area in common. In her study, Cao firstly established a general formulation regarding wrinkles of second order for the "flat plate" scenario. Later, she and X. Wang applied this wrinkling criterion to the case study of

the Yoshida buckling test and square-cup test [Wan00b]. Furthermore, this energy approach was also applied to the Yoshida buckling test in which one side of sheet metal component stay in contact with the tool surface [Cao97].

For the “curved sheet” scenario, namely in the case of geometry with a local curvature, another analytical model (not dependent on the energy approach) was developed by X. Wang and J. Cao in [Wan00a]. In this chapter, only “Cao’s energy approach” is reviewed. It is important to know that the following assumptions must first be considered to establish “Cao’s energy model” for determining critical compressive stress:

- 1) The pre-buckling stress state in the sidewall area is assumed to be in the membrane state, so shear strain and stress are ignored.
- 2) All formulations follow the thin-plate and shell theory. Therefore, it is assumed that the sheet thickness before bending and all the acting stress states through the thickness are uniform.
- 3) The expected strain is low, and it is assumed that the characteristic wavelength is greater than the thickness of the plate, enabling the strain measurement given by the Donnell–Mushtari–Vlasov (DMV) approximation to be used.
- 4) Deformation theory is used in the analysis because it is assumed that the external loading is proportional between force and displacement before the onset of buckling.

Figure 2-26 illustrates a “rectangular-plate model” in a tensile-compressive stress state (σ_x indicates compressive stress and σ_y is tensile stress acting on the investigated region) with an effective length a_c and width b_c . The basic concept of Cao’s energy approach is that, if the value of “internal energy of the buckled plate” ΔU is equal to the value of the “work performed by the in-plane membrane forces” ΔT , the “onset of wrinkling” occurs, see Equation 2.36. Here “d,e = 1,2,3,...” means that the letter d and e can be setted with different number to express the wrinkling models that have relationship with ΔT^C and ΔU^C in Equation 2.38 and 2.39.

$$\Delta T^C = \Delta U^C \quad (2.36)$$

$$w = \frac{w_0}{2} \sin\left(\frac{d\pi x}{a_c}\right) \left(1 - \cos\left(\frac{2e\pi y}{b_c}\right)\right), \quad d, e = 1, 2, 3, \dots \quad (2.37)$$

$$\Delta T^C = -\frac{t}{2} \int_0^{b_c} \int_0^{a_c} \left(\sigma_x \left(\frac{\partial w}{\partial x}\right)^2 + \sigma_y \left(\frac{\partial w}{\partial y}\right)^2 \right) dx dy \quad (2.38)$$

$$\Delta U^C = -\frac{D}{2} \int_0^{b_c} \int_0^{a_c} \left(\sigma_x \left(\frac{\partial w}{\partial x}\right)^2 + \sigma_y \left(\frac{\partial w}{\partial y}\right)^2 - 2(1-\nu) \left(\frac{\partial^2 w}{\partial x^2} \frac{\partial^2 w}{\partial y^2} - \left(\frac{\partial^2 w}{\partial x \partial y}\right)^2 \right) \right) dx dy \quad (2.39)$$

$$\text{Bending stiffness } D \Rightarrow \text{Elastic wrinkling } D^E = \frac{Et^3}{12(1-\nu^2)} \quad (2.40\text{-a})$$

$$\Rightarrow \text{Plastic wrinkling} \quad D^P = \frac{4EE_t}{(\sqrt{E} + \sqrt{E_t})^2} \times \frac{t^3}{9} \quad (2.40-b)$$

To calculate the desired “internal energy of the buckled plate” ΔU and “the work performed by the in-plane membrane forces” ΔT , a “failure model” $w = f(x, y)$ must first be established in Equation 2.37. Here, w_0 is a constant representing the amplitude of the deflection. The letter d indicates the wave number in the direction of the compressive stress. Furthermore, e is the wave number in the direction of the tensile stress.

The critical value of ΔT and ΔU under the given failure model can be calculated using Equations 2.38 and 2.39. Letter D in Equation 2.39 denotes the “bending stiffness”. In the case of “elastic wrinkling”, the value of the elastic modulus can be directly used to calculate the “elastic bending stiffness” D^E . By calculating the “plastic bending stiffness” D^P , the value of the elastic modulus in Equation 2.40-a must be modified with the “von Karman modulus” E_0 , which is defined as:

$$E_0 = \frac{4EE_t}{(\sqrt{E} + \sqrt{E_t})^2} \quad (2.41)$$

Finally, by equating the values of the energies from Equations 2.38 and 2.39 (by $\Delta T = \Delta U$), the critical value of the compressive stress σ_x can be calculated by a given σ_y .

2.3.2.3 Kim’s energy method for determining the critical stress level

J.B. Kim et al. [Kim03] proposed a new method for predicting the onset of wrinkling in flat sheets by defining a “wrinkling factor” W_f . He pointed out that the onset of wrinkling can be influenced by stress, strain values, the thickness of the sheet metal, strain increment, part geometry, and boundary conditions. The following assumptions are presented for using his “wrinkling factor” W_f to detect the onset of wrinkling in complex sheet-forming processes:

- Wrinkling takes place in a flat sheet with a fixed, flat geometry (see Figure 2-28-b) However, according to the works of J. B. Kim, the influence of the sheet geometry was not considered by the “wrinkling factor” W_f since it is difficult to consider the geometry of the investigated area in a general manner.
- Wrinkling occurs as a “sine-wave contour” with a fixed wavelength.
- Wrinkling occurs in the direction of the minor principal stress: that is, in the direction of the maximum compressive stress (see Figure 2-28-b and Figure 2-28-d).
- It is assumed that the material properties in the specimen are considered uniform.

The “wrinkling factor” W_f is defined as a ratio of “deformation energy along the primary path” E_p and “deformation energy along the secondary path” E_s in Equation 2.42. Here, four influencing factors ($\frac{\sigma}{\sigma_y}$, ε , $\Delta\varepsilon$, and $\frac{L}{t}$) are taken into account. According to Kim’s theory, when wrinkling

occurs, the value of ratio $E_{pri.}/E_{sec.}$ Is greater than “1”. This means that bifurcation occurs when the calculated deformation energy along the primary path is greater than the calculated energy along the secondary path (see Figure 2-27-a).

$$W_f = \frac{E_{pri.}}{E_{sec.}} = W\left(\frac{\sigma}{\sigma^Y}, \varepsilon, \Delta\varepsilon, \frac{L}{t}\right); W_f > 1: \text{bifurcation occurs} \quad (2.42)$$

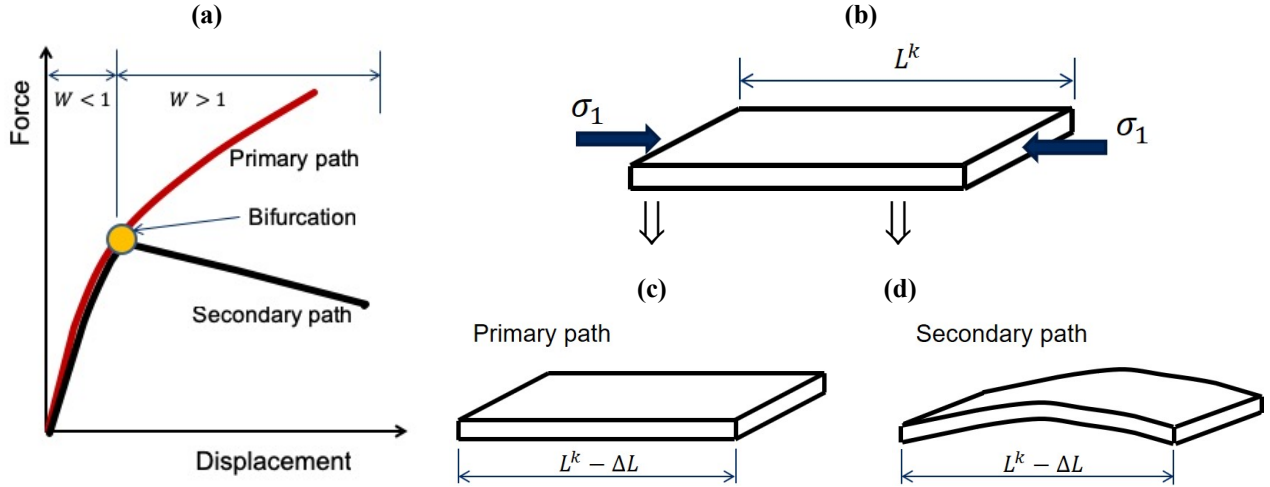


Figure 2-20: Kim’s energy model in [Kim03]: (a) defined primary/secondary path and bifurcation point in Kim’s energy model; (b) assumed specimen under uniaxial compressive stress; (c) deformed specimen along the primary path; (d) deformed specimen along the secondary path

The “deformation energy along the primary path” while considering a uniform sheet subjected to uniaxial compression can be calculated using Equation 2.43-a. Here, “ σ_2 ” indicates the direction of uniaxial compressive stress, and ε_2 is the displacement caused by compressive stress (see Figure 2-28-c), respectively. b_c , t , and L^k are the width, thickness, and length of the assumed uniform sheet, respectively. According to the assumed wrinkling model described in Figure 2-28-b, Equation 2.43-a can be simplified without considering “ σ_1 ” since only the uniaxial compressive stress “ σ_2 ” in Figure 2-28-b is taken into account. Here, $\Delta\varepsilon_2$ indicates the incremental strain in the uniaxial compression direction, and this $\Delta\varepsilon_2$ can be expressed with $\delta\mu/L^k$. Is the length of the assumed specimen, while $\delta\mu$ is the incremental displacement in the direction of σ_2 . The “deformation energy along the primary path” can therefore be simplified as shown in Equation 2.43-b.

$$E_{pri.} = \int_v \sigma_{ij} \Delta\varepsilon_{ij} dv = (\sigma_1 \Delta\varepsilon_1 + \sigma_2 \Delta\varepsilon_2) b_c t L^k \quad (2.43-a)$$

$$\Rightarrow E_{pri.} = \int_v \sigma_{ij} \Delta\varepsilon_{ij} dv = \sigma_2 \Delta\varepsilon_2 b_c t L = \sigma_2 \frac{(\delta\mu)}{L^k} b_c t L^k = \sigma_2 b_c t (\delta u) \quad (2.43-b)$$

Furthermore, to determine the “deformation energy along the secondary path” shown in the Figure 2-27-d, a sheet buckled along the sine wave was assumed. The deformation energy along the

secondary path can be expressed in Equation 2.44-a. As mentioned above, the “ σ_1 ” in Equation 2.44-a will also not be considered for calculating the “deformation energy along the secondary path”. Equation 2.44-a can be simplified as Equation 2.44-b, where M is the moment that can be calculated by considering the case of elastic and plastic wrinkling as shown in Equations 2.45-a and 2.45-b.

$$E_{sec.} = \int_L \frac{1}{2} M d\theta + \sigma_1 \Delta \varepsilon_1 b_c t L^k = \int_L \frac{1}{2} M \frac{d\theta}{dx} dx + \sigma_1 \Delta \varepsilon_1 b_c t L^k \quad (2.44-a)$$

$$\Rightarrow E_{sec.} = \int_L \frac{1}{2} M \frac{d\theta}{dx} dx \quad (2.44-b)$$

$$\text{Bending stiffness} \Rightarrow \text{Elastic wrinkling} \quad M^E = \frac{EI}{\rho(1-v^2)} \quad (2.45-a)$$

$$D \Rightarrow \text{Plastic wrinkling} \quad M^P = \frac{4EE_t \times I}{(\sqrt{E} + \sqrt{E_t})^2 \times \rho(1-v^2)} \quad (2.45-b)$$

$$w = w_0 \sin\left(\frac{\pi x}{L}\right) \quad (2.46)$$

$$\theta = \frac{dw}{dx} = \frac{\pi w_0}{L} \cos\left(\frac{\pi}{L} x\right) \quad (2.47)$$

$$\frac{1}{\rho} = \frac{d\theta}{dx} = \frac{d^2 w}{d^2 x} = -\frac{\pi^2 w_0}{L^2} \sin\left(\frac{\pi}{L} x\right) \quad (2.48)$$

In addition, to calculate the “deformation energy along the secondary path”, a “failure model” ($w = f(x)$) should also be introduced in Equation 2.46. Here, w_0 is a constant representing the amplitude of the deflection. Compared to the “failure model” used in Cao’s energy model, only the sine wave in the direction of compression is considered. In addition, only one sine wave is applied in Equation 2.46. Furthermore, Equations 2.47 and 2.48 must be applied to calculate the value for moment M . θ is defined as the relative angular displacement of the buckled sheet. The slope and curvature $\frac{1}{\rho}$ can be calculated in accordance with Equations 2.47 and 2.48.

In summary, when the “deformation energy along the primary path” E_{pri} . And “deformation energy along the secondary path” E_{sec} . Are equal, the critical compressive stress can be determined at the defined “bifurcation point” as shown in Figure 2-28-a.

3 Objective of this Thesis

In this thesis the main objective is to develop a new wrinkling criterion to predict the surface quality of a drawn part during forming process. To gradually achieve the final goal, five tasks were arranged in this thesis. Each task was treated individual in corresponding chapter. The relationship between the main objective and five tasks are illustrated in Figure 3-1. This new wrinkling criterion is stress based and termed as the Double-Surface Compressive Stress Approach (DSCS-approach). This DSCS-approach was developed to predict the formation of wrinkles and strong waviness during stretch and deep drawing through FEA, especially for predict the surface quality regarding exterior parts in automobile industry. According to the FEA and validation results, this newly developed approach yields better results than the conventional strain based wrinkling criterion which was widely used in commercial software since many years.

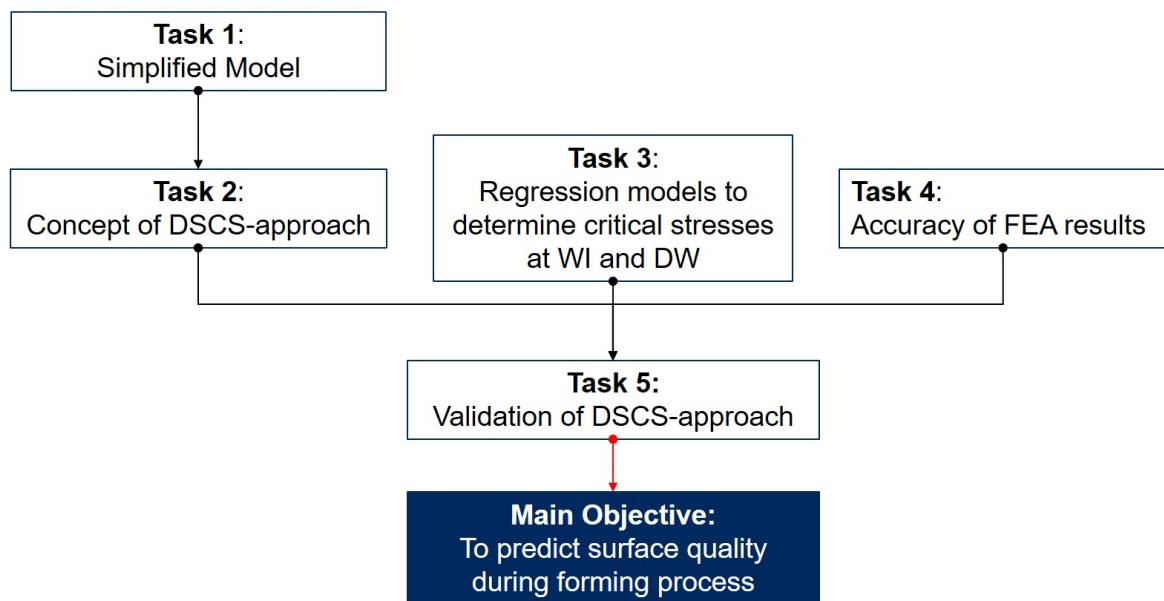


Figure 3-1: Main objective and five tasks in this thesis

In recent years, the development of computer hardware technology has given us new possibilities for performing sheet metal forming simulations with relatively high degrees of quality in predicting process results. In this thesis, a novel stress-based model is used to predict the formation of wrinkles of second order in FEA. This novel approach was desired because “classical” theoretical models described in Chapter 2 do involve too many parameters that cannot be measured precisely by performing physical experiments in order to calculate any critical stress values (and thereby to predict wrinkling formation). The accuracy of the numerical simulation codes in the field of sheet metal forming of today therefore delivers the key to this scientific work. The simulation codes were optimised during recent decades using appropriate and precise material parameters, material and friction models aiming high precision in prediction of forming and spring back results. The results presented in Chapter 7 demonstrate that gained simulation results are to

be evaluated as highly reliable, so they can be directly compared with experimental results obtained from simple tests such as YBT and CCT.

The main purpose of the work undertaken was to develop a new wrinkle criterion for predicting surface defects during the deep drawing process. Later, the developed wrinkling criterion will be implemented as a UDV file in AutoForm to validate the position of the wrinkles and the time at which wrinkling will occur. The three parts comprising outer and inner panels (see Figure 3-2) from a car's body will be validated. To achieve this primary objective, five tasks should be completed and are listed in this section.

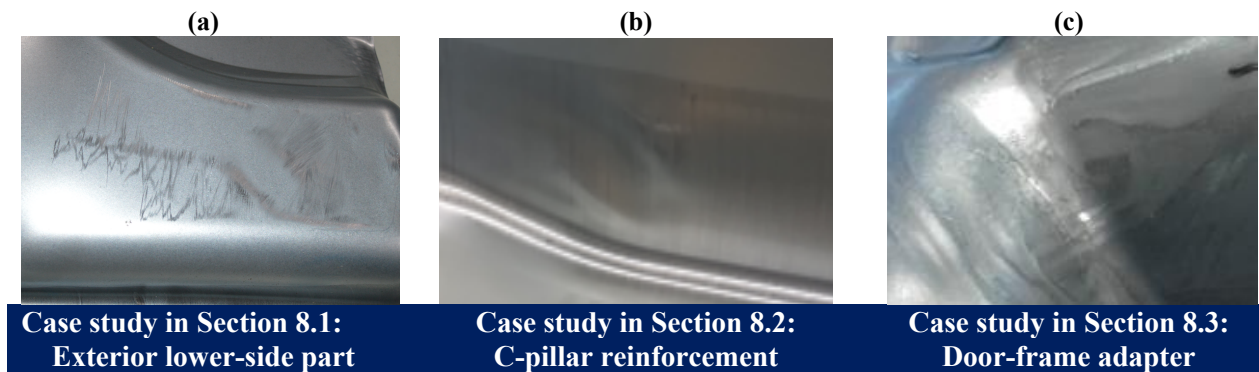


Figure 3-2: Outer and inner panel from car body parts with three different kinds of surface defect patterns: (a) surface low; (b) small wrinkles (visible waviness); (c) severe surface distortion originating from wrinkles of second order

The first task of this work was to create a model or method for describing the overall wrinkling process (wrinkling of second order). According to the traditional method for predicting wrinkles as described in Section 2.3, it seems necessary to evaluate the entire wrinkling process. Normally, a wrinkling limit curve is given for determining whether wrinkling occurred or not. Also, this thesis claims to elaborate appropriate models to identify different kinds of surface defects based on particular in-plane stress conditions as depicted in Figure 3-2, but also for analysing the course of forming process tending to induce any wrinkle formation. To accomplish this task, the following work described in Chapter 5 was to be completed:

- 1) Experiment and simulative investigation to analyse the regularity of wrinkle formation using the Yoshida Buckling Test (YBT) and Conical-Cup Test (CCT)
- 2) Using the “beam-spring” model to simplify the analysis of the stress state
- 3) Definition of a two-phase process course consisting of “wrinkling initiation” and subsequently “developed wrinkling” to describe wrinkling by means of the phenomena observed in the experiments.

Although the new method has yielded satisfying results by predicting wrinkles of second order in the laboratory, it is not suitable for predicting the occurrence of wrinkles in real manufacturing

processes for car body parts in the press shop since the influence of the one side tool contact on the quality of the drawn part during the forming process must also be taken into account. So, it was important to know whether the DSCS-approach can be used to predict the formation of wrinkles with consideration of a one or double side instantaneous tool contact situation.

The second task to solve was to continue developing a suitable software integration of the new model into the post-processing software. In other words, the concept of the DSCS-approach must be “translated” into the software’s language. To complete this task, the following work was to be conducted as described in Chapter 5:

- 1) Influence of tool contact on the simplified model (described in Chapter 4)
- 2) Definition of a two-stage process course consisting of “developed wrinkling” and “wrinkling initiation”, to be finally analysed and displayed in the post-processing code of AutoForm FEA software
- 3) Development of the DSCS-approach considering both sides (outer and inner side) of sheet metal surface compressive stress
- 4) Studying the applicability of the DSCS-approach to post-processing of conventional FEM software

The third task was to establish a complete regression model based on the DSCS-approach that considers important parameter. For this relevant simulation parameters such as material properties and geometric details of sheet metal component disclosing a significant influence on wrinkling formation were defined to calculate the critical compressive surface stress. The DoE (Design of Experiment) method was applied to create an empirical regression model considering such influencing factors. To complete the task, the following work (described in Chapter 6) was to be conducted:

- 1) Selection of important factors for regression model
- 2) Development of empirical regression model from DoE (Design of Experiments) using Minitab software

The fourth task involves establishing the boundary conditions and logic of the DSCS-approach in conventional FEA software (such as AutoForm R6). The developed DSCS-approach does not work properly in AutoForm software unless important boundary conditions are incorporated. The first step in this section is therefore to define the important boundary conditions for the DSCS-approach (i.e. the critical strain values for distinguishing between elastic and plastic wrinkles, and the critical value of stress at the defined “wrinkling initiation” and “developed wrinkling”). According to results gained from YBT tests and mini conical-cup tests, wrinkles or surface defects

can disappear in the elastic deformation state. To complete the task, the following work (described in Chapter 8) was to be undertaken:

- 1) Definition of confidence range without evaluation in post-processing
- 2) Definition of area to be investigated in the FLD
- 3) Setting of critical stress values for both phases “wrinkling initiation” / “developed wrinkling”

The fifth task involves ensuring the accuracy of the simulation results, checking reliability of the simplified model (Task 1) and the usability of the DSCS-approach in general (Task 2). To complete this task, the following work (described in Chapter 7) was to be undertaken:

- 1) Definition of material parameters and application of the appropriate material model
- 2) Optimisation of process parameters in FEA compared to experiments

At last, the above mentioned 5 tasks and corresponding results are listed in Table 3-1.

Table 3-1: Five tasks and corresponding expected results

Task	Presented in	Name of the Task	Expected results
1	Chapter 4	Simplified model	create a model or method for describing the wrinkles of second order
2	Chapter 5	Concept: DSCS-approach	based on the simplified model to create an approach for describing the overall wrinkling process
3	Chapter 6	Regression models: DSCS-approach	By using linear-regression models which determined form DoE method considering sheet thickness and local curvature to calculate critical stresses at wrinkling initiation and developed wrinkle
4	Chapter 7	Accuracy of the FEA results	Though ensuring the material models, boundary conditions in FEA and process parameters to ensure the accuracy of FEA results
5	Chapter 8	Validation: DSCS-approach	Validate the DSCS-approach using real industrial parts

In conclusion, in five steps the DSCS-approach can be used in practice. In this thesis three Materials, namely HC300LA, HC420LA and DX54D will be validated with corresponding drawn parts form automobile industry. The DSCS-approach is auch situable for aluminium Material, like AA6016, and other sheet materials, like sandwich sheet metal material.

4 Development of a simplified model for predicting wrinkles of second order

As described in Chapter 3, the main objective of this thesis is to develop a stress based wrinkling criterion to be applied on numerical simulation of deep and stretch drawing processes. Firstly, in the following section 4.1, the motivation for developing a new stress-based wrinkling criterion will be introduced. Sections 4.2 to 4.3 will present a simplified model for detecting wrinkle formation based on the development of compressive stress development on the inner and outer surface of sheet metal component. By studying the development of surface compressive stress during the wrinkling process, two points (in time) of “wrinkling initiation” and “developed wrinkling” can be defined, which offers an opportunity not only to investigate slight surface defects like “wrinkling initiation”, but also severe wrinkling in a plastic manner. By applying the simplified model introduced in Chapter 4, both surface defects “wrinkling initiation” and “developed wrinkling” can thus be investigated and evaluated using the same criterion.

4.1 Motivation

In this section, the applicability of two conventional criteria (“force–displacement curve” and “strain based criteria”) are discussed. Experimental results have shown that following both wrinkling criteria cannot predict emergence of wrinkles accurately being used in FEA.

The definition of a so called “turning point” as a wrinkling criterion is demonstrated in Section 4.1.1, in which the definition of the “turning point” using a force–displacement curve obtained from the conventional uniaxial tensile test results is presented. The “turning point” phenomenon was shown in Fig. 4-1-a. However, experimental results show that the appearance of the “turning point” phenomenon observed by evaluating the force–displacement curve is affected not only by the geometry of the tested specimen, but also by the tested materials. Therefore, the use of “turning points” as the onset of buckling or wrinkling is limited.

The use of a strain based wrinkling criterion is demonstrated in section 4.1.2, in which experimental results are presented in order to prove that the strain based wrinkling criterion “wrinkling limit curve” (WLC) in FLD could not accurately predict the onset of wrinkling. The results of the experiments conducted can directly prove the statement of Li [Li00], that the use of strain based wrinkling criteria to predict wrinkle formation is limited since critical strain values observed in the case of wrinkling phenomena are not a material property. Geometry of specimen much more influences the location of the wrinkling limit curve within the FLD.

4.1.1 Limitation of the criteria based on the force–displacement curve

According to the works of Schleich [Sch09], the phenomenon of the “turning point” indicated the “beginning of bifurcation” and can thus be defined as the “onset of buckling” to a certain extent. This conclusion is based on the results of experiments being performed with aluminium sheet metal AA6016 and the geometry of the nine specifically in shape modified Yoshida specimens.

The influence of the “specimen topology”, “test materials” on the “turning point” phenomenon.

The “turning point” phenomenon based on the force–displacement curve is shown in Figures 4-1-a and 4-1 c. When the force F measured in the tensile test reaches a critical value, the force first decreases before rapidly increasing again. This kind of change in the force–displacement curve was defined as a “turning point” in [Sch09]. Ton [Ton01] called this phenomenon the “unstable stage” (see. Figure 4-1-a), noting that the phenomenon of decreased force can be observed in real tensile tests. However, the decreased force cannot be observed by performing FEA for a similar load case.

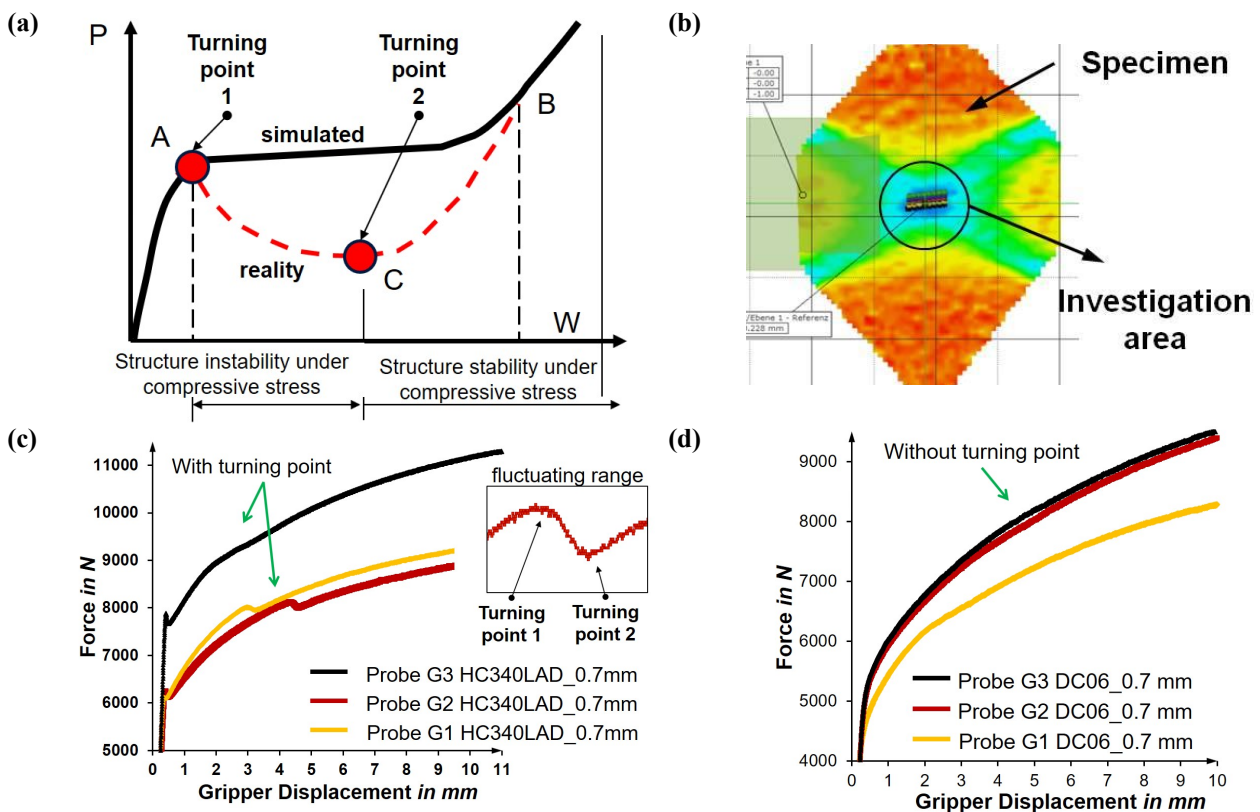


Figure 4-1: (a) Illustration of the “unstable stage” by Ton in reality and in FEA [Ton01]; (b) M-YBT specimen and area investigated using GOM ARAMIS optical-measurement system; (c) experimental results of HX340LAD with 0.7 mm thickness using three kinds of M-YBT specimen; (d) experiment results of DC06 with 0.7 mm thickness using three kinds of M-YBT specimen

Grote [Gro03] explained this phenomenon with the help of structural stability. According to the theory of structural instability, the force decreases after the beginning of bifurcation. He explained that the presence of tensile stress (acting on the specimen) can stabilise the structure of the

specimen, which in turn leads to an increase in force after the observed specimen instability. Due to the continuous action of tensile stress on the specimen, the structural stability of the specimen can be maintained until the end of the experiment. The phenomenon of “the force decreasing rapidly and increasing again” was defined by Grote as “fluctuating range”, from point A to point B in Figure 4-1-a.

However, Schleich’s approach of detecting the onset of buckling by applying the “turning point” cannot be used as a criterion. After testing sheet metal materials HC340LA (thickness 0.7 mm) and DC06 (thickness 0.7 mm) using three different M-YBT specimen geometries, it could be confirmed that the “turning point” phenomenon does not appear inconsistently in each tested sheet metal material (see Figure 4-1-d). The used specimen geometries G1, G2, and G3 are illustrated and described in [Dam14].

For sheet metal material DC06 (0.7 mm thickness), the aforementioned “turning point” (or “unstable phase”) phenomenon could not be observed (Figure 4-1-d). No matter how the specimen changes, no “turning point” was identified during tests performed. In contrast, by experimenting with HC340LA material (0.7 mm thickness), this phenomenon can frequently be observed by using different modified Yoshida specimens (Figure 4-1-c).

Therefore, the application of the “turning point” based on the force–displacement curve (under a uniaxial tensile load) in defining buckling initiation or wrinkling initiation is limited. The appearance of the turning point depends not only on the geometry of the specimen, but also on the material properties being examined.

Detecting the onset of buckling or wrinkling by applying the $d(H^w)/d(T)$ approach

A perspective approach for defining the onset of wrinkling when using M-YBT specimens was not found until 2020. According to the works of Chen [Che16], it can be proved that the approach based on the “gradient of wrinkling height development $d(H^w)/d(T)$ ” (see Figure 4-2) is much more robust than the approach based on the “turning point” for predicting the onset of wrinkling using M-YBT specimens. Here, H^w indicates the buckling height measured using the GOM ARAMIS optical measurement system, where “T” indicates the total time of an experiment. The displacement of the upper tool in the tensile machine (gripper) can be calculated by setting a constant speed for the tensile test and taking photographs every second. However, although this method is much more robust than the “turning-point-based” approach, it still cannot be directly used in FEA. More information and details are discussed in the following section of this chapter.

To better understand the approach of the “gradient of wrinkling-height development $d(H^w)/d(T)$ ”, the results of M-YBT (sheet material HC420LA with a thickness of 0.6 mm) are first shown in Figure 4-2. Figure 4-2-a depicts the wrinkling height as a function of the calculated gripper

displacement. The first derivation of the wrinkling height “ H^W ” as a function of the calculated gripper displacement is illustrated in Figure 4-2-b. It is obvious that the velocity of the development of wrinkling height “ $d(H^W)/d(T)$ ” reaches a maximum value before subsequently decreasing. Here, the point in time (i.e. the maximum value of $d(H^W)/d(T)$) for the onset of wrinkling was identified using M-YBT.

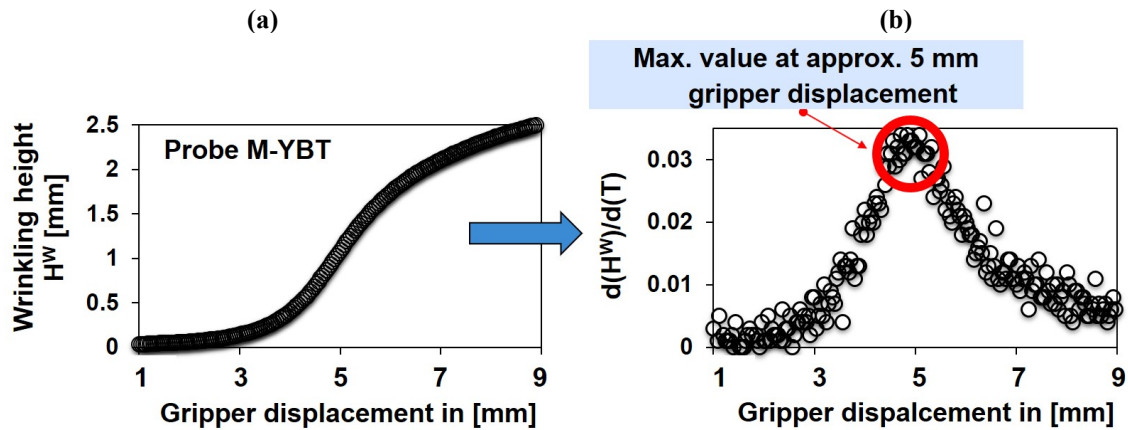


Figure 4-2: (a) Wrinkling height as a function of gripper displacement according to results of M-YBT; (b) definition of maximum velocity regarding the development of wrinkling height as a function of gripper displacement, $d(H^W)/d(T)$

In the following tests, experiments were undertaken in order to identify the relationship between the “ $d(H^W)/d(T)$ ” and the “turning point” by only evaluating the force-displacement curves. Here, the sheet material HC420LA was tested and evaluated with two sheet thicknesses (0.6 mm and 1.0 mm). Used M-YBT specimen geometry is shown in Figure 2-6-b. The experiment results of HC420LA (with a thickness of 0.6 mm and 1.0 mm) are shown in Figure 4-3-a and Figure 4-3-b, respectively.

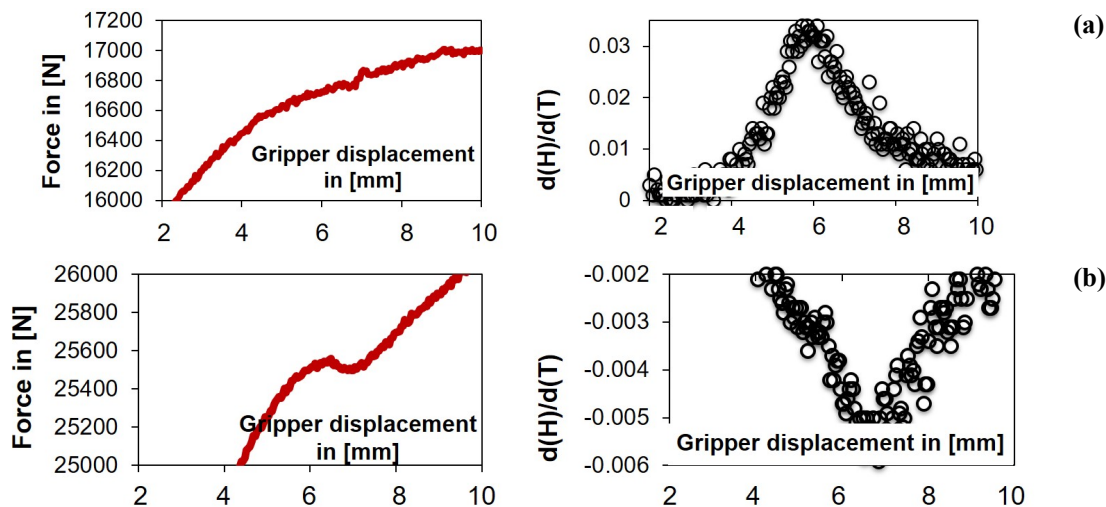


Figure 4-3: Relationship between the “turning point” determined using M-YBT specimens and the “gradient of wrinkling height $d(H^W)/d(T)$ ”: (a) experiment results based on M-YBT specimen with material HC420LA (0.6 mm); (b) experiment results based on M-YBT specimen with material HC420LA (1.0 mm)

Through experiments, it could be proved that the occurrence of this maximum value of $d(H^W)/d(T)$ may be recognized as the “turning point” of the force–displacement curve (see Figure 4-3-a). In this way, the relationship between the “turning point” obtained from the force–displacement curve and the velocity of development of wrinkling height $d(H^W)/d(T)$ is established in [Che16]. The appearance of the maximum value of $d(H^W)/d(T)$ can thus be defined as the “wrinkling initiation”. Although no obvious “turning point” can be discerned in Figure 4-3-b, the onset of buckling can be detected by applying the $d(H^W)/d(T)$ approach. When the gradient of the wrinkling height reaches a maximum value, this point in time is defined as the onset of buckling.

The “ $d(H^W)/d(T)$ approach” and wrinkling phenomenon under uniaxial compressive stress

It is well known that wrinkling not only takes place under tensile compressive stress, but also under uniaxial compressive stress. In this section, the “ $d(H^W)/d(T)$ approach” will be tested to determine whether this approach works in uniaxial compression tests. This test is reviewed in Section 2.1.5 and referred to as the “buckling/bending test” (BBT).

The results based on material HC420LA (sheet thickness 1.0 mm) are shown in Figure 4-4. Figure 4-4-a depicts the tested BBT specimen, which has a length of 190 mm and a width of 50 mm. The effective area (exposed to compressive stress) of the BBT specimen is 90 mm². According to the experiment results (see Figure 4-4-b), a maximum $d(H^W)/d(T)$ value can also be observed in the test using the GOM ARAMIS optical measurement system.

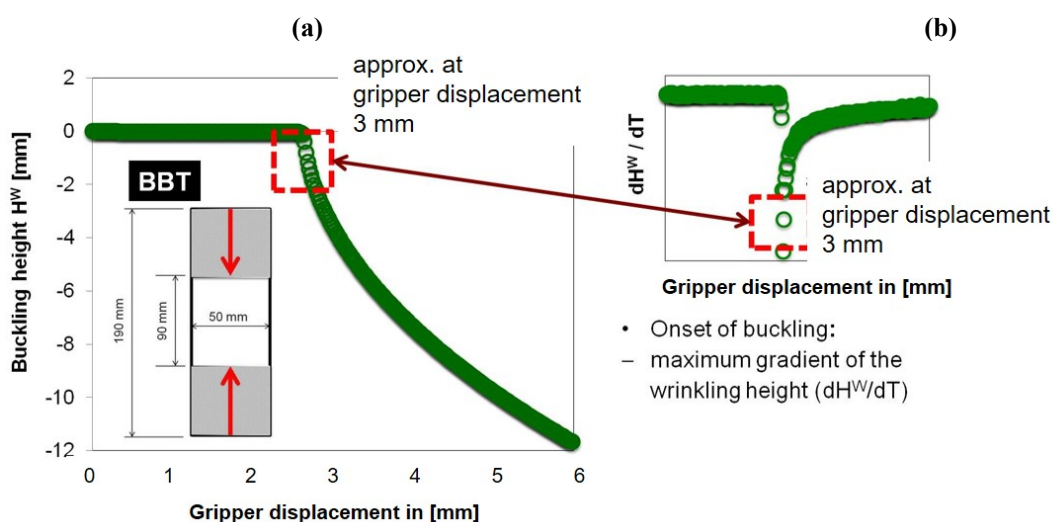


Figure 4-4: Experiment results of the buckling/bending test with sheet metal material HC420LA (thickness 1.0 mm): (a) relationship between wrinkling height H^W and gripper displacement; (b) phenomenon of maximum gradient of wrinkling height $d(H^W)/d(T)$ in buckling/bending test

One phenomenon in the buckling/bending test must be explained. Compared to the M-YBT test, the BBT specimen in the tensile test is only subjected to compressive stress, meaning that there is no tensile stress during the forming process to maintain the structural instability of the BBT

specimen. Therefore, after the maximum force is reached, the force in the BBT test decreases sharply towards the end of the experiment (see Figure 4-13).

The “ $d(H^W)/d(T)$ approach” assumes that $d(H^W)/d(T)$ will continue to reach its maximum until wrinkles occur. This phenomenon is demonstrated and proved by testing several sheet materials with various sheet thicknesses in the M-YBT and BBT tests. The “ $d(H^W)/d(T)$ approach” introduced is suitable for aluminium sheet material AA6016, deep drawing (mild) steels DX54D, DC04, DC06, micro-alloyed steels HC300LA, HC420LA, bake-hardening steel BH180 and BONDAL® sandwich sheet. Some results can be found in [Chen16].

In conclusion, both approaches (“turning point” and “ $d(H^W)/d(T)$ -approach”) can only detect wrinkling initiation under limited conditions in the laboratory. It can be proved that the maximum value of $d(H^W)/d(T)$ indicates the point in time at which the wrinkling area cannot include any more compressive stress. Table 4-1 shows the advantages and disadvantages by determining the wrinkling initiation using the respective “turning point” and “ $d(H^W)/d(T)$ approach”.

Table 4-1: Comparison of different approaches for defining wrinkling initiation in the laboratory

Approaches	Advantage	Disadvantage
Turning point	Can be directly compared to the theory of structure instability	The appearance of the deviation of the curve depends on sheet metal materials and specimen geometries
$d(H^W)/d(T)$	Does not depend on materials or specimen geometry	In the real deep drawn part, the development of wrinkling height cannot be measured.

4.1.2 Limitation of the strain-distribution-based wrinkling criterion

The wrinkling criterion based on strain distribution in FLD has been widely used in the automotive industry to predict and to detect wrinkles in sheet metal parts during metal forming process. In this section, the limitations of strain based criteria are discussed.

“Wrinkling mechanism”, “strain path”, and defined “wrinkling initiation” in FLD

To better understand the concept of the “wrinkling limit curve” (WLC) in FLD, the definition of “wrinkling mechanism” and “strain path” before and after “wrinkling initiation” must first be explained. The “wrinkling initiation” is defined by using the “ $d(H^W)/d(T)$ approach” introduced in Section 4.1.1. According to the results of experiments, the following phenomena can be observed:

- 1) Strain path run through prior defined “wrinkling initiation”: the strain path can be interpreted as a linear function before wrinkling initiation.
- 2) Strain path run through after defined “wrinkling initiation”: the strain path will change due to the altered surface contour in the investigated wrinkling area.

In addition, the phenomenon of the “change of strain path” after wrinkling initiation was observed

in all three wrinkling mechanisms, namely tensile stress induced wrinkles, shear stress induced wrinkles and compressive stress induced wrinkles, that can be observed in the deep drawing process. The details of these three mechanisms are shown in Table 4-2.

Details of the experiments carried out with the M-YBT-K specimen are presented in Figure 4-5-a and Figure 4-5-b. Figure 4-5-c illustrates results from the change in strain path before and after the identified wrinkling initiation (using the $d(H^w)/d(T)$ approach). Figure 4-5-c firstly shows that the strain path changes prior and after the identified wrinkling initiation point (green circle). The red arrow depicts the strain path run through prior wrinkling initiation, while the pink arrow indicates the strain path run through after wrinkling initiation.

Table 4-2: Wrinkling mechanisms and selected specimen geometries

	Investigated specimens	Wrinkling mechanisms
1	Buckling test using modified Yoshida specimen with small shoulder radius (M-YBT-K) [Han14]	Inhomogeneous tensile-stress wrinkling
2	Buckling test using modified Yoshida specimen with wide shoulder radius (M-YBT-G) [Che16]	Shear wrinkling
3	Buckling test with BBT specimen [HOE13]	Compressive stress wrinkling

When the measured data (ε_1 and ε_2) are considered, the strain path before wrinkling initiation can be fitted using the function $\varepsilon_1 = -2.131 * \varepsilon_2$. The M-YBT-K specimen indicates that wrinkles which are caused by inhomogeneous tensile stress (see Table 4-2), can also occur under uniaxial tensile stress together with special specimen geometry. The location of the wrinkling limit curve calculated using the “potential wrinkling” approach in AutoForm is found between the straight lines $\varepsilon_1 = -1 * \varepsilon_2$ and $\varepsilon_1 = -2 * \varepsilon_2$.

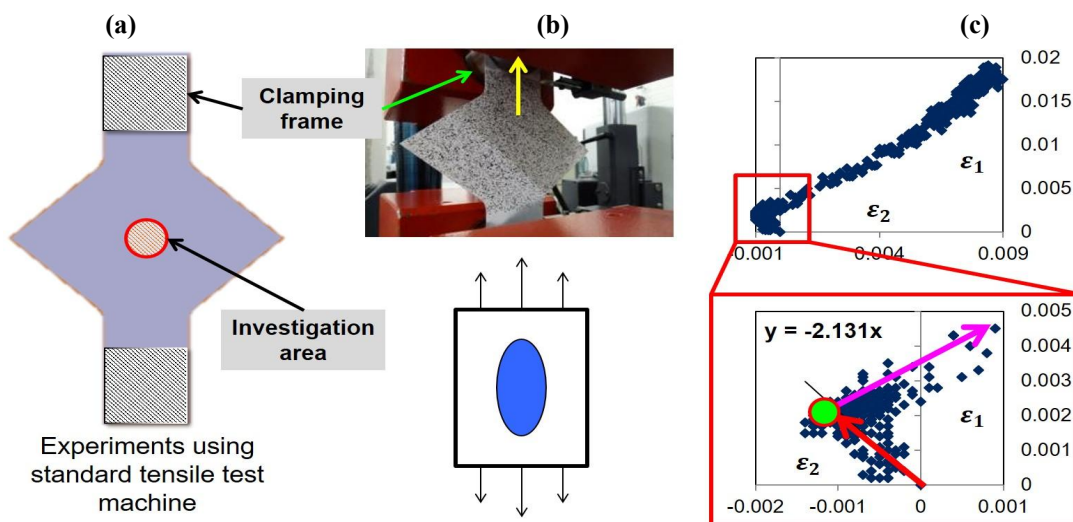


Figure 4-5: (a) Experimental details: M-YBT-K specimen (material HC420LA with 1.0 mm thickness), clamping frame and investigated area; (b) wrinkling mechanism: inhomogeneous tensile-stress wrinkling; (c) defined wrinkling initiation using the $d(H^w)/d(T)$ approach, strain path run through prior (with fit function) and after identified wrinkling initiation in FLD

The details and results of the experiments using the M-YBT-G and BBT specimens are shown in Figures 4-6 and 4-7, respectively. The change in the strain path before and after the identified wrinkling initiation is also illustrated.

M-YBT-G is a special, modified Yoshida specimen used to reduce the bending effect on the specimen [Han14]. Therefore, the critical value of the effective strain recorded by testing of such specimens is higher than the one measured from the specimen M-YBT-K. The reason will be explained in Section 4.3. Based on the experiment results, it can be concluded that the geometry of the tested specimen has a significant effect on the wrinkling behaviour.

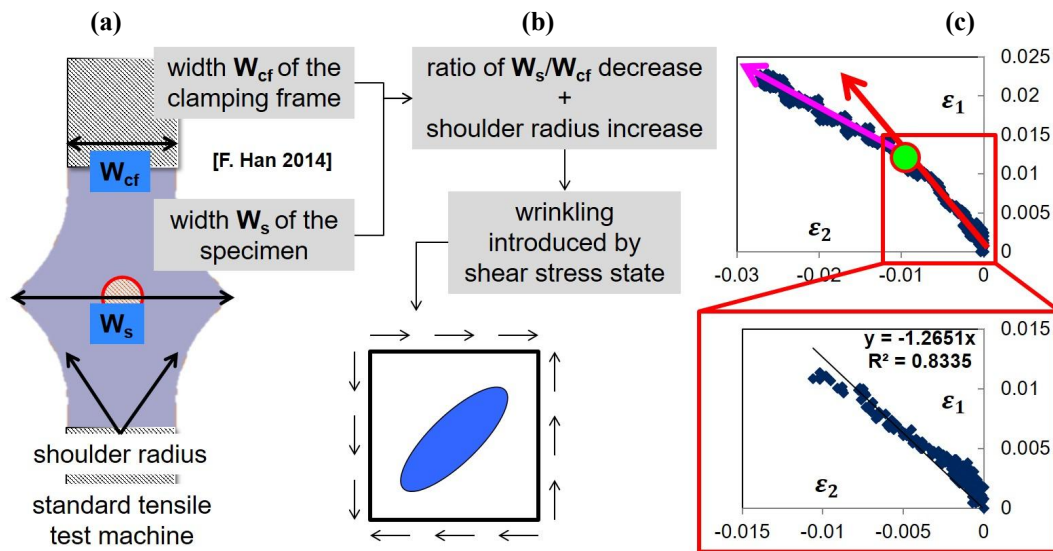


Figure 4-6: (a) Experimental details: M-YBT-G specimen (material HC420LA with 0.6 mm thickness), clamping frame and investigated area; (b) wrinkling mechanism: shear wrinkling; (c) wrinkling initiation identified using $d(H^w)/d(T)$ approach, strain path run through prior (with fit function) and after defined identified initiation in FLD

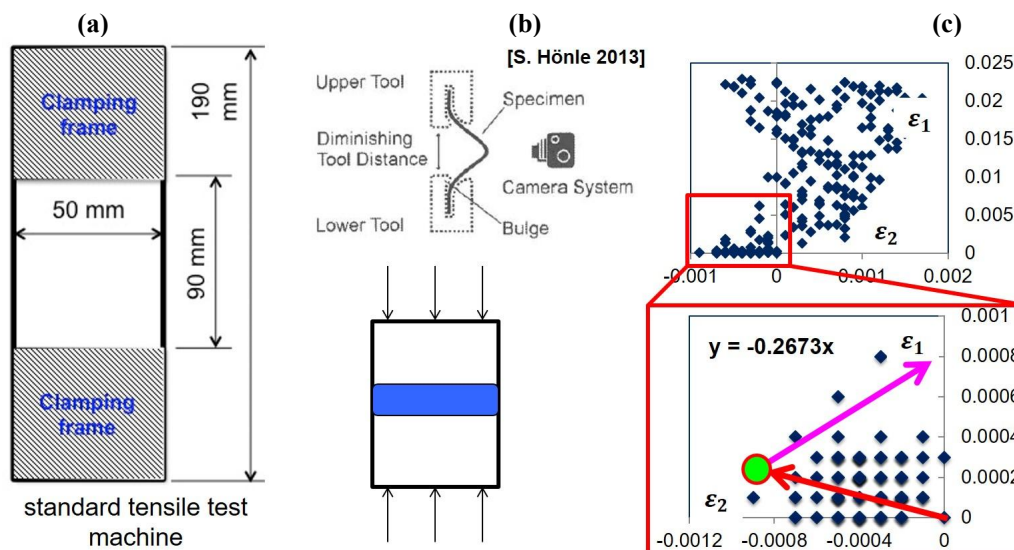


Figure 4-7: (a) Experimental details: BBT specimen (material HC420LA with 1.0 mm thickness), clamping frame and investigation area; (b) wrinkling mechanism: compressive stress wrinkling; (c) wrinkling initiation identified using the $d(H^w)/d(T)$ approach, strain path run through prior (with fit function) and after identified wrinkling initiation in FLD

Development of a wrinkling limit curve (WLC) in FLD

To develop and to design a wrinkling limit curve in FLD, various wrinkling mechanisms must be considered, and corresponding specimens were selected to do so. The details required for constructing a wrinkling limit curve using M-YBT-K specimens (K_1) and BBT specimens (K_2) are presented in Figure 4-8-a. For convenience, a wrinkling limit curve based on two specimens is introduced. Here “K” indicates the tested “K-series” specimens with a small shoulder radius as shown in [Han14].

Three steps must be followed to determine a wrinkling limit curve (see Figure 4-8-b). Firstly, the wrinkling initiation should be identified. Then, at the wrinkling initiation, the coordinates of the strain path ε_1 and ε_2 run through based on specimen K_1 and K_2 are measured by using the GOM ARAMIS optical measurement system. In theory, the accuracy of the wrinkling limit curve depends on the number of repetitions in the experiment. For example, in Figure 4-8-a, the red circles represent the mean value of the experiments. The final step involves fitting the determined strain path (ε_1 and ε_2) of all the specimens with function $\varepsilon_1 = k * \varepsilon_2 + b$.

Obviously, when testing a modified specimen with a large shoulder radius (M-YBT-G), both the strain path and also the critical strain values in the time point “wrinkling initiation” will be changed. The results will be shown in the following section of this chapter. Therefore, the wrinkling limit curve determined using the M-YBT specimens with a small (K-series) and large shoulder radius (G-series) differs between the two. These results show that the wrinkling limit curve is not depending on material properties and therefore the application of strain based wrinkling criterion is limited. Such gained results will be described in the following section.

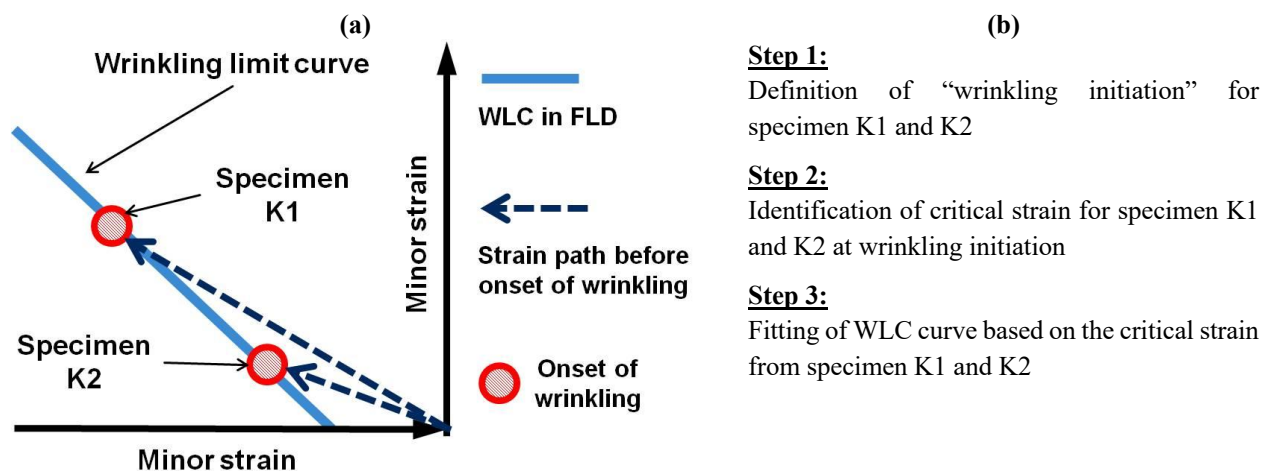


Figure 4-8: (a) Graph showing identification of a wrinkling limit curve in FLD based on modified Yoshida specimens K_1 and K_2 , strain path before wrinkling initiation, onset of wrinkling; (b) introduction of three steps to build up a strain based wrinkling limit curve

Effect of specimen topology on wrinkling limit curve (WLC)

As mentioned above, the wrinkling limit curve can be influenced by the specimen geometry, corresponding experiments and calculated results of simulation runs will be shown in the following. Firstly, the effect of the specimen geometry on the strain path is explained in this section. Since the wrinkling limit curve depends only on the strain path before wrinkling initiation (see the definition in Figure 4-8-a), the influence of the specimen geometry on the wrinkling limit curve can therefore be confirmed if the experiment results are used to prove the influence of the specimen geometry on the strain path before wrinkling initiation. The determined and calculated strain paths run through by this infinite point in volume in the M-YBT-K specimen and M-YBT-G specimen are illustrated in Figure 4-9. The M-YBT specimen used (both K- and G-series) can be found in article [Han14]. Although the FEA results of both M-YBT-K/G-series are predominantly situated between the strain path value of -0.9 and -1.2, the trend is shown and listed in Table 4-3, which was verified in the experiments. The G-series specimens suffer from a higher tensile stress before the defined wrinkling initiation, which results in strain path values of between -1.2 and -2. Due to the large bending moment that occurred in the wrinkling area, the strain paths of the K-series specimens are found between -0.5 and -0.7. Both sets of results gained by simulation and experiment are illustrated and compared in Figure 4-6 and Table 4-3.

In conclusion, the influence of the specimen geometry on the wrinkling limit curve is significant [Han14]. Merely by applying a different shoulder radius, the strain path before wrinkling initiation for the same specimen can be changed, see Figure 2-6-b and Figure 2-6-c. This change in the strain path also results in changes in the position of the wrinkling limit curve of the same material. Therefore, the strain based wrinkling limit curve can only be used for special specimens in limited cases.

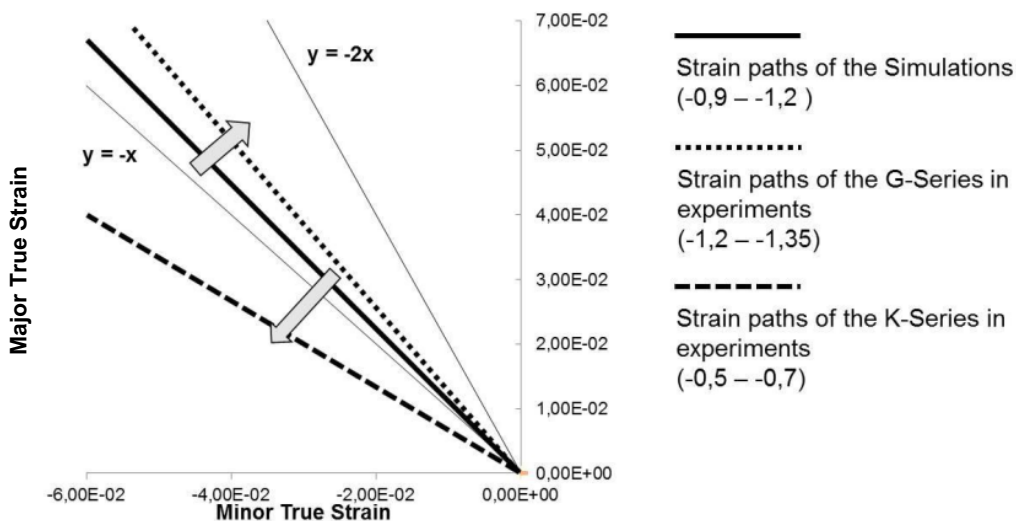


Figure 4-9: Comparison of the simulation and experiment results obtained by investigating the M-YBT specimens (G- and K-series) in [Han14]

Table 4-3: The difference between M-YBT specimens (K- and G-series)

	K-series specimen	G-series specimen
Deformation at wrinkling initiation	Large (2 % to 4.5 %)	Large (2.5 % to 7 %)
Strain path	Tendency towards -1	Tendency towards -2
Deflection height at wrinkling initiation	Large (0.2 to 0.8 mm)	Small (0.04 to 0.13 mm)
Downward movement of the wings	Large (0.3 to 2.0 mm)	Small (0.08 to 1.0 mm)

Plastic and elastic wrinkling

Wrinkling in the plastic forming stage is termed “plastic wrinkling” in this thesis. The results presented in Table 4-3 indicate that specimens with a smaller size and larger shoulder radius (M-YBT-G-series) exhibit “preferable properties” compared to simple deep drawn parts [Han14]. This performed characteristic means that value of effective strain at wrinkling initiation is comparable to real, simply shaped deep drawn parts such as mentioned geometry of the KVG. The experiment results show that the values of effective strain of the M-YBT-K specimens are too low for comparison to actual stretched parts, such as KVG parts and conical cups. In [Han14], the reason for this is given by considering the downward movement of the specimen wing. Cao et al. also pointed out that, according to the value of effective strain, the original Yoshida specimens (with a small shoulder radius) only in a few cases do reflect the actual deep drawing situation [Cao07].

However, according to the validating results mentioned and discussed in Chapter 8, wrinkles can occur at a low strain level in real formed parts. This kind of wrinkling is referred to as “elastic wrinkling” or “small plastic wrinkling” in this paper. This type of wrinkling can be identified and investigated using M-YBT-K series specimens. Due to the measuring deviation of the GOM ARAMIS measurement system used, the critical strain (especially at a low level) could not be precisely determined [Dam14] [Che16].

Validation with simple geometry – KVG geometry

In Section 4.1.2, the application of the strain based wrinkling limit curve (WLC) to KVG geometry for predicting wrinkles of second order is described. As previously mentioned, a strain based WLC can only be used to predict wrinkling in simple geometries like the KVG geometry and conical cups. A conventional WLC in FLD assumes, that a WLC curve can be modelled by a function $\varepsilon_1 = k * \varepsilon_2$ [Doe98]. However, according to the experimental results, this function is only suitable for materials showing a low bending resistance, such as aluminium sheet metal material AA6016 [Han15a]. By studying materials with a higher bending resistance than aluminium, such as HC340LA, the conventional function $\varepsilon = k * \varepsilon_2$ should be modified as $\varepsilon_1 = k * \varepsilon_2 + b$. Here “b” indicates the interception of the ε_2 -axis in FLD.

In 2015, a new approach was introduced for determining the wrinkling limit curve using the

conical cup test (CCT) and tests with modified Yoshida specimens (M-YBT) [Han15b]. Firstly, this approach identified the necessity of modelling a wrinkling limit curve using the function $\varepsilon_1 = k * \varepsilon_2 + b$. The basic idea of this new approach was to develop and to design a WLC based on the following cases of effective strain path run through facing to enhance the accuracy of determined WLC.

- 1) Low effective strain in M-YBT: by using Yoshida and modified Yoshida specimens, the critical strain can only reach a value of around $\varepsilon_1 < 0.05$, $\varepsilon_2 < 0.05$. If the WLC is only determined from M-YBT, the accuracy cannot be ensured since wrinkling might occur at high effective strains in a “real” deep drawing process.
- 2) High effective strain in CCT: by employing the conical cup test, the critical strain can reach a value of around $\varepsilon_1 > 0.1$, $\varepsilon_2 > 0.1$.

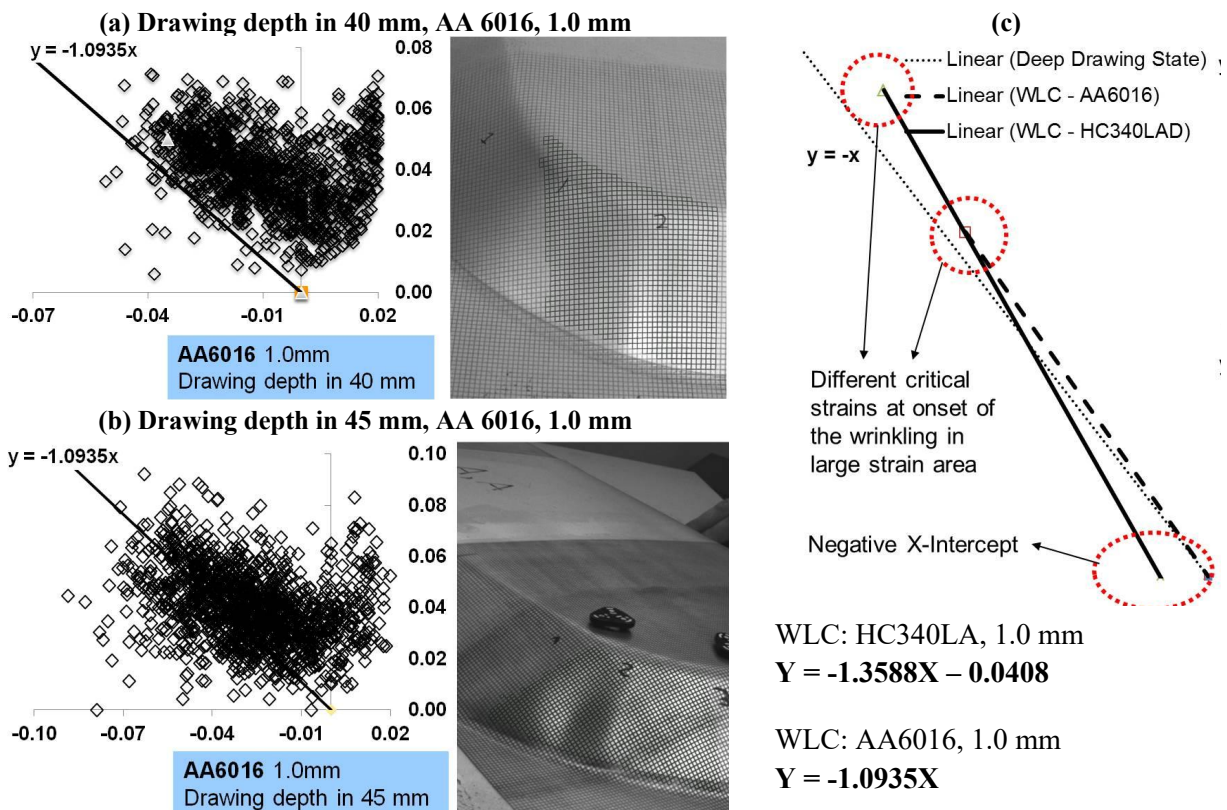


Figure 4-10: (a) Experimental results using VIALUX: strain distribution at wrinkled corner of drawn KVG part with a drawing depth of 40 mm, AA6016 with a thickness of 1.0 mm; (b) experiment results using VIALUX: strain distribution at wrinkled corner of drawn KVG part with a drawing depth of 45 mm, AA6016 with thickness of 1.0 mm; (c) wrinkling limit curve of HC340LA and AA6016 with identical thickness of 1.0 mm

Figure 4-10-a and Figure 4-10-b illustrate the validation results for sheet metal material AA 6016 having a thickness of 1.0 mm. The validating results for sheet material HC340LA having a thickness of 1.0 mm are given in [Han15a]. Figure 4-10-c shows the wrinkling limit curve determined for both materials (HC340LA and AA6015). It is worth noting that the wrinkling limit

curve of AA6016 passes through the original point with a slope of -1.0935 (dotted line in Figure 4-10-b), while the wrinkling limit curve of HC340LA has a negative X-intercept (black line in Figure 4-10-c: slope -1.3588; X-intercept -0.0408).

The high value for the effective strain of material AA6016 can be obtained through CCT tests ($\varepsilon_1 > 0.08$, $\varepsilon_2 > 0.08$). Lower levels of effective strains ($\varepsilon_1 < 0.05$, $\varepsilon_2 < 0.05$) can be obtained by using M-YBT specimen. Moreover, HC340LA material exhibits a higher critical effective strain value than AA6016 as determined through experiments (in the case of CCT, $\varepsilon_1 > 0.1$, $\varepsilon_2 > 0.1$). With the M-YBT specimens, the intercept value “b” can be accurately calculated, thereby improving the accuracy of the wrinkling limit curve.

The validation results for aluminium sheet metal with a thickness of 1.0 mm are shown in Figure 4-10-a and Figure 4-10-b. The former depicts the relationship between the measured ε_1 and ε_2 values (using the VIALUX optical measurement system) and the determined wrinkling limit curve. Results demonstrate that most measured ε_1 and ε_2 values at a drawing depth of 40 mm are located above the wrinkling limit curve. At a drawing depth of 45 mm (see Figure 4-10-b), numerous measurements are found below the defined wrinkling limit curve. So, it is evident that wrinkling initiation can be detected and observed.

4.2 Description of wrinkle formation using a simplified, stress based model

Nowadays, most scientific research focuses only on studying the onset of wrinkling. However, the definition of the “onset of wrinkling” (wrinkling initiation) is still well defined in the sheet metal-forming industry and refers to the fact, that different wrinkling criteria lead to different critical wrinkling heights when the onset of wrinkling occurs.

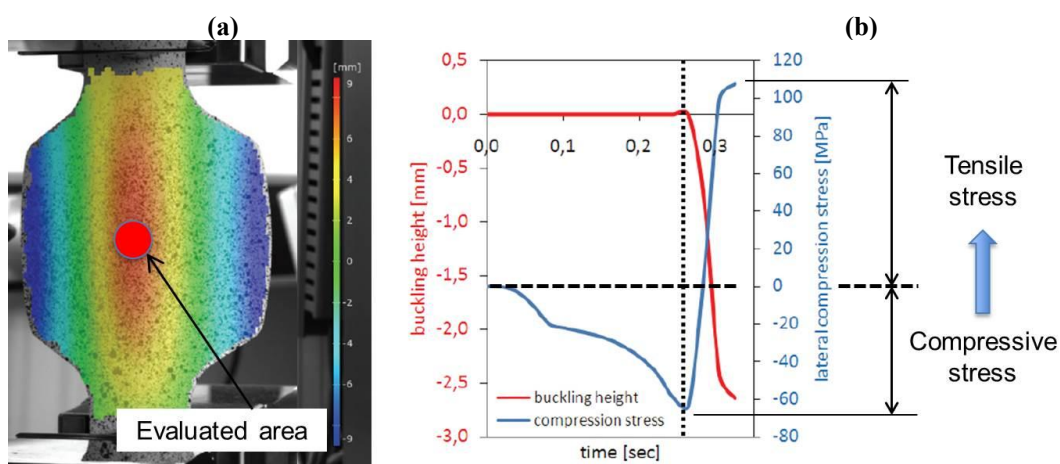


Figure 4-11: Relationship between buckling height and compressive stress in [Sch09]: (a) visualisation of the wrinkling height of a modified buckling specimen after bifurcation, AA6016 with thickness 1.0 mm; (b) lateral compressive stress, development of wrinkling height with modified specimen, change in the stress state of lateral compressive stress after defined bifurcation

In certain situations, the critical wrinkling height determined in accordance with specific wrinkling criteria is unacceptable. A suitable approach for predicting wrinkles in the sheet metal forming process is therefore desired. In this section, a new method for predicting the onset of wrinkling is described. This method is based on analysing the development of compressive stress throughout the wrinkling process. The purpose of this new approach is to ascertain the relationship between surface defects and the development of compressive stress in the wrinkling region. Only in this way a wrinkling criterion based on critical wrinkling height can be developed.

Schleich focused on the relationship between the development of compressive stress and wrinkling height in his thesis [Sch09][Sch10], investigating this relationship using modified Yoshida specimens. According to his results, he claimed, that after a maximum value for compressive stress is reached (blue curve in Figure 4-11-b), the buckling height (red curve in Figure 4-11-b) increases dramatically towards the end of experiment. Furthermore, the compressive stress tends to turn into tensile stress. Following the results of Schleich, two questions should be investigated before developing a simplified model for describing the process of wrinkling formation:

- 1) Does a maximum value for compressive stress exist at the defined wrinkling initiation and how can the development of compressive stress be measured or observed directly or indirectly through experiments? This question will be addressed in Section 4.2.1.
- 2) Does a change of stress state exist in the wrinkling process and can this change of stress state be measured or observed directly or indirectly through experiments? This question will be addressed in Section 4.2.2.

4.2.1 Analysis of maximum compressive stress emerging at wrinkling initiation

Simplify the “thin-walled plates under tensile compressive stress” with “single-beam-spring system”

According to the work of N. Fridl [Fri99], the behaviour of thin-walled plates under tensile and/or compressive stress can be simplified using the “double-beam system” (see Figure 4-12-a). Here, F_1 represents the tensile force in the first principal direction, while F_2 stands for the compressive force in the second principal direction.

In FEA software (e.g. AutoForm), only two principal directions are defined when addressing the FEA of thin-walled plates, namely the “major” (or maximum) and “minor” (or minimum) direction. According to the definition of principal stress [Her17], if the system is in a state of tensile/compressive stress, the major principal stress is tensile stress and the minor principal stress is compressive stress.

The “double-beam system” can be simplified to give the “single-beam-spring system” described in Figure 4-12-b [Sed00]. Here, the spring stiffness is considered a relevant parameter for materials

and structures. Assuming that the section area (S) of the beam stays constant, the compressive stress can be calculated using the equation $\sigma = F/S$. Therefore, to understand the wrinkling behaviour, only the compressive stress in the minor direction should be studied.

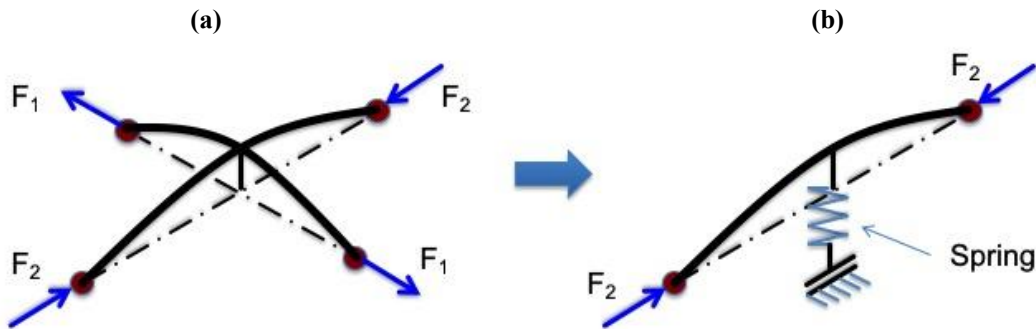


Figure 4-12: Effective stress state for investigation the wrinkling behaviour of pates: (a) simplified “double-beam system” in [Fri99]; (b) simplified “single-beam-spring system” in [sed00]

To summarise, the “single-beam-spring system” simplifies the behaviour of thin-walled plates under tensile/compressive stress under compressive stress in the minor principal direction.

Buckling bending test (BBT) and maximum compressive stress

the concept of the “single-beam-spring system” was introduced above. It is now obvious why the maximum compressive stress is studied using the BBT. In this case, the BBT can be understood as a single-beam-spring system without spring effects (see Figure 4-12-b), since there is only a compressive force F_2 induced by the upper and lower clamping jig (grripper, see Figure 2-5-a/b/c/d). By conducting the buckling bending test, the buckling behaviour can be studied using the GOM ARAMIS optical measurement system.

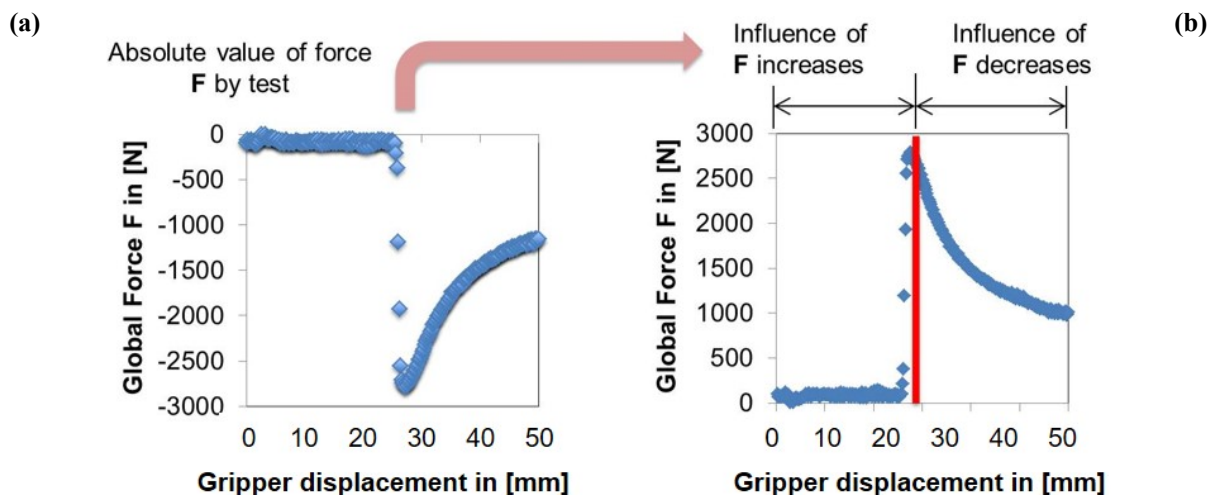


Figure 4-13: Buckling bending test with material HC420LA, thickness of 1.0 mm: (a) original force–displacement curve measured using tensile test machine; (b) absolute value of force F as a function of gripper displacement)

Results obtained with material HC420LA (1.0 mm thickness) were shown to provide better

comprehension of the test results gained by this. The originally measured compressive force F_2 is shown in Figure 4-13-a. For a clearer overview (comparable with the results of the force–displacement curve obtained with M-YBT specimens), the development of the “absolute value” of compressive force F_2 is presented in Figure 4-13-b. Compressive force $|F_2|$ decreased after reaching a specific maximum value of around 2.700 N, when the upper tool of the tensile machine reached a displacement of 4 mm.

When the maximum compressive-force value is reached, instability of the BBT specimen occurs (the red line in Figure 4-13-d). Naturally, after the instability occurs, the influence of compressive stress F_2 on the BBT specimen decreases significantly. The experiment results show that instability will occur when the BBT specimen cannot withstand the compressive load. The surface profile changes from a “pre-instability” profile to a “post-instability” profile.

In this Thesis, the pre-instability profile is defined as a state in which the surface profile of the specimen has a small, local surface curvature. The local surface curvature value is defined by $k = 1/R^L$, where R^L indicates the radius of the “local surface contour”. After instability, the value of R^L decreases rapidly. This decreased value of R^L results into a high value for k . This phenomenon is termed the “local bending process” in this chapter.

Relationship between “ $d(H^W)/d(T)$ approach” and maximum compressive stress

Figure 4-14-a illustrates the relationship between compressive force F_2 and the “ $d(H^W)/d(T)$ ” approach (as a function of the gripper displacement). According to experimental results obtained with HC420LA material (1.0 mm thickness), the compressive force reaches its maximum value when the value of $d(H^W)/d(t)$ is also at its maximum.

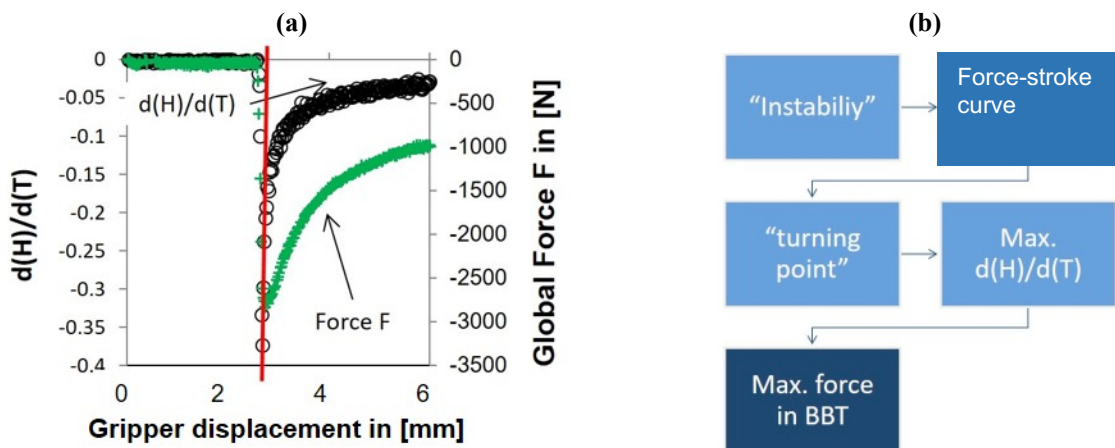


Figure 4-14: (a) Results gained from the buckling bending test: the relationship between $d(H^W)/d(T)$ and development of compressive force F_2 , HC420LA specimen with a sheet thickness of 1.0 mm; (b) logic from instability to maximum value of $d(H^W)/d(T)$, maximum compressive force appears at wrinkling initiation defined by applying $d(H^W)/d(T)$ approach

From the experimental results it can be concluded that, when the compressive force reaches its maximum value in the buckling bending test, the $d(H^W)/d(T)$ approach does too. The following conclusions can be drawn from the buckling bending test in Section 4.2.1:

- 1) The maximum compressive force indicates the “wrinkling initiation” defined by applying the $d(H^W)/d(T)$ approach based on the buckling bending test.
- 2) At wrinkling initiation, a maximum compressive stress exists in accordance with the formula $\sigma = F/S$ (assuming that the section area S of buckling bending specimen remains constant).

4.2.2 Analysis of the change in stress state after wrinkling initiation

Explaining the change in stress state after instability using the modified Yoshida specimen

In Schleich’s work [Sch10], no information is given on the “compressive stress” as shown in Figure 4-11-b. Consequently, the trend of “compressive stress” was first examined with the M-YBT specimens. Figures 4-15 and 4-16 show why the compressive stress in the wrinkling area first increases to the maximum value, then decreases to zero, while the stress state changes from compressive stress to tensile stress after instability.

As shown in Figure 4-15, the red circle in the middle of the modified Yoshida specimen indicates the measurement area. Some factors for the development of the wrinkling height and the minor strain were measured with GOM ARAMIS. It is worth noting that only the outside of the specimen was measured and evaluated during the test (see Figure 4-15-b).

Before the defined “wrinkling initiation”, the investigated wrinkling area was subjected to tensile/compressive stress as shown in Figure 4-16-a and Figure 4-16-b. In this stage, the influence of the “local bending effect” on the wrinkling area is small, since the local curvature k is also small.

After the defined “wrinkle initiation”, the surface compressive stress decreases as the surface profile (wrinkling area) changes. On the outer side (side measured using GOM ARAMIS cameras) of a wrinkle, the stress state will change from compressive stress to tensile stress due to “the local bending process” (area marked red in Figure 4-17).

The “local bending process” results in a moment $M(x)$ in the M-YBT specimen: this moment results in a tensile stress (in the minor principal direction) on the outer side of the tested specimen. Figure 4-16-c illustrates that the compressive stress decreases after instability (see Figure 4-13 and 4-14).

Meanwhile, the tensile stress induced by moment $M(x)$ increases because of the increased local curvature. When the resulting stress in the minor principal direction is considered, the compressive stress will eventually become tensile stress. The details concerning the change of stress state will be explained in greater depth in Chapter 5.

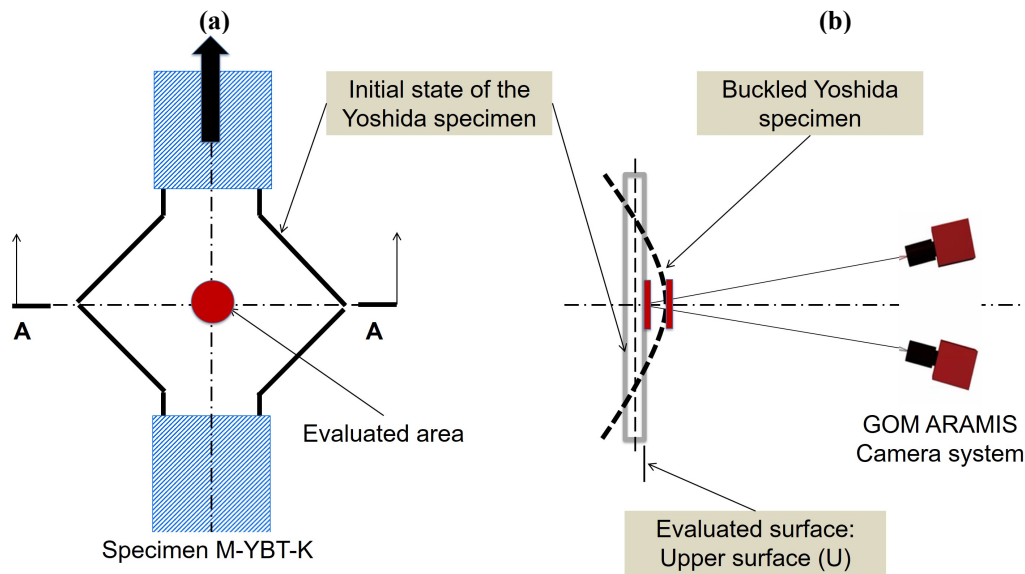


Figure 4-15: (a) M-YBT specimen with evaluated area; (b) initial position and buckled section profile A-A, evaluated specimen side: outer side and position of GOM ARAMIS cameras

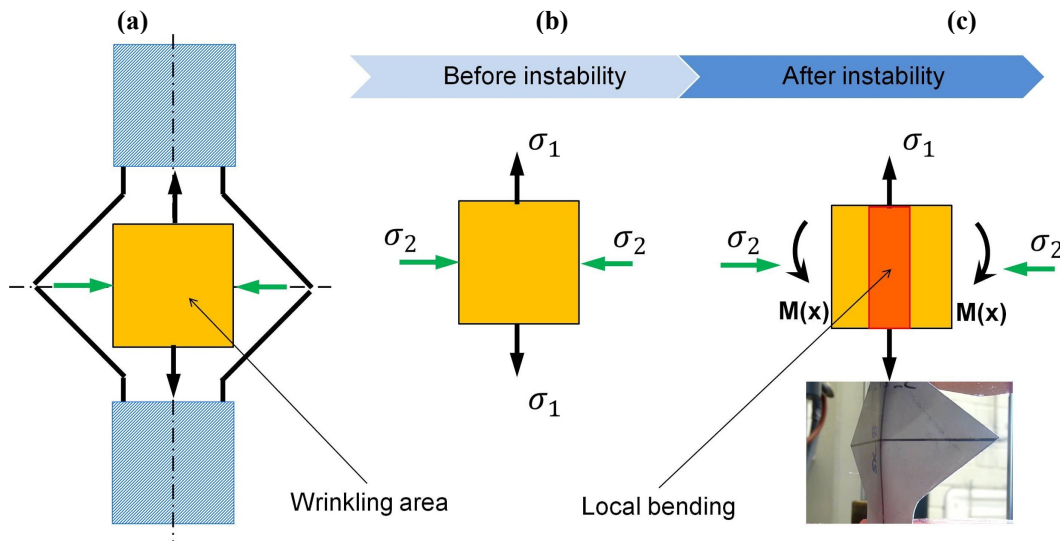


Figure 4-16: (a) Wrinkling area of the tested M-YBT specimen; (b) illustration of the stress state before the identified wrinkling initiation; (c) stress state after the identified wrinkling initiation and the “change in the stress state” due to the illustrated local bending process

Proving the change in stress state by observing the development of minor strain during the forming process with regard to the YBT test

The development of surface stress in the minor principal direction cannot be measured directly. To overcome this inconvenience, a new method based on the “development of minor strain” in the wrinkle area was proposed to observe the change of stress state during the experiment [Hor15]. Since the compressive stress tendency on the outer side (measured side) can be observed by evaluating minor strain, this approach was used in the conical-cup test and buckling test with modified Yoshida specimens in [Hor15].

However, the relationship between the “development of minor strains” and the “ $d(H^W)/d((T))$ ”

approach first should be established. Subsequently, the change in stress state can be observed by evaluating the development of minor strains after wrinkling initiation.

The relationship (according to the results from the M-YBT-K specimen) of “the development of minor strains” and “ $d(H^W)/d(T)$ value”, as a function of gripper displacement, is illustrated in Figure 4-17-a. It seems that, when $d(H^W)/d(T)$ reaches its maximum value, the “value of minor strain” also reaches its maximum. This phenomenon is called the “short transition” phenomenon and will be explained later in Figure 4-18-a.

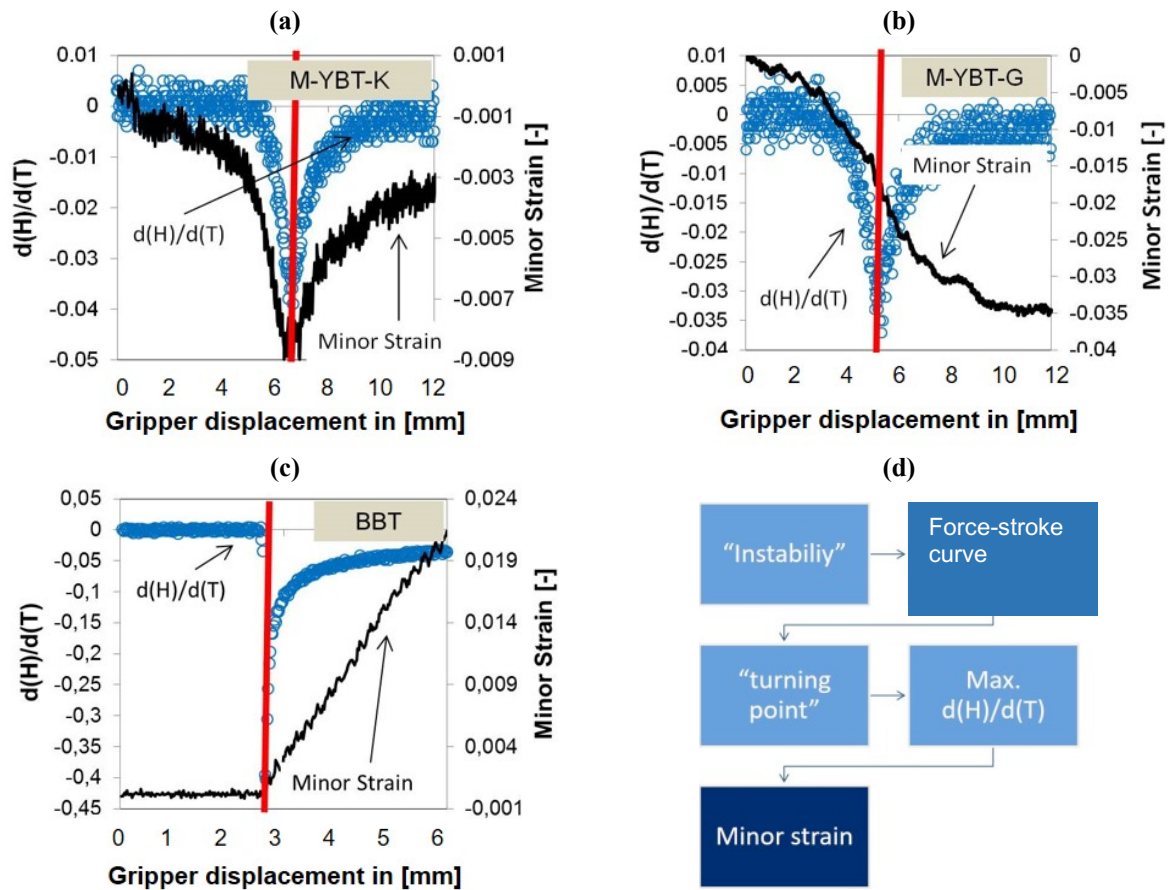


Figure 4-17: Experiment results gained for the modified Yoshida specimen using GOM ARAMIS: the relationship between the development of minor strain and $d(H^W)/d(T)$ value in (a) M-YBT-K; (b) M-YBT-G; (c) BBT, the development of minor strain can also be used to predict the onset of wrinkling; (d) relationship between minor strain and instability induced by compressive stress

The relationship (according to the results from the M-YBT-G specimen) between the “development of minor strains” and “ $d(H^W)/d(T)$ value” (as a function of gripper displacement) is illustrated in Figure 4-17-b. The maximum value of the minor strain appears at the end of the test. This phenomenon is defined as the “long transition” phenomenon and is explained below in Figure 4-18-b.

The relationship (according to the results from the BBT specimen) between the “development of minor strains” and “ $d(H^W)/d(T)$ value”, as a function of gripper displacement, is illustrated in

Figure 4-17-c. According to the experiment results, when the maximum value of $d(H^W)/d(T)$ is reached, the value of the minor strain starts to change its sign from “-“ to “+” and increases rapidly towards the end of the experiment. In this context, Figure 4-17-d shows why the development of the minor strain should be used in YBT testing to determine the maximum compressive stress.

As mentioned above, the “short transition” (see Figure 4-18-a/b/c) and “long transition” phenomena (see Figure 4-18-d/e/f) will now be discussed. Results from research published in [Han15] explain the various phenomena encountered with modified G- and K-series specimens using the development of minor strain determined by GOM ARAMIS during the wrinkling process. As shown in Figure 4-18-a and Figure 4-18-d, the development of minor strain ε_2 in M-YBT-G and -K specimens can generally be divided into the following three steps with two points in time based on Figure 4-18:

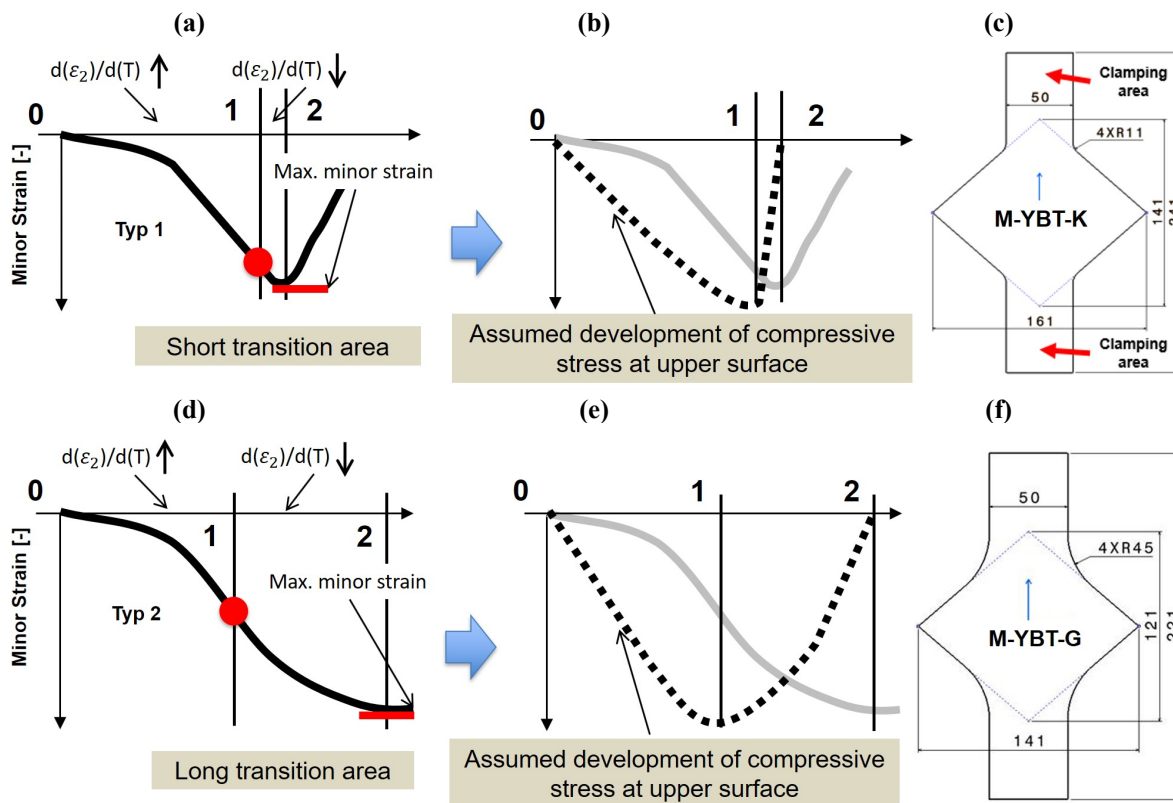


Figure 4-18: “Short transition” and “long transition” phenomena in M-YBT-K/G: (a) illustration of the development of minor strain with definition of three stages in the case of “short transition” phenomena; (b) depicted development of the compressive stress during the test, “short transition”; (c) specimen geometry of M-YBT-K; (d) illustration of the development of minor strain with definition of three stages in the case of “long transition” phenomena; (e) depicted development of the compressive stress during the test, “long transition”; (f) specimen geometry of M-YBT-G

- Step 1, from stage 0 to stage 1: the value of $d(\varepsilon_2)/d(T)$ increases until point 1; see Figure 4-18 a/d. During this step, the compressive stress on the outer side also increases until point 1, see Figure 4-18-b/e.

- Point 1, stage 1: “ $d(\varepsilon_2)/d(T)$ ” at point 1 reaches its maximum value (see Figure 4-18-a/d, before the appearance of the maximum value of minor strain ε_2), see Figure 4-18 a/d. The compressive stress also reaches its maximum value at this point, see Figure 4-18-b/e.
- Step 2, from stage 1 to stage 2: the value of $d(\varepsilon_2)/d(T)$ decreases (see Figure 4-18-a/d) due to the decrease in compressive stress on the outer side, see Figure 4-18-b/e.
- Point 2, stage 2: minor strain ε_2 reaches its maximum value (see Figure 4-18-a/d) since the compressive stress at point 2 disappears (see Figure 4-18-b/e).
- Step 3, from the end of stage 2: after stage 2, the compressive stress is completely transformed into tensile stress due to the “local bending process” in the wrinkling area. Therefore, the compressive stress disappears after point 2, after which obvious wrinkling profiles in the formed part can be identified.

The “short transition” phenomenon can be analysed by using the M-YBT-K specimen. In this case (see Figure 4-18-a), the transition phase from stage 1 to stage 2 is “too fast” because of the influence of the additional bending moment acting on the wrinkling area that is induced by the specimen wings. This phenomenon was explained in [Han14]. For this reason, and sometimes in practice, point 1 (the maximum value of $d(\varepsilon_2)/d(T)$, denoted red circle) cannot be clearly captured in experiments. Examples are shown in Figure 4-19-a. In other words, the value of $d(\varepsilon_2)/d(T)$ decreases very quickly in a short time and reaches its maximum value in stage 2 (point 2).

However, the “short transition” phenomenon can be changed into a “long transition” phenomenon by modifying the geometry of the tested specimen. Using the M-YBT-G specimen (see Figure 4-18-f), the effects of additional bending moments caused by the specimen wings can be significantly reduced. In this way, the transition phase from stage 1 to stage 2 is extended. The critical point between the increase and decrease of “ $d(\varepsilon_2)/d(T)$ ” can be detected. According to the experiment results, the maximum value of $d(\varepsilon_2)/d(T)$ can be clearly captured when the transition phase from stage 1 to stage 2 is prolonged; see Figure 4-18-d.

Proving the change in stress state by observing the development of minor strain in the forming process with regard to mini-CCT tests

The “short transition” and “long transition” phenomena can be also observed in the mini conical-cup test (see Figure 4-19-a and Figure 4-19-b). Mini-CCT tests were performed with material HC420LA in varying sheet thicknesses.

Figure 4-19-a illustrates the “short transition” phenomenon by testing HC420LA in a thickness of 0.6 mm (green points) and a thickness of 1.0 mm (black points). Compared to the “short transition” phenomenon explained in M-YBT-K, the GOM ARAMIS measuring system was not able to clearly capture “point 1” in case of specimen’s thicknesses of both 0.6 mm and 1.0 mm; see Figure

4-19-a. However, “point 2” (denoted by a red line) indicates that the compressive stress is equal to zero and can be easily detected, especially during when deep drawing low sheet thickness (see Figure 4-19-a). Therefore, in this case of a “short transition” phenomenon, “point 2” can be immediately identified at the “maximum value of minor strain ε_2 ”.

Figure 4-19-b illustrates the “long transition” phenomenon by testing HC420LA with a thickness of 0.6 mm (green points) and 1.0 mm (black points). Compared to the “long transition” phenomenon explained with M-YBT-G using GOM ARAMIS and testing the thickness of the two sheets, “point 1” (depicted by red dots) can be clearly captured. Therefore, in this case of the “long transition” phenomenon, “point 1” can be directly identified at the “maximum value of $d(\varepsilon_2)/d(T)$ ”, while “point 2” can be identified at the “maximum value of minor strain ε_2 ”.

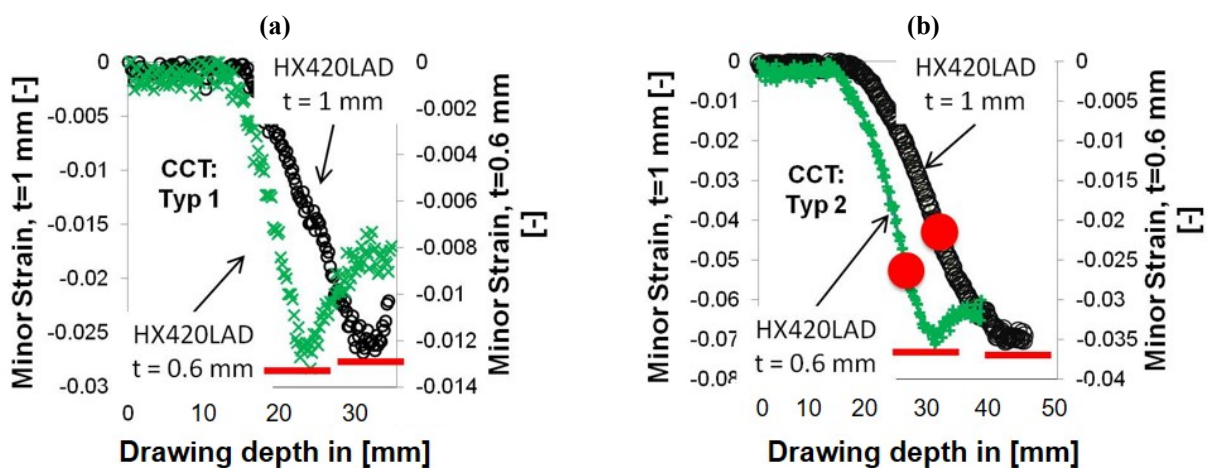


Figure 4-19: “Short transition” and “long transition” phenomena in mini-CCT test, experiment results with material HC420LA: (a) illustration of the development of minor strain with definition of “point 2” in the case of “short transition” phenomena; (b) illustration of the development of minor strain with definition of “point 1” and “point 2” in the case of “long transition” phenomena

By analysing tests with M-YBT-K/G and performing mini-CCT tests, the following conclusions can be drawn for the findings presented in Section 4.2.2:

- 1) After the defined “wrinkling initiation” (point 1), compressive stress tends to decrease until point 2, at which the value of the compressive stress is equal to zero.
- 2) After the defined point 2, the state will change from compressive stress to tensile stress.

4.2.3 Using development of surface compressive stress to establish a simplified model

In Sections 4.2.1 and 4.2.2, the following phenomena were proved:

- 1) The existence of a maximum compressive stress at defined “wrinkling initiation”
- 2) The existence of a change in state from compressive stress to tensile stress

The “compressive stress” proposed here will be named “compressive stress on the outer side” since only the outside of the specimen is tested and analysed in Sections 4.2.1 and 4.2.2. Chapter 4 does not discuss changes in the stress state on the inner side of the specimen.

Section 4.2.3 only describes changes in surface quality associated with the development of compressive stress on the outer side. The results listed in Figure 4-20 solely are based on the mini-CCT tests performed. From stage 0 to stage 1, the sidewall of the conical cup indeed show an acceptable buckling height. After the defined “wrinkling initiation” (namely from stage 1 to stage 2), noticeable wrinkles tend to appear on the sidewall surface of the conical cup. Finally, after the defined “point 2”, severe wrinkling can be observed on the entire sidewall surface.

In summary, the change in surface quality can be described using three stages and by defining two points in time:

- 1) “Wrinkling initiation” at point 1 in Figure 4-20
- 2) “Developed wrinkling” at point 2 in Figure 4-20

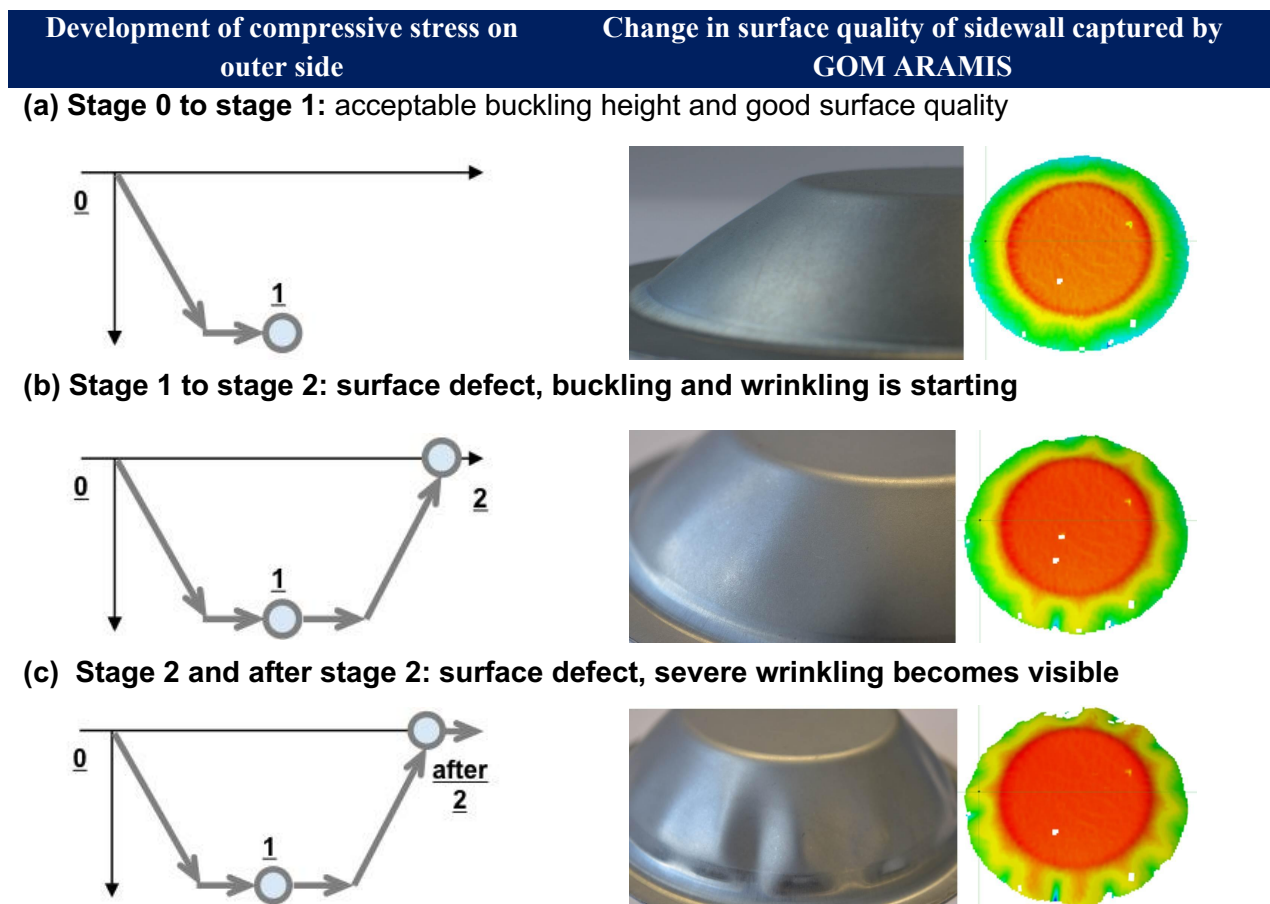


Figure 4-20: Description of the change in surface quality by considering the development of surface compressive stress, tested material HC420LA with thickness of 0.6 mm; (a) illustration of development of surface compressive stress from stage 0 to stage 1, specimen with acceptable buckling height and 3D surface profile; b) illustration of development of surface compressive stress from stage 1 to stage 2, specimen with noticeable wrinkles and 3D surface profile; b) illustration of development of surface compressive stress after stage 2, specimen with severe wrinkling and 3D surface profile

4.3 Conclusion on the simplified model for predicting wrinkles of second order

Development of compressive stress on outer side and surface quality in wrinkling area

In Section 4.2.3, the newly developed simplified model defines the wrinkling process based on the change in compressive stress on the outer side. By analysing the formation of wrinkles during the drawing process, the following results can be obtained:

- The new, simplified model for predicting wrinkles of second order is independent of sheet metal materials and specimen geometries. This approach can be used for detecting wrinkles of second order and will be developed further in Chapter 5 for application in a scenario considering tool contact under real deep drawing conditions.
- Wrinkling initiation occurs when the wrinkling area can no longer withstand compressive stress. The structural stability of the wrinkling area is lost.
- The phenomena of buckling and wrinkling are different (for details, see Figure 4-20 a/b).
- The transition from buckling to wrinkling initiation in real deep drawn parts is dependent on the bending stiffness of the wrinkling area.
- The surface defects in the buckling and wrinkling stages are different. First, the resulting buckling in fact lead to a slight deviation in the geometry of the part compared to the wrinkles that occur after the buckling stage. Compared to the reference geometry, wrinkles greatly change the surface quality as the deviation increases.

In Section 7.2, this newly developed simplified model for detecting wrinkling will be validated through FEA with mini-CCT tests. The wrinkling process can be divided into three phases in accordance with Figure 4-20, while the development of the surface quality is summarised in Figure 4-21 [Lie16]:

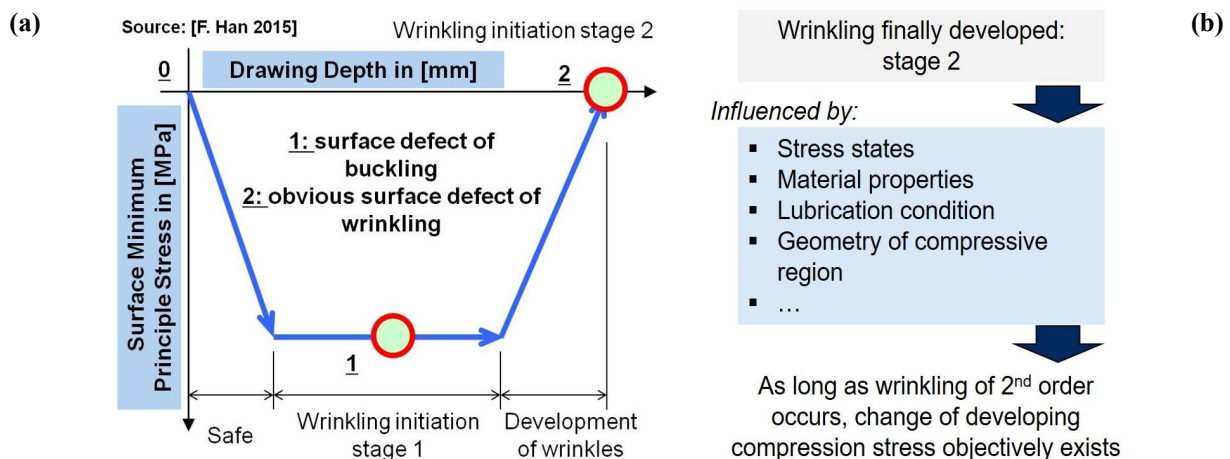


Figure 4-21: (a) Simplified approach for describing wrinkling formation using the development of surface compressive stress, considering the change in surface quality [Lie16]; (b) the simplified model developed remains independent from material property and specimen geometries

- Stage 0–1: surface even and flat, straight line between punch corner and die radius
- Point 1 to “wrinkling initiation”: wrinkling area has lost its stability. Surface defects will change from buckling to obvious wrinkling
- Stage 1–2: mixed surface defect (buckling and subsequent wrinkling) can be observed in experiments performed with deep drawn parts in laboratory

Point 2 and after stage 2, “developed wrinkling”: from this point onwards, surface defects are mainly caused by wrinkling. Severe surface defects mainly caused by wrinkling.

The relationship between the development of surface compressive stress and minor strain

Section 4.1 describes how to define “wrinkling initiation” using a force–displacement curve. Since the development of the force in the sidewall of the conical cups cannot be determined during the CCT test, the method of evaluating the force–displacement curve determined from the tensile test can only be used in M-YBT tests. The approach involving the “development of minor strain” aims to prove the change in stress state (Section 4.2.2) and is suitable for both M-YBT and mini-CCT tests.

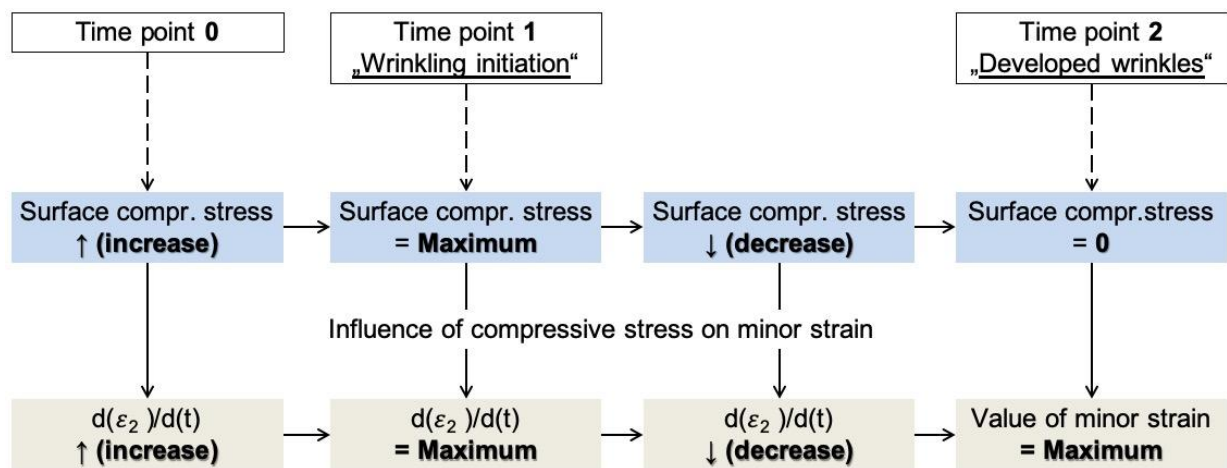


Figure 4-22: Wrinkling process according to theoretical analysis – relationship between the development of surface compressive stress and minor strains

According to the theoretical analysis of the wrinkling process in [Lie15], a particular dependency between the “compressive stress” and the “minor strain” during wrinkling formation can be drawn from Figure 4-22 since theoretical analysis claims that compressive stress during wrinkling increases up to the defined “wrinkling initiation” before the change in the stress state do emerge. Figure 4-22 explains the relationship between “compressive stress” and “minor strain” during the wrinkling process on the outer side.

Narayanasamy identified the tensile compressive stress state in his research as a possible stress state for inducing wrinkles during the forming process [Nar00]. Combined with Selman’s analysis, where in fact the biaxial compressive stress state produces severe wrinkles, it can be concluded

that an investigated region will be defined as having a “wrinkling tendency” when compressive stress exists. This assumes that the investigated region is subjected to compressive stress at the beginning of the forming process (from point 0 to point 1, see Figure 4-22). Furthermore, the value of the compressive stress increases from point 0 onwards.

During wrinkling formation, the compressive stress reaches its maximum value at point 1 as shown in Figure 4-22. The behaviour from point 1 to point 2 describes the “superposition” between “compressive stress” and “tensile stress” caused by bending moment $M(x)$ (induced by the “local bending process”) on the outer side of the tested specimen. Details of this are given in Chapter 5. At point 2, the minor strain reaches its maximum value.

In summary, the formation of wrinkles can be evaluated using the development of minor strain determined through experiments. However, like the force-based approach, it cannot be used as an approach in FEA for detecting wrinkling. Therefore, this thesis in the following will focus on the stress based approach.

5 Criterion considering tool contact – Concept of newly developed approach

Chapter 4 presents a simplified model to predict the onset of wrinkles of second order based on the development of compressive stress during deep drawing process. This model only is suitable for detecting wrinkles of second order while considering tool contact. To predict wrinkling initiation under those conditions this simplified model must be developed further, which is described in Chapter 5. Here the development of surface compressive stress on both the outer and inner side of the workpiece will be taken into account in post-processing of FEA.

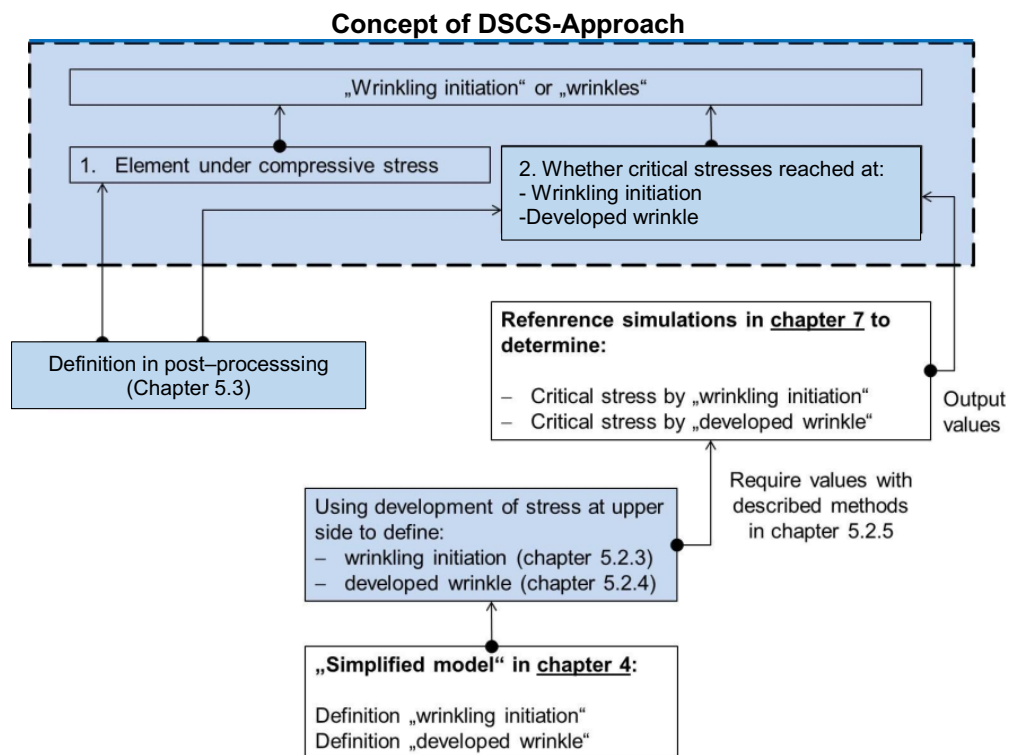


Figure 5-1: Further development of the “simplified model” as described in Chapter 4 into the new concept of the DSCS-approach in Chapter 5

Main objective of Chapter 5 is to develop a concept for the DSCS-approach that can be used in post processing codes of FEA. The expression “concept” means that a critical value should be set for detecting the points in time for “wrinkling initiation” and “developed wrinkling”, both of which are defined based on the simplified model in Chapter 4. This new concept is called “concept of DSCS-approach” and was first established by the author in 2016 by evaluating the critical value of the “difference in resultant stress between the outer and inner side in the minor principal direction” (abbreviated as “outer/inner side stress difference”) for predicting wrinkling formation. In Sections 5.1.2 to 5.1.4, the development of the outer/inner side stress difference was evaluated to demonstrate the surface quality of the formed part during wrinkling formation (see Figure 5.1). Considering such concept of the DSCS-approach will be used in FEA, the definition of “wrinkling

initiation” and “developed wrinkling” must be rewritten by using such given parameters and values in the post processing code. By applying the concept of the DSCS-approach, it is only necessary to check the two boundary conditions presented in Figure 5.1 to simplify the detection of wrinkles in FEA. Details of this will be given in Section 5.1.

By applying the simplified model presented in Chapter 4, the “wrinkling initiation” and “developed wrinkling” were defined further by evaluating the development of compressive stress in the minor principal direction on the outer side of the sheet metal component. Further details of this are given in Sections 5.1.2 to 5.1.4. The reason and approach for determining the critical value of the outer/inner side stress difference based on the concept of DSCS-approach will be outlined in Section 5.1.5. Finally, the basic concept of the DSCS-approach can be realised in a particular code, so finally its application for post processing objectives in FEA is presented in Section 5.2.

In summary, if the FEA-calculated value of the outer/inner side stress difference exceeds the given critical stress value, “wrinkling initiation” or “developed wrinkling” will occur. Further information on the application of the DSCS-approach will be provided in Section 5.4.

5.1 Basic concept of the developed approach

The basic concept of the DSCS-approach will be explained in Section 5.2.1 using corresponding boundary conditions. Furthermore, by applying the DSCS-approach, three stages of the wrinkling process can be defined. The defined “bifurcation” will be introduced in Section 5.2.2. In Sections 5.2.3 and 5.2.4, the defined “wrinkling initiation” and “developed wrinkling” will be described.

5.1.1 Definition of wrinkling using two boundary conditions

Section 5.2.1 is intended to introduce two boundary conditions for detecting wrinkles in FEA. Three steps should be considered for developing the basic concept of this new approach, namely:

- Boundary condition 1: the element investigated through FEA is loaded with compressive stress in the minor principal direction.
- Boundary condition 2: the element investigated is also subjected to a bending effect.

“Boundary condition 1” can be defined by calculating the value of $\varepsilon_1/\varepsilon_2$ for the element investigated in FLD (this method was used for UDV1 and UDV2 in Chapter 8), or directly by analysing the stress state (this method was used for UDV3 in Chapter 8). If the approach of calculating the value of $\varepsilon_1/\varepsilon_2$ is adopted, then the FEA employed in the UDV is a strain based UDV. In this way, the UDV must thus consider the influence of the forming history of each particular node. Conversely, if the first boundary condition is analysed with stress states, the UDV used is termed as a “stress based UDV”. The forming history is not considered in this case. Theoretical difference between strain based UDVs and stress based UDVs is shown in Chapter 8.

However, it is more difficult to define “element under bending effect” (in boundary condition 2) in post processing using FEA software than boundary condition 1. The solution is to calculate the difference of stress between outer and inner side of the investigated element. The critical value of the outer/inner side stress difference then can be used to determine the degree of wrinkling. This idea is based on an analysis of the relationship between the “stress states” and “surface profile” on the outer and inner side. To understand this relationship, the following steps should be explained:

- **Step 1:** studying stress states (see Figure 5-2-c and Figure 5-2-d) by considering the compressive stress and bending effect that act on the “flat sheet part” and “buckled sheet part” proposed by J. B. Kim [Kim03]; see Figure 5-2-a and Figure 5-2-b.
- **Step 2:** analysing the resultant stress of the adopted “sheet part” at the points O_0 and O_1 to determine the outer/inner side stress difference; see Figure 5-2-e and Figure 5-2-f.

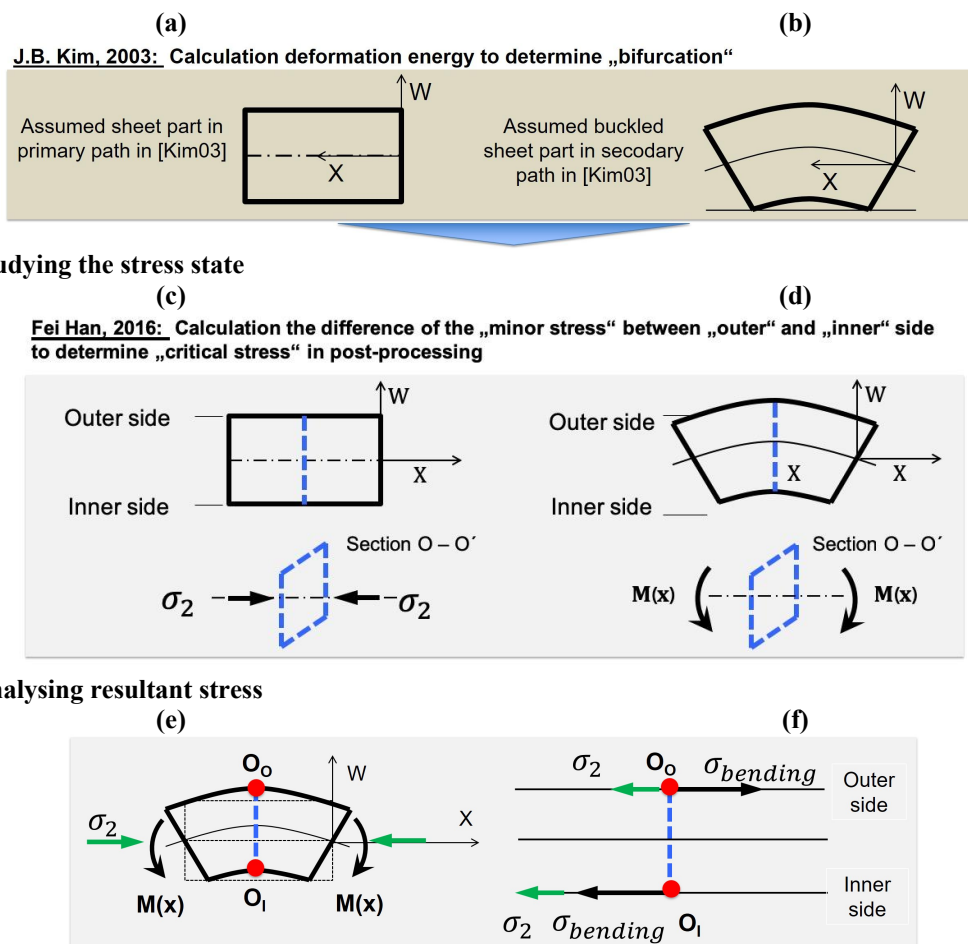


Figure 5-2: (a) Assumed “flat sheet part in primary path” according to [Kim03]; (b) Assumed “buckled sheet part in primary path” according to [Kim03]; (c) compressive stress acting on “flat sheet part” in FEA considering outer and inner side; (d) bending moment acting on “buckled sheet part” in FEA considering outer and inner side; (e) defined “wrinkling tendency” of an element in FEA considering outer and inner side and given O_0 and O_1 points; (f) resultant stress at investigated points O_0 and O_1 in minor principal direction considering compressive stress and stress induced by bending moment $M(x)$

Two states of the sheet part were assumed in order to study the change in energy during the deformation in accordance with the approach of J. B. Kim [Kim03], namely “flat sheet part in primary path” (see Figure 5-2-a) and “buckled sheet part in secondary path” (see Figure 5-2-b). Compared to the method of J. B. Kim, this section considers the three layers of the investigated element (outer side, middle layer and inner side). In addition, no “changes in energy” during the forming process have been studied. However, the stress state considering compressive stress (σ_2 ; see Figure 5-2-c) and the stress values induced by “local bending effect” (bending moment $M(x)$, see Figure 5-2-d and σ_{bending} ; see Figure 5-2-f) on both the outer side and inner side of the adopted sheet part are studied. When an element in FEA is subjected to compressive stress in the minor principal direction and bending moment $M(x)$ simultaneously, a “wrinkling tendency” can be identified in accordance with the DSCS-approach (see Figure 5-2-e).

In this way, the surface quality can be scored solely depending on the critical value of the “outer/inner side stress difference” (see Figure 5-2-f). The red point O_O (point o on the outer side) and O_I (point c on the inner side) indicates the location of “maximum tensile stress” induced by bending moment $M(x)$ and “maximum compressive stress” induced by bending moment $M(x)$, respectively. For the sake of clarity, only the stress state at points O_O and O_I will be investigated in the following sections. According to the critical value of the “outer/inner side stress difference”, four levels of surface quality can be defined:

- “No surface defect” before bifurcation and “surface defect initiation” (see Section 5.2.2)
- Surface defect at “wrinkling initiation” and “developed wrinkling” (see Sections 5.2.3 / 5.2.4)

The difference between Kim’s “energy model” and the proposed “concept of the DSCS approach” in Chapter 5 is summarised as follows:

- 1) In the “energy model” based on the work of Kim, the deformation energy was calculated in the “unbuckled part” as well as “buckled part”, respectively. According to his approach, only one time point – “Moment of bifurcation” – can be identified.
- 2) The concept of the “DSCS-approach” is based on the “unbuckled part” as well as “buckled part” also proposed by Kim. However, in the DSCS-approach, only the “outer/inner side stress difference” is considered. With this, not only “bifurcation”, but also the “wrinkling initiation” and “developed wrinkling” can be identified. Details will be shown in the next section.

By applying the concept of the DSCS approach, an overview of the wrinkling process can be established. Details about the defined “bifurcation”, “wrinkling initiation”, and “developed wrinkling” will be provided in the following chapters.

5.1.2 Detecting bifurcation by analysing the stress state

In this section, the “surface defect initiation” is defined as the point in time at which the resultant

stresses at point O_o (outer side) and O_i (inner side) exhibit a difference in terms of a threshold (see Figure 5-3-b). This “surface defect initiation” can also be viewed as a kind of bifurcation, since the outer/inner side stress difference occurs when surface deviation Δw exists. The point in time when “surface defect initiation” takes place indicates a similar bifurcation phenomenon that was introduced by Kim and his energy model. Before the defined “bifurcation” occurs, no surface deviation (Δw) is observed and the outer/inner side stress difference is found balanced; see Figure 5-3-b.

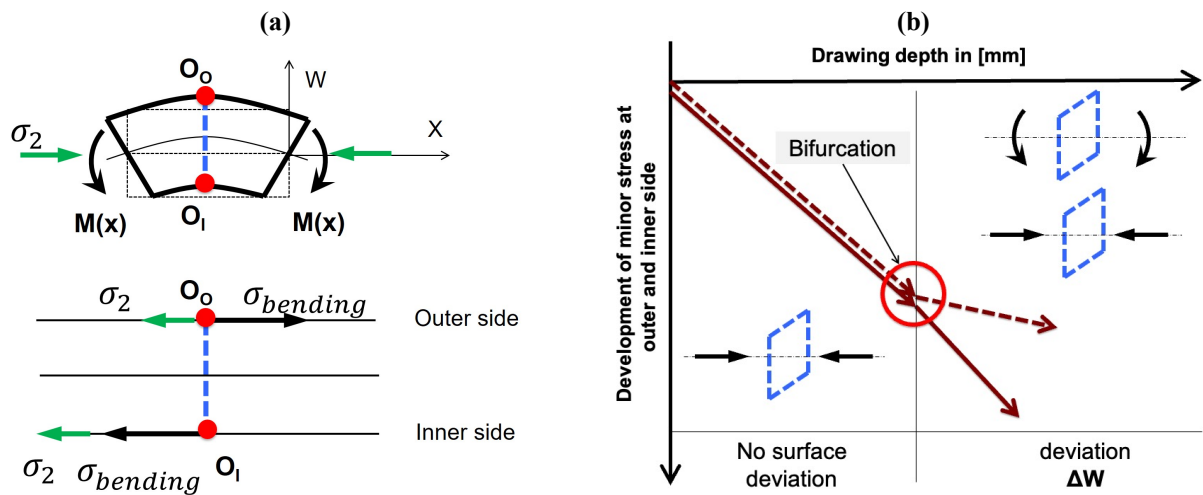


Figure 5-3: Development of outer/inner side stress difference: (a) definition of surface deviation Δw and resultant stress at O_o and O_i considering tensile stress and compressive stress induced by the bending moment; (b) identification of “bifurcation” by evaluating the resultant stress difference between O_o and O_i on the outer/inner side

To better understand the “outer/inner side stress difference” acting on an element in the FEA, the “resultant stress” at both O_o and O_i will first be investigated. After the “surface defect initiation”, the bending moment $M(x)$ induces tensile stress at point O_o (see $\sigma_{bending}$ at O_o) and compressive stress at point O_i (see $\sigma_{bending}$ at O_i). Therefore, the change in the resultant stress values at points O_o and O_i emerge after the time point “surface defect initiation” and can be calculated by Equations 5.1 and 5.2.

$$\sigma_{resultant}^{O_o} = -\sigma_{comp.}^{O_o} + \sigma_{bending} \quad (5.1)$$

$$\sigma_{resultant}^{O_i} = -\sigma_{comp.}^{O_i} - \sigma_{bending}$$

$$\text{before surface defect initiation } \sigma^{outer.} = \sigma^{inner} \rightarrow \text{after: } \sigma^{outer} \neq \sigma^{inner} \quad (5.2)$$

Assuming that an element in FEA is suffering compressive stress and has wrinkling tendency. Under such a situation this element can be described as a cylindrical bending area defining by a radius of curvature ρ (see Figure 5-3-a). According to the sheet thickness coordinate y , the resulting stress can be calculated as follows:

$$\sigma_{resultant}^{O_o}(y) = -\frac{F_2}{S} + \sigma_{bending} \quad (5.3)$$

The tensile stress at a coordinate y from the neutral axis can be calculated as follows, when E represents Young's modulus and ϑ is Poisson's ratio, respectively. S is the cross-sectional area of the finite element. Besides F_2 represents the compressive force along the minor direction. Therefore, the resultant stresses at points O_o and O_I can be expressed as follows:

$$\sigma_{resultant}^{O_o}(y) = -\frac{F_2}{S} + \frac{E}{1 - \vartheta^2} \times \frac{y}{\rho} \quad (5.4-a)$$

$$\sigma_{resultant\ stress}^I(y) = -\frac{F_2}{S} - \frac{E}{1 - \vartheta^2} \times \frac{y}{\rho} \quad (5.4-b)$$

When y is set to sheet thickness $t/2 \rightarrow y = t/2$, the resultant stresses on both surfaces can be determined as follows:

$$\sigma_{resultant\ stress}^{O_o} = -\frac{F_2}{S} + \frac{E}{1 - \vartheta^2} \times \frac{t}{2\rho} \quad (5.5-a)$$

$$\sigma_{resultant\ stress}^{O_I} = -\frac{F_2}{S} - \frac{E}{1 - \vartheta^2} \times \frac{t}{2\rho} \quad (5.5-b)$$

5.1.3 Identification of both wrinkling initiation and developed wrinkling

Models for calculating tensile stress and compressive stress induced by bending moment $M(x)$

Since the resultant stresses $\sigma_{resultant}^{O_o}$ and $\sigma_{resultant}^{O_I}$ are mainly affected by the local bending process after instability ($+\sigma_{bending}$ and $-\sigma_{bending}$), it is first necessary to select a model for determining the tensile and compressive stresses induced by bending moment $M(x)$ on the outer side and inner side. It can be assumed that the strain-hardening model of the investigated material follows Hollomon's power law described in Equation 2.21-a. The value of the tensile and compressive stresses at coordinate thickness direction $t/2$ with local curvature $1/\rho$ (where ρ is the radius of local curvature) can be calculated with Equation 5.6 [Mar02]:

This equation indicates that both the tensile stress $\sigma_{bending}^{O_o}$ and the compressive stress $\sigma_{bending}^{O_I}$ increase as the local curvature $1/\rho$ increases. Figure 5-4-a illustrates the relationship between $\sigma_{bending}^{O_o}$ and the local curvature $1/\rho$. Since the change in the local curvature $1/\rho$ is related to drawing depth, the relationship between $\sigma_{bending}^{O_o}$ and can be estimated; see Figure 5-4-b.

$$\sigma_{bending}^{O_o} = K \left(\frac{t}{2\rho} \right)^n, \text{ and } \sigma_{bending}^{O_I} = -K \left(\frac{t}{2\rho} \right)^n \quad (5.6)$$

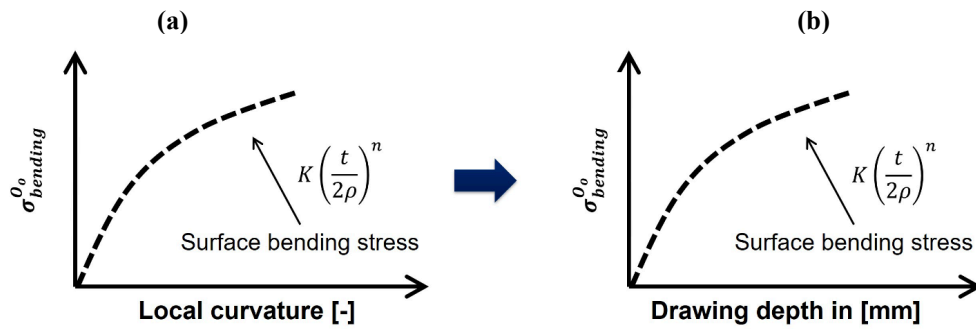


Figure 5-4: Explanation for the development of the term “ $\sigma_{bending}^{Outer}$ ” in Equation 5.6: (a) development of tensile stress $\sigma_{bending}^{Oo}$ induced by bending moment $M(x)$ at point O_o as the function of local curvature; (b) development of tensile stress $\sigma_{bending}^{Oo}$ induced by bending moment $M(x)$ at the O_o as the function of drawing depth

Stress state on the outer side (O) – change of state in resultant stresses

Considering the effect of the force F_2 the development of the resultant stresses on the outer and inner side during the test can be presented as follows:

$$\sigma_{resultant}^{Oo} = -\frac{F_2}{S} + K \left(\frac{t}{2\rho} \right)^n, \text{ and } \sigma_{resultant}^{Oi} = -\frac{F_2}{S} - K \left(\frac{t}{2\rho} \right)^n \quad (5.7)$$

To better understand the development of the term “ $-\frac{F_2}{S}$ ” in Equation 5.7, the change in force $|F_2|$ during the forming process is illustrated in Figure 5-5-a. The force–displacement curve used is derived from the BBT test introduced in Chapter 4.

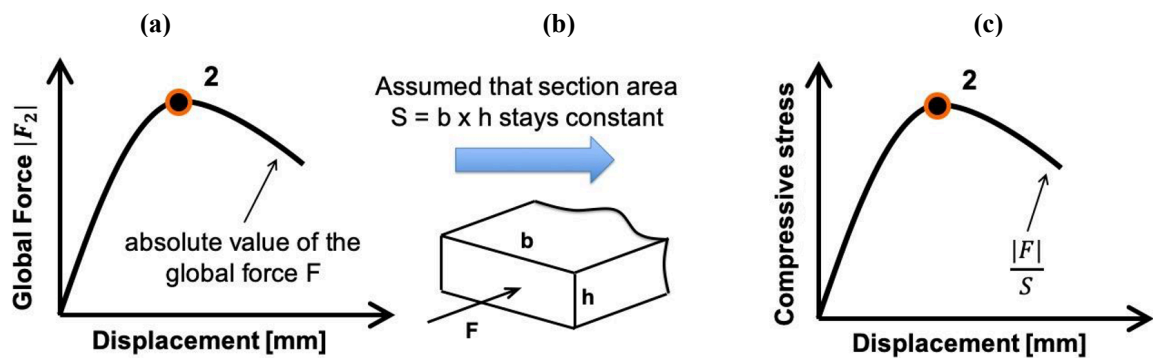


Figure 5-5: Explanation of development of the term “ $-\frac{F_2}{S}$ ” in Equation 5.7: (a) absolute value of development of the compressive force F_2 at point O_o as a function of tool displacement; (b) assumed constant section area S of the tested BBT specimen; (c) compressive stress induced by $|F_2|$ at point O_o as a function of tool displacement by considering a constant specimen section S

By assuming a constant specimen section S (depicted in Figure 5-5-b), the relationship between compressive stress $-\frac{F_2}{S}$ and drawing depth can be presented in Figure 5-5-c. The point in time “2” in Figure 5-5-a and Figure 5-5-c indicates the “wrinkling initiation” as introduced in Chapter 4.

As mentioned, the value of the resultant stresses $\sigma_{resultant}^{Oo}$ can be determined in Equation 5.7.

According to the results of the BBT test described in Chapter 4, before the defined “wrinkling initiation” emerge the compressive stress $-\frac{F_2}{S}$ played an important role (dominating the stress state on the outer side) compared to tensile stress $K\left(\frac{t}{2\rho}\right)^n$ caused by bending moment $M(x)$.

After the defined point of time “wrinkling initiation” is passed, the force F_2 decreases significantly since the structure of the buckled specimen cannot withstand any more external force (see experiment results in Chapter 4). Furthermore, the local curvature $1/\rho$ increases rapidly after wrinkling initiation. In turn, this rapidly increased curvature leads to an increase in tensile stress $K\left(\frac{t}{2\rho}\right)^n$ too. To better understand this phenomenon (before and after wrinkling initiation), Figure 5-4-b and Figure 5-5-c are investigated together in Figure 5-6. The analysis of the tensile stress $K\left(\frac{t}{2\rho}\right)^n$ and compressive stress $-\frac{F_2}{S}$ is depicted in Figure 5-6-a.

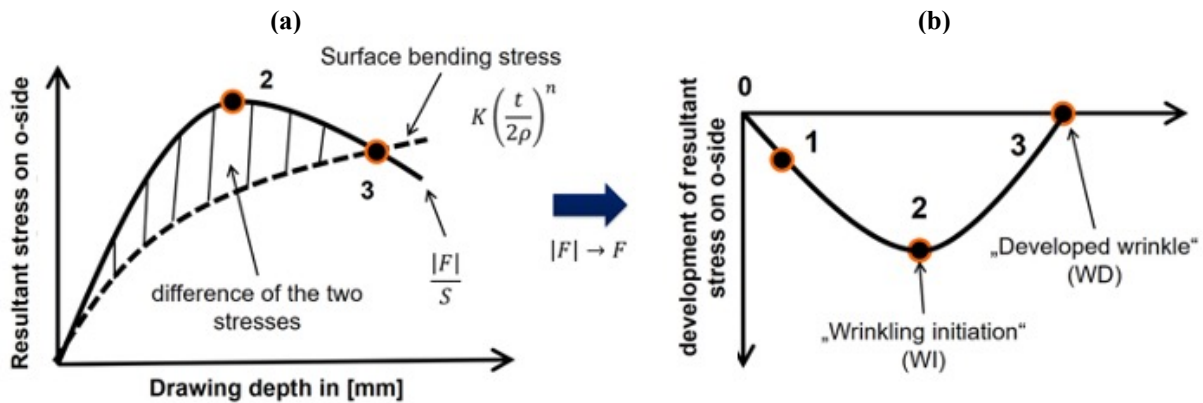


Figure 5-6: Explanation for the development of $\sigma_{resultant}^{Outer}$ in Equation 5.7: (a) definition of “wrinkling initiation” and “developed wrinkling” by evaluating the resultant stress on the outer side considering terms $-\frac{F}{S}$ and $K\left(\frac{t}{2\rho}\right)^n$ in Equation 5.7; (b) actual development of resultant stress at O_o (outer side) without considering absolute value of force ($|F| \rightarrow F$)

The value of the $\sigma_{resultant}^{O_o}$ on the outer side can be presented as the difference between these two stress values $K\left(\frac{t}{2\rho}\right)^n$ and $-\frac{F_2}{S}$ (see shaded area in Figure 5-6-a). Obviously, the difference between both stress values increases towards point 2, i.e. the wrinkling initiation point. After “wrinkling initiation” (WI), due to the continual increase of tensile stress $K\left(\frac{t}{2\rho}\right)^n$ and simultaneous decrease in the stress $-\frac{F_2}{S}$ on the outer side, the sign of the value of $\sigma_{resultant}^{O_o}$ in Equation 5.7 ultimately changes from “-” to “+” (at point 3). When the value of the compressive stress $-\frac{F_2}{S}$ is equal to the tensile stress $K\left(\frac{t}{2\rho}\right)^n$ at point 3, “developed wrinkling” (DW) is identified as occurring, as illustrated in Figure 5-6.

Finally, the development of the resultant stress $\sigma_{resultant}^{O_o}$ can be transformed from Figure 5-6-a

into Figure 5-6-b, which shows the same tendency as the FEA results of buckling tests with an M-YBT specimen and mini-CCT tests presented in Section 7.1 and 7.2.

Therefore, “point 2” and “point 3” are defined as “wrinkling initiation” and “developed wrinkling”, which each take into account the development of stress states on the outer side. Section 5.2.4 will discuss the development of stress on the inner side. According to this logic, “wrinkling initiation” (WI) and “developed wrinkling” (DW) can be defined and presented in Equations 5.8 and 5.9.

After defining the stress threshold corresponding to the wrinkling initiation, it was observed that the local curvature was further increased due to the occurrence of local instability. In order to detect wrinkles that have occurred, two phases (before and after wrinkling initiation) should be distinguished in Table 5-2.

$$WI = MAX. \left[-\frac{F}{S} + K \left(\frac{t}{2\rho} \right)^n \right], \text{ with } \left[-\frac{F}{S} + K \left(\frac{t}{2\rho} \right)^n \right] \in (-\infty, 0) \quad (5.8)$$

$$WD = \sigma_{resultant}^{O_o} = 0 \quad (5.9)$$

Table 5-2: Change of sign of resultant stress on outer/inner side before and after wrinkling initiation

	Phase 1: Before wrinkling initiation	Phase 2: After wrinkling initiation
Influence of the stress caused by force F_2 :	Large (Figure 5-5)	Small (Figure 5-5)
Sign of the stress caused by global force F_2 on outer side:	“-” (Figure 5-3)	“-” (Figure 5-3)
Sign of the stress caused by global force F_2 on inner side:	“-” (Figure 5-3)	“-” (Figure 5-3)
Influence of the bending stress:	Small (when ρ is large)	Large (when ρ is small)
Sign (bending stress) on outer side:	“+” (Figure 5-6)	“+” (Figure 5-6)
Sign (bending stress) on inner side:	“-” (Eq. 5-7)	“-” (Eq. 5-7)
Stress state of outer side:	Compressive stress	Turns into tensile stress
Stress state of inner side:	Compressive stress	Compressive stress

5.1.4 Characterising the degree of wrinkling by evaluating the development of stress

According to the analysis described in Sections 5.2.2 to 5.2.4, the definitions of “bifurcation”, “wrinkling initiation”, and “developed wrinkling” are shown in Table 5-4. For the detection of “bifurcation”, the stress $\sigma_{resultant}^{O_o}$ on the outer side and stress $\sigma_{resultant}^{O_i}$ on the inner side should be checked, as already explained. If these two values differ, surface defect initiation will be defined as “occurring”. The time point of bifurcation can be understood as the “onset of buckling”.

For detecting “wrinkling initiation” and “developed wrinkling” it is only possible to judge whether both effects exist by investigating the development of $\sigma_{resultant}^{O_o}$. Since post processing cannot

evaluate the entire stress curve from point 0 to point 3 as illustrated in Figure 5-6-b, new definitions of these “three phases” should be formulated.

Table 5-4: Comparison of different methods for defining wrinkling initiation

Surface quality	Definition	Applicability in FEA
Bifurcation	Resultant stress between outer/ inner side differs	Possible
Wrinkling initiation	Resultant stress on outer side reaches maximum	Impossible
	Resultant stress between outer and inner side	Possible
Developed wrinkling	Resultant stress on outer side equal to 0	Impossible
	Resultant stress between outer and inner side	Possible

The “outer/inner side stress difference” is therefore introduced as a criterion for evaluating the “degree of surface quality” and predicting “wrinkling initiation” and “developed wrinkling” in the wrinkling process. Figure 5-7 illustrates the development of $\sigma_{resultant}^{Oo}$ (see Figure 5-7-a) and the development of $\sigma_{resultant}^{Oi}$ (see Figure 5-7-b).

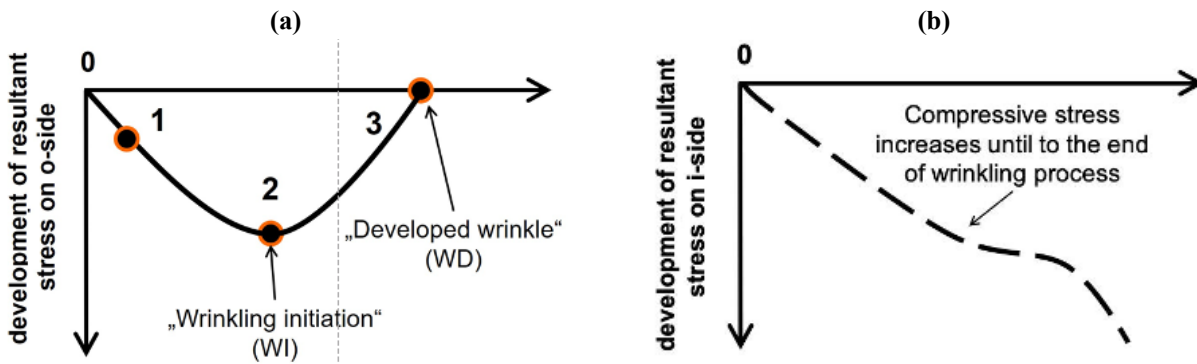
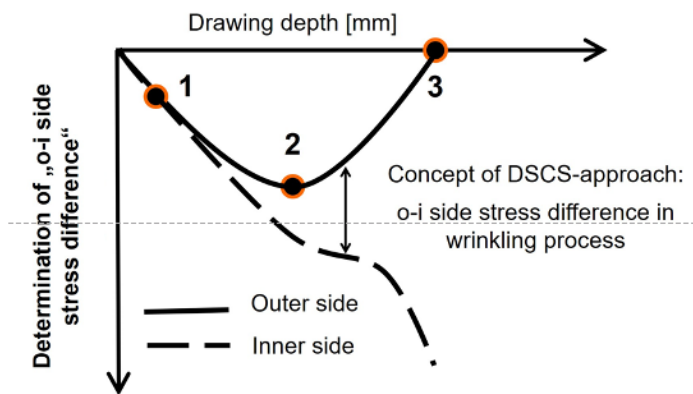


Figure 5-7: Development of resultant stress: (a) development of resultant stress on the outer side with definition of “bifurcation” at point 1, “wrinkling initiation” at point 2, and “developed wrinkling” at point 3; (b) development of resultant stress on the part inner side

Considering outer and inner side of an element in FEA:



Input parameters:

- Material properties
- Lubrication condition
- Geometries of effective compressive region

Output parameters:

- Development of the compressive stress on the outer and inner side
- Outer/inner side stress difference

Figure 5-8: Concept and fundamental idea of the DSCS-approach – difference in resultant stress between the outer side and inner side increases towards the end of the wrinkling process

The black curve in Figure 5-7-a indicates the development of the resultant stress on the outer side, while the dotted black curve in Figure 5-7-b indicates the development of the resultant stress on the inner side.

In order to better understand the changes in the resultant stresses on both the outer and inner side of the investigated element in the wrinkling area, the development of $\sigma_{resultant}^{Oo}$ and $\sigma_{resultant}^{OI}$ is shown in Figure 5-8.

Under a tensile-compressive stress state, a studied region is considered to have no surface defects when the drawing depth is located between time interval phase 0 and 1. When surface defect initiation occurs at point 1, the resultant stress on the outer and inner side begins to exhibit a slight difference: the introduced “outer/inner side stress difference”. At point 3 (“developed wrinkling”), the outer/inner side stress difference increases significantly because of the increasing influence of the local bending effect in the wrinkling area.

Regardless of material properties, lubrication conditions, and specimen geometry, the outer/inner side stress will differ for as long as wrinkles occur, and this stress difference will increase towards the end of the wrinkling process. For a given material, the critical value of the outer/inner side stress difference at “wrinkling initiation” and “developed wrinkling” can be determined. The details for determining the critical value considering other parameters like sheet thickness and local curvature can be found in Chapter 6.

5.2 Application of the newly developed concept in post processing FEA code

Chapter 4 and Section 5.2.4 explain the reasons for using outer/inner side stress difference to detect wrinkle formation in FEA. The advantages of using the concept of the DSCS-approach in a post processing code are listed below:

- The DSCS concept not only can be applied for detecting wrinkles of second order, but also for other scenarios considering tool contact and for manufacturing complex deep drawn parts in industry (see Chapter 8).
- Every element located in an area potentially exposed to a wrinkling tendency can be observed and evaluated separately.
- The dimension of the wrinkling area does not have to be considered. In general, the effective size of the wrinkling area should be given when using the analytical model to calculate the critical compressive stress. In practice, wrinkling areas are difficult to define.
- The desired values for the resultant surface stress on both the outer and inner side of sheet metal component can be taken directly from commercial FEA software (e.g. “minor stress” in AutoForm, or “minor principal stress” in LS-Dyna). This is convenient for preparing UDV files.

- “Wrinkling initiation” and “developed wrinkling” can be detected by means of the critical stress level with the same criterion. The extremely high “bifurcation” requirements introduced in Section 5.2.1 can also be taken into account when using the DSCS approach.

Potential application for predicting wrinkling height

It is well known that the strain based wrinkling criterion “potential wrinkling” used in AutoForm cannot predict height of emerging wrinkles. Therefore, the degree of surface quality only can be described by the calculated “wrinkling factors”. These kinds of “wrinkling factors” are applied in post-processing to predict the wrinkling degree. Compared to defined parameter “potential wrinkling” used in AutoForm, the wrinkling height can be measured at the time points “bifurcation”, “wrinkling initiation”, and “developed wrinkling” based on the definition of DSCS approach. The measured wrinkling height based on the M-YBT tests and mini-CCT tests are explained more deeply in Chapter 7. In the buckling test performed with the M-YBT specimen (material HC420LA, thickness 1.0 mm), the wrinkling height emerges as very small (approximately 0.002 mm) at the defined “bifurcation” point. The wrinkling height at “wrinkling initiation” and “developed wrinkling” was approximately measured to 0.04 mm and 1.1 mm in that test, respectively.

For the validation in Chapter 8, the introduced surface defect “bifurcation” is therefore not considered in the UDV file to save evaluation time in post processing. Here, “wrinkling initiation” was defined with the colour yellow, while “developed wrinkling” is defined with the colour red, see Fig. 5-9-b. An overview of the surface condition at each drawing depth can be realised.

Application of the concept of the DSCS-approach in a post processing code

According to the analysis from Chapter 4/5, the DSCS-concept was developed into a regression model as discussed in Chapter 6, and, in addition, deep drawn parts from industry will be validated too in Chapter 8 based on the new DSCS-approach. This approach is using two boundary conditions for detecting “wrinkling initiation” and “developed wrinkling” according to Fig. 5-9.

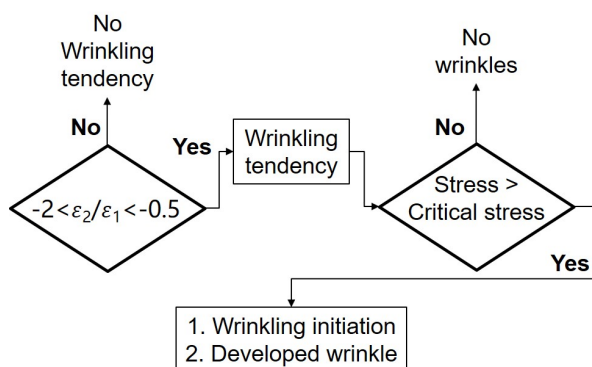


Figure 5-9: (a) Concept of the strain based UDV used in Chapter 8 for detecting “wrinkling initiation” and “developed wrinkling”; (b) defined colours for predicting wrinkling height in FEA

Boundary condition 1 is used to select elements in FEA exposed to risk of “wrinkling tendency”. First of all, the value of $\varepsilon_2 / \varepsilon_1$ should be determined (using a strain based UDV; see Figure 5-9) to select the elements located in that potentially critical area of “wrinkling tendency”. The workflow for a stress based UDV will be explained in Chapter 8 in Figure 8-1.

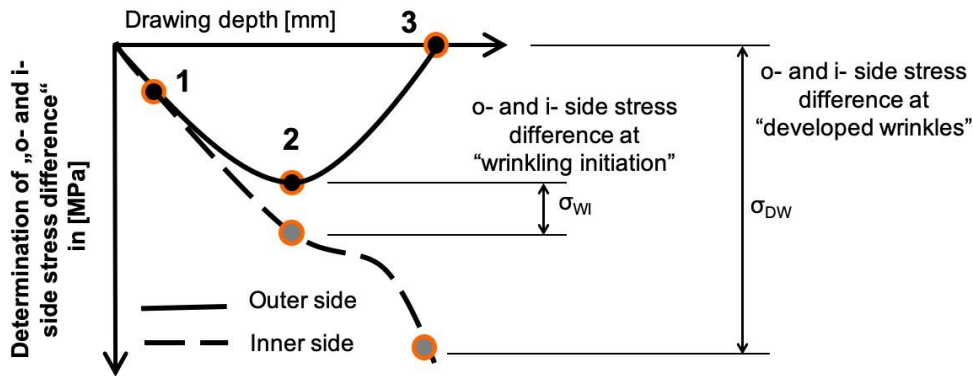


Figure 5-10: Illustration of definition of outer/inner side stress difference at “wrinkling initiation” (σ_{WI}) and “developed wrinkling” (σ_{DW})

Proposed method for determining those critical stresses is illustrated in Figure 5-10. Resultant surface stresses at “wrinkling initiation” and “developed wrinkling” are written as “ σ_{WI} ” and “ σ_{DW} ”, respectively. Utilizing both stress values, a simple sketch of the concept of the DSCS approach for integration in an enhanced post processing code can be drawn (see Figure 5-11, where the black curve shows the outer/inner side stress difference). The red dotted line indicates the safe range of the element under investigation in FEA. When the calculated outer/inner side stress difference in that concerning element is located within the safe range, wrinkling is not initiated.

In addition, if the values of the outer/inner side stress difference are greater than a certain critical value (e.g. the critical value of the safe range), wrinkling starts. If the value of the outer/inner side stress difference is greater than the defined critical value of “developed wrinkling”, severe wrinkles will occur (see blue dotted lines in Figure 5-11).

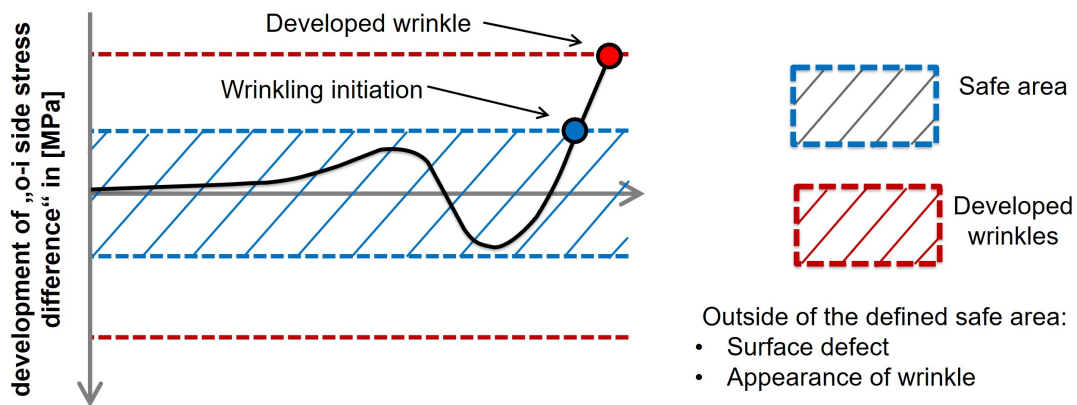


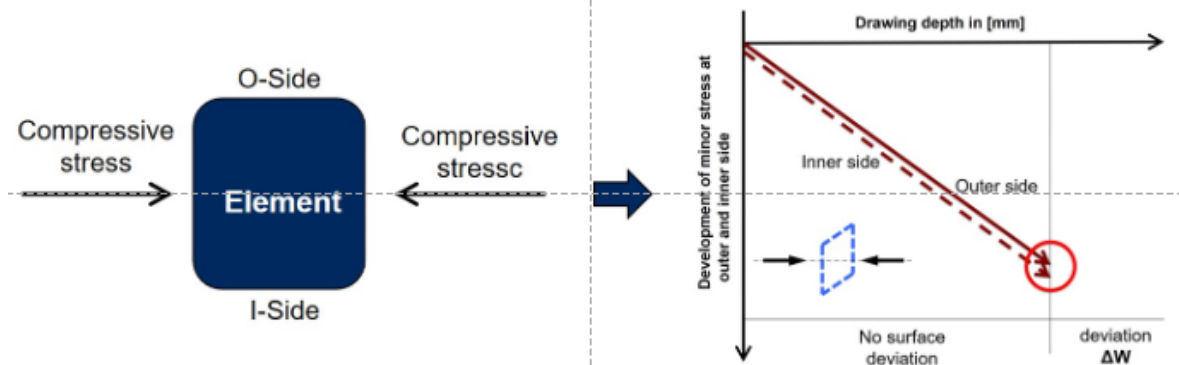
Figure 5-11: Illustration of the application of the concept of DSCS-approach in post processing with definition of the “safe range” and “developed wrinkling”

5.3 Conclusion

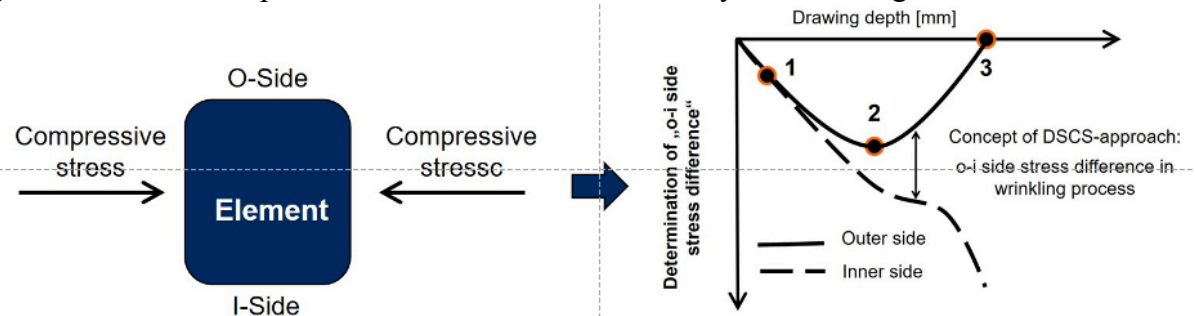
Importance of the DSCS-approach

As mentioned above, the stress state leading to “wrinkling tendency” does not refer to wrinkles. In other words, if an element is suffering from compressive stress, as long as this element can hold the stability itself, wrinkling initiation will not take place. A good example can be shown by using a shear specimen (see. Fig. 5-12-c). This case was described in Figure 5-12 (case 1)

(a) **Case 1:** under compressive stress and **hold** it’s stability \Rightarrow wrinkling will not take place



(b) **Case 2:** under compressive stress and **loose** it’s stability \Rightarrow wrinkling initiation



(c) Shear specimen belongs to the situation in case 1

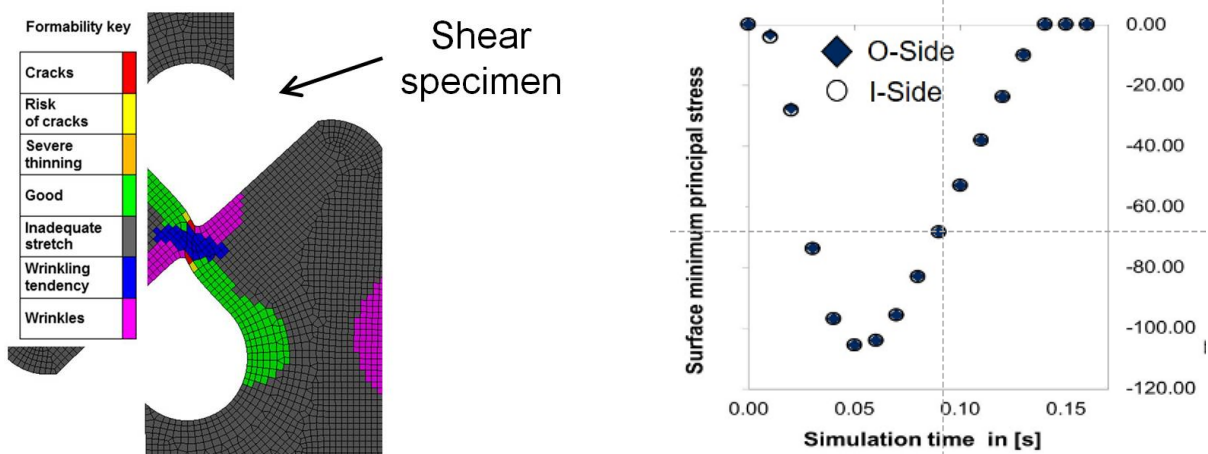


Figure 5-12: Illustration of the application of the concept of DSCS-approach in post processing with definition of the “safe range” and “developed wrinkling”

According to the concept of DSCS-approach, in FEA when an element suffering compressive stress can hold it’s structure stability, the stresses on O-side and I-side show no deviation, see

Figure 5-12-a. When an element cannot hold the structure stability, the stresses on O-side and I-side will show a deviation. This phenomenon was presented in Figure 5-12-b.

FEA Results by using LS-Dyna regarding the case study of shear specimen was shown in Figure 5-12-c. FEA results shown that the centre part of the shear specimen has wrinkling tendency (colour blue) and wrinkles (colour pink). However, according to experimental results no wrinkling or buckling phenomenon was observed during the test. The reason can be explained by using DSCS-concept. The centre part of the shear specimen can hold the structure stability, thus stresses on O-side and I-side show no deviation during the forming process, although the centre part of the specimen suffering compressive stress.

Practical case: Wrinkles considering two sides tool contact and change of wrinkling direction

As an example, the simulation results from part Door-Frame-Adapter was shown in Fig. 5-13. By evaluating the stress state at O-side and I-side, the changed wrinkling direction can be observed by using FEA. In Figure 5-13-b, the first wrinkle marked with number “1” changes its wrinkling direction and the second wrinkle marked with number “2” takes place. Then the second wrinkle changes the wrinkling direction again. The wrinkling direction turns back into the direction of the first wrinkle.

No matter how the wrinkling direction changes, the wrinkling formation and wrinkling initiation can be detected by applying DSCS-approach. Since the DSCS-approach uses the deviation of the stress values between O-side and I-side. No matter how the wrinkling direction changes, the position of the O-side and I-side will be changed, but the deviation still exists.

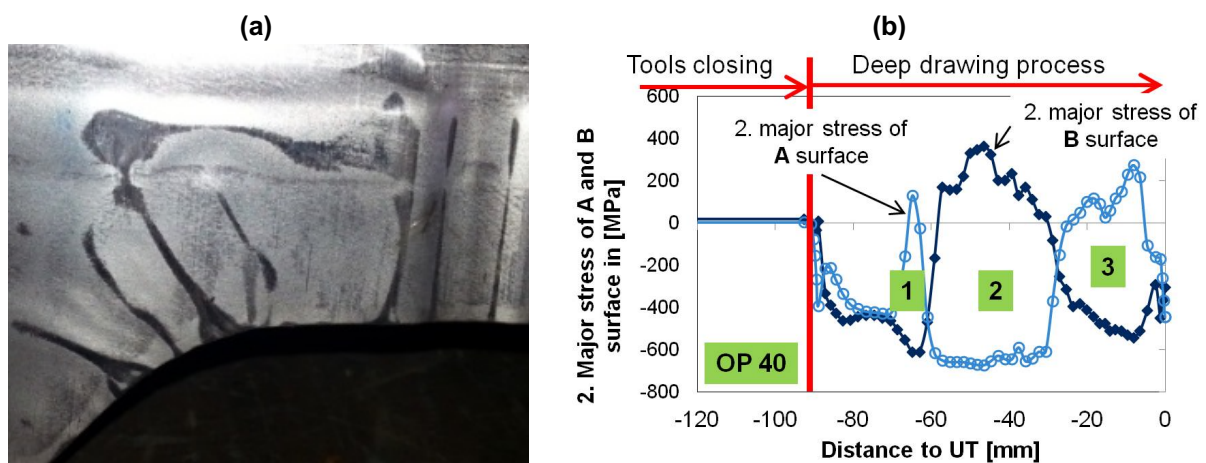


Figure 5-13: Simulation results of Door-Frame-Adapter: (a) Pattern of wrinkles under two sides tools contact during the forming process; (b) Change of the wrinkling direction under condition double side tools contact

6 Regression models considering essential factors affecting wrinkling process

According to the second task for developing the DSCS-approach was completed in Chapter 5. The third task is to develop regression models for predicting the critical values of the difference between the outer and inner side at “wrinkling initiation” and “developed wrinkling” considering entire set of influencing factors (see Figure 6-1). Factors that influence the wrinkling behaviour significantly (such as material properties, sheet thicknesses “ t ” and initial local curvature “ K^{lc} ” were reviewed in Chapter 2. Two of the most critical influencing factors (namely sheet thickness “ t ” and local curvature “ K^{lc} ”, which were taken into account when developing regression models for a given material) are investigated using LS-DYNA in Sections 6.2 to 6.4. The preferred method of designing regression models is introduced in Section 6.5.

In Chapter 6, all linear-regression models are developed based on the “Design of Experiments” (DoE) approach. Three different sheet materials were studied in Chapter 6 with two different sheet thicknesses of 0.6 mm and 1.0 mm. These three materials are micro-alloyed sheet metal HC300LA, HC420LA, and the mild steel DX54D. The determined regression models will be used in terms of UDV files to validate complex shaped sheet metal forming parts from industry in Chapter 8.

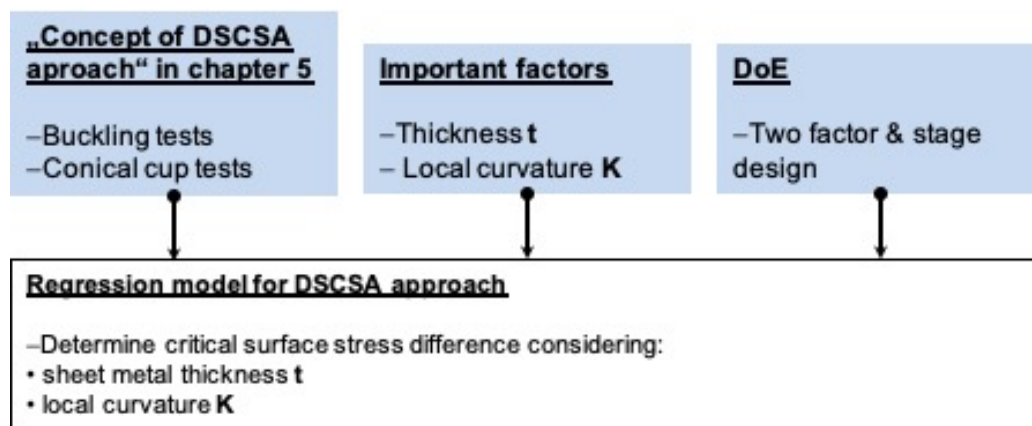


Figure 6-1: Further development of the concept of the DSCS-approach (proposed in Chapter 5) using DoE to yield regression models considering essential factors

6.1 Essential factors affecting the wrinkling process

There are several reasons to choose sheet thickness “ t ” and local curvature “ K^{lc} ” as crucial factors when determining linear-regression models for calculating value of critical stress which will be used as criteria in FEA. Firstly, according to the results of research by Y. S. Kim, wrinkling formation can be more effectively controlled by changing sheet thickness “ t ” than the strain-hardening coefficient “ n ”, yield stress “ $R_{p0.2}$ ”, and anisotropy value “ R ” [Kim99]. He points out that the metallurgical process influences parameters such as the strain-hardening coefficient “ n ”, yield stress “ $R_{p0.2}$ ”, and anisotropy value “ R ”. Since these values cannot be changed, the factors

concerned cannot be used to establish a regression model from a DoE perspective. J. W. Hutchison et al. studied the relationship between local curvature and critical stress [Hut74]. This relationship has been adopted by many other researchers over the past 30 years. Furthermore, the influence of the factor “local curvature” on wrinkling behaviour during metal forming process was confirmed directly through experiments by Han and Liewald [Han15]. The influence of the local curvature was considered in this paper using the DoE and considering two stages: K^{lc} -value = 0 (buckling test with modified Yoshida specimen) and K^{lc} -value = 0.025 (mini-CCT test). The anisotropy values R in different rolling directions do indeed influence effective strains when performing such tests. Therefore, by designing a strain based wrinkling limit curve (WLC) in FLD, anisotropy values R should be taken into account. In opposite to that, the anisotropy value R is not important in the case of a stress based wrinkling criterion like the energy approach described in Section 2.2.2 since the critical stress depends solely on the mechanical properties of the investigated sheet metal.

6.2 Influence of material on the difference in surface stress

To evaluate the influence of materials on the outer/inner side stress difference, three materials (namely HC300LA, HC420LA, and DX54D) are tested. The results and conclusion are given in the following Sections 6.2.1 and 6.2.2.

6.2.1 Influence of sheet thickness on the difference in surface stress

Investigated sheet metal material with a thickness of 0.6 mm

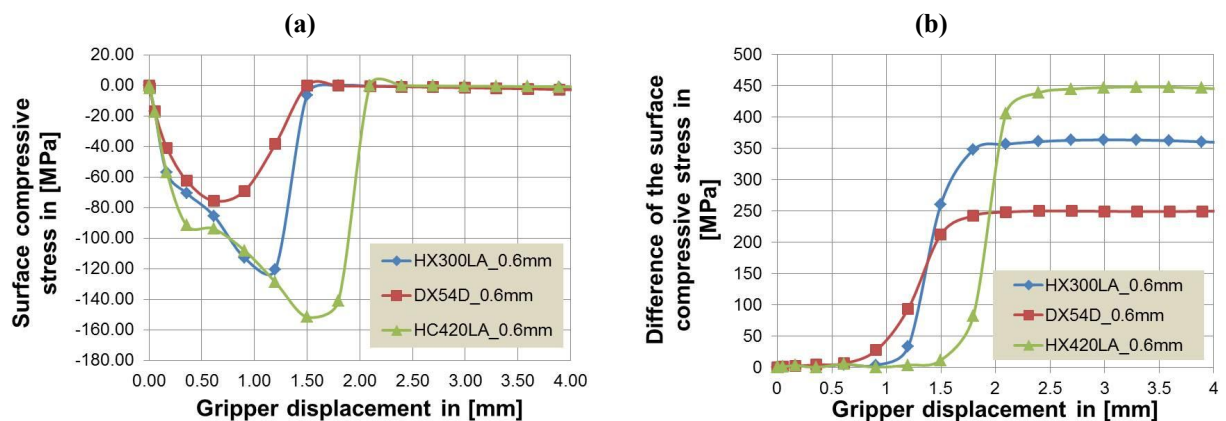


Figure 6-2: Based on the simulation results for a sheet thickness of 0.6 mm with the M-YBT specimen: (a) the development of the lateral surface stress as a function of the gripper displacement; (b) the difference between the internal and external stresses as a function of the gripper displacement

As previously mentioned, the minor principal stress cannot be directly measured through experiments. Therefore, FEA analyses were performed for stretching M-YBT specimens having a thickness of 0.6 mm. The results of the minor principal stress on the outer side of the investigated M-YBT specimen are illustrated in Figure 6-2-a. Obviously, the development of minor principal stress on the outer side of all the specimens made from materials HC300LA, HC420LA, and

DX54D shows the same tendency introduced in Section 4.2. The only difference is the gripper displacement when “wrinkling initiation” and “developed wrinkling” occur.

According to Figure 6-2-a, the point in time of the “wrinkling initiation” for all three materials can be determined by finding the maximum value for the minor principal stress on the outer side. When the minor principal stress on the outer side decreases to zero, the defined “developed wrinkling” occurs. For the sake of clarity, the point of “wrinkling initiation” and “developed wrinkling” for those three materials is replaced by “gripper displacement” as shown in Table 6-1.

In addition, the development of the outer/inner side stress difference between the beginning and the end of the test is shown in Figure 6-2-b. According to the gripper displacement determined at “wrinkling initiation” and “developed wrinkling” in Figure 6-2-a, it can be observed that different materials yield different critical values for the outer/inner side stress difference at wrinkling initiation (σ_{WI}) and developed wrinkling (σ_{DW}), respectively. The same tendency can also be identified when performing FEA analysis for conducting conical-cup tests.

6.2.2 Conclusion on the influence of sheet metal materials on wrinkling behaviour

Influence of materials on the defined “wrinkling initiation” and “developed wrinkling”

Taking the results of the FEA (Figure 6-2 and 6-3; Table 6-1 and 6-2), it can be confirmed that sheet metal materials do indeed have an influence on the following:

- 1) Development of minor principal stress on the outer side of sheet metal component
- 2) The value of the outer/inner side stress difference

Obviously, changing the value of the “outer/inner side stress difference” results in a change of point in time at which “wrinkling initiation” and “developed wrinkling” occur. Furthermore, the critical value of the “outer/inner side stress difference” is crucial for defining the “safe range” and “developed wrinkling range”.

Further information and outlook

Combining gained results and data listed in Figure 6-2 and 6-3, and Table 6-1 and 6-2, the following conclusions can be drawn:

- 1) The “K”-value used in the Swift material model primarily affects the critical value of the outer/inner side stress difference in the DSCS-approach. Figure 6-4 shows this trend. Since only three different materials were studied in this work, a linear-regression model was determined to describe the relationship between the “K” value and the critical value of the outer/inner side stress difference in the DSCS-approach.

To better understand material properties, the determined material parameters of sheet metals HC420LA, HC300LA, and DX54 are listed in Table 6-3.

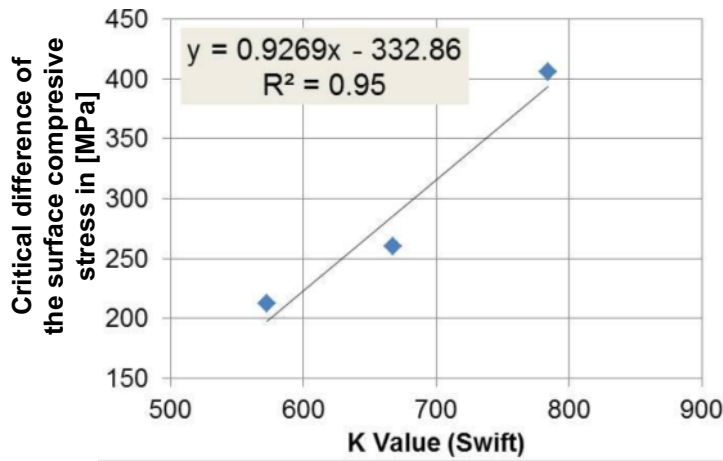


Figure 6-4: Relationship between critical surface-stress difference at developed wrinkling and K-value

Table 6-3: Material parameters of sheet metals used in Chapter 6

Sheet materials	K^{lc}	n	E_0	R-0°	R-45°	R-90°	Mean value of R
HC420LA	784.14	0.130	0.006388	0.6	1.2	1.7	1.17
HC300LA	667.75	0.179	0.011189	0.9	0.9	1.15	0.98
DX54D	572.66	0.244	0.005970	1.5	1.2	1.9	1.53

- 2) According to Table 6-3, the effect of anisotropy value R on the critical value of the outer/inner side stress difference σ_{WI} and σ_{DW} emerges as lower than the effect of sheet metal thickness t and local curvature K^{lc} . When determining the critical stress value by applying the DSCS-approach, the influence of the R values do not need to be taken into account.
- 3) According to the FEA results, there is a small difference between the values of σ_{DW} in Table 6-1 (material thickness 0.6 mm) and Table 6-2 (material thickness 1.0 mm).

In summary, according to the FEA results, the thickness of the sheet has no significant effect on the critical value of the outer/inner side stress difference at “developed wrinkling”. However, the factor “sheet thickness” used in the DSCS-approach does affect the formation of wrinkles significantly in another way, which is discussed in depth in Section 6.3 below.

6.3 Influence of sheet thickness on the difference in surface stress

In Section 6.2.2, it was confirmed that sheet thickness has no significant influence on the critical value of the outer/inner side stress difference at “developed wrinkling” according to the FEA results based on M-YBT specimens. However, experiments conducted have shown that sheet metal thicknesses do indeed have a significant impact on the wrinkling process. In Section 6.3, the reason will be investigated in depth and then explained in Section 6.3.2.

6.3.1 Wrinkling initiation when materials have different thicknesses

As an example, the FEA results based on material HC420LA with a thickness of 0.6 mm and 1.0 mm are shown in Figure 6-5-a and Figure 6-5-b, respectively. For the sheet thickness of 0.6 mm

in Figure 6-5-a, wrinkling initiation takes place at a gripper displacement of 1.5 mm. The developed wrinkling then occurs rapidly at a gripper displacement of 2.1 mm. In contrast, after reaching “wrinkling initiation”, the M-YBT specimen with a thickness of 1.0 mm provides a significantly longer transition area between “wrinkling initiation” and “developed wrinkling”, see Figure 6-5-b.

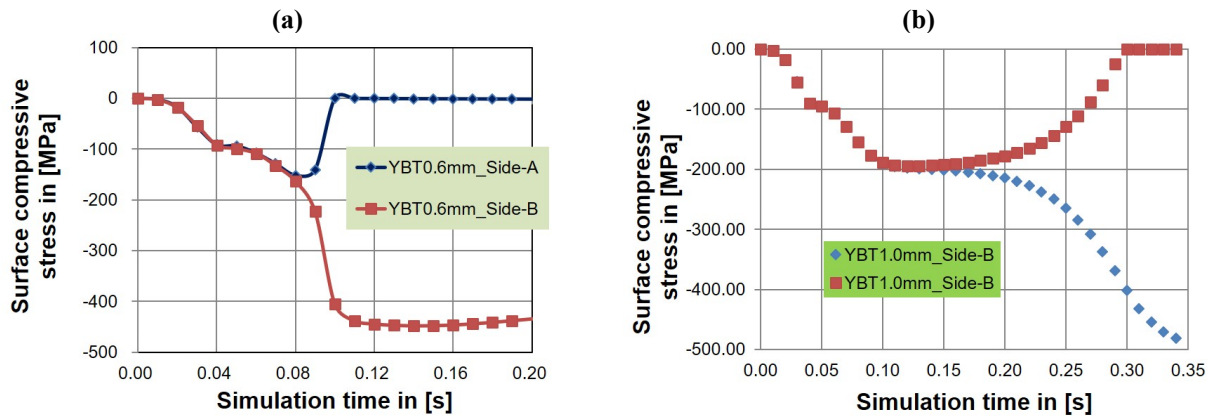


Figure 6-5: Simulation results based on M-YBT specimens, material HC420LA: (a) development of minor principal stress on both the outer and inner side of M-YBT specimen, sheet thickness of 0.6 mm; (b) development of minor principal stress both on the outer and inner side of M-YBT specimen, with sheet thickness of 1.0 mm

6.3.2 Conclusion on the influence of sheet thickness

According to the results of the FEA (Figure 6-5-a and Figure 6-5-b), it was confirmed that sheet thickness does indeed have an influence on “wrinkling initiation” and “developed wrinkling”. Although the critical value of σ_{WI} and σ_{DW} at “wrinkling initiation” and “developed wrinkling” among specimens with a thickness of 0.6 mm and 1.0 mm exhibits a small difference, the gripper displacement clearly differs; see Table 6-4.

Table 6-4: Influence of the sheet thickness on wrinkling initiation and developed wrinkling

Material and sheet thickness	WI at gripper displacement in [mm]	DW at gripper displacement in [mm]	σ_{WI} in [Mpa]	σ_{DW} in [Mpa]
HC420LA – 0.6 mm	1.5	2.1	11.5	405.6
HC420LA – 1.0 mm	3	8.2	12.4	431.6

In the case of the specimen with a sheet thickness of 0.6 mm, the “wrinkling initiation” and “developed wrinkling” occur at a gripper displacement of 1.5 mm and 2.1 mm, respectively (see Table 6-4; values compiled from Table 6-1 and Table 6-2). If the sheet thickness increases to 1.0 mm, the wrinkling initiation and developed wrinkling occur much later (at a gripper displacement of 3.0 mm and 8.2 mm). This phenomenon can be explained by varying bending stiffness of specimen, as described in Section 6.2.2.

To better understand this phenomenon, Figure 6-6 shows an additional graph. In essence, the wrinkling process can be imagined of as a change in local curvature. The bending stiffness of the

M-YBT specimen with a thickness of 0.6 mm is less than that of the specimen having a thickness of 1.0 mm. Therefore, in a specimen with a thickness of 0.6 mm, the change in local curvature is more sensitive, consequently a specimen having a small thickness (and therefore lower bending stiffness) reaches a critical local curvature more easily.

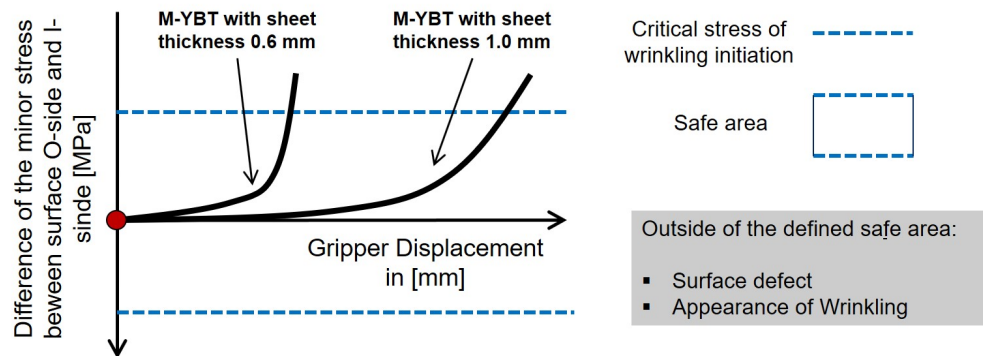


Figure 6-6: Diagram to explain the influence of sheet thickness on the wrinkling process using the FEA results based on material HC420LA with a thickness of 0.6 mm and 1.0 mm

In summary, if the local curvature of the studied wrinkling area reaches a critical value, wrinkling will occur regardless of the drawing depth. As previously mentioned, the following two further results can be concluded:

- 1) The critical value of σ_{WI} and σ_{DW} alone cannot represent all the influences on wrinkling behaviour of specimen. The “drawing depth” or “gripper displacement” at which “wrinkling initiation” and “developed wrinkling” occur are also important for indicating the “wrinkling tendency”.
- 2) By applying the DSCS-approach, the wrinkling process can be understood as a phenomenon of a change in the local curvature. Wrinkling tends to occur where the lowest bending stiffness can be found at that moment of load application.
- 3) If the value of “outer/inner side stress difference” reaches a critical value (see Figure 5-11) when “wrinkling initiation” or “developed wrinkling” occur.

6.4 Influence of local curvature on the critical stress level

Sections 6.2 and 6.3 describe the results of the FEA performed with M-YBT specimens to explain the effect of the material and sheet thickness on the wrinkling process. In the following sections, the conical-cup test (CCT) is used to show the effect of local curvature on the wrinkling process.

6.4.1 Determination of principal local curvature in experiments

Approaches for determining the local curvature of formed specimens – such as the CCT, M-YBT and KVG specimen – are illustrated in Figure 6-7. According to the work of H. Simon [Sim89], the very first wrinkle in a deep drawing process appears near the first third of the drawing depth.

For this reason, the curvature radii of a conical cup and a simplified part geometry likely to a passenger car fender were evaluated near the first third of the drawing depth. The line segment $O-O'$ in Figures 6-7-a and 6-7-c (both left and right) indicates the level of the first third of the drawing depth in the conical-cup test and in the experiment with a geometry based on that simplified car fender shape.

Figure 6-7-a depicts a simple cylindrical cup. As this part is symmetrical, the geometry can be used to derive the curvature of the sidewalls in the conical-cup test. The method for calculating the local curvature of the conical cup (near the first third of the drawing depth) is introduced in [Sel99]. The value of local curvature ($1/R$) in the sidewall of the conical cup is 0.025. This value will be used in the following chapters to finalize regression models. For KVG geometry, since the curvature of the left and right corners (see Figure 6-7-c) is too complex to calculate, these curvatures can be directly obtained by using the “curvature analysis” feature provided in the CAD program CATIA 5 (see Figure 6-7-c).

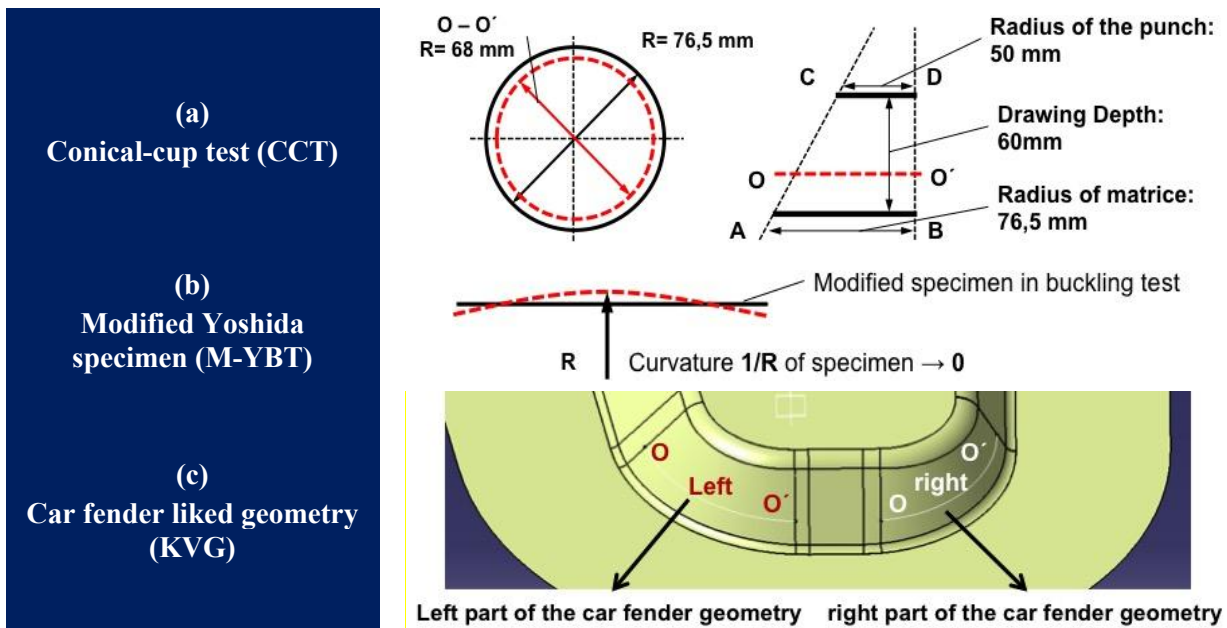


Figure 6-7: Methods for determining the local curvature of drawn component: (a) the geometric method for calculating the local curvature of the conical cup; (b) the geometric method for determining the local curvature of the M-YBT specimen before wrinkling initiation; (c) the method for determining the local curvature of the KVG part

The value of the local curvature of M-YBT is presented in Figure 6-7-b. Before wrinkling initiation, the wrinkling area of the M-YBT specimens reveal a small local curvature value ($1/\rho$). This value was therefore recognised as “0” in the following sections for the purpose of assembling regression models.

6.4.2 FEA results gained from the conical-cup test

Investigated sheet metal material with a thickness of 1.0 mm

As previously mentioned, the minor principal stress cannot be accurately measured. Therefore, the FEA was performed using a CCT specimen with a thickness of 1.0 mm. Figure 6-8-a shows the results of the minor principal stress on the outer side of CCT parts. CCT parts made from materials HC300LA, HC420LA, and DX54D showed the same trend as discussed in Section 6.2.1 (M-YBT specimens). According to the results of the study, when “wrinkling initiation” and “developed wrinkling” occur, the difference in drawing depth is small.

In addition, the development of the critical value of the outer/inner side stress difference from the beginning to the end of the test is shown in Figure 6-8-b. According to the determined gripper displacement at “wrinkling initiation” and “developed wrinkling” in Figure 6-2-a, it can be observed that different materials yield different critical values for the outer/inner side stress difference at the defined “wrinkling initiation” (σ_{WI}) and “developed wrinkling” (σ_{DW}) points, respectively. Results from different materials are presented in Table 6-6. Here, “WI” denotes the “wrinkling initiation”, and “DW” the “developed wrinkling”.

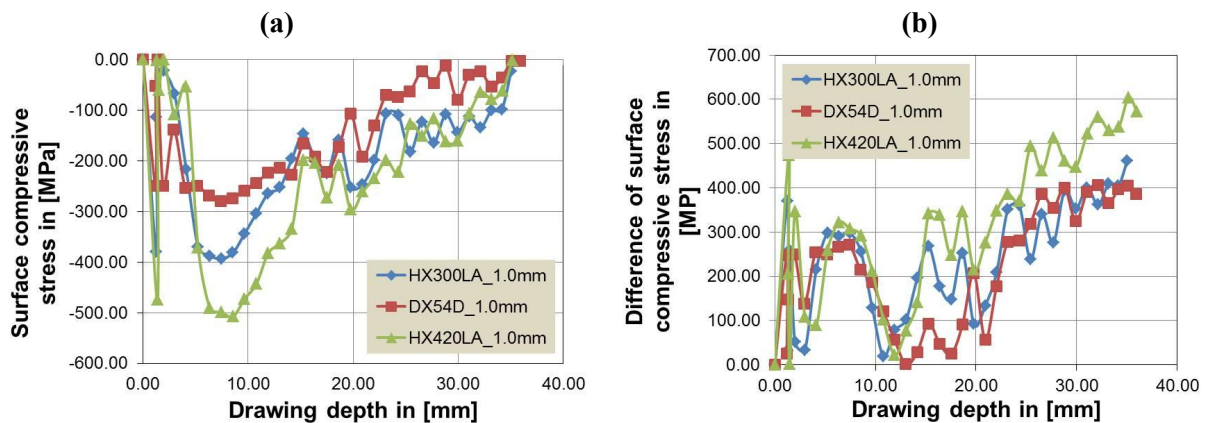


Figure 6-8: FEA results of the conical-cup test (sheet thickness 1.0 mm): (a) surface stress of outer side with a large fluctuating region before wrinkling initiation; (b) development of outer/inner side stress difference

Table 6-5: Simulation results gained when analysing the CCT specimen consisting of different materials (thickness of sheet materials 1.0 mm)

Sheet materials	WI at drawing depth in [mm]	σ_{WI} in [Mpa]	DW at drawing depth in [mm]	σ_{DW} in [Mpa]
HC420LA	8.6	307	35	604
HC300LA	7.5	297	35	461
DX54	7.4	271	35	385

When comparing the results of the CCT specimen with gained results of the M-YBT specimen, obviously a fluctuating region in the wrinkling process of CCT tests for specimens can be found when using a sheet metal thickness of 1.0 mm (see Figure 6-8-a and Figure 6-8-b). This phenomenon can be explained by the results presented in Chapter 7.2.6. The kind of surface defect

in the CCT tests is mainly caused by elastic buckling. The buckling process is a transition process from a surface without any defects to a surface that reveals the very first trends for wrinkling. This phenomenon will be explained in depth in Chapter 7 using the FEA results. The situation for M-YBTs is much simpler. To evaluate the point of wrinkling initiation by means of a conical-cup test, the approach described in Figure 6-7 can be used to reduce evaluation errors if the maximum value of the surface compressive stress cannot be evaluated. The development of compressive stress on the outer side of sheet thicknesses of 0.6 mm and 1.0 mm show similar characteristics. The surface compressive stress reaches its maximum value and then decreases to zero. The threshold can therefore be determined in the manner shown in Figure 6-8-b.

Investigated sheet metal material with a thickness of 0.6 mm

The simulation results show that the development of the minor principal stress on the outer side when using the HC420LA with a thickness of 0.6 mm has the same tendency as the curve presented in Figure 6-8-a. The value of the outer/inner side stress difference at “wrinkling initiation” (σ_{WI}) and at “developed wrinkling” (σ_{DW}) can be found in Table 6-6. Due to the low bending stiffness of the cross section of this specimen, the developed wrinkling appears at a drawing depth of around 25 mm for the material HC420LA. In the case of a 1.0 mm sheet thickness, the developed wrinkles take place at a drawing depth of around 35 mm.

Table 6-6: Simulation results obtained when analysing the CCT specimen consisting of different materials (thickness of sheet materials 0.6 mm)

Sheet materials	WI at drawing depth in [mm]	σ_{WI} in [Mpa]	DW at drawing depth in [mm]	σ_{DW} in [Mpa]
HC420LA	7.7	281	27	536
HC300LA	7.2	268	24	391
DX54D	6.1	218	28	305

Pattern of wrinkling with different thicknesses

The experiment results show that patterns of wrinkling differ among materials with different thicknesses due to the varying degrees of bending stiffness in the circumferential direction. Figure 6-9 shows the experiment results of the mini-CCT test on material HC420LA (thickness 1.0 / 0.6 mm).

For mini-CCT specimens with a sheet thickness of 1.0 mm there is no typical, recognisable wrinkling profile. According to the FEA results presented in Figure 6-8, an obvious fluctuating region can also be found in the pre- and post-wrinkling stages during the deep drawing process, although only a buckled surface in the sidewall can be observed (see Figure 6-9-a). Specimen having a sheet thickness of 0.6 mm shows a typical, wrinkled surface profile in the sidewall of drawn part.

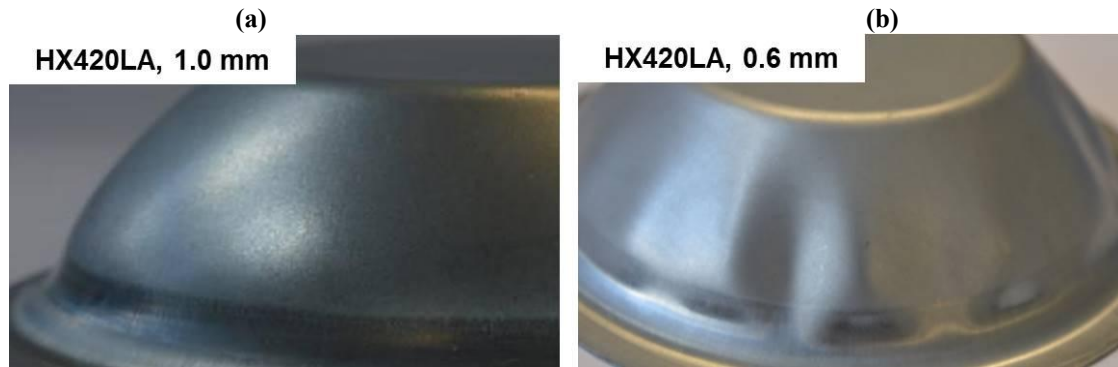


Figure 6-9: Influence of the sheet metal thickness on the wrinkling behaviour of HX429LA material: (a) surface defect buckling in the case of a 1.0 mm material thickness; (b) surface defect of buckling and wrinkling in the case of 0.6 mm material thickness

6.4.3 Conclusion on the influence of local curvature on wrinkling behaviour

To evaluate the influence of local curvature on the wrinkling process, both the FEA results of the M-YBT and the mini-CCT tests (sheet metal thickness of 1.0 mm) for all three investigated materials are shown in Table 6-7.

Table 6-7: Influence of local curvature on the wrinkling process (material thickness of 1.0 mm)

Sheet materials	WI at drawing depth or gripper displacement in [mm]	σ_{WI} in [Mpa]	DW at drawing depth or gripper displacement in [mm]	σ_{DW} in [Mpa]
HC420LA – CCT	8.6	307	35	604
HC420LA – M-YBT	3	12.4	8.2	432
HC300LA – CCT	7.5	297	35	461
HC300LA – M-YBT	3	26.3	6.3	277
DC54D – CCT	7.4	271	35	385
DC54D – M-YBT	4	27.7	6.2	221

Together with the data from Table 6-5 and Table 6-6, the following conclusions can be drawn:

- 1) The local curvature has a significant effect on the value of the outer/inner side stress difference. Therefore, the effect of local curvature cannot be ignored (see regression model in Chapter 6).
- 2) For a sheet thickness of 1.0 mm (both the M-YBT and mini-CCT test), the defined “wrinkling initiation” occurs later than the “wrinkling initiation” compared to specimens investigated with a thickness of 0.6 mm. This means that the wrinkling tendency of 1.0-millimetre-thick sheet metal is less pronounced than the one with a thickness of 0.6 mm (different bending stiffness between a thickness of 0.6 mm and 1.0 mm).
- 3) Sheet thickness indeed has an effect on the patterns of the surface defects. Investigation results show that a specimen with a low bending stiffness will tend earlier to develop wrinkles.

6.5 Linear-regression models for predicting the critical value of surface stress

From Section 6.1 to 6.4, the difference at “wrinkling initiation” and “developed wrinkling” was introduced by using the DSCS-approach to determine the critical value of the outer-/inner-side stress. Furthermore, in this section, the conventional analytical method (Cao’s and Kim’s model) was not used because relationships between the value of the critical stress and influencing factors (e.g. sheet thickness and local curvature) cannot be accurately determined by using physical experiments. Besides, by using DoE the relationship between critical stress values and influencing factors can be presented in a statistical way, like linear-regression model.

The desired parameters and stages (see Table 6-8) according to the DoE method are listed in Table 6-8. The value of the local curvature of M-YBT was previously mentioned in Chapter 6.4, while the K^{lc} -value is equal to zero. Having utilized calculations based on the geometric method, the local curvature of the mini-CCT specimen used was determined to be 0.025. The DoE sequence (sequence means the plan of experiments) is presented in Table 6-9. Listed results from the simulation do not exhibit any deviation. All simulations were performed once.

Table 6-8: Influence parameters and it’s values at stage 1 (min. value) and stage 2 (max value)

Parameters	Stage 1 in DoE	Stage 2 in DoE
Local curvature (K^{lc})	0 (M-YBT)	0.025 (CCT)
Sheet metal thickness (t)	0.6 mm	1.0 mm

Table 6-9: Sequence of the DoE for determining a linear-regression model to predict a critical difference in surface-compressive stress levels on the outer and inner side

Sequence of the DoE	Local curvature in [1/mm]	Sheet thickness in [mm]	σ_{WI} in [Mpa]	σ_{DW} in [Mpa]
1	0	1.0	16	431
2	0	0.6	12	401
3	0.025	0.6	350	550
4	0.025	1.0	400	600

The critical stress levels for the safe range (σ_{WI} –wrinkling initiation) and developed wrinkling (σ_{DW} –developed wrinkling) are listed in Table 6-10 for sheet material HX420LA. Information on the critical stresses of the sheet metal materials HC300LA and DX54 is not shown here. Regression models for HC300LA and DX54 are described in Section 6.5.2. To evaluate the results of the DoE, Minitab 17 software was used, which is a statistics package widely used for solving statistical problems in the field of engineering and economics. Table 6-9 shows that, the influence of local curvature on the critical stress cannot be ignored. Because local curvature has a great influence on the critical stress by wrinkling initiation. According to the results, the value of critical stress has increased by about 30 times from $K^{lc} = 0$ to $K^{lc} = 0.025$.

6.5.1 Linear-regression models for sheet metal material HC420LA

As mentioned at the beginning of Section 6.5, Table 6-10 consists of results for ‘wrinkling initiation’ and ‘developed-wrinkle’ gained by simulating M-YBT and CCT using material HC420LA with a thickness of 0.6 mm and 1.0 mm.

Table 6-10: Data for sheet metal material HC420LA used for DoE objectives

HX420LA	WI at drawing depth or gripper displacement in [mm]	σ_{WI} in [Mpa]	DW at drawing depth or gripper displacement in [mm]	σ_{DW} in [Mpa]
YBT 1.0 mm	4	16	8	431
YBT 0.6 mm	1.2	12	1.5	401
CCT 1.0 mm	15	400	40	600
CCT 0.6 mm	9	350	20	550

These values are used to determine a linear-regression model, which was calculated through a DoE analysis. The linear-regression models can be used to estimate the stress differences $\Delta\sigma_{WI}$ and $\Delta\sigma_{DW}$. Parameters that influence the linear-regression models are the local curvature K^{lc} of the unwrinkled geometry and the sheet metal thickness t . In this way, the critical stress difference at “wrinkling initiation” and “developed wrinkle” can be calculated in this work by using the following equation 6.1:

$\Delta\sigma_{WI/DW} = A^{LR} + B^{LR} * X_1 + C^{LR} * X_2 + D^{LR} * X_1X_2$			(6.1)
	$A^{LR}, B^{LR}, C^{LR}, D^{LR}$	X_1, X_2	X_1X_2
Meaning of the parameters used in Equ. 6.1	Coefficients of regression models	The first parameter and the second parameter	Interaction parameter

Determining the critical value for “outer/inner side stress difference” at “wrinkling initiation”, HC420LA

The main-effect diagram and interaction-effect diagram of the critical stress level at “wrinkling initiation” are presented in Figure 6-10.

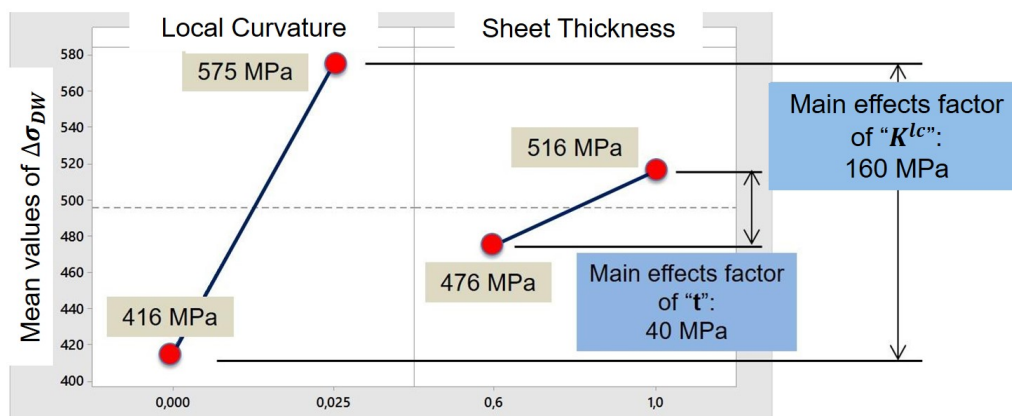


Figure 6-10: Main-effect diagram for local curvature and sheet thickness with regard to critical stress value at “wrinkling initiation”. Results determined for HC420LA material

Obviously, the influences of the local curvature and sheet thickness on the critical surface stress are highly significant. Moreover, a significant interaction effect from the influence of the local curvature and sheet thickness was also discernible. A significant interaction effect between sheet thickness and local curvature was not identified using the results from the Minitab software.

Determining the critical value for “outer/inner side stress difference” at “developed wrinkling”, HC420LA

The main-effect diagram and interaction-effect diagram of the critical stress level at “developed wrinkling” are presented in Figure 6-11. Obviously, the influences of the local curvature and sheet thickness on the critical surface stress are also significant. Moreover, a significant interaction effect between the influence of local curvature and the sheet thickness was not identified using the results from the Minitab software.

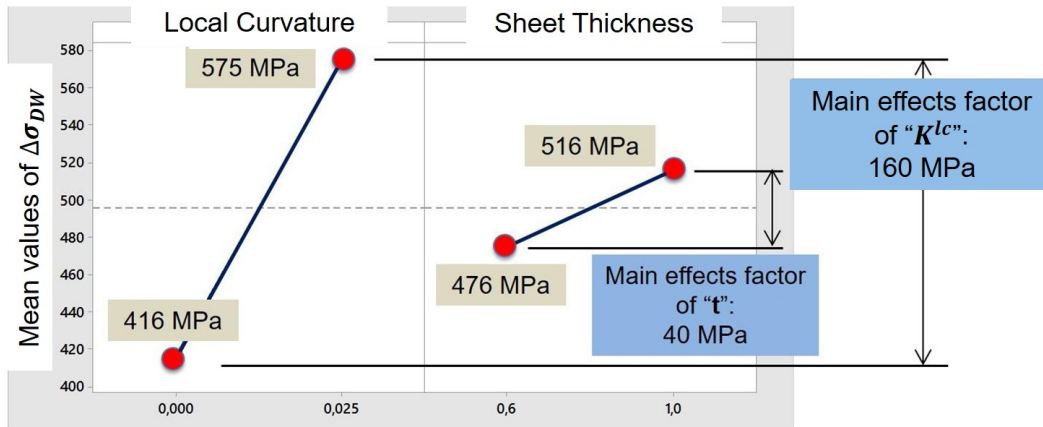


Figure 6-11: Main-effect diagram for local curvature and sheet thickness with regard to critical stress value at “developed wrinkling”. Results determined using material HC420LA

Linear-regression model for critical value of “outer/inner side stress difference” at “wrinkling initiation” and “developed wrinkling” using Minitab 17 for material HC420LA

The results of the critical value of “outer/inner side stress difference” at “wrinkling initiation” and “developed wrinkling” are given in Equations 6.2-a and 6.2-b, respectively. The value of the local curvature in AutoForm R6 can be directly used in the equation for calculating Δσ_{WI} and Δσ_{DW}. The “current sheet metal thickness” in AutoForm R6 can be used for the equations for determining the critical value of “outer/inner side stress difference”. By using the following equations, determined by applying the DoE analysis, the critical value of the “outer/inner side stress difference” for material HC420LA can be estimated.

$\Delta\sigma_{WI} = 6.0 + 10,760 \times K^{lc} + 10 \times t + 4,600 \times K^{lc} \times t$	(6.2-a)
$\Delta\sigma_{DW} = 356.0 + 4,760 \times K^{lc} + 75 \times t + 2,000 \times K^{lc} \times t$	(6.2-b)

More details on these equations are given in the appendix.

6.5.2 Linear-regression models for material HC340LA and DX54D

Linear-regression model for critical value of “outer/inner side stress difference” at “wrinkling initiation” and “developed wrinkling” using Minitab 17 for material HC300LA

The critical stress of $\Delta\sigma_{WI}$ and $\Delta\sigma_{DW}$ regarding material HC300LA determined in the same way as for material HC420LA described above. The values for calculating the safe ranges (σ_{WI}) and developed wrinkling (σ_{DW}) range are listed in Table 6-11 for sheet material HC300LA. The determined regression models are presented in Equation 6.3 with regard to the critical value of the “outer/inner side stress difference” at “wrinkling initiation” and “developed wrinkling”. More details on these regression models are given in the appendix (see page 148).

Table 6-11: Data for sheet metal material HC300LA used for DoE objectives

HC300LA	WI at drawing depth or displacement in [mm]	σ_{WI} in [Mpa]	DW at drawing depth or displacement in [mm]	σ_{DW} in [Mpa]
YBT 1.0 mm	3.2	33	6.8	340
YBT 0.6 mm	1.2	20	1.8	260
CCT 1.0 mm	15	300	40	550
CCT 0.6 mm	9	200	20	470
$\Delta\sigma_{WI} = 52.5 - 100 \times K^{lc} - 32.5 \times t + 11,300 \times K^{lc} \times t$				(6.3-a)
$\Delta\sigma_{DW} = 140 + 8,400 \times K^{lc} + 200 \times t$				(6.3-b)

Linear-regression model for critical value of “outer/inner side stress difference” at “wrinkling initiation” and “developed wrinkling” using Minitab 17 for material DX54D

The critical stress of $\Delta\sigma_{WI}$ and $\Delta\sigma_{DW}$ regarding material DX54D determined in the same way as for material HC300LA described above. The values for calculating the safe regions (σ_{WI}) and developed wrinkling (σ_{DW}) are listed in Table 6-12 for sheet material DX54D. The determined regression models are presented in Equation 6.4 with regard to the critical value of the “outer/inner side stress difference” at “wrinkling initiation” and “developed wrinkling”. More details on these regression models are given in the appendix.

Table 6-12: Data for sheet metal material DX54D used for DoE objectives

HDX54D	WI at drawing depth or displacement in [mm]	σ_{WI} in [Mpa]	DW at drawing depth or displacement in [mm]	σ_{DW} in [Mpa]
YBT 1.0 mm	3	13	6.3	220
YBT 0.6 mm	0.6	10	1.2	210
CCT 1.0 mm	15	270	40	500
CCT 0.6 mm	9	175	20	400
$\Delta\sigma_{WI} = 5.5 + 1,080 \times K + 7.5 \times t + 9,200 \times K \times t$				(6.4-a)
$\Delta\sigma_{DW} = 195.0 + 2,200 \times K + 25 \times t + 9,000 \times K \times t$				(6.4-b)

7 Examining the simulation accuracy and reference simulations

Chapters 5 and 6 introduce the “concept” of the DSCS-approach and the “regression model” of the DSCS-approach, respectively. As mentioned in Chapter 6, all the values of o-I side stress difference, like σ_{WI} and σ_{DW} , used for constructing regression models came from simulation results in Chapter 7. Therefore, the accuracy of the simulation, especially the buckling test with modified Yoshida sample (M-YBT) and the mini conical cup test (mini-CCT), plays a crucial role in the current work. The tasks in Chapter 7 are as follows:

- Enhance the simulation accuracy
- Examine the development of minimum principal stress on the outer side
- Examine the development of the critical value (o-I side stress difference) during the wrinkling process presented in chapter 5
- Comparison between simulation and experimental results

Firstly, in Chapter 7.1 and 7.2, the reference simulations M-YBT and Mini-CCT are introduced to prove the wrinkling process described in Chapter 5. Both simulation results provide good suggestions for experimental work. To apply the new methodology to more practical oriented sheet metal components, experimental works with car-fender-based specimen (KVG) [Ran15] will be performed later in Chapter 7.3. According to the experimental results, the wrinkling tendency can be decreased by applying segment-elastic blankholder (SEB) introduced in Chapter 2.1.5. The reduced wrinkling tendency can be directly predicted by only using the simplified model introduced in Chapter 4. In summary, two aspects should be done to improve the accuracy of the simulation results in Chapter 7:

- Material input parameters and material models
- FEM – Models to eliminate real forming process

7.1 Case study 1 – Buckling test with modified Yoshida specimen

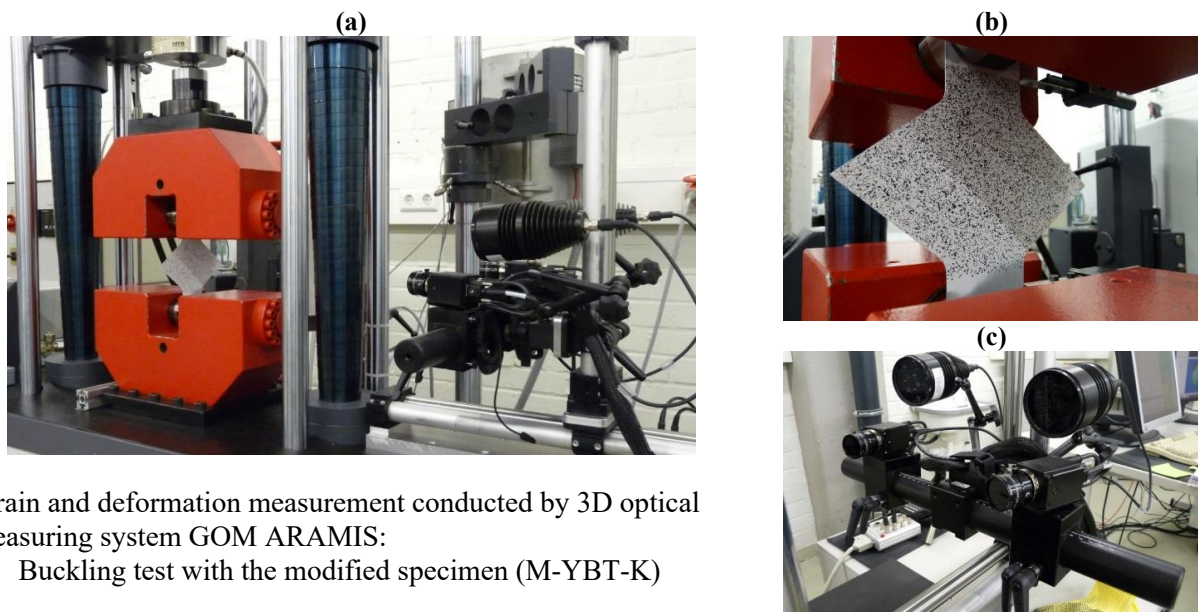
First, Chapters 7.1.1 and 7.1.2, respectively describe the experimental work and simulation details of the buckling test using the modified Yoshida sample. Combined with the results of the FEA, the experimental results will be shown in Chapter 7.1.3. The experimental results will be compared with the simulation results obtained from LS-Dyna in Chapter 7.1.3.

The sheet metal material HC420LA was used as reference material with the sheet thickness of 1.0 mm. Since in the M-YBT and mini-CCT, the change of the surface quality during the forming process can be observed directly using GOM ARAMIS optical measuring system, M-YBT and Mini-CCT were chosen as reference for testing and FEA. The FEA accuracy of the M-YBT depends mainly on material input parameters and material model. In this way, the interference

from FEM-Model can be eliminated by treating with material issues. The FEA investigation for the KVG geometry is much more difficult because the accuracy of the results depends also on FEM models and set lubrication conditions in the simulation.

7.1.1 Experiment details – Buckling test with modified Yoshida specimen

In this work, the buckling tests with modified Yoshida specimens were performed on the conventional tensile test machine with a speed of 20 mm/min (see Fig. 7-1-a). The optical measuring system GOM ARAMIS was placed near the machine to get the best digital images of the process sequence. The frequency of the GOM ARAMIS system trigger was set to 10 pictures per second. The essential experimental results like stroke force F , stroke displacement ΔL and buckling height H^W were captured by using a 3D module of GOM ARAMIS (see Fig.7-1-c). In Fig7-1-b, the M-YBT specimen with small shoulder radius is shown as reference specimen for testing.



Strain and deformation measurement conducted by 3D optical measuring system GOM ARAMIS:

- Buckling test with the modified specimen (M-YBT-K)

Figure 7-1: (a) Experimental work of buckling test performed in uniaxial tensile test machine with modified Yoshida specimen; (b) Modified Yoshida buckling specimens with reduced shoulder radius; (c) Cameras and lamps of 3D optical measuring system GOM ARAMIS

7.1.2 Simulation details – Buckling test with modified Yoshida specimen

The main objective of studying the buckling test is to examine the validity of the stress-based simplified model (described in Chapter 4) and the concept of DSCS-approach (introduced in Chapter 5) using FEA based on M-YBT specimens. Both simulation and experimental works were performed using M-YBT-K specimen. The adopted M-YBT-K specimen is introduced in [Han14]. The geometry will be illustrated later in Fig. 7-2-a.

In order to evaluate the bending effect in the wrinkling area, the material models presented in [Hoe13] were adopted. According to S. Höhle, the combination of “material model *Mat_3-

Parameter_Barlat” and “flow curve model based on Swift equation”, allows the most accurate prediction of the bending strain determined from FEA analysis compared with experimental results. Therefore, this combination will be used in FEA regarding buckling test with M-YBT-specimen (in Chapter 7.1) and mini-CCT test (see Chapter 7.2).

The material parameters used by the FEA were determined using the ISO120014 standard method. The true stress-true strain curve is calculated directly from the GOM ARAMIS system. The true stress-true strain curve of the plastic stage is fitted with the Swift hardening model. Only Swift parameters and the material parameters determined from tensile test are listed in Table 7-1.

Table 7-1: Material parameters of sheet metal material HC420LA used in FEA, thickness of 1.0 mm

Parameter	Swift parameter 1	Swift parameter 2	Lankford anisotropy R00	Lankford anisotropy R45	Lankford anisotropy R90
Value	703.576	0.181	0.889	0.964	1.099

A schematic of the M-YBT-K specimen used in the experimental and FEA analysis is shown in Figure 7-2-a. This specially designed specimen has a length of 221 mm and a width of 161 mm. In addition, the tensile machine has a clamping length and a width of 50 mm and 50 mm, respectively. Therefore, the effective length of the M-YBT-K sample used (see Figure 7-2-a) is 121 mm. The blue arrow indicates the gripper movement (the upper tool of the tensile machine) during the test. The initial position (dotted line) and section profile O-O' (black curve) after forming of M-YBT-K specimen are presented in Fig. 7-2-b.

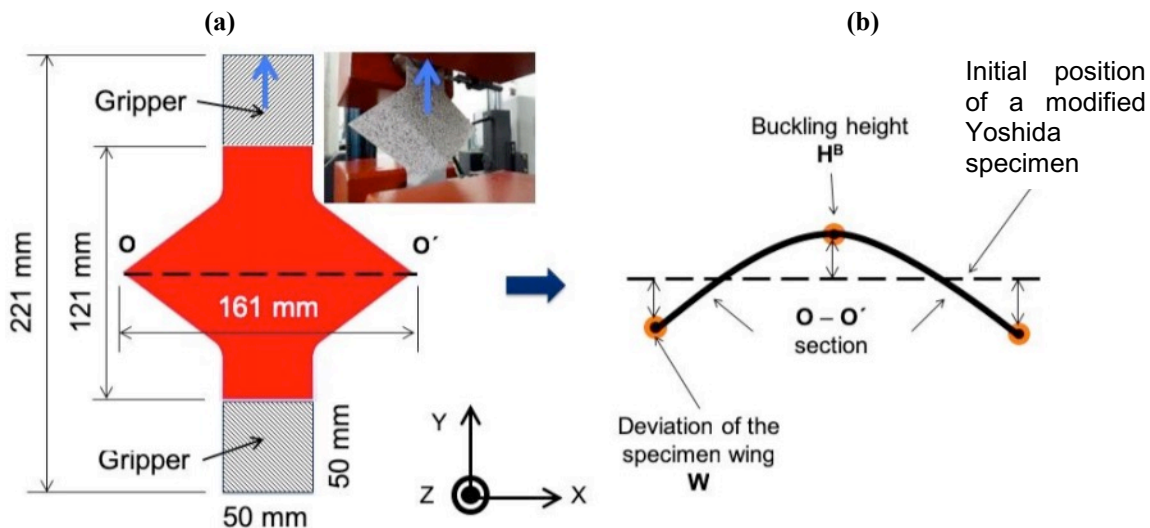


Figure 7-2: Details in FEA with LS-Prepost, (a) Geometry of modified Yoshida specimen, effective area in FEA using LS-PrePost; (b) Investigating area of buckling test with modified Yoshida specimen and definition of buckling height, initial position, and deviation of the specimen wings

Comparing the initial position and profile after forming process, the buckling height H^B and the deviation of the specimen wing H^{Wing} can be defined in Fig.7-2-b. In this case study, the buckling

height H^B is defined as the distance between the buckled middle surface area and the initial position of the M-YBT specimen. A schematic principle is presented in Figure 7-2-b.

Furthermore, two boundary conditions were set in the FEA analysis of modified Yoshida specimens. First with the “boundary condition 1” (black line m-m’ in Fig. 7-3-a), only the displacements in direction Y and rotation in direction X, Y and Z were allowed. For the second boundary condition (black line n-n’ in Fig. 7-3-a), the displacement and rotation of all elements in X, Y and Z directions were not allowed. In experiment and FEA analysis, the region to be analysed is sampled in the middle area of the specimen (see Figure 7-3-b).

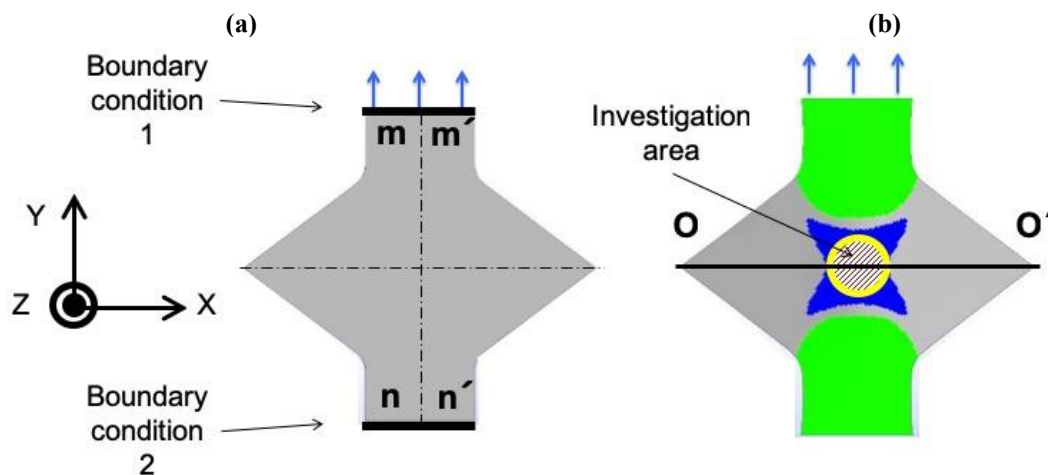


Figure 7-3: Details in FEA with LS-Prepost, (a) Defined boundary conditions “m-m’” and “n-n’” in initial state; (b) Investigation area and formability after forming shown in FEA

7.1.3 Examining of surface stress development on outer and inner side of specimen

Examining the development of minimum principal stress at outer side in FEA

According to Figures 4-9 and 4-10, the beginning of wrinkling is determined by evaluating only the development of the minimum compressive stress at outer side. Figure 7-4 shows the development of this stress determined from FEA analysis by forming with M-YBT specimen.

In Figure 7-4-a, the general trend of minimum principal stress (outer side) development is illustrated. When the minimum principal stress reaches its critical value, the defined “wrinkling initiation” occurs (at gripper displacement of 4 mm). In the case of material HC420LA with thickness 1.0 mm, this critical value is around 200 Mpa. After “wrinkling initiation” the observed minimum principal stress at outer side decreases to zero. This time point was defined as “developed wrinkles” (at gripper displacement of 8 mm).

Since the tendency of minimum principal stress at outer side can be fit with the quadratic function shown in Figure 7-4-a, the beginning of wrinkling initiation can be predicted according to the first derivative of the fitted function. The results show that the “wrinkling initiation” of the modified Yoshida specimen occurs at the gripper displacement of 4 mm. When the gripper reaches a displacement of 8 mm, the defined “developed wrinkles” takes place.

Checking the development of o-I side stress difference in the wrinkling area

As mentioned earlier, the critical value of “o-I side stress difference” cannot be directly measured in the experiment. Therefore, FEA analysis was performed to obtain this information. Figure 7-4-b illustrates the development of both minimum principal stress on the o- and i-sides. The stress difference between the o- and i-sides first occurs at a 1.5 mm gripper displacement. Within this 1.5 mm displacement range, the surface stress deviation fluctuates between -0.5 and 1.5 Mpa based on the FEA results. After the gripper displacement larger than 1.5 mm, the stress difference increases until the end of the FEA.

According to the approach mentioned in Chapter 5, “bifurcation” is defined at the gripper displacement of 1.5 mm in this case study. After beginning of “bifurcation”, the wrinkling height can be measured using GOM ARAMIS based on M-YBT specimen.

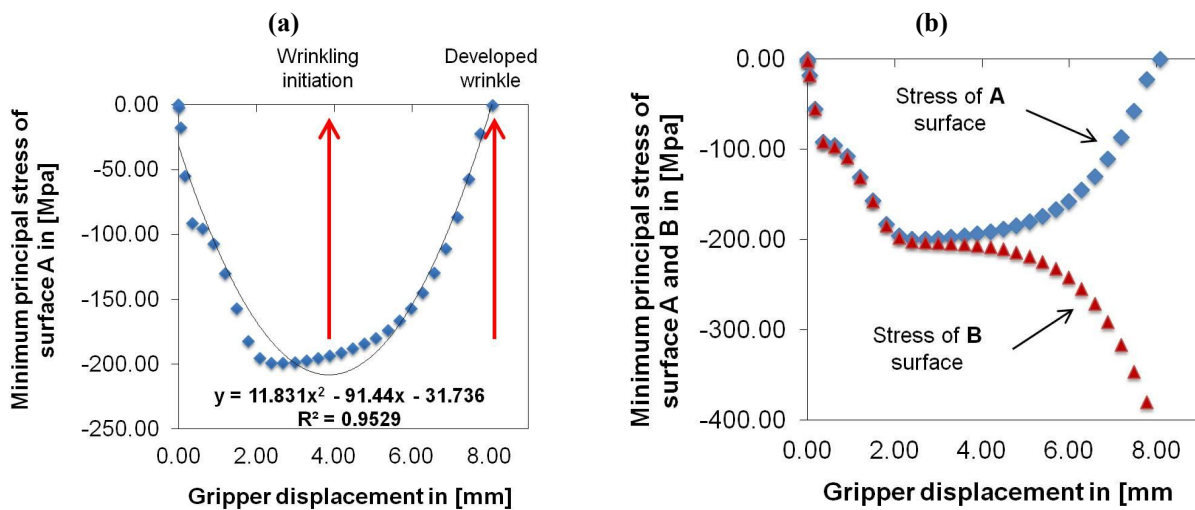


Figure 7-4: FEA results based on M-YBT-K specimen, material HC420LA with thickness of 1.0 mm, (a) Development of the minimum principal stress at outer side during the test; (b) Development of the O-side stress difference during the buckling test with definition of “bifurcation” introduced in chapter 5

7.1.4 Results and conclusion – Buckling test with modified Yoshida specimen

First in Chapter 7.1, the development of minimum principal stress at the outer side introduced in Chapter 4 was examined. By analysing “the development of minimum principal stress at outer side”, “wrinkling initiation” and “developed wrinkle” can be detected. Furthermore, the development of the critical value of “o-I side stress difference” was examined. From the definition, “bifurcation” on, the “o-I side stress difference” increases continuously until the end of the simulation.

The comparison of experimental and numerical results is shown in Figure 7-5. The wrinkling height H^W calculated in FEA is in good agreement with the experimental results from beginning of the test until the defined “developed wrinkle”.

“Bifurcation” (first stage, in Fig. 7-5-a) occurs at gripper displacement of 1.5 mm. “Wrinkling

initiation” (second stage, in Fig. 7-5-a) and “developed wrinkle” (third stage, in Fig. 7-5-a) takes place, when gripper displacement reaches 4 mm and 8 mm, respectively. The wrinkling height H^W at each stage is listed in Fig. 7-5-b.

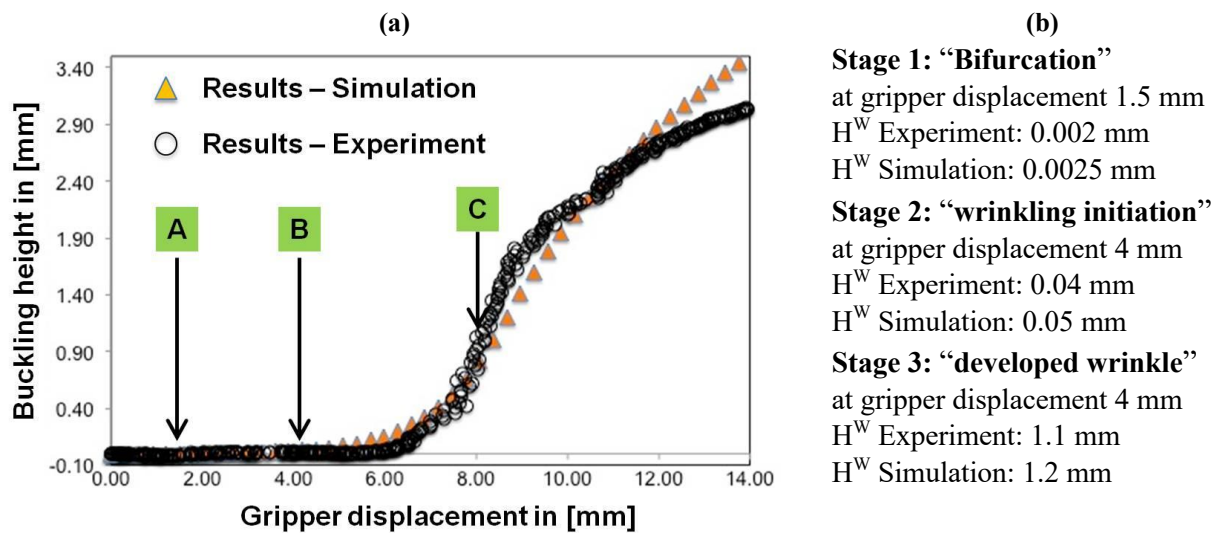


Figure 7-5: Comparison of simulation and experimental results, M-YBT-K specimen with material HC420LA, thickness of 1.0 mm, (a) Development of wrinkling height H^W from FEA and experiments as the function of gripper displacement; (b) Wrinkling height H^W at defined “bifurcation”, “wrinkling initiation” and “developed wrinkle”.

7.2 Case study 2 – Mini conical cup test

Mini conical cup test was chosen as another referent simulation in Chapter 7. The main purpose of Chapter 7.2 is to check the accuracy of the FEA and to verify the concept of the DSCS-approach for simple symmetric deep drawing parts. The development of minimum principal stress at outer side in FEA and the development of o-I side stress difference in the wrinkling area will be checked in Chapter 7.2.

First, the Chapters 7.2.1 and 7.2.2 describe the experimental work and simulation details of the mini conical cup test with sheet metal material HC420LA having thickness of 1.0 mm. Surface quality assessment methods for unsupported areas between the punch and the die are described in 7.2.3 and 7.2.4. Combined with the results of the FEA, the experimental results will be shown in the later part of 7.2.5, and a short conclusion can be drawn.

7.2.1 Experiment and simulation details – Mini conical cup test

Traditional conical cup test was performed in the conventional press, as introduced in the work of Beck [Bec04]. However, the experimental work of IFU shows that GOM ARAMIS cannot stably measure the side wall of the conical cup because the drawing process in the press is mainly performed and is accomplished with the vibration of the tools. If the frequency of GOM ARAMIS is set to 10 pictures per second, the camera of GOM ARAMIS will not work robustly. In order to

solve this problem, the mini-CCT test was carried out using the deep drawing equipment modified from the Nakajima test (see Figure 7-6-a).

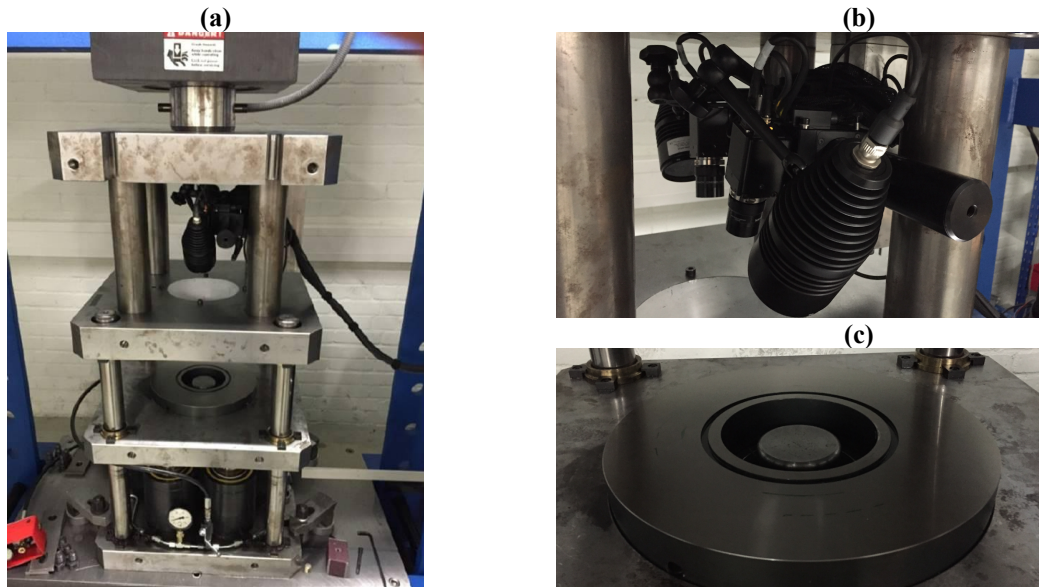


Figure 7-6: Test equipment of the Mini-CCT tests at IFU, (a) overview of the equipment; (a) Cameras of GOM ARAMIS optical measurement system fixed in the test device; (c): blank holder and punch used in Mini-CCT test

The mini-CCT tests were performed at room temperature in a hydraulic press. The experiments were carried out with a constant punch speed of 2 mm/s. At this speed, optical measurement GOM ARAMIS can work steadily in the presented hydraulic press with a frequency of 10 frames per second. Because wrinkle occurs circumferentially in the part region without any tool contact, the values of major/minor strain and 3D shape of wrinkling area can be directly measured and stored (see Fig. 7-7). The experimental results gained that way are shown and compared later together with simulation results from LS-Dyna in Chapter 7.2.6.

Mineral oil lubricant M100 was applied to both sides of the specimen to reduce the frictional force. The maximum drawing depth Z_d in the mini-CCT test was limited to 40 mm.

The tools for mini-CCT test involves three symmetric tools (die, punch, and blankholder, see Fig. 7.6 and Fig. 7-7) and is schematically illustrated in Fig. 7-7-a. The applied punch is depicted in Figure 7-7-a, which has a diameter of 70 mm. The diameter of the die is 105 mm. The blank holder plate and the position of cameras of GOM ARAMIS are depicted in Figure 7-6-a as well.

Compared with the buckling test in the tensile test machine mentioned in Chapter 7.1, an “effective measured depth” Z_{eff} . Exists in the mini conical cup test (see Figure 7-7-b). “Effective measured depth” Z_{eff} . Indicates the effective measured area of a side wall. This is because the entire side wall cannot be prepared with stochastic white and black patterns in practice.

Figure 7-8 explains why the sample diameter of the Mini-CCT test was 145 mm (see Figure 7-8-a). However, the white (paint) and black (carbon) patterns (in the circle with the dashed curve, see

Figure 7-8-a) applied stochastic on the sample can only be prepared in the diameter range of 105 mm.

When stochastically white and black patterns are not prepared between the dotted circle and the blank circle, no white and black samples will be drawn into the die. This region cannot be captured by GOM ARAMIS. However, the quality of the drawn part is robust due to controlled lubrication conditions, see Figure 7-8-b. However, in this way, only the side wall with stochastic white and black pattern can be measured (informations about major/minor strains, surface profile at side wall) using GOM ARAMIS during the tests

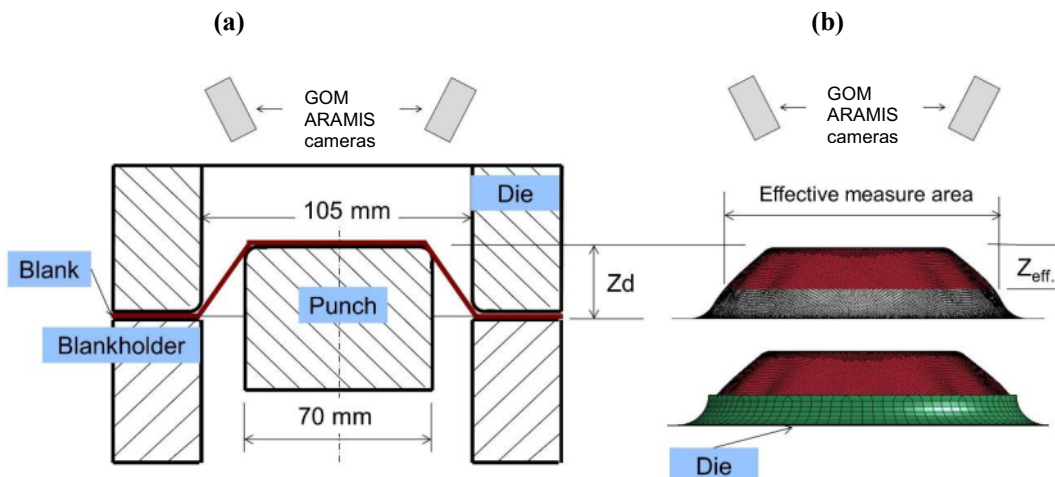


Figure 7-7: Mini-CCT test depicted at a certain drawing depth, (a) Tools of the Mini-CCT test (punch, die, specimen and blank holder) and position of the cameras of GOM ARAMIS, (b) Definition of “effective measured depth” Z_{eff} .

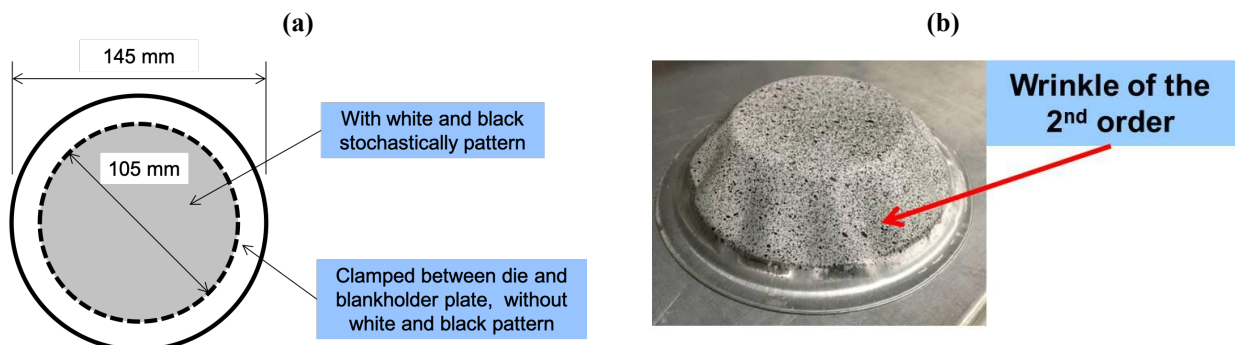


Figure 7-8: Illustration of stochastic white and black pattern at specimen, (a) Dimension of the specimen and die area, where the stochastic white and black pattern was prepared in the test, (b) drawn part of conical cup with presented effective measured area, material HC420LA with sheet thickness 0.6 mm

7.2.2 Examining of surface stress development on outer and inner side of wrinkling area

Examining the development of minimum principal stress at outer side in FEA

The value of minimum principal stress at outer side in the Mini-CCT test cannot also be directly measured in experiments. Therefore, FEA was performed to get corresponding values of minimum principal stress at the outer side at “wrinkling initiation” and “developed wrinkle”.

The FEA result only in the rolling direction (see Figure 7-9-b, selected elements in FEA) is

described as an example. Figure 7-9-a illustrates the general trend of the development of the minimum principal stress at outer side. When the minimum principal stress at outer side reaches its maximum at drawing depth of 15 mm, the defined “wrinkling initiation” occurs. In the case of material HC420LA with thickness of 0.6 mm, the minimum principal stress at outer side is located around 200 MPa. After “wrinkling initiation”, the calculated stress decreases to zero at drawing depth of 25 mm. This time point was defined as “developed wrinkles”.

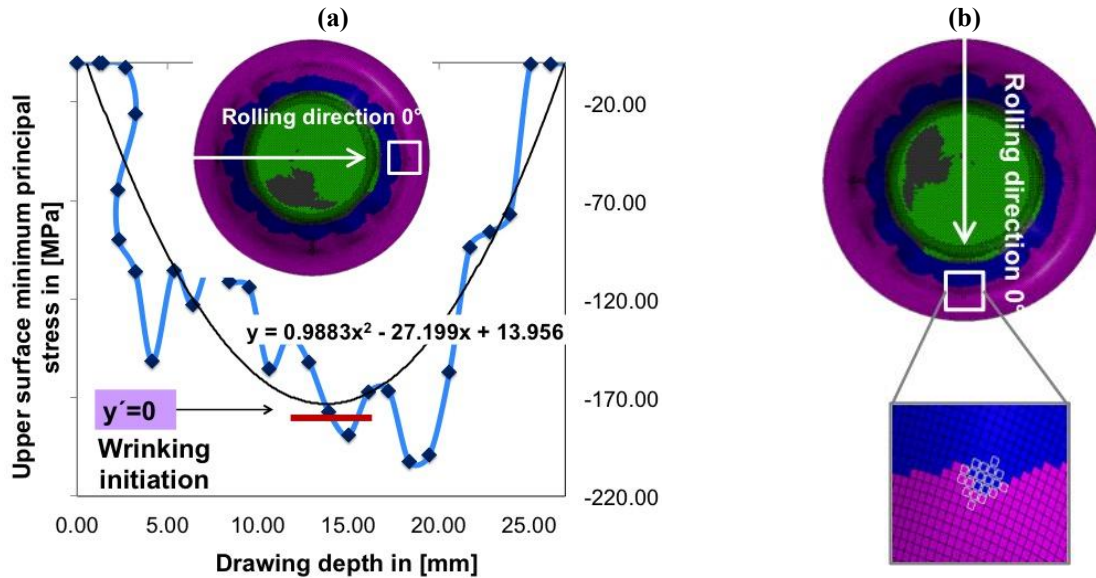


Figure 7-9: FEA results based on Mini-CCT test, material HC420LAD with thickness 0.6 mm, (a) Development of minimum principal stress at outer side with the method to find out “wrinkling initiation”; (b) Rolling direction and selected elements for analysing

Since the development of minimum principal stress at outer side can be fit with the quadratic function shown in Fig. 7-9-a, the time point of “wrinkling initiation” can be predicted according to the first derivative of the fitted function (see Fig 7-9-a). This method can be applied in the situation, when the minimum principal stress at outer side shows a “fluctuation” phenomenon. “Fluctuation” phenomenon of the stress means that, the maximum value of minimum principal stress at outer side cannot be obviously obtained because of the fluctuation of the critical stress value in FEA analysis.

Checking the development of o-I side stress difference in the wrinkling area

As mentioned earlier, the critical value (the difference in minimum principal stresses between the o- and i-side) cannot be directly measured in the experiment. Therefore, a simulation was performed to obtain this information. Figure 7-10 illustrates the development of minimum principal stress both on the o- and i-sides.

The black and blue curve in Fig. 7-10-a indicates the development of minimum principal stress at outer side and inner side, respectively. Compared with results from M-YBT in Chapter 7.1.2, the whole wrinkling process in the case of Mini-CCT test can be divided into two phases:

Verifying the development of outer/inner side stress difference in the wrinkling area

As mentioned above, the critical value (i.e. the difference between minor principal stresses on the outer and inner side) cannot be directly measured in the experiment. Figure 7-10 illustrates the development of the minor principal stress on both the outer and inner side.

The black and blue curves in Figure 7-10-a indicate the development of minor principal stress on the outer side and inner side, respectively. Compared with results from M-YBT in Section 7.1.2, the entire wrinkling process can be divided into two phases in the case of the mini-CCT test:

- 1) First surface defect process (from the beginning to a drawing depth of 3 mm)
- 2) Wrinkling process (from a drawing depth of 3 mm to a drawing depth of 30 mm)

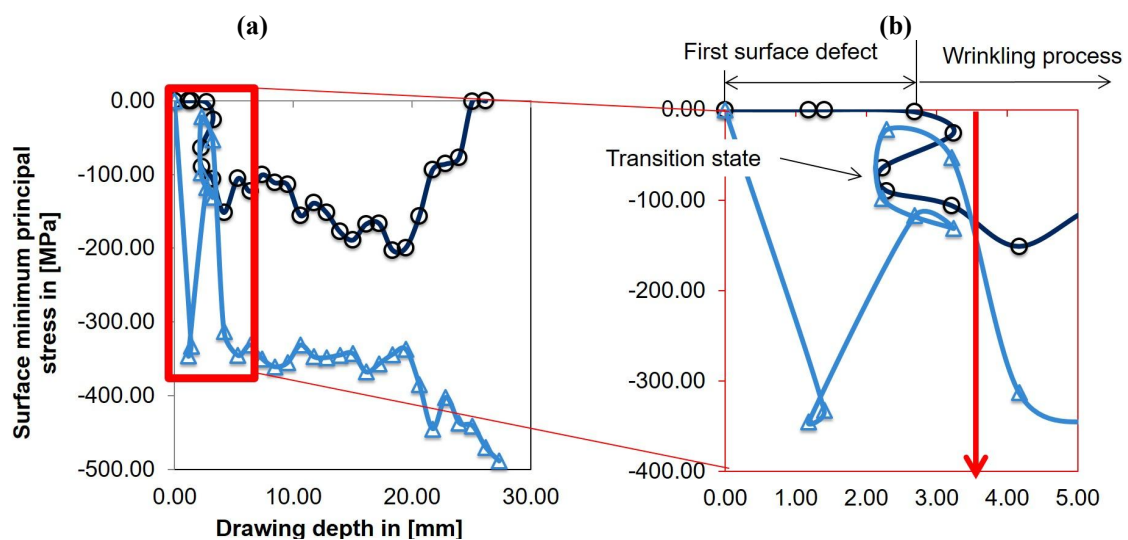


Figure 7-10: FEA results based on the mini-CCT test, material HC420LAD with a thickness of 0.6 mm: (a) development of minimum compressive stress on outer side (black curve) and inner side (blue curve) during the forming process; (b) details of the point in time from which the “first surface defect” and “wrinkling process” can be distinguished

First surface defect process in the case of the mini-CCT test

In the “first surface defect process” from a drawing depth of 0 mm to 3 mm (see Figure 7-10-b), the difference in the minor principal stress between the outer side and inner side increases rapidly from 0 Mpa to around -350 Mpa at a drawing depth of 1.5 mm. Then, at a drawing depth of 3 mm, the difference between the minor principal stresses on the two sides is continuously reduced to a small value of around zero.

Besides, according to the FEA results wrinkling initiation take place with small effective strains. This kind of surface defect is defined as “elastic wrinkling” for the purposes of this paper since the investigated wrinkling area involves elastic deformation. This phenomenon was introduced by L. Ton as the “change of the equilibrium state” from the original equilibrium state to a new equilibrium state, see Figure 7-11.

Chapter 8 presents elastic wrinkles on a complex deep drawn part from the automobile industry. Elastic wrinkles can be observed through testing in a press at a small drawing depth (less than 10 mm). One characteristic of this type of elastic wrinkling is that it will disappear as the drawing depth increases.

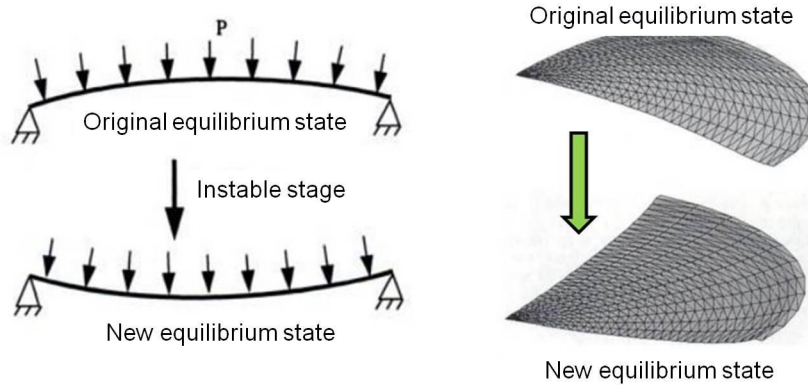


Figure 7-11: Definition of change in equilibrium state according to L. Ton [01]

Wrinkling process in the case of the mini-CCT test

A steady wrinkling process takes place during the mentioned “wrinkling process” between a drawing depth of 3 mm and a drawing depth of 30 mm; see Figure 7-10-a. This wrinkling process is part of the “plastic wrinkling” process, which indicates that the wrinkling process occurs after the beginning of plastic deformation on the forming part. The mini-CCT test thus defined that “wrinkling initiation” and “developed wrinkling” involve plastic deformation.

Compared with M-YBT, the same tendency can be observed in the FEA results of mini conical-cup tests. From the defined “wrinkling initiation”, emerging at a drawing depth of 15 mm, the difference in the minor principal stress between the outer and inner side steadily increases up to a drawing depth of 27 mm, where the value of the minor principal stress on the outer side is equal to zero.

7.2.3 Evaluating surface quality by applying Eisele’s approach

There is almost no research that aims to evaluate the difference between the “buckling initiation” and “wrinkling initiation” during CCT tests. Furthermore, scientific work focusing on the change in surface quality on the sidewall in CCT tests has been insufficient. Eisele proposed an approach for predicting the onset of sidewall wrinkling based on simple symmetrical parts. According to Eisele’s approach, the wrinkling height H^W and the position deviation V^P can be defined to evaluate the sidewall surface quality of a conical cup. The definition of the wrinkling height H^W and position deviation V^P will be introduced in this section.

The program LS-PrePost offers the option of exporting all “nodal coordinates” (X, Y, Z) of a drawing part to other analysis tools. By using these “nodal coordinates”, the critical region of the

conical cup – one-third of the drawing depth in the sidewall – can be identified and investigated. To investigate wrinkling formation and to measure the wrinkling height H^W in the sidewall of a conical cup, Eisele introduced an approach based on “polar coordinates” as illustrated in Figure 7-13-a. The deviation between the peaks and troughs of the black curve (section profile in X–Y surface, see Figure 7-12-a/b) is defined as the wrinkling height H^W in this case. Later, with the definition of “vector_length $|MP_i|$ ” and “angle θ in polar coordinates”, the “polar coordinates” can be transformed into the “wrinkling height H^W ” as the function of “angle θ in polar coordinates”, which are depicted in Figure 7-14-a. Furthermore, to investigate the buckling behaviour and to measure the buckling height H^B in the sidewall of a conical cup, Duan-Mu proposed a concept of “position deviation V^P ” [Dua16], which is defined as the deviation (at one third of drawing depth in the sidewall) between “ideal radius R in X–Z section” and “real radius R' in buckled X–Z section”, see Figure 7-12-d. According to the results of Duan-Mu, the development of sidewall surface quality in a conical cup can be described by the “wrinkling height H^W ” and “positional deviation V^P ”. Details will be given in Section 7.2.4 below.

$$|MP_i| = \sqrt{X^2 + Y^2} \quad (7.1)$$

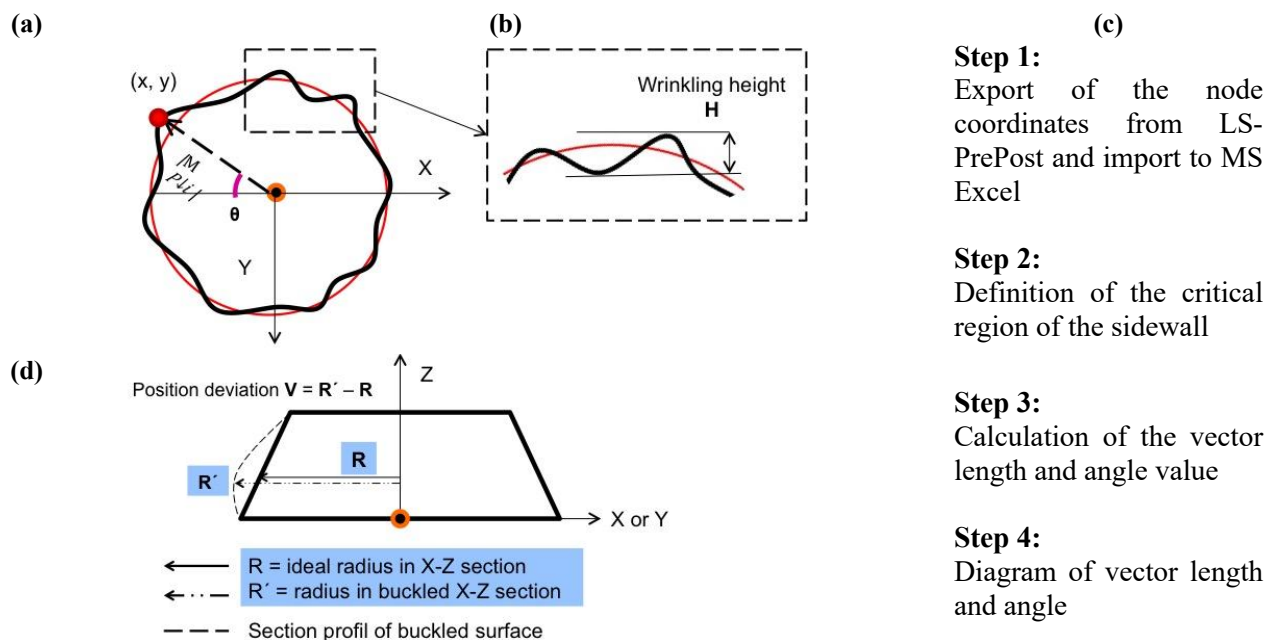


Figure 7-12: Eisele’s approach for investigating the sidewall quality of a conical cup: (a) definition of the position deviation; (b) four steps for determining diagram of vector length and angle; (c) identification of vector length and its relationship with angle; (d) identification of the wrinkling height

The vector length $|MP_i|$ can be calculated in four steps using X and Y coordinates as described in Figure 7-12. Furthermore, the “ideal radius R in X–Z section” is equal to “radius R_Z ” (see Figure 7-13-b and Equation 7.2), while the “real radius R' in buckled X–Z section” is equal to “vector length $|MP_i|$ ”. The value of “position deviation V^P ” is thus defined (see Equation 7.3) as the “average value of the deviation between vector length $|MP_i|$ and radius R_Z ” of every point in

Figure 7-14-b. Therefore, by evaluating the vector length–angle diagrams for various deep drawing steps, the surface profile can be determined with the aim of evaluating its quality.

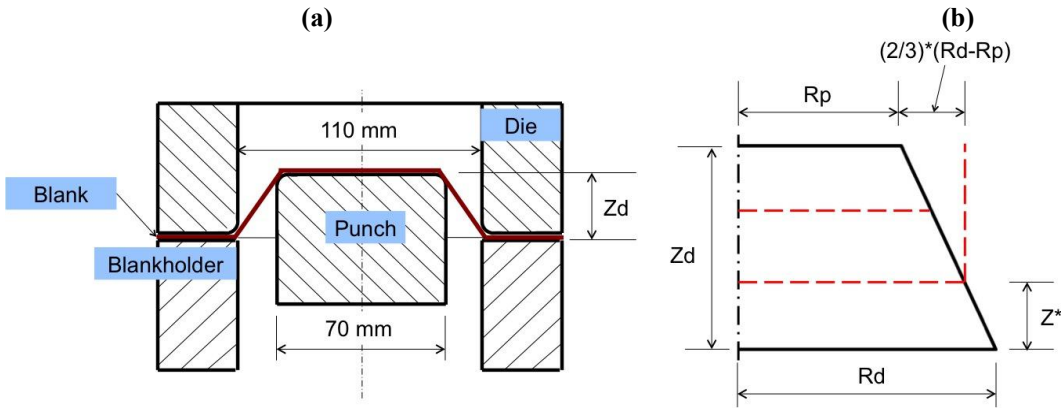


Figure 7-13: Illustration of the definition of “radius R_z ” in the case of mini-CCT test: (a) illustration of the tools used for the mini-CCT test at a certain drawing depth Z_d ; (b) schematic diagram of “drawing depth Z_d ”, “radius of die R_d ”, “radius of punch R_p ”, “position at one-third of drawing depth in the sidewall Z^* ”, and “radius at Z^* - R_z ”

$$R_z = R_p + \frac{2}{3}(R_d - R_p) \tag{7.2}$$

$$Position\ deviation\ V = \frac{\sum_{i=1}^n (|MP_i| - R_z)}{n} \tag{7.3}$$

$$\theta = \frac{Y}{X} \tag{7.4}$$

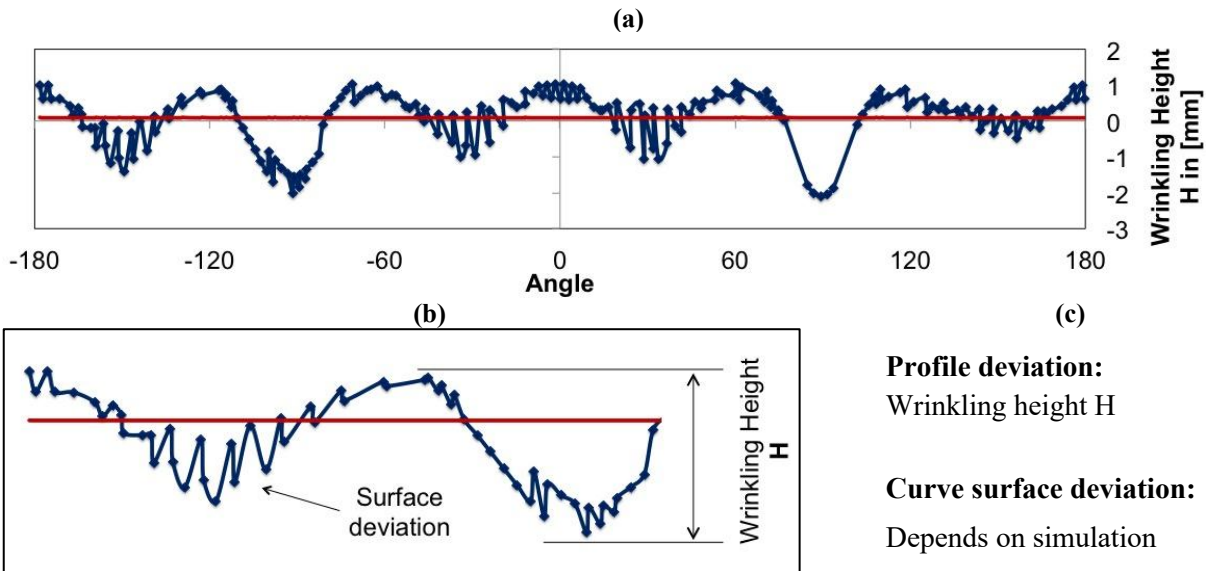


Figure 7-14: Wrinkling height H^W and position deviation V (red line) using angle–vector diagram

In this case, the wrinkling behaviour of the part during the drawing process is defined by the undulating waves formed along the circumferential path of the unsupported sidewall region. The profile of the wrinkles that appear along the sidewall first appears at a height of one-third of the drawing depth (R_d , see Figure 7-13) and can be represented by the vector–angle diagram (the blue curve in Figure 7-12). The x-axis in Figure 7-14 indicates the change of angle θ (see Equation 7.3)

along the circumferential path, while the y-axis represents its vector length $|MP_i|$ calculated with Equation 7.1.

7.2.4 Surface defect – wrinkling height and surface deviation

Using the drawing depth as the abscissa and the wrinkling height H^W and height of occurring buckles H^B as the ordinates, the development of the surface contour can be described in accordance with Figure 7-15. The dark-blue curve indicates the development of the position deviation V^P during the deep drawing process, while the light-blue curve indicates the development of the wrinkling height H^W .

During the “first surface-defect process”, defined in Section 7.2.2, drawing depth between 0 mm and 4 mm, the sidewall has no wrinkles (value of light-blue curve equal to zero). The positional deviation V^P has a maximum value of 0.3 mm. At the defined “wrinkling initiation” – at a drawing depth of 15 mm – the conical cup exhibits a “wrinkling height” of around 0.4 mm. At the “wrinkling initiation”, the positional deviation V^P reaches a maximum value of buckling. 1.3 mm. From a drawing depth of 4 mm (after occurrence of first surface defect) to a drawing depth of 15 mm (wrinkling initiation), the wrinkling height H^W slowly increases from 0 mm to approximately 0.4 mm.

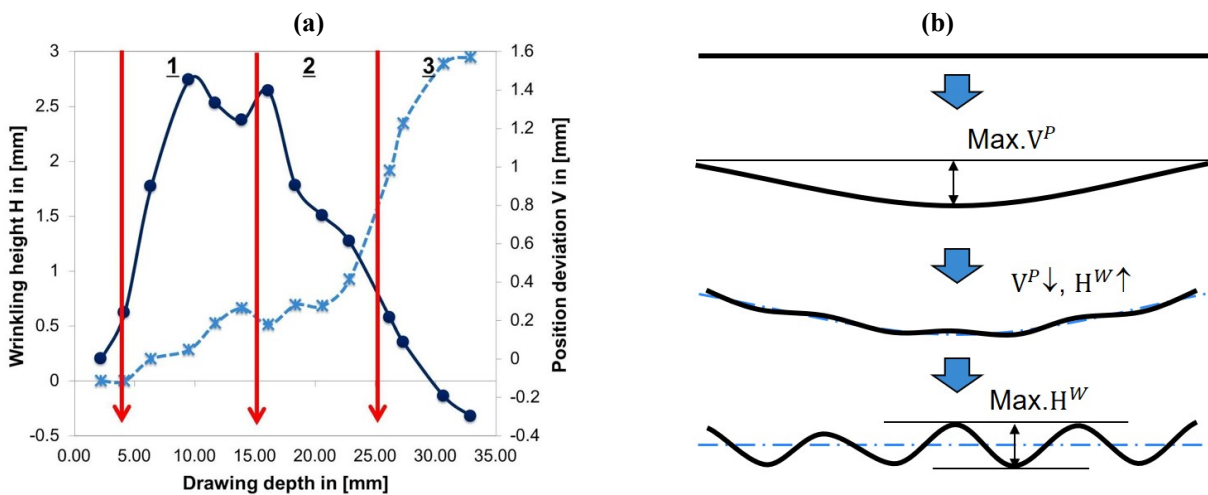


Figure 7-15: (a) Determination of the buckling and wrinkling phenomena in the conical-cup test; dark blue line: position deviation; light blue line: wrinkling height; (b) Max. positional Deviation and max. wrinkling height during the forming process

After the wrinkling initiation, the value of “positional deviation V^P ” decreases rapidly after the sine wave appears in the sidewall of the conical cup. Therefore, the positive and negative parts of the wrinkles are balanced. The positional deviation was steadily reduced to zero before the end of the experiment. Compared to the tendency of positional deviation V^P , the growth of the wrinkling height H^W increases dramatically between the “wrinkling initiation” and the end of the experiment.

7.2.5 Conclusion on the mini conical-cup test

Comparison of modified Yoshida buckling test to mini-CCT test

The wrinkling process of the mini conical-cup test cannot be compared to the modified Yoshida buckling test. The reasons are as follows:

- In the conical-cup test, there was a surface defect (“surface depression”), after which the investigated wrinkling process starts. This phenomenon was not observed in the YBT tests.
- The buckling profile in the modified Yoshida buckling test is different from the wrinkling profile of the sidewall wrinkles in conical cups.
- The wrinkling process of the sidewall of the conical cup is a process involving a mixture of wrinkling and buckling. The wing motion of the modified Yoshida specimen caused a bending moment, which affected the wrinkling process of the buckling test on the M-YBT specimen. The mixing process therefore cannot be observed in the buckling test.

Comparison of simulation and experiment results

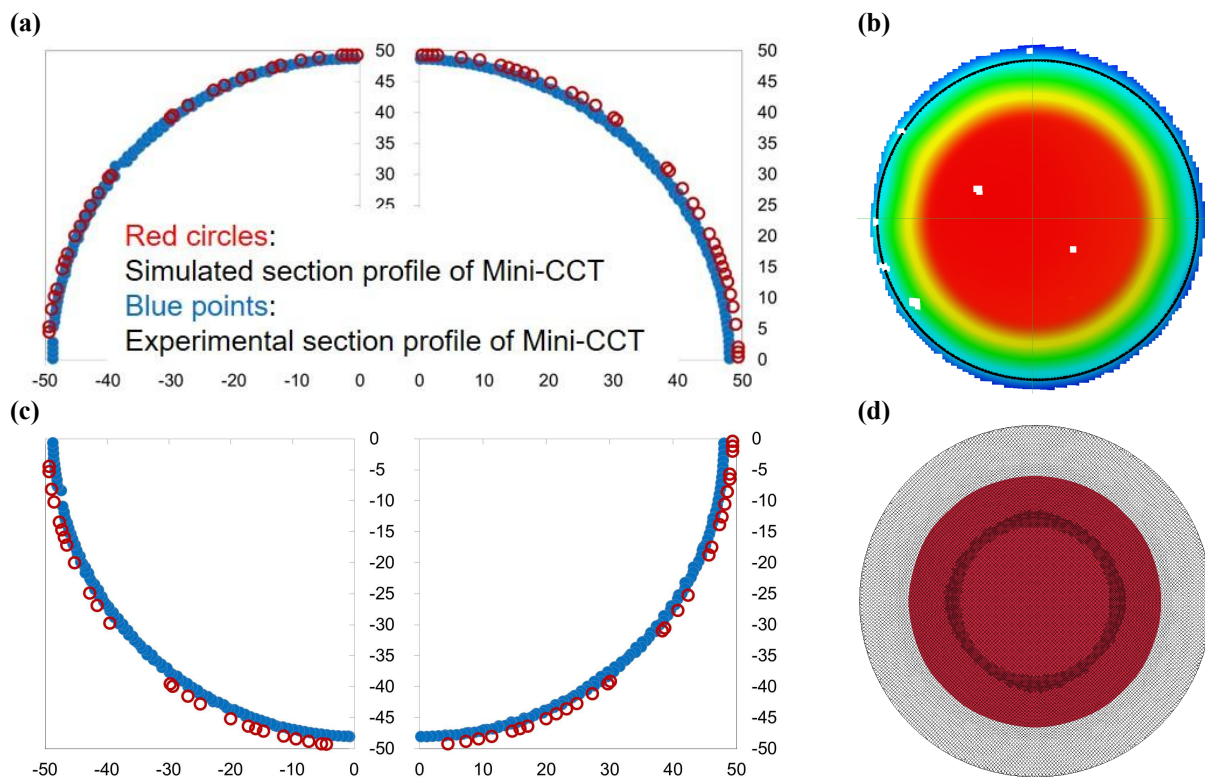


Figure 7-16: (a) and (c) comparison of results from experiments (blue points) and FEA (red circles) at maximum buckling height with homogeneous enlargement in the sidewall, tested material HC20LA with thickness of 0.6 mm; (b) 3D surface profile captured by GOM ARAMIS; (c) 3D surface profile exported from LS-PrePost

In this section, the simulation results are compared with the experiment results. Material HC420LA with a thickness of 0.6 mm was used for investigation of the wrinkling behaviour.

The comparison of the X–Z section profile at maximum “position deviation V^P ” (at maximum buckling height) is shown in Figure 7-16. The X–Z section profiles at the defined “wrinkling initiation” and “developed wrinkling” points are presented in Figure 7-17 and Figure 7-18.

Results of the comparison between results of FEA and experiments at the maximum buckling height (described in Figure 7-15 by “position deviation V^P ”) is shown in Figure 7-16. At this drawing depth, the wrinkle profile was not observed since the “surface defect” before “wrinkling initiation” is presented as a “buckling” phenomenon, which enlarged the part perimeter homogeneously.

Figure 7-16-b, Figure 7-17-b, and Figure 7-18-b show the 3D surface profile measured using GOM ARAMIS at a corresponding drawing depth. The colour indicates the displacement of the surface profile in the direction of action. The colour red denotes the maximum displacement in the drawing direction, while blue denotes the minimum displacement. The area of the sidewall in the conical cup is shown in green. The blue circles in these figures indicate the positions of the X–Z sections evaluated in Figures 7-16, 7-17, and 7-18. The blue circle is exported from GOM ARAMIS and illustrated in Figure 7-16-a/c, Figure 7-17- a/c, and Figure 7-18- a/c.

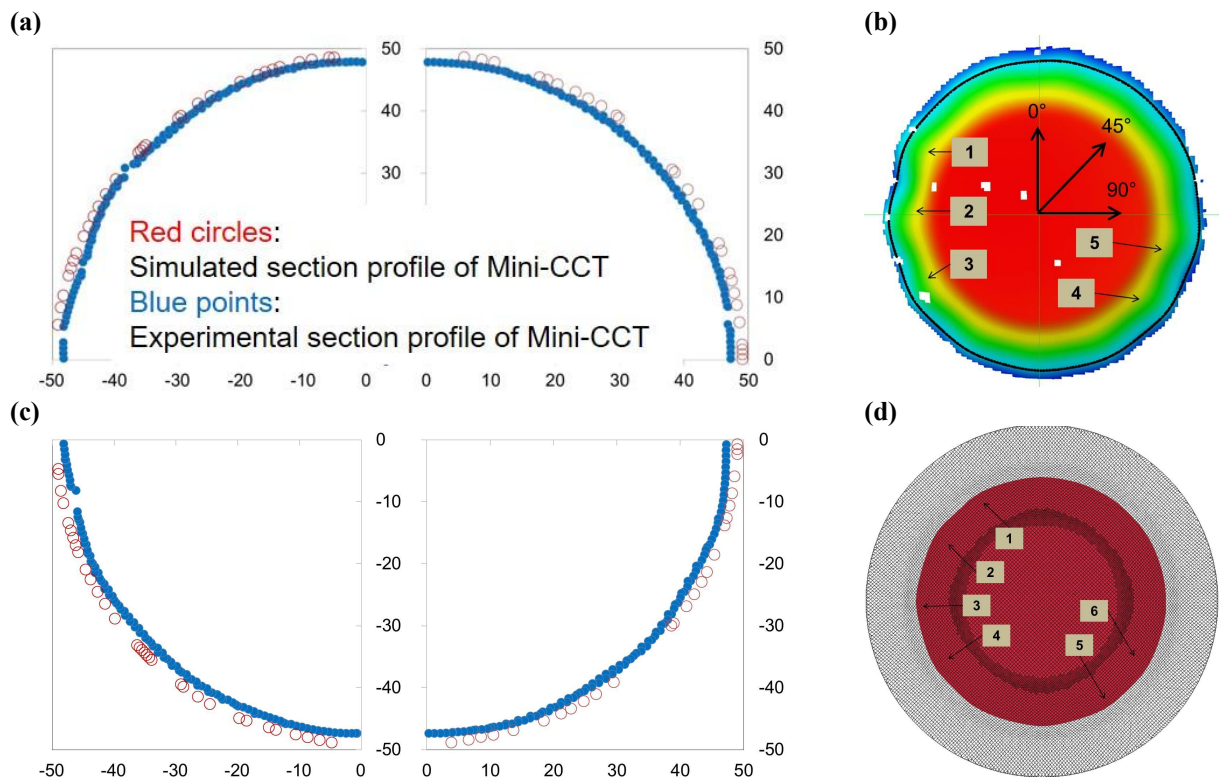


Figure 7-17: (a) and (c) comparison of results from experiments (blue points) and FEA (red circles) at “wrinkling initiation” in sidewall, tested material HC20LA with thickness of 0.6 mm; (b) 3D surface profile with 5 observed slight wrinkles captured by GOM ARAMIS; (c) 3D surface profile exported from LS-PrePost with 6 observed wrinkles

Figure 7-16-b, Figure 7-17-b and Figure 7-18-b show the 3D surface profile of the conical cup exported from LS-PrePost. An X–Z-section at the same position in the Z-direction (the same Z-direction as the blue circle) was also exported and depicted as small red circles in Figure 7-16-a/c, Figure 7-17- a/c, and Figure 7-18- a/c.

Figure 7-17 shows the results at “wrinkling initiation” (drawing depth of 15 mm). From this stage onwards, the development of wrinkles can be observed. From this drawing depth onwards, severe wrinkles in the sidewall can be observed. In the labelled sidewall, 5 wrinkles were observed when using GOM ARAMIS during deep drawing. Six wrinkles were also observed by investigating the three-dimensional surface profile derived from the FEA, the results of which can be compared to the experiment results.

Results of the comparison at “developed wrinkling” (drawing depth of 25 mm) are shown in Figure 7-18. From this drawing depth onwards, severe wrinkles in the sidewall could be observed. In the sidewall, 12 wrinkles were observed using GOM ARAMIS. 12 wrinkles could also be observed by investigating the exported 3D surface profile from the FEA. It can be concluded that the results of the FEA are comparable to the experiment results.

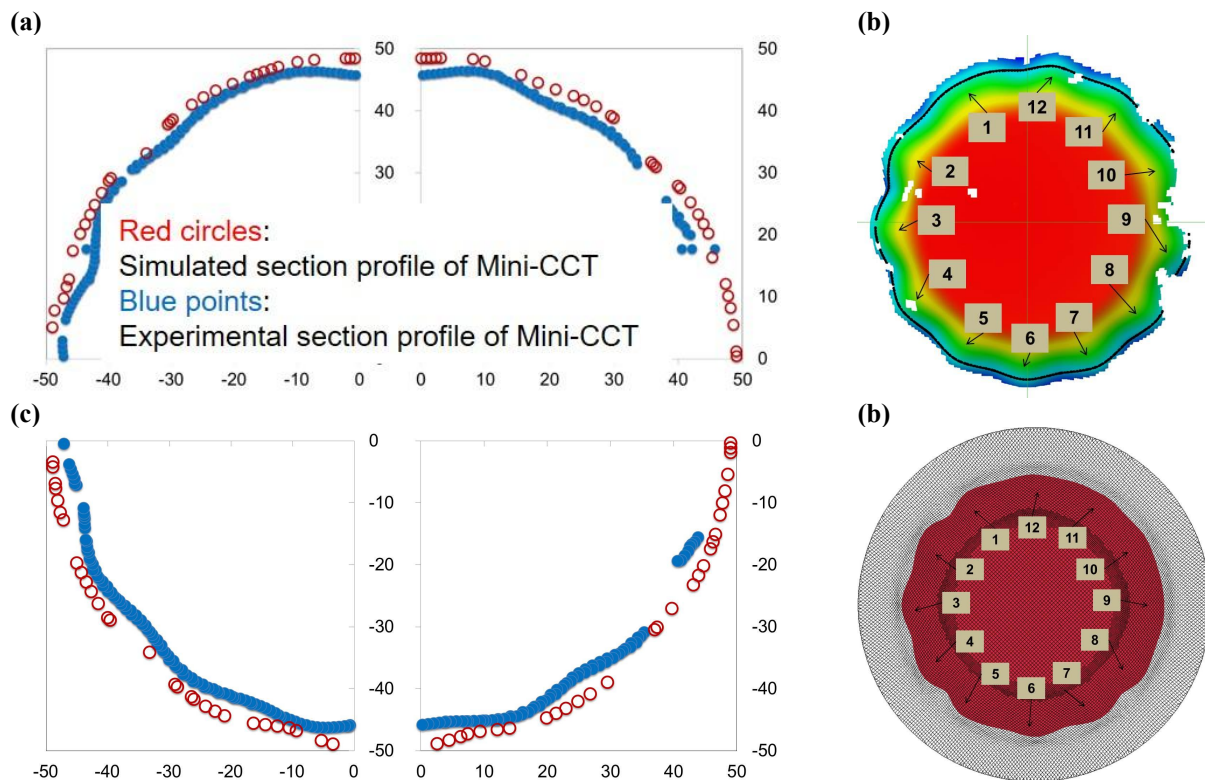


Figure 7-18: (a) and (c) comparison between results of experiments (blue points) and FEA (red circles) at “developed wrinkling” in sidewall, tested material HC20LA with thickness of 0.6 mm; (b) 3D surface profile with 12 observed severe wrinkles captured by GOM ARAMIS; (c) 3D surface profile exported from LS-PrePost with 12 observed wrinkles

7.3 Case study 3 – car-fender-based geometry

Section 7.3 described the use of FEA for studying wrinkles in KVG geometry. Two finite-element models were created for the “rigid blank holder” and the “elastic blank holder”. The simulation details were published in [Ran15a] and [Ran15b].

7.3.1 FE model for rigid blank holder

Deep drawing process with a rigid blank holder was simulated using the LS-Dyna FE code. The complete tool in the simulation consists of the die, blank holder, and punch, as presented in Figure 7-19-a. Properties for the investigated material HC340LA with a thickness of 1.0 mm were obtained from a uniaxial tensile test. The flow curve was approximated by means of the Swift rule. In the FEA, blank material model *MAT 36 (3-parameter Barlat plasticity) was used. This material model enables Lankford parameters R_{0° , R_{45° , and R_{90° to be incorporated into the FE modelling and includes a variety of material depending on the rolling directions.

The tool geometry has been meshed with the “Belytschko–Tsay shell” element type. For all tool parts, material model “MAT-RIGID” was applied. For the punch and die also depicted in Figure 7-19-a, “*CONTACT-FORMING-ONE-WAY-SURFACE-TO-SURFACE” with “soft constraint 4” was applied.

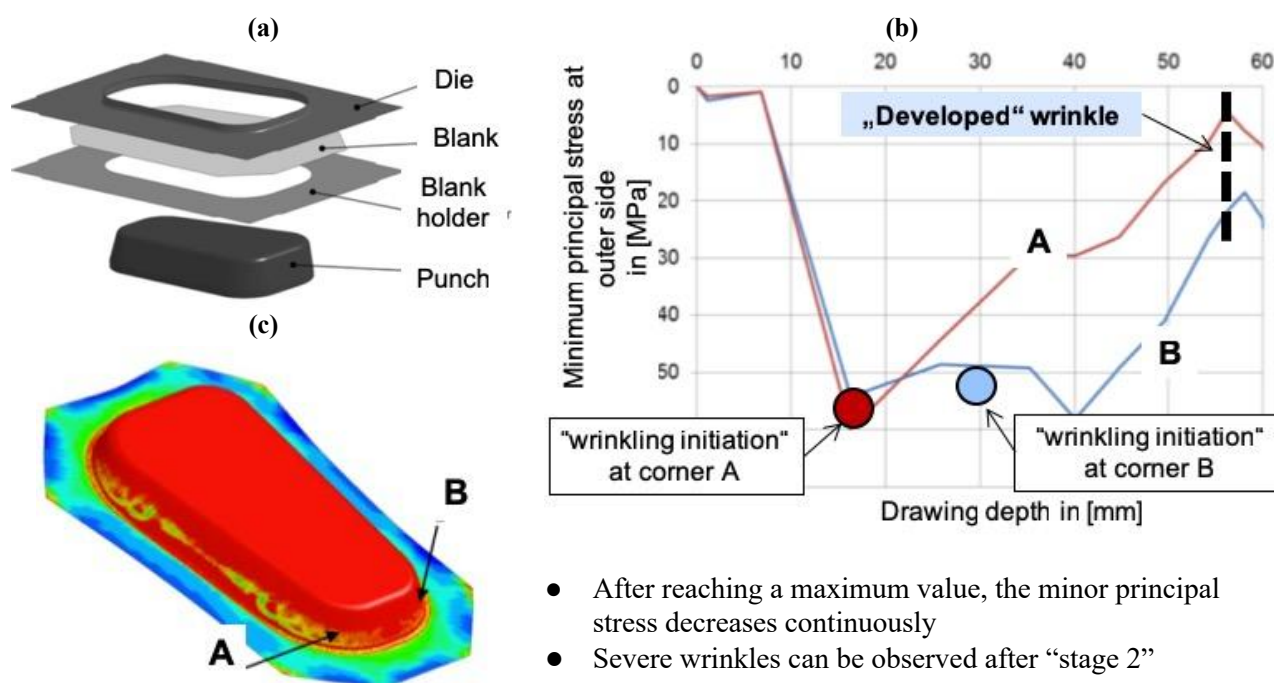


Figure 7-19: FEA for rigid blank holder with material HC340LA, sheet thickness of 1.0 mm: (a) FE model for deep drawing process using a rigid blank holder; (b) analysis of the stress conditions through investigation of selected elements at corner A and corner B of formed part [Ran15a]; (c) relationship between minor principal stress on outer side of investigated elements of corner A and corner B and deep drawing depth in the case of rigid blank holder [lie16]

or modelling the contact physics between the blank holder and blank, the contact type “*CONTACT-FORMING-SURFACE-TO-SURFACE” with “soft constraint 0” was used. The blank has also been meshed with the “Belytschko–Tsay shell” element type. Figure 7-19-a shows the FE model for the deep drawing process considering rigid tool surfaces.

Figure 7-19-a shows the FEA results using a rigid tool component. The blank holder force applied in this case was 900 kN, and the maximum drawing depth was set to 60 mm. Here, two finite elements near “corner A” and “corner B” (critical areas of the part in terms of the occurrence of wrinkles; see Figure 7-19-c) were selected. Figure 7-19-b presents and defines correlations between the “minor principal stress on the outer side” and “drawing depth” used to analyse the wrinkle formation process. With this it became obvious, that the first wrinkle occurs at corner A at a drawing depth of approximately 17 mm.

The “wrinkling initiation” process required a drawing depth of 30 mm for the investigated element at “corner B” and a drawing depth of 17 mm being found for the investigated element at “corner A”. After reaching the defined “wrinkling initiation”, both of the minor principal stresses on the outer side reduced steadily. At the achieved drawing depth of approximately 57 mm, the minor principal stress on the outer side of the element at “corner A” was found very close to value “0”. With regard to the previously described assumption, a wrinkle is fully formed in the investigated “corner A” at this drawing depth.

7.3.2 FE model for the elastic blank holder

The objective of the defined FE model was to analyse the influence of blank holder elasticity on the material draw-in and to accurately predict the achievable part height without cracking, as well as the second-order wrinkling formation. The motion of the die was disabled during the simulation. To form the required part shape, in FE the motion function was applied to the punch. The punch motion was modelled as a sine function [Tra16].

To increase the deep drawing depth while considering requirements for part surface quality (wrinkles, cracks, etc.), the finite-element simulation was performed with an elastic blank holder in order to apply various surface pressures onto the part flange. This can be achieved by varying the blank holder stiffness using the appropriate order and type of blank holder supporting element (as depicted in Figure 7-20).

According to Figure 7-20, the blank holder consists of a cover plate, which is supported by numerous elastic pyramids made of cast iron. To properly model the elastic behaviour of the cover plate supported that way, the blank holder plate and corresponding supporting elements are meshed with solid elements. The elastic material model “*MAT- ELASTIC” was assigned to those tool

parts, and the tool parts were designed using CATIA V5 software. To model the deep drawing process, DynaForm 5.8.1, LS-PrePost 4.1, and text editor Notepad++ software were used.

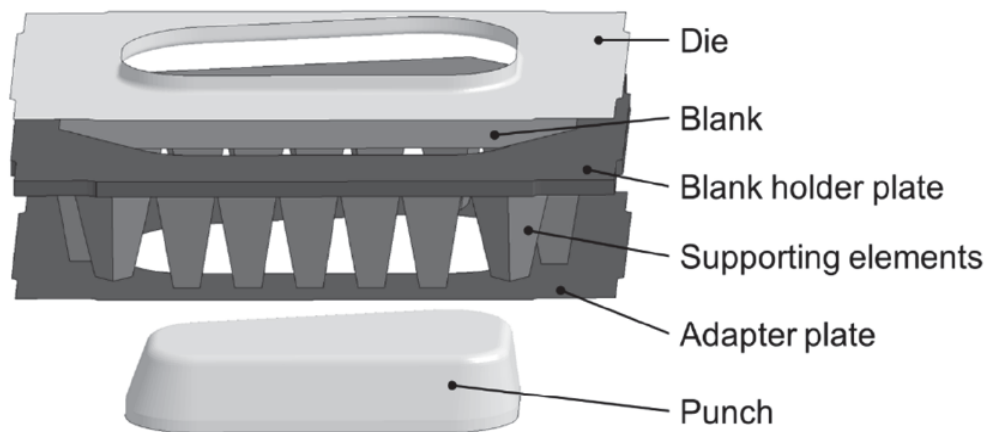
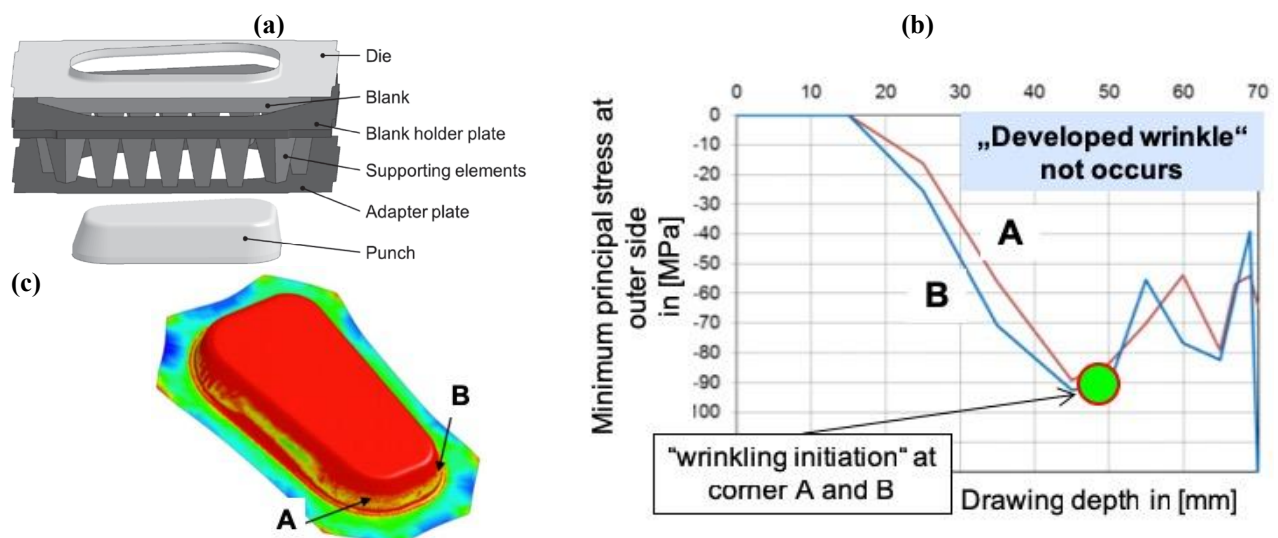


Figure 7-20: FE model for deep drawing process using elastic blank holder design [Ran15a]

In the section on the development of wrinkles, two finite elements were selected at corner A and B (Figure 7-22-c) to observe the development of stress values during the drawing process in detail. For these selected elements, the interdependence of the minor principal compressive stress and deep drawing depth was analysed (Figure 7-21-b).



- Later appearance of time point of maximum compression stress
- After achieving a maximum value, compression stress does not tend towards a value of zero
- In the corners A and B tendency towards development of wrinkling is noticeably reduced when using elastic blank holder

Figure 7-21: FEA for elastic blank holder with material HC340LA, sheet thickness of 1.0 mm: (a) FE model for deep drawing process using an elastic blank holder; (b) analysis of the stress conditions through investigation of selected elements at the corners A and B of formed part [Ran15a]; (c) relationship between minor principal stress on outer side of investigated elements at both corners A and B and deep drawing depth in the case of rigid blank holder [lie16]

It can be seen that both minor principal stress values on the outer side of the investigated elements (corner A and corner B) do achieve their maximum value at a deep drawing depth of approximately

45 mm (wrinkling initiation). After this defined “wrinkling initiation” (see Figure 7-21-b), the value of the minor principal stress on the outer side starts to reduce and, furthermore, does not tend towards zero. After reaching its maximum, the value changes cyclically. According to the obtained results depicted in Figure 7-21-b, it can firstly be confirmed that the deep drawing depth is significantly increased without any wrinkles of second order occurring when compared to deep drawing with a “rigid” blank holder that has not been optimised. The tendency for wrinkles to develop was also noticeably reduced. The “developed wrinkling” point of time as marked in Figure 7-19-b was not detected based on the FEA results using the elastic blank holder concept.

7.3.3 Results – experiments conducted with car-fender-based geometry

To determine the wrinkle height occurring in the deep drawing process for car-fender-like geometry, selected parts were digitised using the GOM ATOS optical-measuring system. To avoid reflection during measurement, the test objects were coated with white paint. It was necessary to ensure that an extremely thin layer of paint was applied to reduce measurement failure.

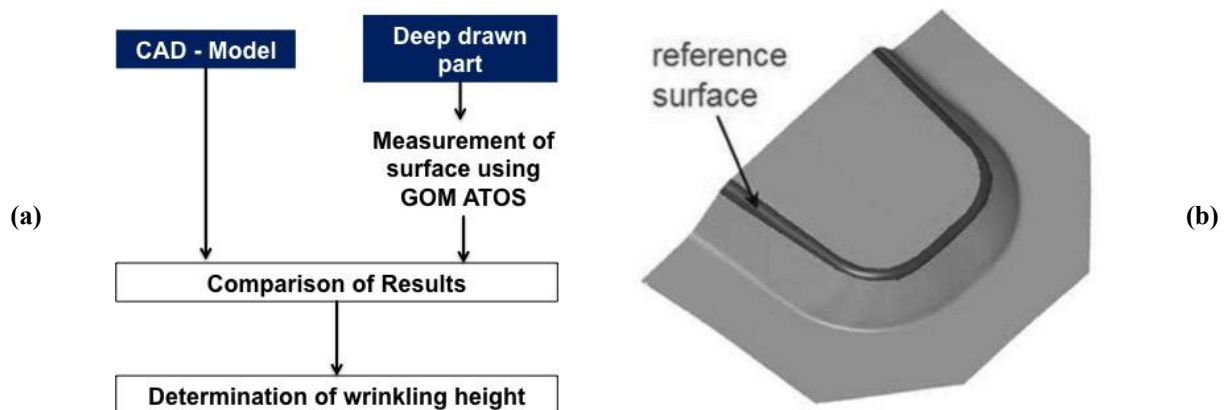


Figure 7-22: (a) Approach for determining the wrinkling height by comparing the CAD model with the measured “car-fender-like” specimen; (b) CAD image of the part’s reference geometry with the defined reference surface [Ran15a]

After the parts were successfully digitised, obtained results were converted into an STL (stereolithography) file format before being compared to the reference geometry of the part as represented in CAD. GOM Inspect software was used for this purpose. Firstly, the measurement results and reference geometry of the part were imported into the software for optimum alignment of both geometries and to determine the wrinkle height as precisely as possible. For this purpose, the selected surface was chosen as a reference for part positioning (see Figure 7-22).

Figure 7-23 shows differences in dimensions with regard to part shape deviations. The deep drawing depth of the parts was 60 mm. In this experiment, the blank holder was modelled with a uniform stiffness. In the first case (Figure 7-23-a), the part was deep drawn at a blank holder force of 900 kN. Experiment results showed that larger part shape deviations occurred. These deviations consisted of wrinkles as well as springback effects (sidewall curl and angle change; see Figure 2-10). The greatest measured deviation was +2.42 mm, and wrinkles of second order are visible in

this area of the part. The other deviations in the sidewall area of the part are the result of elastic recovery or springback after the part was from the drawing tool.

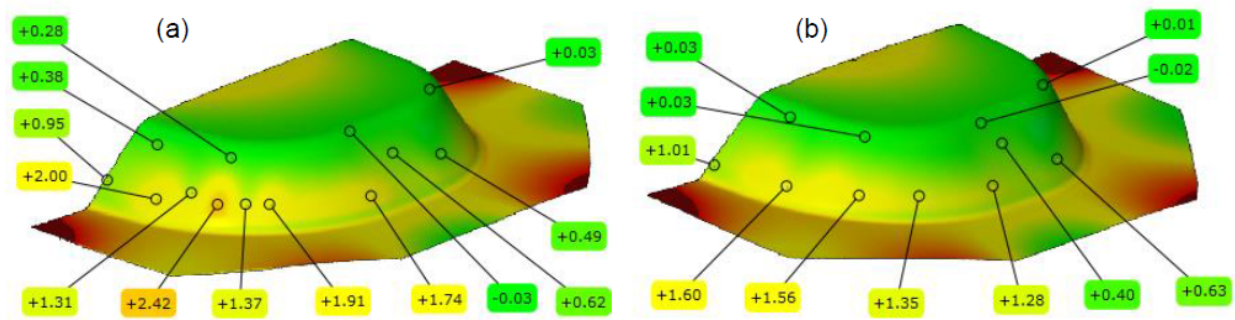


Figure 7-23: Comparison of occurring wrinkle height when using rigid blank holder; (a) part deep drawn at a blank holder force of 900 kN; (b) part deep drawn at a blank holder force of 1,050 kN

In the second case (Figure 7-23-b), the part is deep drawn by applying a blank holder force of 1,050 kN. Measurement results showed that the greatest deviation in the analysed part area is +1.60 mm. There was no visible wrinkling development observed on this part. Any deviations occurring on this part were identified as “springback”, which means that residual elastic stresses caused the change in the part’s shape after its removal from the die cavity. The shape deviations in the sidewall area near the part flange occurred as a result of angular change and sidewall curl. When comparing measurement results in Figure 7-20-a, it can be seen that part shape deviations have been generally reduced for a part deep drawn through application of higher blank holder force

Application of a higher blank holder force ($> 1,050$ kN) led to the development of cracks when a uniform blank holder stiffness was used to further reduce part shape deflections. A lower blank holder force resulted in severe wrinkling. The appropriate blank holder stiffness was assembled to achieve simulation results for a deep drawing depth of 70 mm. The blank holder consists of the blank holder plate and corresponding supporting elements with appropriate Young’s modulus with regard to results shown in Figure 7-20-b.

Drawing depths of 70 mm without cracks were achieved in corresponding experiments. Figure 7-24 depicts experimental results for a part that was deep drawn using the optimised blank holder structure. The greatest shape deviation values range around +1.35 mm. No visible wrinkles in the part sidewall area were detected. The deviations that occurred in the part’s sidewall are a result of elastic recovery (springback), which occurs after the part’s removal from the tools cavity. When comparing these results obtained by FEA results for parts that were deep drawn using the “rigid” blank holder, it can be seen that the part-shape deviations were significantly reduced.

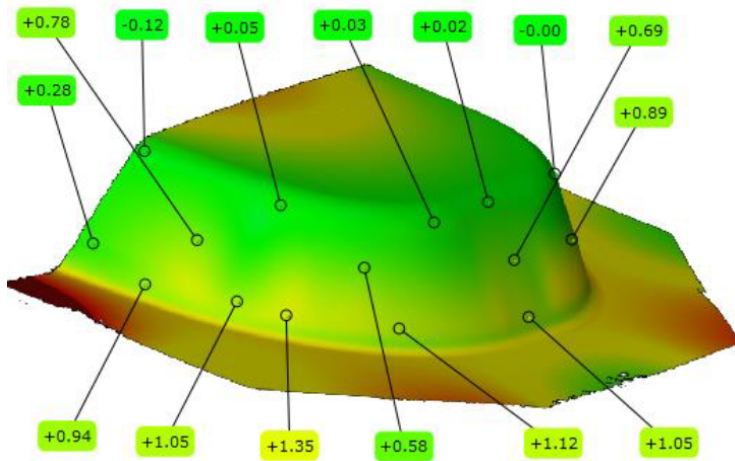


Figure 7-24: Shape deviation for a part deep drawn using the optimised blank holder stiffness (drawing depth of 70 mm; applied blank holder force of 1,000 kN)

7.3.4 Conclusion on experiments performed with car-fender-based geometry

Due to the modelling of the blank holder's stiffness, it is possible to influence part deflection in areas of extreme sheet thickening, which occurs during deep drawing. The tool load optimisation is of great importance, especially when forming steel grades with a high tensile-strength level.

When compared with corresponding experiments, the simulation results evaluated using the described simplified model (regarding the development of compressive stress) in Chapter 4 demonstrate the following:

1. It is feasible to predict the process of wrinkling formation on the KVG geometry using a simplified model since the investigated wrinkles on the KVG geometry are located in the free (unsupported) forming region. The simplified model in Chapter 4 is sufficient for predicting wrinkling of second order.
2. In addition, the influence of the optimised blank holder stiffness on wrinkling formation can be observed solely by evaluating the simplified model.
3. The influence of increased drawing depth on wrinkling formation can be observed solely by evaluating the simplified model.
4. Results of the investigation performed in Section 7.3 showed that it is possible to increase drawing depth significantly when forming with an optimised elastic blank holder design.

In general, the simplified model (without considering tool contact) can be successfully applied to predict the formation of wrinkling of second order (e.g. on car-fender-based geometry.) In addition, the influence of the blank holder stiffness and drawing depth on wrinkling formation can be predicted by applying the simplified model introduced in Chapter 4.

8 Validation of newly developed approach by applying in industrial part analysis

After evaluating the accuracy of the simulation results, the last task to be completed is described in Chapter 8, whereby complex deep drawn parts from industry will be validated using the DSCS-approach. Here, the DSCS-approach were implemented together with boundary conditions in post-processing of the Fem software AutoForm R6 to investigate four kinds of surface defects as introduced in Section 3.1, namely “wrinkles”, “surface low”, “small dimension of wrinkles”, and “surface distortion”.

In Section 8.1, the logic of the DSCS-approach used for post-processing in AutoForm R6 was explained more broadly. In Section 8.2, possible surface defects like “wrinkles” and “surface low” were predicted using the DSCS-approach based on an exterior part from industry with the name of “exterior-lower-side-part”. Here, not only the position of “wrinkles” and “surface low”, but also the time point of those defects during the drawing process will be predicted by employing the DSCS-approach. In Sections 8.2 and 8.3 and below, the surface defects like “small dimension of wrinkles” and “surface distortion” were also predicted by using the DSCS-approach based on the specimens of “C-pillar reinforcement” and “door-frame adapter”, respectively, taken from a real passenger car.

8.1 User-defined-variable files in AutoForm software

Three types of UDV were tested in Chapter 8 to evaluate the impact of the type of UDV file on the detection of surface defects mentioned above when validating industrial car body parts. Further details are listed in Table 8-1.

Strain based and stress based UDV file

Table 8-1: Comparison of UDV1, UDV2, and UDV3 implemented in post-processing

	UDV1	UDV2	UDV3
Evaluation region:	Major/minor strain	Major/minor strain	Major/minor stress
Influence of non-linear strain paths:	Not considered	Not considered	/
Critical strain level:	0.006	0.004	0.004

As mentioned in Figure 5-1, the main challenge when preparing UDV files in post-processing is identifying the “wrinkle” or “surface defect” in the “wrinkling tendency” area. In the strain based files UDV1 and UDV2, the evaluation region was defined by the ratio of major and minor strain in FLD. By contrast, in stress based file UDV3, the evaluation region solely was checked by considering the stress acting on an element. The major advantage of stress based UDV3 compared

to strain based UDV1 and UDV2 is that, by using UDV3, the influence of a non-linear strain path does not need to be considered.

Furthermore, the “recoverable wrinkles” and “non-recoverable wrinkles” will be distinguished using a critical strain value. If the critical strain value of a wrinkle is smaller than the given critical value, wrinkling will manifest itself as elastic wrinkles that disappear during the subsequent or ongoing forming process. Only wrinkles with a critical strain value larger than the critical value are evaluated. To save calculation time, especially for a simulation with small elements, it is recommended to set such a critical strain value. The only difference between UDV1 and UDV2 is the set “critical strain value”. In this way, the influence of the “critical strain value” on the accuracy of wrinkle prediction can be investigated. In UDV1, this value is set to 0.006, while in UDV2 and UDV3 the amount of 0.004 is previously set.

Details on UDV1 and UDV2 in post-processing

The logic for implementation of UDV1 and UDV2 in post-processing using AutoForm FE software is shown in Figure 8.1.

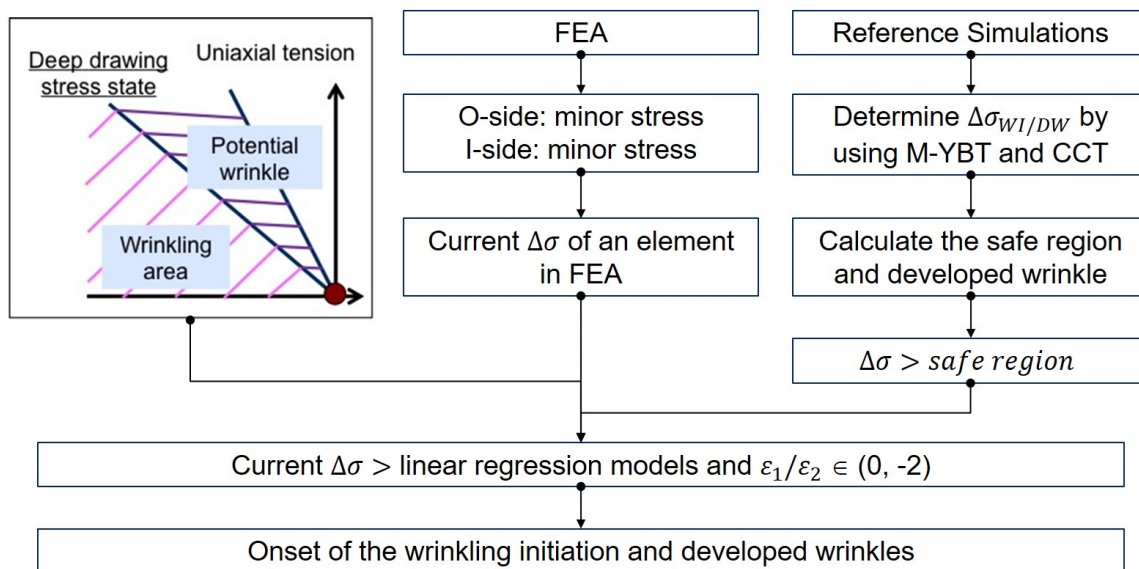


Figure 8-1: Logic for implementation of UDV1 and UDV2 in AutoForm R6 without considering the non-linear impact on defined “wrinkling initiation” and “developed wrinkles”

1) Definition of an “evaluation region” for detecting “wrinkling tendency”

Firstly, at every drawing depth, the value of the major strain/minor strain is calculated. If the calculated value is located between -1 and -2, the corresponding element is recognised as having a “wrinkling tendency” in FEA. Normally, when the calculated value ranges between the region of major strain/minor strain (between 0 and -2), the corresponding element can be recognised as having “wrinkles” or “surface defects”. Values ranging between -2 and 1 do indicate no “wrinkling tendency”.

2) Identification of the “difference between the minor principal stresses on the outer and inner

side” using linear-regression models

The value for the “difference between the minor principal stresses on the outer and inner side” of all the elements, which have a “major strain/minor strain” value of between -1 and -2 in FLD, was calculated in post-processing. If the “values calculated in post-processing” exceed the “values calculated through linear-regression”, the defined “wrinkling initiation” or “developed wrinkling” will occur.

The value of the local curvature in AutoForm R6 can be directly read and used since the local curvature of the simulated parts can be represented by factors like the maximum/minimum curvature and Gaussian curvature, etc. Since the initial sheet thickness cannot be used in post-processing, the value of the “current thickness” is used to calculate “critical stress values calculated in linear regression”.

Details on other issues in post-processing

The element in AutoForm R6 without surface defects will be marked in green. The elements located in “wrinkling initiation” and “developed wrinkling” are shown in yellow and red, respectively.

8.2 Validation study 1 – exterior lower-side part

In this case study, the deep drawn “exterior lower-side part” made of sheet metal DX54D (0.65 mm) was first investigated to validate the DSCS approach. The process plan of the exterior lower-side part is shown in Table 8-1.

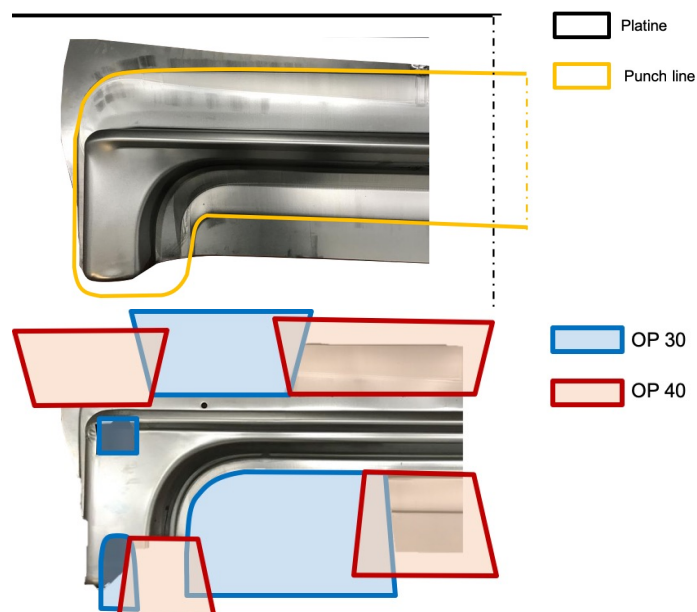
Table 8-1: Process plan for deep drawing and trimming

OP 20

- Deep drawing with open head
- Drawbead

OP 30 and OP40

- Trimming in direction of action
- Piercing in direction of action



OP 50:

- Trimming in direction of action
- Down flanging



Prediction of wrinkle formation in OP 20 using “potential wrinkling”

Since the very first wrinkle occurred in OP 20 according to experiment results, the analyses of the surface quality change in the formed part were carried out in OP 20, and the final forming operation in OP 50. To better evaluate emerging wrinkle formation, a drawn part was produced at every 10 mm drawing depth. Corresponding photographs are shown in Figure 8-2. Furthermore, every drawn part produced was treated by “stoning” to detect “small wrinkles” or “surface defects”. The photos before and after treatment by “stoning” are listed in Figure 8-2.

As shown in Figure 8-2, elastic wrinkles occur around the free forming area between die and tool at a drawing depth of 10 mm. When the drawing depth in OP 20 reaches 30 mm, this kind of elastic wrinkles disappear, as shown in Figure 8-2 (OP 20, at drawing depth of 30 mm). based on the FEA results and the real specimens from press shop, it can be summeried that elastic wrinkles may “disappear” during the deep drawing process. More accurate expression is, elastic wrinkles cannot be observed under certain drawing conditions with human eye. Thus, it is meaningful to distinguish between elastic and plastic wrinkles in order to enhance the accuracy of FEA to evaluate the surface quality of a drawn part.

From a drawing depth of 30 mm and beyond, the surface defects in the drawn part are not discernible by human eye. Using quadratic grinding stones being moved on sheet metal part surface such “stoning” treatment disclose s light surface defect types of “buckling” and “surface low”, so wrinkling effects can be recognised from a drawing depth of 40 mm to 60 mm in OP 20. At a drawing depth of 60 mm, the surface defect region was expanded to cover the entire evaluated surface (see the photo of treatment by “stoning”).

However, no surface defects or wrinkles were recognised by using AutoForm R6 between a drawing depth 10 mm and 60 mm by applying the wrinkling criterion “potential wrinkles”, the FEA results were shown in Figure 8-2.

In summary, “potential wrinkling” used in AutoForm cannot predict surface defects accurately during the forming process, for example for the case of “exterior lower-side part”. The possible reason is elastic wrinkles occurs with small ture stain value (ε_1 and ε_2 have the value around 0.005 according to the Yoshida test) . Strain based wrinkling criterion like “potential wrinkles” ignore the wrinkles with small strain value during the wrinkling process.

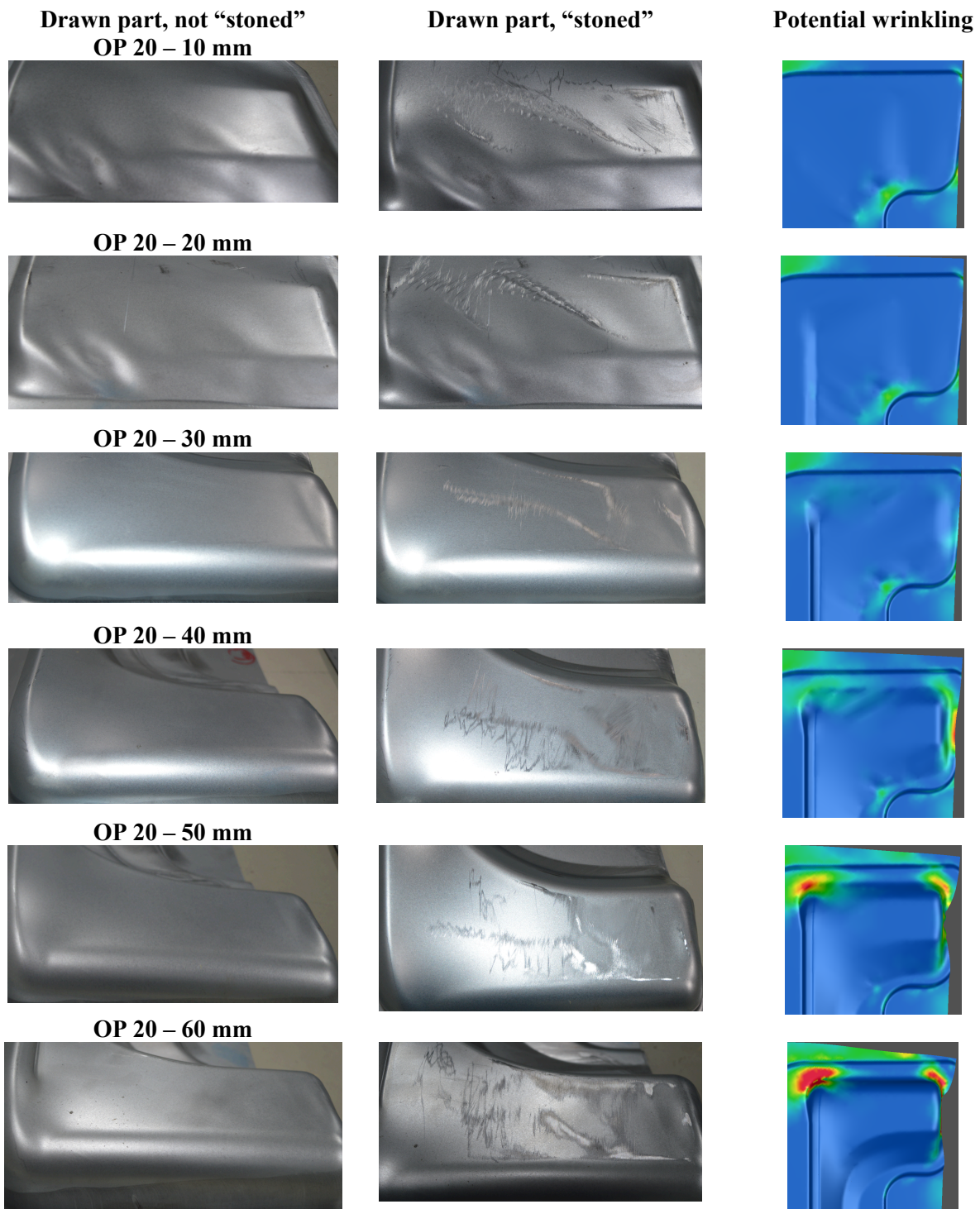
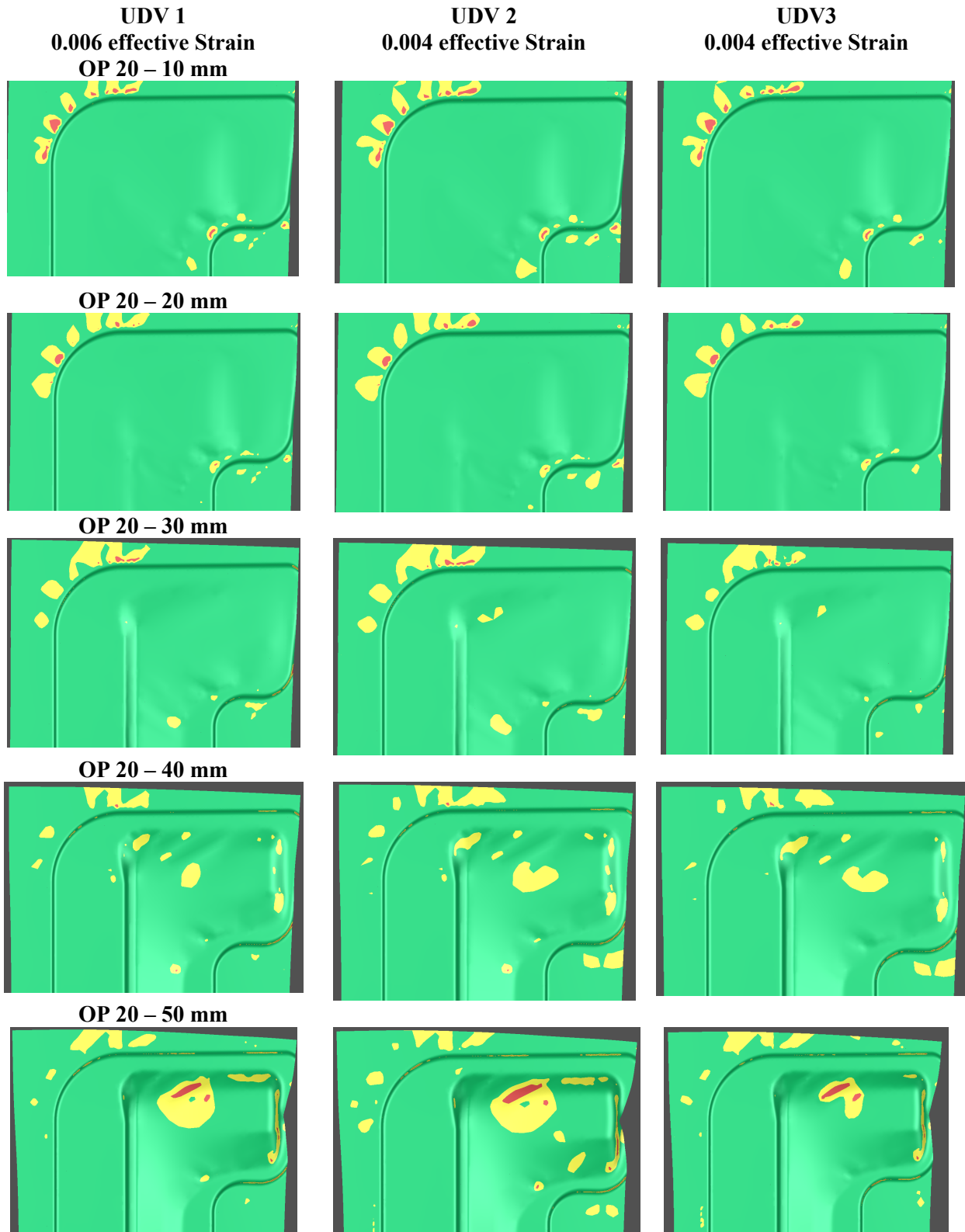


Figure 8-2: Experiment results (with and without “stoning” and simulative evaluation using potential wrinkling in AutoForm) for the surface quality of the exterior lower-side part from a drawing depth of 10 mm to 60 mm in OP 20

Prediction of wrinkles formation in OP 20 using DSCS-approach with effective strain between 0.004 and 0.006

Figure 8-3 shows the simulation results (OP 20) using UDV-1 (with 0.006 effective strain), UDV-2 (effective strain 0.004), and UDV-3 (effective strain 0.004). As described in Section 8.1, elastic wrinkles are not considered by setting critical strain values.

After recovery from the elastic wrinkles, the first wrinkles occur between 30 mm and 40 mm (see Figure 8-2). The simulation results show that only UDV-2 and UDV-3 can predict the first surface defect, because after the effective strain reaches 0.004, the post-processing can detect wrinkles. In UDV-1, the effective strain is set to 0.006, so wrinkles are detected later than UDV-2 and UDV-3. In addition, based on the simulation results, the expansion of the surface defects was observed from drawing depth of 30 mm to 60 mm.



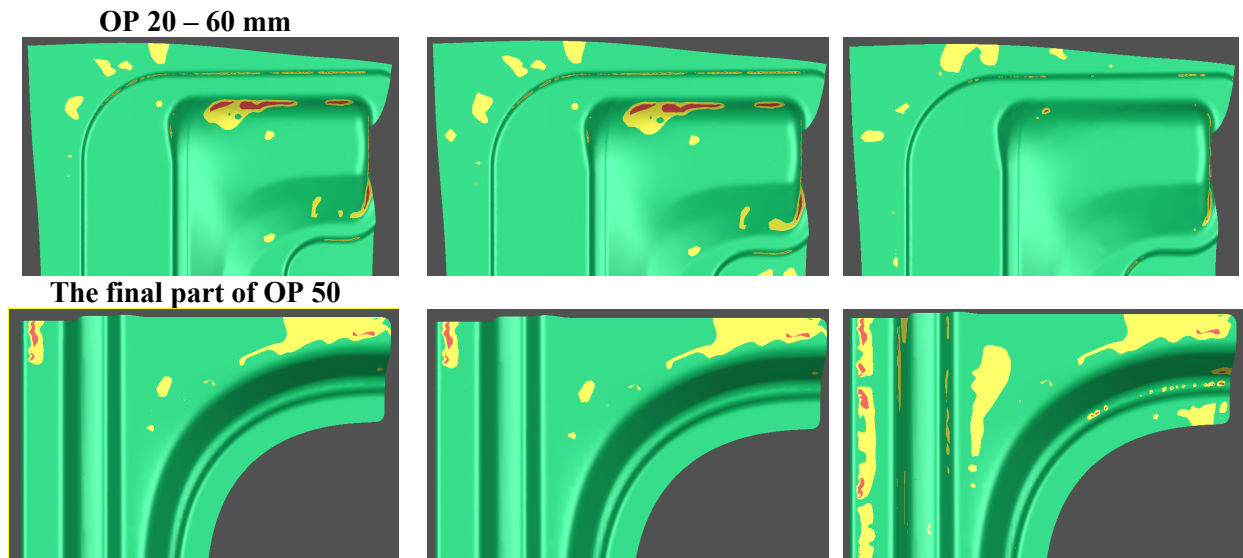


Figure 8-3: Simulative evaluation of the surface quality of part Side-Low-Outer using UDV-1, UDV-2 and UDV-3 from drawing depth of 10 mm to 60 mm in OP20 and final part in OP40

Since the type of the surface defects by part Side-Low-Outer are “surface low”, rather than “wrinkles”, the simulation results with UDV-3 was compared with another criterion in AutoForm R6 – “surface low”. (see Fig. 8-5). By using the DSCS-approach, the position of the critical regions predicted in the simulation with UDV-3 is comparable with validated parts. The accuracy of the predicted region of “surface low” with the approach in AutoForm is not sufficient in the case of part Side-Low-Outer.

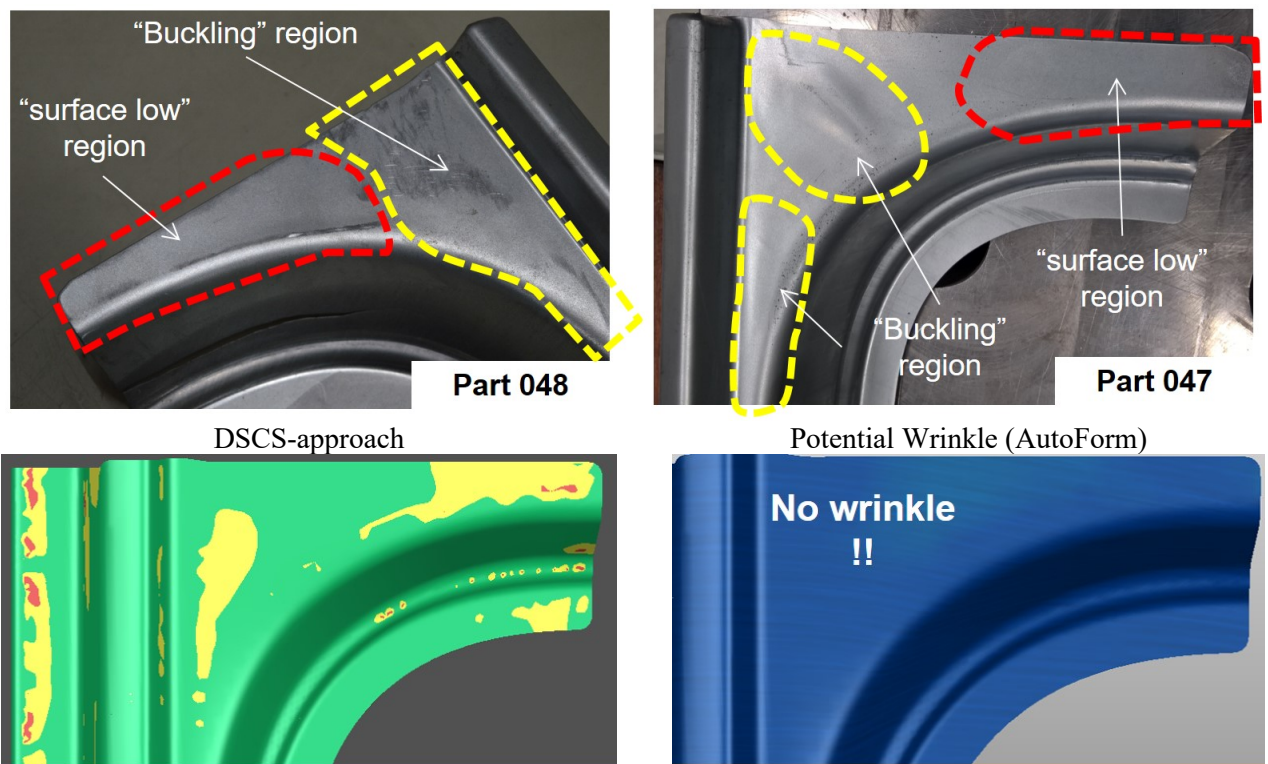


Figure 8-4: (a) Formed part Side-Low-Outer with surface defects surface low and buckling; (b) Comparison of the simulation results between “DSCS-approach” and “potential wrinkles” used in AutoForm in the OP40

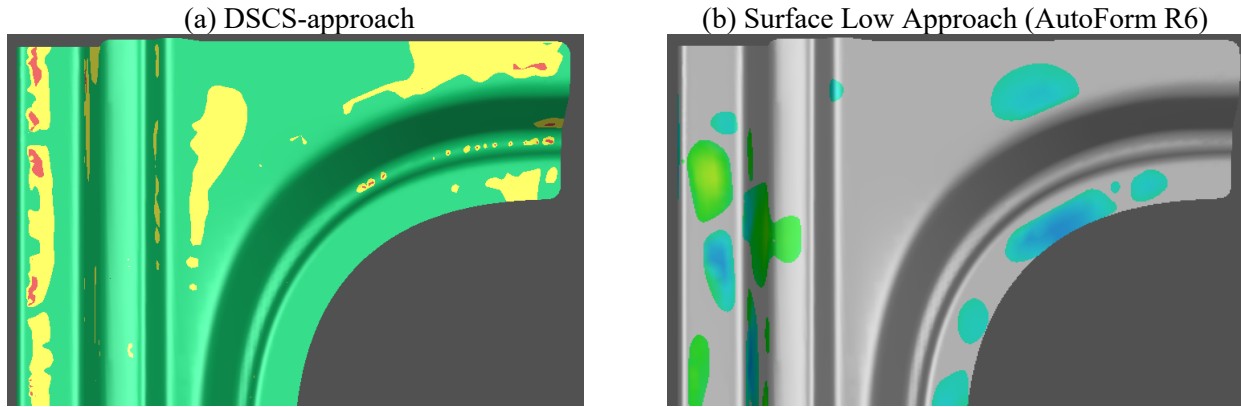


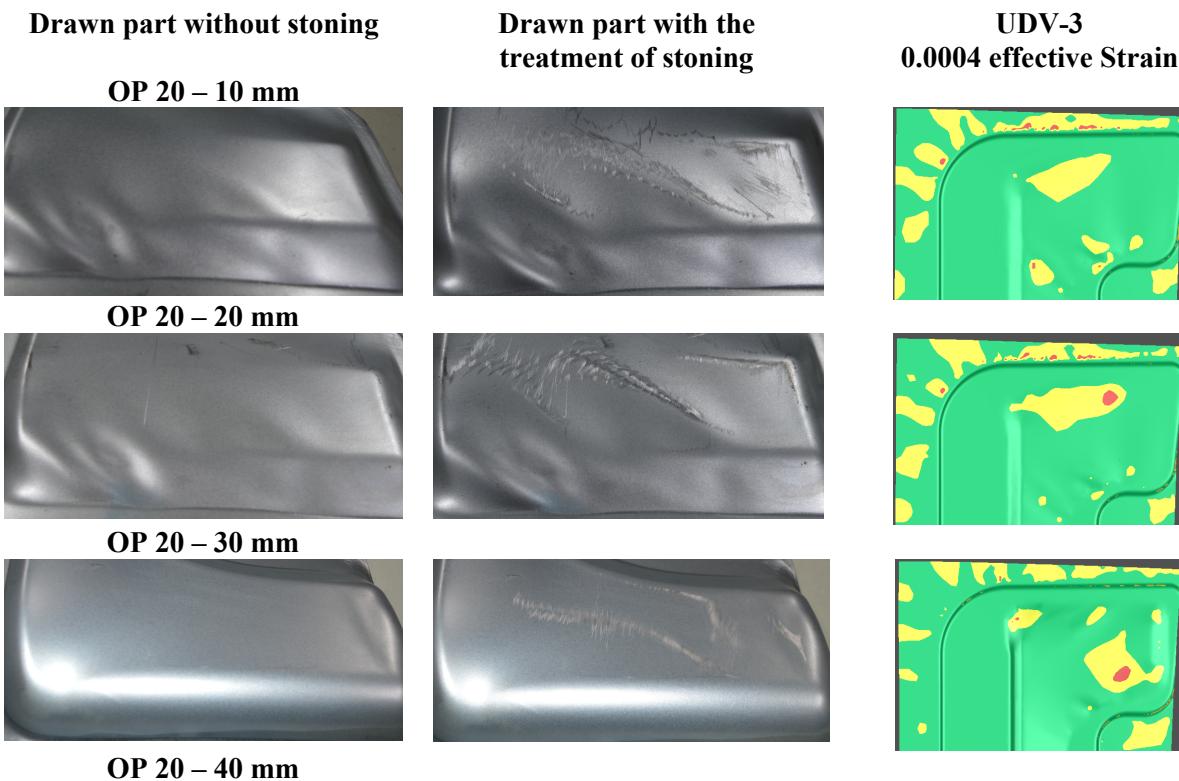
Figure 8-5: (a) Simulation results of the finished part before springback using DSCS-approach with UDV-3; (b) Simulation results of the finished part after springback using the surface low approach in AutoForm R6

In summary, the “DSCS-approach” can be used for predicting surface defects like surface low, buckling. The reason will be discussed in Chapter 9.

Prediction of wrinkles formation in OP 20 using “DSCS-approach” with effective strain 0.0004

To predict “elastic wrinkles”, which took place by the closing of tools and can be observed at drawing depth of 10 mm and 20 mm, the value of effective strain should be reset.

For example, the simulation results for an effective strain value of 0.0004 in the UDV-3 are shown in Figure 8-6. The results show that wrinkles have occurred at a depth of 10 mm. In addition, the wrinkled area significantly reduces itself from drawing depths of 10 mm to 60 mm. Since the marked wrinkling area (position) could not be stored in the simulation, the surface of the drawn part was considered to be free of defects at a drawing depth of 60 mm.



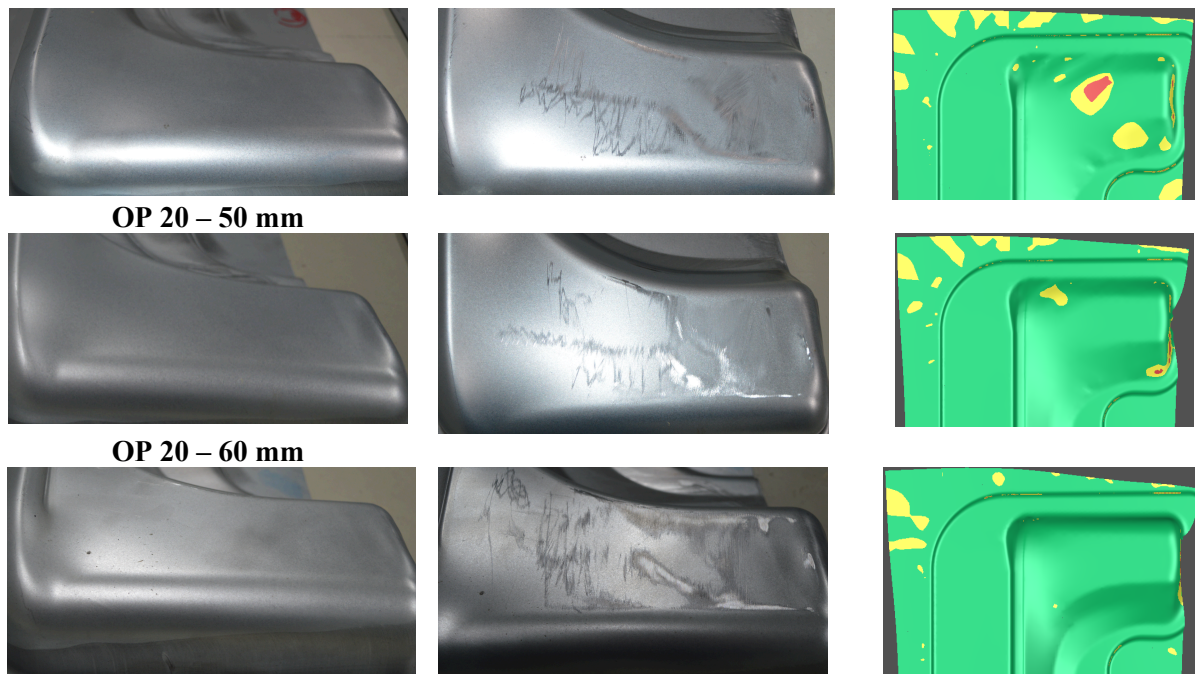


Figure 8-6: Experimental (with and without treating of stoning) and simulated evaluation (using potential wrinkles in Autoform) of the surface quality of part Side-Low-Outer from drawing depth of 10 mm to 60 mm in OP20

8.3 Validation study 2 – Part C-Pillar-Reinforcement

In this case study, the deep drawn part of the C-Pillar-Reinforcement is used to validate the new wrinkling criteria – DSCS-approach. Since there is no chance to produce a drawn part every 10 mm in OP 20 (as the situation in case study 1), only the wrinkling position at the finished drawn part will be validated. The occurrence of the first wrinkles is not validated in case study 2. The part C-Pillar-Reinforcement was produced with sheet material HC300LA (thickness 0.9 mm).

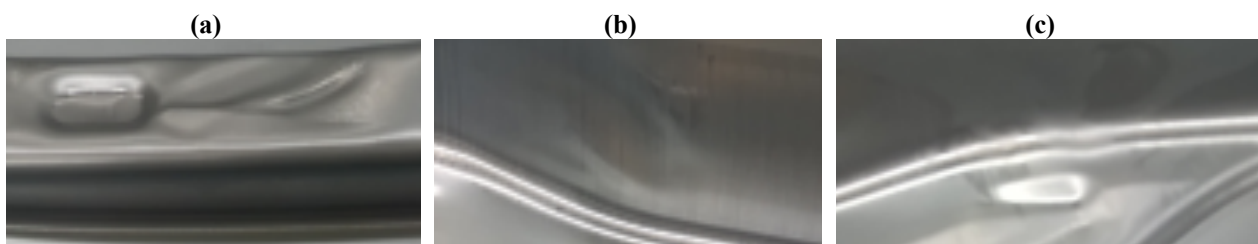


Figure 8-7: (a) Wrinkling area 1; (b) Wrinkling area 2; (c) Wrinkling area 3

After studying the finished drawn part, three wrinkling areas can be observed (Fig. 8-7 a/b/c). The validating results of the final drawn part are presented in Fig. 8-9, Fig 8-10, and Fig. 8-11.

The comparison of FEA results in OP 20 using “potential wrinkles” and “DSCS-approach” is presented in Fig. 8-8. The wrinkles which can be observed took place at a “distance to the bottom dead center” (Dist.BDC) of -30 mm. According to the simulation results using the “DSCS-approach”, there are no wrinkles at the edges of the sample. Severe wrinkles occur in the position marked with a red circle in Figure 8-8-b. On the other hand, results based on the “potential wrinkle” approach indicate that severe wrinkles are located at the edge of the finished product and are

marked as “colour red” in the FEA automatically.

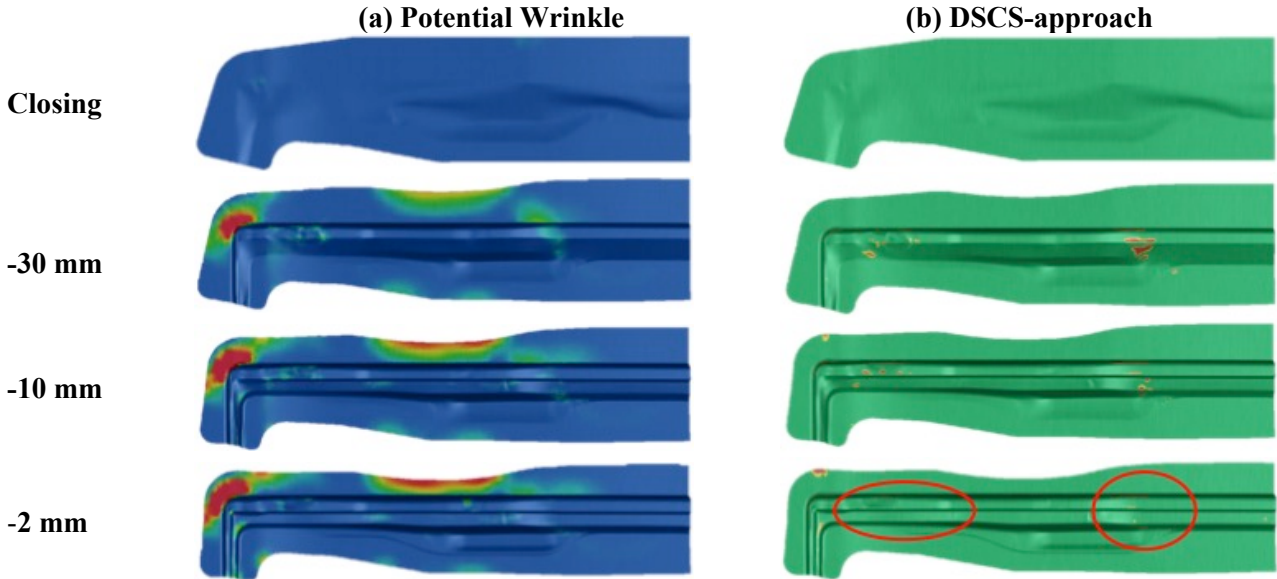


Figure 8-8: FEA results in OP 20 using AutoForm, material HC300LA with thickness of 0.9 mm: (a) Results using “potential wrinkles” approach; (b) Results using “DSCS-approach”

When compared with the simulation results using the DSCS-approach, it can be concluded that results from “DSCS-approach” are in good agreement with deep drawn parts (see Fig. 8-9/10/11). After the deep drawing process, severe wrinkles can be observed in wrinkling area 1, see Fig. 8-9-a/b, which was marked with red circles in Fig. 8-8-b. In summary, both wrinkling criteria are feasible to identify this wrinkling area. However, by using “potential wrinkles”, only slight wrinkles (marked with colour hell green) are detected, see Fig. 8-9-c.

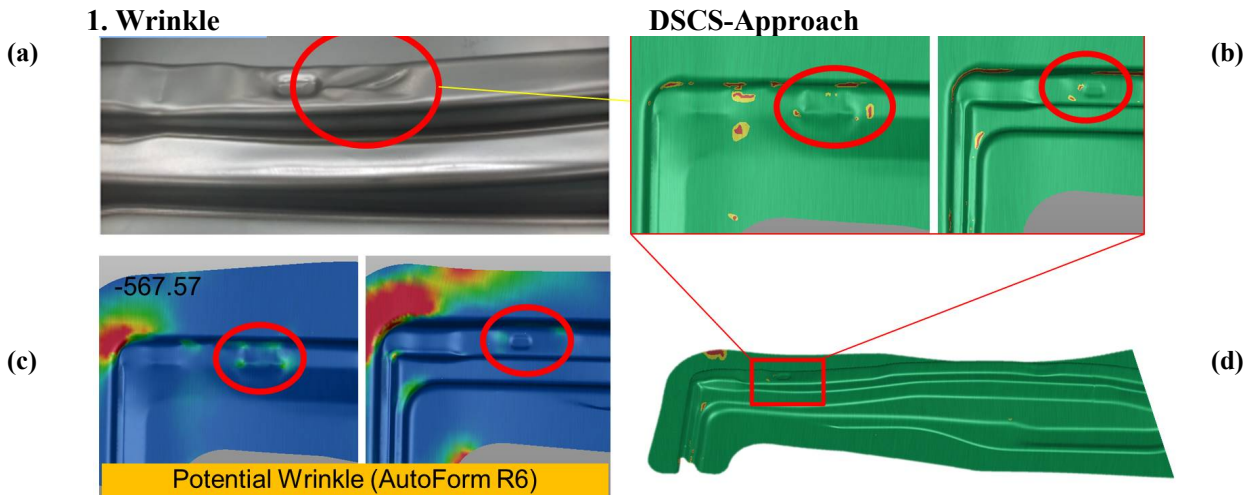


Figure 8-9: Comparison between “potential wrinkles“ approach and “DSCS-approach” at wrinkling area 1, (a) Experimental results; (b) FEA results based on “DSCS-approach”; (c) FEA results based on “potential wrinkles” approach; (d) Location of the wrinkling area 1 in FEA

The second wrinkling area is located in the side wall of this deep drawn part (marked with a red circle). The wrinkling position is presented in Fig. 8-10-a. When using “potential wrinkles” approach, this wrinkling area cannot be detected (see Fig. 8-10-c). However, by using the DSCS-

approach, this wrinkling area was marked in yellow (see Fig. 8-10-b). This means “wrinkling initiation” occurs in this area. It can also be shown that the results of “DSCS-approach” are in good agreement with deep drawn parts and can be used as criteria for the deep drawn parts in AutoForm R6. This is because wrinkles emerge with the change of local surface profile because of “local bending process”. As soon as the local curvature has been changed, the difference of the stress between O-side and I-side can be detected.

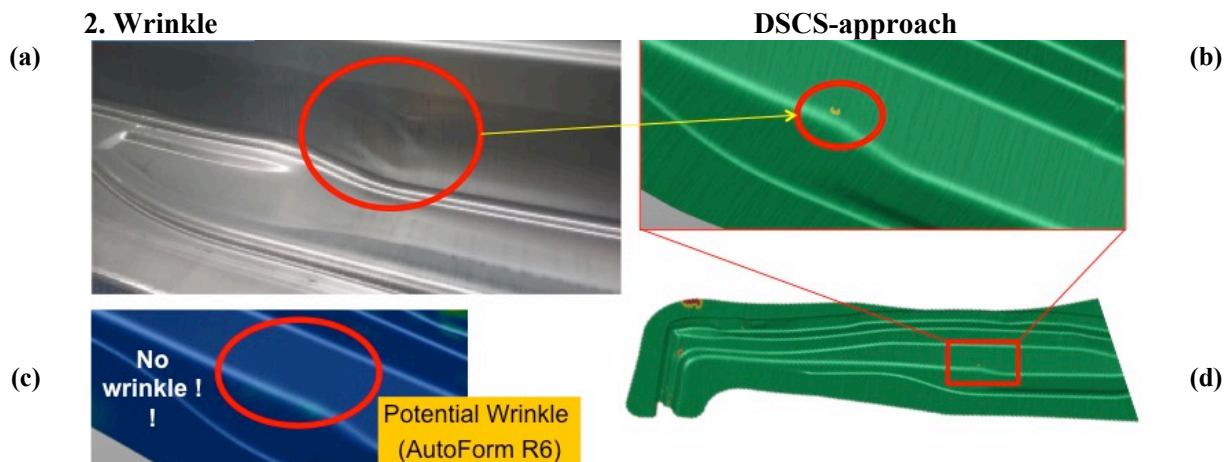


Figure 8-10: Comparison between “potential wrinkles” approach and “DSCS-approach” at wrinkling area 2, (a) Experimental results; (b) FEA results based on “DSCS-approach”; (c) FEA results based on “potential wrinkles” approach; (d) Location of the wrinkling area 2 in FEA

The third wrinkled area is located in the transition zone of this deep drawn part (marked with a red circle), as shown in Figure 8-11. When using the results of variable “Potential wrinkles” from AutoForm, this wrinkling area can be detected. Moreover, when using the DSCS-approach, this wrinkling area was marked in yellow and red. Both wrinkling criteria can detect this area.

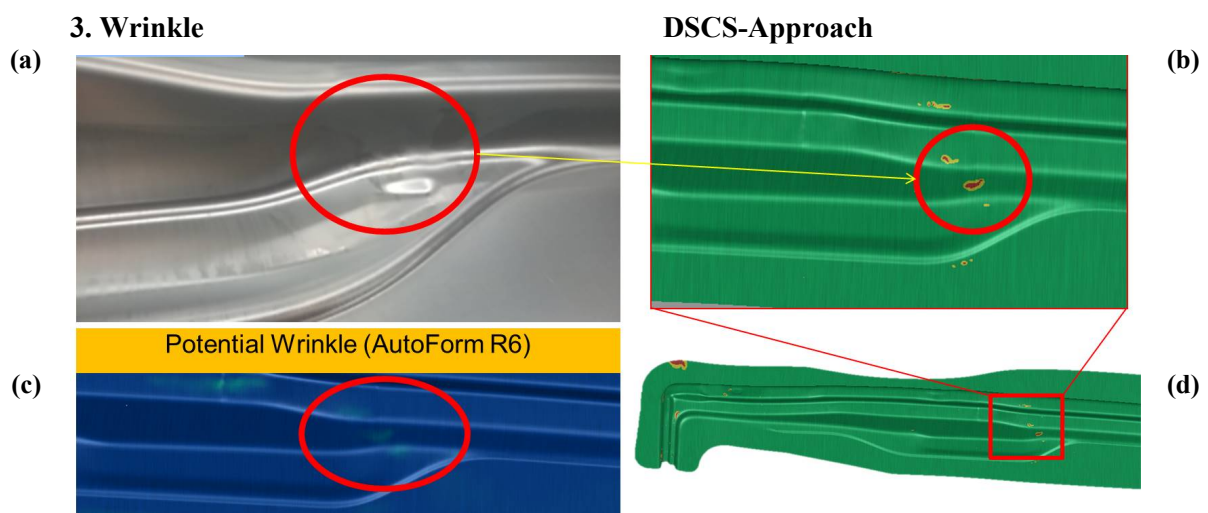


Figure 8-11: Comparison between “potential wrinkles” approach and “DSCS-approach” at wrinkling area 3, (a) Experimental results; (b) FEA results based on “DSCS-approach”; (c) FEA results based on “potential wrinkles” approach; (d) Location of the wrinkling area 3 in FEA

8.4 Validation study 3 – Part Door-Frame-Adapter

In this case study, the formed part of Door Frame Adapter is used to validate the new wrinkling criteria – DSCS-approach. Since there is no chance to produce a drawn part every 10 mm in OP 20 (like the situation in case study 1), only the wrinkling position at the finished drawn part will be validated. The occurrence of the first wrinkles is also not validated in case study 3. The part Door Frame Adapter was produced with sheet material HC300LA having thickness of 0.9 mm.

Door-Frame-Adapter, HX300LA 0.9 mm

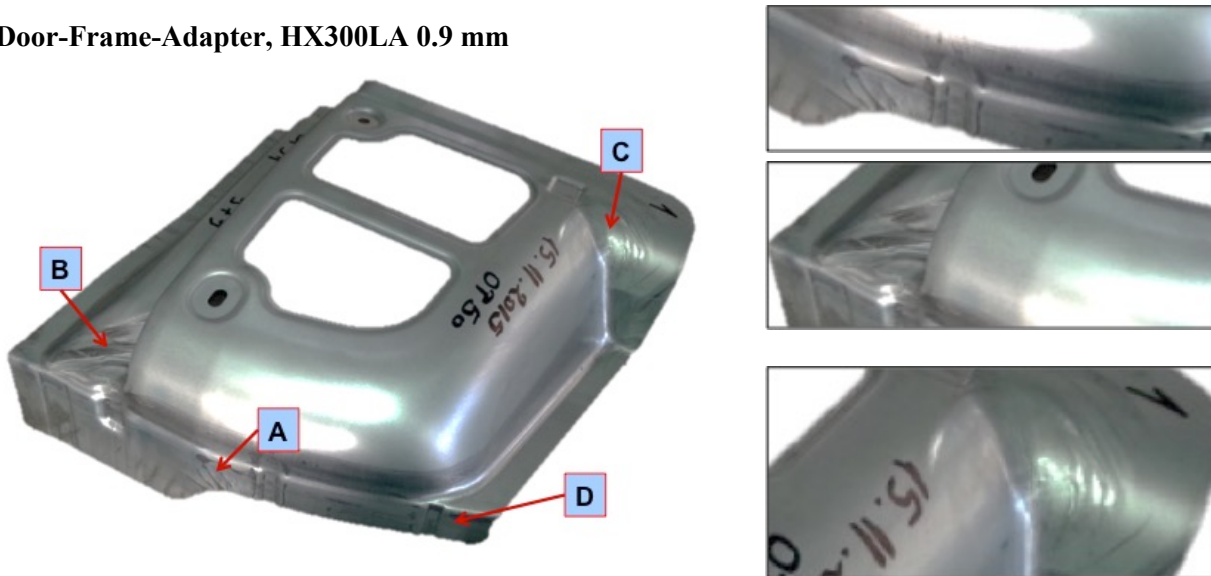


Figure 8-12: Four wrinkle formation areas indicated in the part Door-Frame-Adapter

In the deep-drawn part of the Door-Frame-Adapter, four wrinkling areas were observed. When drawing the part, the comparison of the simulation results between the Potential-wrinkles-AutoForm and the DSCS-approach are presented in Figures 8-11, 8-12 and 8-13.

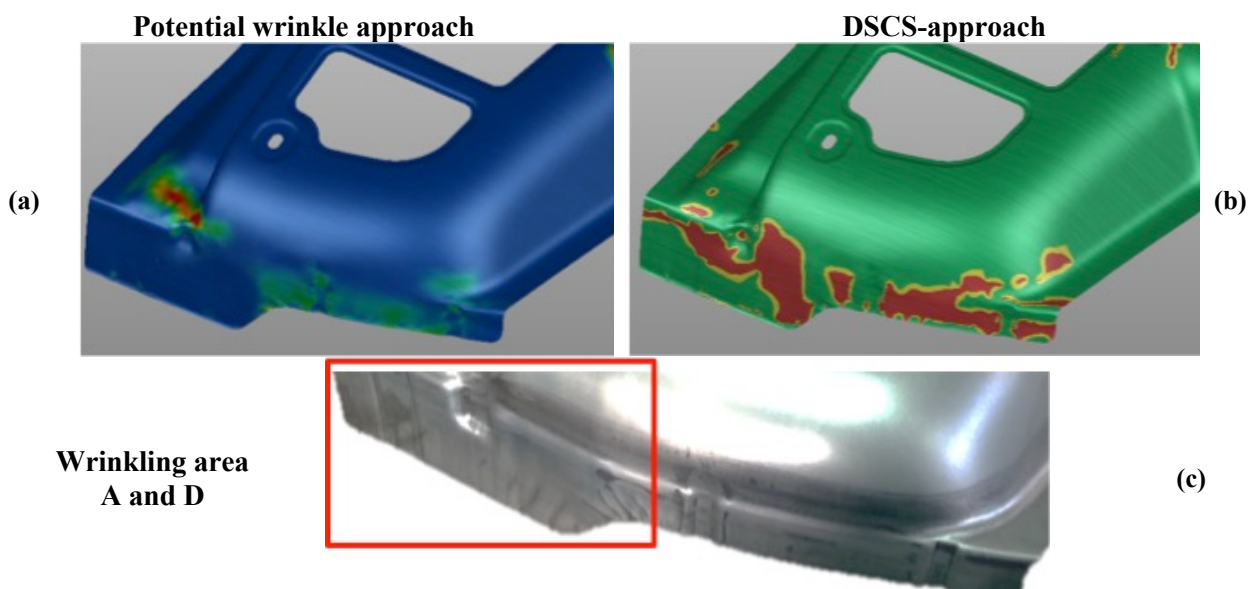


Figure 8-13: Comparison between the “potential wrinkles” and “DSCS-approach” regarding wrinkling area A, (a) FEA results according to “potential wrinkles” approach; (b) FEA results according to “DSCS-approach”; (c) wrinkling area A and D in formed part

In Fig. 8-13, the results of the comparison of wrinkling areas A and D are shown. In the formed part Door-Frame-Adapter, the wrinkle can be found from wrinkling region A to wrinkling region D marked in Fig. 8-12. The FEA results using the “DSCS-approach” (see Fig. 8-13-a) were in good agreement with the proposed method and the deep drawn parts. When using the “potential wrinkles” approach (see Figure 8-13-a), not all wrinkles in the wrinkle area can be recognised. By using the “potential wrinkles” approach, only the wrinkle area A (marked in green hell green) is predicted. In the wrinkling area D, severe wrinkles can also appear in the real drawn part.

In summary, the type of wrinkles in Zones A and D (type: “flat developed wrinkles”) is caused by two main causes. First, the geometry of the flanging area which is caused by the flanging down process leads to wrinkles. The contact line is convex (as viewed from the top) and there is a compressive stress by the flanging down process in the working direction. Therefore, wrinkles will occur. The second is that the clearance between the forming tool and the lower tool is too small. Usually, in order to obtain good quality of the flanging surface, the clearance between flanging tool and lower tool is planned to be small. For these two reasons, the wrinkles that are developed during the flanging down process are forced to flatten.

In Figure 8-14, the results for wrinkle zone B are compared. “Wrinkle Zone B” occurs during the deep drawing process OP 20. These two approaches are in good agreement with the actual formation of severe wrinkles in Zone B. The difference between the “potential wrinkles” approach and the “DSCS-approach” is the time at which wrinkles appear (the “time” draw depth can be understood as drawing depth).

According to the FEA results using the “potential wrinkles” approach, the slight wrinkles (marked in green) detected occurred at a drawing depth of 55 mm. The first severe wrinkles (marked with colour red in Fig. 8-14-a) in wrinkling area B occurs at a drawing depth of 90.3 mm. After the appearance of the wrinkles, the wrinkles remain stable in the B area. According to the FEA results using the “DSCS-approach”, the slight wrinkles (marked with colour green) which are detected by using “potential wrinkles” approach occurs at the drawing depth of 45 mm. The first severe wrinkles (marked with colour red in Fig. 8-14-a) in wrinkling area B occurs at a drawing depth of 65 mm.

In Fig. 8-15, the comparison of the results regarding wrinkling area C is presented. Wrinkling area C” occurs also at deep drawing process OP 20, like wrinkling area B. The two approaches were in good agreement with deep drawn parts. The difference between “potential wrinkles” approach and “DSCS-approach” is the time (drawing depth) at which wrinkles take place. According to the FEA results using the “potential wrinkles” approach, the slight wrinkles (marked in green) detected in the FEA occurred at a depth of 25 mm. In the wrinkle area B, the first severe wrinkle (marked in

red in Figure 8-14-a) occurs at a drawing depth of 80 mm after the wrinkles appear, and the wrinkles in the B area remain stable. According to the FEA results using the “potential wrinkles” approach, the slight wrinkles (marked in green) occurred at a depth of 25 mm. The first severe wrinkle in the wrinkle area B (marked red in colour in Figure 8-14-a) occurs at a depth of 45 mm.

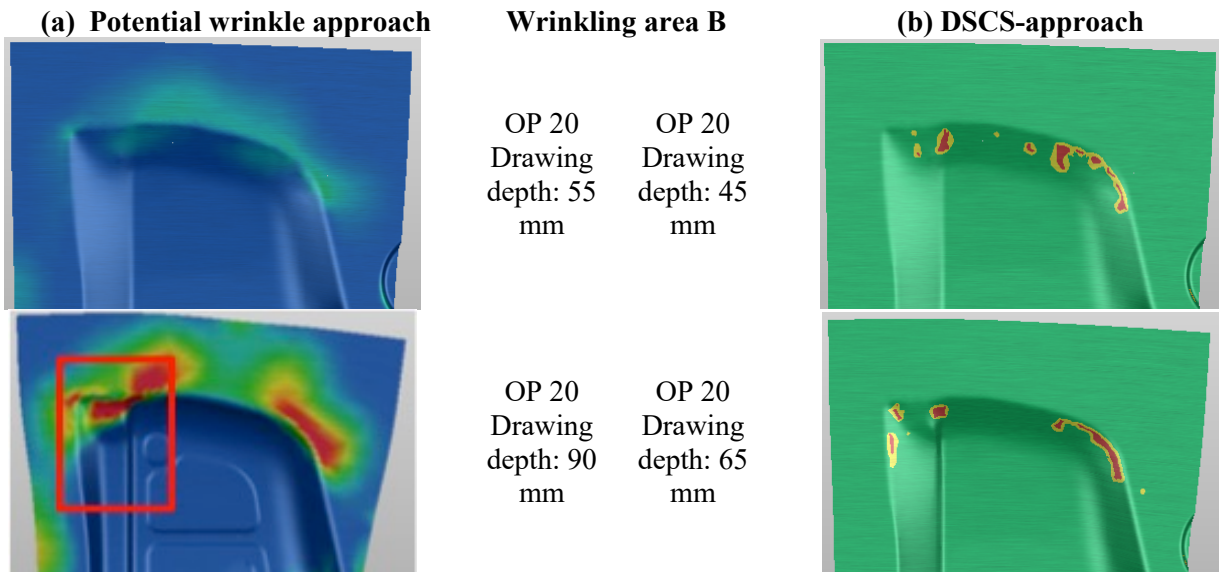


Figure 8-14: Comparison between the “potential wrinkles” and “DSCS-approach” regarding wrinkling area B, (a) FEA results according to “potential wrinkles” approach at drawing depth of 55 mm and 90 mm; (b) FEA results according to “DSCS-approach” at drawing depth of 45 mm and 65 mm

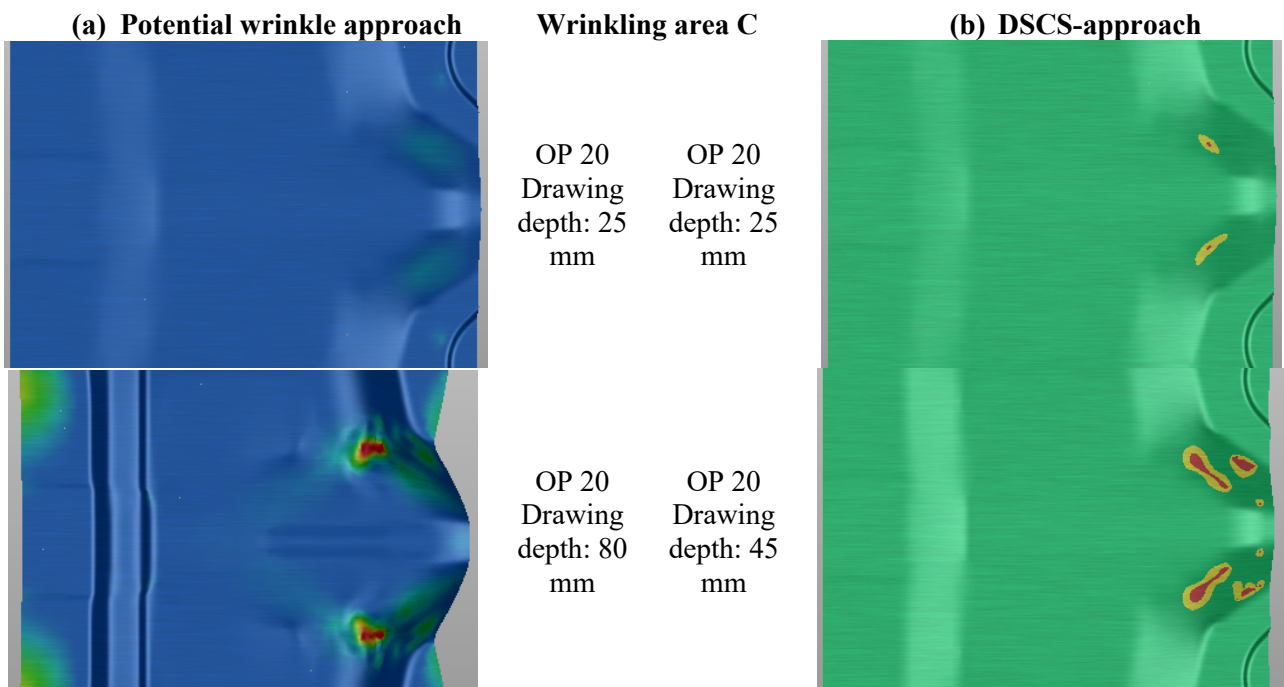


Figure 8-15: Comparison between the “potential wrinkles” and “DSCS-approach” regarding wrinkling area C, (a) FEA results according to “potential wrinkles” approach at drawing depth of 25 mm and 80 mm; (b) FEA results according to “DSCS-approach” at drawing depth of 25 mm and 45 mm

9 Conclusion and Outlook

9.1 Conclusion of this work

In this work, multiple wrinkle criteria have been mentioned in state of the art. In general, it is possible to predict wrinkles of sheet metal components during deep drawing using FEA analysis based on strain-based or stress-based criteria. However, by using conventional strain or stress based criteria some restrictions should be mentioned as following:

Restrictions of conventinal strain-based wrinkling criteria

- Application of strain-based criterion on simple geometry

As mentionened in Chapter 2, usually strain based wrinkling criterion cannot predict wrinkling formation accurately. However, FLD based wrinkling limit curve can be used to predict wrinkling formation regarding simple desined part, like conical cup test and Yoshida buckling test. As explained before, wrinkling behavior can be affected by part geometry. Thus, when the part geometry can stay consistent, the wrinkling tendency of the used material can be characterized.

- Strain based wrinkling criterion cannot be applied for predicting elastic wrinkles

In the case of elastic wrinkling, the value of strain values are too small to identify both in FEA and experimental works. The reason why FEA has low sensitivity towards wrinkling initiation regarding low strain values in the case of elastic wrinkles and wrinkles with small plastic deformation.

Restrictions of convetional stress-based wrinkling criteria

- Change of the surface quality cannot be predicted

According to Cao's and Kim's model, a critical stress value should be calculated and used as criterion to judge, whether the wrinkling initiation on a drawn part takes place or not. Furthermore, by using conventional stress-based wrinkling criteria, wrinkling height cannot be defined as a criterion, because only at the difined wrinkling initiation the wrinkling height can be determined. By using DSCS-approach the whole wrinkling process can be evaluated und the relationship between actual stress and wrinkling height can be obtained. Thus, by using DSCS-approach the wrinkling height can be used as criterion to predict wrinkling behavior of drawn parts.

- Kim's Bifurcation method to define wrinkling initiation

Validation results of Kim shows that, the defined wrinkling initiation take place very soon in deep drawing process. His conclusion can be verified by performing modified Yoshida buckling test (see Figure 7.5). By Using Kim's bifurcation method, the bifurcation takes place at gripper displacement 1.5 mm. the ensprechend wrinkling height is about 0.002mm. According to DSCS-approach the wrinkling initiation occurs when the gripper has the displacement of 4 mm. The

wrinkling at this gripper displacement is 0.04 mm. Under normal requirement in automobilindustry, the wrinkling/buckling of 0.002 mm for exterior parts is acceptable. Thus, Kim's bifurcation method can be widely applied for the surface evaluation where has a high requirement on surface quality regarding sheet metal parts or components.

- Hutchinson's bifurcation method to predict wrinkling initiation

Compared with Kim's bifurcation method, the characteristic of Hutchinson's method is much more conservative. According to his method, the bifurcation occurs after the defined developed wrinkles by using DSCS-approach. Thus, Hutchinson's bifurcation method was not widely used in practice. The reason is, according to DSCS-approach the wrinkling height at "developed wrinkle" is 1.1 mm. In practice, 1.1 mm wrinkling height for exterior parts is already unacceptable.

- Cao's energy method, require accuracy of experimental results

The advantage of Cao's energy method is, the critical stress value can be calculated according Cao's model. However, her formula contains many parameters which must be determined by performing corresponding experiments. Thus, the results from performed experiments affect directly the accuracy of the formula. In addition, one calculated critical value can only predict when wrinkling initiation occurs. At wrinkling initiation, if the critical wrinkling height should be setted as 0.02, the Cao's method will be cannot used. In Conclusion, According Cao's method, only one value can be calculated passively.

Restrictions of simplified model introduced in Chapter 4 for predicting wrinkling formation

- simplified model can be used as criterion of wrinkling second order

By using of simplified model presented in chapter 4, the wrinkling initiation can be only manual evaluated. For the wrinkles in free forming area in simple geometry like conical cup test and Yoshida buckling test, the wrinkling formation can be predicted by using FEA.

- no considerision of change of the wrinkling direction

by using the simplified model only the development of minor stress at O-side should be considered. When the wrinkling direction changes in another direction, in this case the minor stress at I-side will be used to determine the wrinkling initiation and developed wrinkles.

- Problem by implementing in postprocessing of FEM software.

As shown in Figure 7-9, the time point regarding wrinkling initiation and developed wrinkles can be evaluated according to the first derivative of the fitted function. In postprocessing of FEA, the most of the FEM software dosen't have the ability, the first derivation of a fitted function to calculate.

For these above mentioned reasons, the new stress-based wrinkling criterion named with "Double-

Surface-Compressive-Stress-Approach” (DSCS-approach), should be developed and introduced as soon as possible to predict the surface quality of a part.

The DSCS-approach which has been developed between 2015 and 2016. This new criterion for predicting of wrinkling time phases is based on the stress differences (in minor principal direction) between the outer and inner surfaces of deep drawn components in FEA. When the critical values are reached, the in post-processing defined wrinkling time phases like “wrinkling initiation” and “developed wrinkle” will take place.

To identify regions with potential wrinkling tendency and developed wrinkles, to distinguish different time phases of wrinkling and to get a deeper understanding of the whole wrinkling process, two basic experiments and reference simulations have been conducted (modified Yoshida buckling test, conical cup test) made of three different sheet metal materials (HC300LA, HC420LA, and DX54D). Results of these fundamental tests and simulations were used in a DoE-analysis to calculate linear regression models for critical stress at wrinkling initiation and developed wrinkle, for each material. These regression models were used later on for the implementation of the DSCS-approach in AutoForm R6 as UDV files (User-Defined-Variable).

Results gained by newly developed DSCS-approach were compared to wrinkling criterion “Potential Wrinkles” which is used in AutoForm R6. Three parts used in BIW were validated as case studies introduced in Chapter 8, namely Side-Low-Outer panel, Door-Frame-Adapter panel and C-Pillar-Reinforcement panel. Validation results show that DSCS- approach is more sensitive to low strain values than the criterion “Potential Wrinkles” used in AutoForm and demonstrates much better agreements with real deep drawing parts. By using conventional strain or stress based criteria some restrictions should be mentioned as following:

Advantages of DSCS-approach

- Stress based wrinkling criterion

DSCS-approach is stress based. For DSCS-approach, the critical stress value is the deviation between minor stress at O-side and I-side. Here the critical stress can be understood as a time depended curve.

- Wrinkling degree can be defined according to wrinkling height

The form FEA determined critical stress is not only time depended, but also wrinkling height depended. The deviation between minor stress at O-side and I-side can be directly determined from FEA. Besides informations about wrinkling can also be determined in FEA.

- Considering “local curvature” and “sheet thickness” by using DoE method

With the help of DoE, the relationship between local curvature/sheet thickness and wrinkling

height at wrinkling initiation and developed wrinkle can be determined

- Directly used in post-processing of FEM software

DSCS-approach can be prepared as UDV-files and directly used in postprocessing.

Disadvantages of DSCS-approach

- Special specimens design and modified specimens

Until today Yoshida buckling tests are not standard test to evaluate the wrinkling tendency of sheet metal materials. Thus, Yoshida specimen should have to be modified according to experimental equipments and sheet material. The question is, how to ensure the consistency of experiments between different laboratories.

- Critical compressive stress determined by FEA

In this thesis, the needed critical stress at wrinkling initiation and developed wrinkles were determined directly from FEA (see reference simulations in Chapter 7). Thus, the boundary conditions of the simulation, like material parameter, element parameter and process parameter must be consistent to ensure the consistency of FEA results between different simulation operator.

- Experimental limit regarding conical cup test and Yoshida buckling test

In this thesis, the tested materials have a sheet thickness is less than 1 mm. However, during the research work it was found that, conical cup test and Yoshida buckling test will doesn't work, if the sheet thickness is more than 1.5 mm. Thus, for the wrinkling tendency regarding thick sheet metal, the new experimental equipments should be developed.

9.2 Outlook and future works

Based on the short overview in Chapter 9.1, it can be conducted that further investigations for improving usability and prediction quality of the new developed DSCS-approach are highly recommended. Especially the following tasks need to be studied in depth:

Automatically presented wrinkling positions (at each drawing depths) in the FEA

By using stress-based wrinkling criterion like DSCS-approach, the wrinkling position cannot be stored automatically in AutoForm R6. Conversely, by using strain-based criterion like "potential wrinkles", the wrinkle area can be automatically stored and marked in the FEA. To overcome this disadvantage and to show the fixed wrinkling position in FEA, a new method of implementation (UDV-files in post-processing of FEM software) should be developed.

Improved regression model in the future work

Since only three sheet metal materials have been studied. The critical stress difference at "wrinkling initiation" and "developed wrinkle" can be firstly predicted in this work with the following equation: $\Delta\sigma = A + BX_1 + CX_2 + D X_1 * X_2$. Details have been explained in Chapter 6.

In the future work, more sheet metal materials should be investigated to determine a more proper and effective empirical regression model. Results based only on this work show that the K^{lc} value of the Swift model mainly influences the critical difference of surface compressive stress. This tendency is shown in Fig. 6-14. By investigating further different sheet metal materials, the influence of K value based on Swift model on critical stress differences should be determined.

Models to predict wrinkling height during the wrinkling process in FEA

According to the validation results, DSCS-approach provides the potential of more precise prediction of surface quality regarding wrinkling initiation and wrinkle development. Wrinkling height is an important factor to characterise surface condition. In this work, the critical wrinkling height can only be predicted at corresponding time point, as “wrinkling initiation” and “developed wrinkle”. In the future, models to describe wrinkling height can be introduced and disclosed during the FEA in the future. In addition, using “wrinkling height” to define surface quality during the whole wrinkling process is essential for the following next point.

Useful Informations by using DSCS-approach in FEA

According to the analysis above, it is possible to obtain more accurate informations about surface quality of forming parts. Further developed wrinkling criteria based on DSCS-approach should be implemented with models to predict wrinkling height directly at each drawing depths. Using those informations, the impact of surface defects on crash performance can be more appropriately determined in the future.

10 Appendix

10.1 Applied sheet metal materials

Table 10-1: Chemical composition [VW14] and mechanical properties [Bec13] regarding deep drawing sheet material DX54D used in Chapter 8

	C [%] Max.	Si [%] Max.	Mn [%] Max.	P [%] Max.	S [%] Max.	Ti [%] Max.
DX54D +Z140MB	0.06	0.50	0.40	0.025	0.025	0.3
	Yield strength Rp0.2 [Mpa]		Tensile strength Rm [Mpa]		Elongation A ₈₀ [%]	
DX54D +Z140MB	151		289		45,3	

Table 10-2: Chemical composition [VW14] and mechanical properties [Bec13] regarding micro-alloyed sheet material HC300LA, HC340LA and HC420LA used in Chapter 2/7 and Chapter 8

	C [wt%] Max.	Si [wt%] Max.	Mn [wt%] Max.	P [wt%] Max.	S [wt%] Max.	Al [wt%] total	Ti [wt%] Max.	Nb [wt%] Max.
HC300LA +Z100MB	0.12	0.50	1.4	0.03	0.025	≥0.015	0.15	0.09
HC420LA +Z100MB	0.12	0.50	1.6	0.03	0.025	≥0.015	0.15	0.1
	Yield strength R _{p0.2} [Mpa]		Tensile strength R _m [Mpa]			Elongation A ₈₀ [%]		
HC300LA +Z100MB	368		457			23.4		
HC420LA +Z100MB	463		561			20.4		

Table 10-3: Chemical composition [DIN09] and mechanical properties regarding deep drawing sheet material AA6016 used in Chapter 2

	Si [wt%] Max.	Fe [wt%] Max.	Cu [wt%] Max.	Mn [wt%] Max.	Mg [wt%] Max.	Cr [wt%] total	Zn [wt%] Max.	Ti [wt%] Max.
AA6016	1.0 – 1.5	0.50	0.2	0.2	0.25 – 0.6	0.1	0.2	0.15
	Yield strength R _{p0.2} [Mpa]		Tensile strength R _m [Mpa]			Elongation A ₈₀ min. [%]		
AA6016 T4	300 – 380		380 – 480			23		

10.2 Results regarding regression models using Minitab 17

Table 10-4: Results of critical surface stress by „wrinkling initiation“, HC300LA

Coded Coefficients

Term	Effect	Coef	SE Coef	t-Value	p-Value	VIF
Constante		138,3	*	*	*	
Local Curvature	223,5	111,8	*	*	*	1,00
Sheet Thickness	43,50	21,75	*	*	*	1,00
Local Curvature*Sheet Thickness	56,50	28,25	*	*	*	1,00

1)

Regression equation in non-encoded units

2)

$$\Delta \sigma_{WI} = 52,50 - 100,0 * \text{Local Curvature} - 32,50 * \text{Sheet Thickness} \\ + 11300 * \text{Local Curvature} * \text{Sheet Thickness}$$

Table 10-5: Results of critical surface stress by „developed wrinkle“, HC300LA

Coded Coefficients

Term	Effect	Coef	SE Coef	t-Value	p-Value	VIF
Constante		138,3	*	*	*	
Local Curvature	223,5	111,8	*	*	*	1,00
Sheet Thickness	43,50	21,75	*	*	*	1,00
Local Curvature*Sheet Thickness	56,50	28,25	*	*	*	1,00

3)

Regression equation in non-encoded units

4)

$$\Delta \sigma_{DW} = 140,0 + 8400 * \text{Local Curvature} + 200,0 * \text{Sheet Thickness} \\ - 0,000000 * \text{Local Curvature} * \text{Sheet Thickness}$$

Table 10-6: Results of critical surface stress by „wrinkling initiation“, HC420LA

Coded Coefficients

Term	Effect	Coef	SE Coef	t-Value	p-Value	VIF
Constante		194.5	*	*	*	
Local Curvature	361.0	180.5	*	*	*	1.00
Sheet Thickness	43,50	13.50	*	*	*	1.00
Local Curvature*Sheet Thickness	23.00	11.50	*	*	*	1.00

Regression equation in non-encoded units

$$\Delta \sigma_{WI} = 6,000 + 10760 * \text{Local Curvature} + 10,00 * \text{Sheet Thickness} \\ + 4600 * \text{Local Curvature} * \text{Sheet Thickness}$$

Table 10-7: Results of critical surface stress by „developed wrinkle“, HC420LA

Coded Coefficients

Term	Effect	Coef	SE Coef	t-Value	p-Value	VIF
Constante		495.5	*	*	*	
Local Curvature	159.00	79.50	*	*	*	1.00
Sheet Thickness	40.00	20.00	*	*	*	1.00
Local Curvature*Sheet Thickness	10.000	5.000	*	*	*	1.00

Regression equation in non-encoded units

$$\Delta \sigma_{DW} = 356.0 + 4760 * \text{Local Curvature} + 75.00 * \text{Sheet Thickness} \\ + 2000 * \text{Local Curvature} * \text{Sheet Thickness}$$

11 Bibliography

- [Ach13] Achouri, M.; Germain, G.; Santo, P. D.; Saidane, D.: Experimental characterization and numerical modeling of micromechanical damage under different stress states, *Materials & Design*, Vol. 50, p. 207-222, 2013
- [And95] Anderson, T.L.: *Fracture mechanics – Fundamentals and applications*, Texas A&M University, CRC press, second edition, ISBN 0-8493-4260-0, 1995
- [And15] Andrade, F.; Erhart, T.; Haufe, A.; Feucht, M.; Prediction of material failure under nonlinear strain paths using incremental models, in 8th Forming Technology Forum Zurich – Advanced constitutive models in sheet metal forming, P. 65-70, Zurich, 2013
- [Aut19] AutoForm Online Support Document: Material models and Forming criteria for the version R7 and R8, 2.-Version, Esslingen, 2019
- [Ban10] Banabic, D.: *Sheet metal forming processes – Constitutive modeling and numerical simulation*, ISBN 978-3-540-88112-4, Springer-Verlag Berlin Heidelberg, 2010
- [Ban13] Banabic, D.; Lazarescu, L.; Paraiianu, L; Ciobanu, I.; Nicodim, D.S. Comsa: Development of a new procedure for the experimental determination of the forming limit curve, *CIRP Annals – Manufacturing Technology*, Vol. 62, p. 255-258, 2013
- [Bar87] Barlat, F.; Richmond, O.: Prediction of tricomponent plane stress yield surfaces and associated flow and failure behavior of strongly textured FCC polycrystalline sheets, *Materials Science and Engineering*, Vol. 91, P. 15-29, 1987
- [Bar17a] Barthau, M.; Liewald, M.: New approach on controlling strain distribution manufactured in sheet metal components during deep drawing process, *International Conference on the Technology of Plasticity, Cambridge (ICTP)*, Cambridge, United Kingdom, 2017,
- [Bar17b] Barthau, M.; Liewald, M.; Held, C.: Improved process robustness by using closed loop control in deep drawing applications, *Journal of Physics: Conference series*, Volume 869, 36th IDDRG Conference – Materials Modelling and Testing for Sheet Metal Forming, Munich, 2017
- [Bec02] Becker, W.T.: *Principles of failure analysis – Ductile and brittle fracture*, ASM International, The materials information society, OH 44073-0002, 2002
- [Bec04] Beck, S.: Optimierung der Zargenspannung beim Ziehen unregelmäßiger Blechformteile, Dr.-Ing. Dissertation, Beiträge zur Umformtechnik, Institut für Umformtechnik der Universität Stuttgart, Band 46, DGM, ISBN: 3883553336, 2004
- [Bec11] Becker, C.: Untersuchung eines Messdübelsensor zur Spannungsermittlung und Versagenserkennung beim Tiefziehen, Studienarbeit im Fach Umformtechnik, IFU, 2011
- [Bec13] Becker Stahl-Service GmbH: *Produktinformationen und Chemische Zusammensetzung und mechanische Eigenschaften*, 2013
- [Ben04] Benzerga, A.A.; Besson, J.; Pineau, A.: Anisotropic ductile fracture, Part 1: experiments, *Acta Materialia*, Vol. 52, p. 4623-4638, 2004

- [Bla08] Blaich, C.; Liewald, M.: New approach for closed-loop control of deep drawing processes, International conference – New development in sheet metal forming, Fellbach, Germany, 2008
- [Bla10] Blaich, C.; Liewald, M.: Erfassung und Regelung lokaler Zargenspannungen zur Optimierung von Tiefziehprozessen, Internationale Konferenz – Neuere Entwicklung in der Blechumformung, Fellbach, Deutschland, 2010
- [Bla12] Blaich, C.: Robuster Tiefziehprozess durch Erfassung und Optimierung der örtlichen Bauteilqualitaet, Dr.-Ing. Dissertation, Beiträge zur Umformtechnik, Institut für Umformtechnik der Universität Stuttgart, Band 66, DGM, ISBN: 3883553069, 2012
- [Ble52] Bleich, F.: Buckling strength of metal structures, McGraw-Hill international Book Company, International student edition, 1952
- [Bol14] Bolanos, J.A.; Cobos, O.F. Hinguera; Marrero, J.M. Cabrera: Strain hardening behavior of ARMCO iron processed by ECAP, IOP Cnf. Series: Materials Science and Engineering, 63-012143, 2014
- [Bru14] Bruschi, S.; Altan, T.; Banabic, D.; Bariani, P.F.; Brosius, A.; Cao, J.; Ghiotti, A.; Khraisheh, M.; Merklein, M.; Tekkaya, A.E.: Testing and modeling of material behavior and formability in sheet metal forming, CIRP Annals – Manufacturing Technology, Vol. 63, P. 727-749, 2014
- [Cao97] Cao, J.; Boyce, M.C.: A predictive tool for delaying wrinkling and tearing failures in sheet metal forming, Transaction of the ASME, Vol. 119, P. 354-365, 1997
- [Che04] Cheng, H.S; Cao, J.; Yao, H.; Liu, S.D.; Kinsey, B.: Wrinkling behavior of laminated steel sheets; in Journal of Materials Processing Technology, 151(2004); P. 133-140, 2004
- [Che07] Chen, F.K.; Liao, Y.C.: Analysis of draw-wall wrinkling in the stamping of a motorcycle oil tank; in: Journal of Materials Processing Technology 192-193, P: 200-203, 2007
- [Col87] Colangelo, V.J.; Heiser, F.A.: Analysis of metallurgical failures, published by Wiley, second edition, ISBN: 978-0-471-89168-0, 1987
- [Dav04] Davis, J.R.: Tensile Testing, ASM Internatianl, Materials Park, Ohio 44073-0002, Second Edition, ISBN: 0-87170-806-X/SAN: 204-7586, 2004
- [Den11] Denninger, R.; Liewald, M.; Held, C.; Sindel, M.: Investigation on bendability of lightweight materials for various load path, ESAFORM, Conference Proceeding 1601-1604, 2001
- [DIN01] DIN EN 10002-1: Metallische Werkstoffe Zugversuch – Teil 1: Prüfverfahren bei Raumtemperatur (Deutsche Fassung EN 10002-1:2001
- [DIN09] DIN EN 573-3:2009: Aluminium und Aluminiumlegierungen – Chemische Zusammensetzung und Form von Halbzeug – Teil 3: Chemische Zusammensetzung und Erzeugnisformen, Deutsche Fassung EN 573-3:2009
- [Doe86] Doege, E.; Meyer-Nolkemper, H.; Saeed, I.: Fließkurvenatlas metallischer Werkstoffe – mit Fließkurven für 73 Werkstoffe und einer grundlegenden Einführung, ISBN 3-446-14427-7, Hanser Verlag München Wien, 1986
- [Doe95] Doege, E.; Rosoki, T.E.; Seibert, D.: Prediction of necking and wrinkling in sheet metal forming, Journal of Materials Processing Technology, Vol. 50, P. 197-206, 1995

- [Doe98] Doege, E.; Kracke, M.: Vorhersage der Faltenbildung in geneigten Ziehteilzargen mit elementaren Ansätzen, Blech Rohre Profile, Vol. 11, S. 54-61, 1998
- [Doe10] Doege, E.; Behrens, B.: Handbuch Umformtechnik, Springer-Verlag, Heidelberg, 2010
- [Fri14] Friebe, H.: Optical 3D metrology for sheet metal analysis and material parameters determination, FLC Workshop, Institut fuer virtuelle Production, ETH Zuerich, 2014
- [Fri99] Friedl, N.; Rammerstorfer, F.G.; Fischer, F.D.: Zum Beulen von Platten unter globalem Zug, in: Zeitschrift für angewandte Mathematik und Mechanik 79, S. 545-546, 1999
- [Gao16a] Gao, Q.; Han, F.; Wortberg, D.; Bleck, W.; Liewald, M: The impact of hydrogen on the formability of AHSS in Nakajima tests, Online DOI: 10.1063/1.4963626, 19th International ESAFORM Conference on Material Forming, Nantes, France, 2016
- [Gao16b] Gao, Q.; Han, F.; Wortberg, D.; Bleck, W.; Liewald, M: Influence of hydrogen on formability and bendability of DP 1180 steel for car body application, IDDRG International Conference, p. 61-68, 2016
- [Gao17] Gao, Q.: Investigation on Hydrogen Embrittlement of advanced high strength steels for automotive applications, Dr.-Ing Dissertation, IEHK der Rheinisch-westfaelische Technische Hochschule, 2017-08357, HBZ: HT019487618, 2017
- [Gib82] Gibson, T.J.; Hobbs, R.M.: Observations on the Yoshida buckling test, IDDRG, Genoa, Proceedings of Working Group 3
- [Gon15] Gong, P.; Palmiere, E.J.; Rainforth, W.M.: Dissolution and precipitation behavior in sheets microalloyed with niobium during thermomechanical processing, Acta Materialia, Vol. 97, p. 392-403, 2015
- [Gro03] Grote, H.: Zum Einfluss des Beulens auf die Tragfähigkeit von Walzprofilen aus hochfestem Stahl, Dr.-Ing. Dissertation, Ruhr-Universität Bochum, 2003
- [Gro09] Gross, D.; Schnell, W.; Hauger, W.; Wriggers, P.: Technische Mechanik 4: Hydromechanik, Elemente der Hoeheren Mechanik, Numerische Methoden, 7. Auflage, Springer, Berlin, ISBN 978-3-540-89390-5
- [Hae02] Häussermann, M.: Zur Gestaltung von Tiefziehwerkzeugen hinsichtlich des Einsatzes auf hydraulischen Vielpunktzieheinrichtungen, Dr.-Ing. Dissertation, Beiträge zur Umformtechnik, Institut für Umformtechnik der Universität Stuttgart, Band 28, DGM, ISBN: 3883553069, 2002
- [Han14] Han, F.; Liewald, M.: A new method to enhance the accuracy of the buckling test using modified Yoshida sample, Advanced Materials Research, Vol. 1018, P. 199-2016, 2014
- [Han15a] Liewald, M.; Han, F.; Radonjic, R.: New criterion for prediction of the wrinkle formation in the deep drawing process, Key Engineering Materials, Vol. 651-653, P. 71-76, 2015
- [Han15b] Han, F.; Radonjic, R.: New approach for wrinkle prediction in deep drawing process, Key Engineering Materials, Vol. 639, P. 459-466
- [Has16] Hassan, H.U.; Maqbool, F.; Güner, A.; Hartmaier, A.; Khalifa, N.B.; Tekkaya, A.E.: Springback prediction and reduction in deep drawing under the influence

- of unloading modulus degradation, *International Journal of Material Forming*, DOI 10.1007/s12289-015-1248-5, 2015
- [Her17] Herakovich, C.T.: *A concise introduction to elastic solids – An overview of the mechanics of elastic materials and structures*, ISBN: 978-3-319-45601-0, Springer Verlag, 2017
- [His93a] Hishida, Y.; Wagoner, R.: *Experimental analysis of blank holding force control in sheet metal forming*, SAE Transactions, 930285, *Journal of Materials and Manufacturing, Section 5, Volume 102*, P. 93-99, 1993
- [His93b] Hishida, Y.; Wagoner, R.: *Analysis of blank holding force control forming using hydraulic forming simulator*, *Advanced Technology of Plasticity, Proceedings of the fourth International Conference on Technology of Plasticity*, P. 1740-1746, 1993
- [Hoe13] Hoenle, S.: *Influence of material modelling parameters on the prediction of bending loads in sheet metal forming simulation*, *Advanced Materials Research, Vol. 769*, P. 165-172
- [Hoe16] Honle, S.: *Methode zur Bewertung und Prognose der Anmutungsqualitaet und der Herstellbarkeit von Falzschlaufen an Karosserieanbauteilen aus Aluminium*, Dr.-Ing. Dissertation, *Beiträge zur Umformtechnik, Institut für Umformtechnik der Universität Stuttgart, Band 79, DGM*, ISBN: 978-3-946818-04-5, 2016
- [Hoj17] Hojna, A.: *Overview of interanular fracture of neutron irradiated austenitic stainless steels*, *Metals – Open Access Metallurgy Journal, Vol. 7-292*, doi:10.3390/met7100392, 2017
- [Hor12] Hora, P.; Manopulo, N.; Tong, L.: *Numerical and experimental methods for the prediction of failure in sheet metal forming*, P. 1-10, *Forming Technology Forum 2012, ETH Zurich, Switzerland*
- [Hos07] Hosford, W.F.; Caddell, R.M.: *Metal forming – Mechanics and metallurgy*, Cambridge university press, Third edition, ISBN-13: 978-0-511-35453-3, ISBN-10: 0-511-35453-3, 2007
- [Hu08] Hu, Y.; Zhu, X.; Lee, W.: *Surface low prediction using LS-Dyna and Dynaform*, P. 779-785, *Numisheet 2008*
- [Hut74] Hutchinson, J.W.: *Plastic buckling*, *Advances In Applied Mechanics, Vol. 14*, P. 67-144, 1974
- [Hut85] Hutchinson, J.W.; Neale, K.W.: *Wrinkling of curved thin sheet metal*, *Plasticity Instability*, p. 71-78, 1985
- [Isi14] Isik, K.; Silva, M.B.; Tekkaya, A.E.; Martins, P.A.F.: *Formability limit by a fracture in sheet metal forming*, *Journal of Materials Processing Technology, Vol.214*, P. 1557-1565, 2014
- [ISO08] ISO 12004-2: *Metallic materials – Sheet and strip – Determination of forming limit curve – Part 2: Determination of forming limit curves in the laboratory*, 2008
- [ISO14] ISO 16808:2014-08: *Methallic materials – Sheet and strip – Determination of biaxial stress-strain curve by means of bulge test with optical measuring*, Technical committee: ISO/TC 164/SC 2 *Ductility testing*, 2014
- [Jan05] Jann, B.: *A general theory of uniqueness and stability in elastic-plastic solids*, *Journal of the Mechanics and Physics of Solids, Vol. 6*, P. 236-249

- [Kau13] Kaupper, M.; Merklein, M.: Bendability of advanced high strength steels – A new evaluation procedure, *CIRP Annals – Manufacturing Technology*, Vol. 62, P. 247-250, 2013
- [Kim99] Kim, Y.S.; Son, Y.J.; Park, K.C.: Bifurcation analysis of wrinkling formation for anisotropic sheet, *KSME International Journal*, Vol. 13, P. 221-228, 1999
- [Kim00a] Kim, J.B.; Yang, D.Y.; Yoon, J.W.; Barlat, F.: The effect of plastic anisotropy on compressive instability in sheet metal forming, *International Journal of Plasticity*, Vol. 16, P. 649-676, 2000
- [Kim00b] Kim, J.B.; Yoon, J.W.; Yang, D.Y.: Wrinkling initiation and growth in modified Yoshida buckling test: Finite element analysis and experimental comparison, *International Journal of Mechanical Sciences*, Vol. 42. P. 1683-1714, 2000
- [Kim03] Kim, J.B.; Yoon, J.W.; Yang, D.Y.: Investigation of wrinkling behavior of thin sheets in the cylindrical cup drawing process using bifurcation theory, *International Journal for Numerical Methods in Engineering*, Vol. 56, P. 1673-1705, 2003
- [Kle15] Klein, B.: *FEM – Grundlagen und Anwendungen der Finite-Elemente-Methode im Maschinen- und Fahrzeugbau*, 10. Auflage, Springer Vieweg, ISBN 978-3-658-06054 (eBook)
- [Klo10] Klocke, F.: Sheet metal forming 2: Simulation techniques in manufacturing technology – Lecture 4, Werkzeugmaschinenlabor (WZL) der Rheinisch-westfälische Technische Hochschule (RWTH) und Fraunhofer Institut fuer Produktionstechnologie (IPT), 2000
- [Koc12] Koch, N.; Liewald, M.; Bäcker, F.: Vorhersage der Oberflächenqualität von Tiefziehteilen im Automobilbau mittels virtuellem Yoshida-Buckling-Test (YBT), Liewald, M. (Hrsg.): *Neue Entwicklungen in der Blechumformung*, MAT INFO (Frankfurt a. M), Stuttgart-Fellbach, 2012
- [Koc14] Koch, N.: *Neue Ansätze und Methoden zum kombinierten Streck- und Tiefziehen von flachen Aussenhautteilen moderner Fahrzeugkarosserien*, Dr.-Ing. Dissertation, Beiträge zur Umformtechnik, Institut für Umformtechnik der Universität Stuttgart, Band 72, DGM, ISBN: 978-3-88355-406-8, 2014
- [Kop99] Kopp, R.; Wiegels, H.: *Einführung in die Umformtechnik*, Verlag: G. Verlag, 2. Edition, ISBN-10: 3860738216, ISBN-13: 978-3860738214, 1999
- [Lan90] Lange, K.: *Umformtechnik Handbuch für Industrie und Wissenschaft Band 3: Blechumformung*, Springer Verlag, 1990
- [Li00] Li, M.; Brazill, R.L.; Chu, E.W.: Initiation and growth of wrinkling due to nonuniform tension in sheet metal forming, *Experimental Mechanics*, Vol. 40, No. 2, P. 180-189, 2000
- [Li12] Li, Si.P.; Tekkaya, A.E.; Verhoeven, H.: *Numerische Simulation von Sandwichblechen in Umformprozessen*, LS-DYNA Forum, 09.-10. Oktober, Ulm, 2012
- [Lie08] Liewald, M.; Blaich, C.: *Versagensfälle in der Blechumformung – Ein Ueberblick; Teil 2*, Veröffentlicht in Tagungsband des 11. Workshop Simulation in der Umformtechnik, Stuttgart, Deutschland, 2008
- [Lie14] Liewald, M.; Wagner, S.; Radonjic, R.; Proc. 14th Stuttgart Int. Symposium Automotive and Engine Technology, P. 496, Stuttgart, 2014

- [Lie15] Liewald, M.; Han, F.: A new approach for determination of the wrinkling limit curve (WLC) in deep drawing, P. 75-80, Forming Technology Forum, Switzerland, 2015
- [Lie16] Liewald, M.: State of the art – perspectives of strain and stress-based approaches to determine wrinkles of second order in deep drawing processes, presentation in 19th International ESAFORM Conference on Material Forming, Nantes, France, 2016
- [Lie18] Liewald, M.; Barthau, M.: Adaptive control strategies for deep drawing of high-performance sheet metal materials, in 37th IDDRG Conference, Waterloo, Canada, 2018
- [Loh05] Lohse, W.: Stahlbau 2, B.G. Teubner 2005, Wiesbaden, ISBN 978-351925259
- [Lsd12] LS-DYNA Keyword user's manual, Volume 2 Material Models, Livermore software technology corporation (LSTC), Version 971 R6.1.0, 2012
- [Mar02] Marciniak, Z.; Duncan, J.L.; Hu, S.J.: Mechanics of sheet metal forming, Butterworth-Heinemann press, ISBN 0 7506 5300 0, 2002
- [Mid20] Midea Group: Marketing research and consumer habits report – Aisa region, KWHA, 2020
- [Nar08] Narayanasmy, R.; Loganathan, C.: Study on wrinkling limit of interstitial free steel sheets of different thickness when drawn through conical and tractrix dies, Material and Design, Vol. 29, P. 1401-1411, 2008
- [Nas71] NASA Apace Vehicle Design Criteria (Structures): Buckling strength of structural plates – Designs for determining buckling strength of structural plates for spacecraft, National Aeronautics and space administration, Document-ID: 19710023855, NASA SP-8068, 1971
- [Nea90] Neale, K.W.; Tugcu, P.: A numerical analysis of wrinkle formation tendencies in sheet metals, Inter. Journal for Numerical Methods in Engineering, Vol. 30, P. 1595-1608, 1990
- [Neu09] Neukamm, F.; Feucht, M.; Haufe, A.: Considering damage history in crashworthiness simulations, 7th European LS-Dyna Users Conference, Salzburg, 2009
- [Now10] Nowotnik, A.; Siwecki, T.: The effect of TMCP parameters on the microstructure and mechanical properties of Ti-Nb microalloyed steel, Journal of Microscopy, doi: 10.1111/j.1356-2818.2009.03238, Vol. 237(3), P. 258-262, 2010
- [Pap16] Papaioanu, A.: Einsatz eines neuartigen Verfahrens zum kombinierten Recken und Tiefziehen von Aussenhautbeplankungen aus Feinblech, Dr.-Ing. Dissertation, Beiträge zur Umformtechnik, Institut für Umformtechnik der Universität Stuttgart, Band 81, DGM, ISBN: 978-3-946818-06-9, 2016
- [Pin16] Pineau, A.; Benzerga, A.A.; Pardoën, T.: Failure of metals: Brittle and ductile fracture, Acta Materialia, Vol. 107, P. 424-483, 2016
- [Pok10] Pokluda, J.; Šandera, P.: Micromechanisms of fracture and fatigue – In a multi-scale context, Engineering Materials and Processes, ISBN 978-1-84996-266-7, Springer Verlag, 2010
- [Por08] Port, A. L.; Thuillier, S.; Manach, P.Y.; Garabed, J.: Experimental and numerical characterization of the surface defects of an automotive door, P. 773-778, Proceeding of 144, Numisheet 2008

- [Rad15a] Radonjic, R.; Liewald, M.; F. Han: Optimisation of the blank holder stiffness in deep drawing processes by using FEA,” in 10th European LS-DYNA Conference, Würzburg, 2015
- [Rad15b] Radonjic, R.; Liewald, M.; F. Han: Influence of blank holder stiffness on part surface quality in deep drawing process, in DEMI 2015, 12. International Conference on Accomplishments in Electrical and Mechanical Engineering and Information Technology, Serbien, P. 205-212, 2015
- [Rad16] Radonjic, R.; Liewald, M.: Approaches for springback reduction when forming ultra high-strength sheet metals, IOP Conf. Series: Materials Science and Engineering, 159, 012028, doi: 10.1088/1757-899X/159/1/012028, 2016
- [Ran20] Radonjic, R.: Kompensationsstrategien von Ruckfederungseffekten beim Umformen von hochfesten Stahlblechwerkstoffen, Dr.-Ing. Dissertation, Beiträge zur Umformtechnik, Institut für Umformtechnik der Universität Stuttgart, Band 87, DGM, ISBN: 978-3-946818-12-0, 2020
- [Roo08] Roos, E.; Maile, K.: Werkstoffkunde fuer Ingenieure: Grundlagen, Anwendung, Prüfung, 3. Auflage, Springer, Berlin, Heidelberg 2008, ISBN 978-3-540-68398-8
- [Roy01] Roylance, D.: Stress-Strain Curves, MIT Open-Course-Ware, Department of material science and engineering, Massachusetts Institute of Technology (MIT), Document-ID: MA 02139, 3.11-Mechanics of Materials, 2001
- [San13] Panich, S.; Barlat, F.; Uthaisangsuk, V.; Suranuntchai, S.; Jirathearanat, S.: Experimental and theoretical formability analysis using strain and stress-based forming limit diagram for advanced high strength steels, Materials and Design, Vol. 51, P. 756-766, 2013
- [Sel99] Selman, A.: Wrinkling prediction procedure in thin sheet metal forming processes with adaptive mesh refinement, Part 1: Contact fress wrinkling, The University of Twente, Project number: WB.99/NIMR-0183, 1999
- [Sel01] Selman, A.: Wrinkling prediction procedure in thin sheet metal forming processes with adaptive mesh refinement, Part 2: Wrinkling with contact, University of Twente, Project number: ME97033, 2001
- [Sch53] Schmidt, E.: Tiefziehen konischer Teile, Dr.-Ing. Dissertation, Technische Hochschule Stuttgart, 1953
- [Sch98] N. N.: Schuler Handbuch der Umformtechnik, Schuler GmbH, Springer-Verlag Berlin, London, New York, ISBN 3-540-14760-8, 1998
- [Sch09] Schleich, R.; Albiez, C.; Papaioanu, A.; Liewald, M.: Investigation on simulation of buckling of aluminum sheet alloys, 7th European LS-DYNA Conference, 2009
- [Sch10] Schleich, R.: Entwicklung eines Versagensmodells fuer Aluminiumlegierungen zur praediktiven Bestimmung von lastabhaengigen Versagensfaellen in der Blechumformung, Dr.-Ing. Dissertation, Beiträge zur Umformtechnik, Institut für Umformtechnik der Universität Stuttgart, Band 64, DGM, ISBN: 978-3-88355-383-2, 2010
- [She04] Sheng, Z.Q.; Jirathearant, S.; Altan, T.: Adaptive FEM simulation for prediction of variable blank holder force in conical cup drawing, International Journal of Machine Tools and Manufacture, Vol. 44, P. 487-494, 2004

- [Sie98] Siegert, K.; Hohnhaus, J.; Wagner, S.: Combination of hydraulic multipoint cushion system and segment-elastic blankholders, SAE-Paper 980077, P. 31-40, 1998
- [Sie15] Siegert, K.: Blechumformung – Verfahren, Werkzeugen und Maschinen, Springer-Verlag, ISBN 978-3-540-02488-0, 2015
- [Sim89] Simon, H. (1989): Rechnerunterstützte Ziehtheilauslegung mit elementaren Berechnungsmethoden, Dr.-Ing. Dissertation, ISBN: 318148802X, Institut für Umformtechnik und Umformmaschinen, Hannover, 1989
- [Sim90] Simon, H.: Computer based part development using elementary calculation methods, VDI, ISBN 318148802X
- [Tim85] Timoshenko, S.P.; Gere, J.M.: Theory of elastic stability, McGraw-Hill international Book Company, International student edition, Second edition, ISBN 0-07-Y85821-7, 1985
- [Ton01] Tong, L.; Hora, P.; Reissner, J.: Modified stiffness method for the FE prediction of wrinkling in sheet forming processes. In: Simulation of Materials Processing: Theory, Methods and Applications; Swetz&Zeitlinger Verlag, ISBN 90 2651 822 6, P. 621–626, 2001
- [Vol11] Volk, W.; Kim, Jae-K: Modellierungsansätze fuer ausgewählte Aspekt der Umformsimulation, LS-Dyna Anwenderforum, Stuttgart, 2011
- [VW14] VW-50065: Flacherzeugnisse aus Stahl zur Kaltumformung – Werkstoffanforderungen, Version-Nr.: 51251, Ausgabe 2014-05
- [Wan00a] Wang, X.; Cao, J.: An analytical prediction of flange wrinkling in sheet metal forming, Journal of Manufacturing Processes, Vol. 2, P. 100-107, 2000
- [Wan00b] Wang, X.; Cao, J.: On the prediction of side-wall wrinkling in sheet metal forming processes, International Journal of Mechanical Sciences, Vol. 42, P. 2369-2394, 2000
- [Wan08] Wang, H.P.; Xu, S.G.; Cao, J.; Chen, W.; Cheng, H.S.; Wang, C.T.: Preliminary study on a surface distortion prediction for sheet metals: Validation in Yoshida buckling problems, P. 787-795, Proceeding of 144, Numisheet 2008
- [Wer13] Werber, A.; Liewald, M.; Nester, W.; Grünbaum, M.; Wiegand, K.; Simon, J.; Timm, J.; Hotz, W.: Assessment of forming limit stress curves as a failure criterion for non-proportional forming processes, Production Engineering Research and Development., Vol. 7(2-3), P. 213-221, doi: 10.1007/s11740-013-0446-6, 2013
- [Wur11] Wurster, K.; Liewald, M.; Blaich, C.: Procedure for automated virtual optimization of variable blankholder force distributions for deep drawing process with LS-Dyna and OptiSLang, in 8th Weimar Optimization and Stochastic Days, P. 1-16, Weimar, 2011
- [Yos81] Yoshida, K.; Hayashi, H.; Miyauchi, K.; Hirata, M.; Hira, T.; Ujihara, S.: Assessment of fitting behavior and shape fixation by Yoshida buckling test – a way to overall formability, Proc. Int. Symp. New Asp. Sheet Met. Form, Japan, 1981

Curriculum Vitae

PERSONAL DATA

Name Han, Fei
 Geburtsdatum 03th August 1985
 Geburtsort Nanjing, Jiangsu Province, P.R. China
 Familienstand Married, one child

EDUCATION

RWTH Aachen University

10/2009 bis 02/2013: Material Engineering
 Degree: Master of Science (M.Sc.)

Nanjing Institute of Technology

09/2005 bis 07/2007: Material Engineering
 Degree: Bachelor of Science (B.Sc.)

Nanjing College of Information Technology

09/2005 bis 07/2007: Material Engineering
 Change of university in 2005

WORK AND SCIENTIFIC EXPERIENCE

Midea Group

SHBG, KWHA-PPRC, Technology Research

07/2021 until now: Senior Director – Forming Technology
 03/2021 bis 06/2021: Director – Forming Technology
 09/2020 bis 03/2021: Technical Supervisor – Forming Technology
 02/2020 bis 08/2020: Process Research Engineer

EDAG Production Solution GmbH & Co. KG

09/2017 bis 09/2019: SE-Process Planer (Sheet metal forming)

University of Stuttgart

Institute for Metal Forming Technology (IFU)

04/2013 bis 08/2017: Research Fellow (Material department)

Daimler AG

08/2012 bis 02/2013: Internship
Research center of Access e.V.

01/2012 bis 07/2012: Student Research Assistant

Nanjing Progressive Stamping GmbH

08/2007 bis 12/2007: Internship